UNIVERSITY OF CAPE TOWN
IYUNIVESITHI YASEKAPA • UNIVERSITEIT VAN KAAPSTAD

Development of low-clinker concrete: Partial replacement of cement with calcined clay and limestone, based on selected African raw materials

By

Emmanuel Safari Leo

Thesis Presented for the Degree of
DOCTOR OF PHILOSOPHY
in the Department of Civil Engineering
Faculty of Engineering and the Built Environment
UNIVERSITY OF CAPE TOWN

February 2022

Supervisor: Emeritus Professor Mark Alexander
Co-supervisor: Professor Hans Beushausen

Declaration

I, Emmanuel Safari Leo, hereby declare that this Thesis is my own, unaided work. All the work in this document, apart from that which is properly acknowledged, is my own. It is being submitted for the degree of DOCTOR OF PHILOSOPHY at the University of Cape Town. It has not been submitted before for any degree or examination in any other University.

Signed by candidate

Emmanuel Safari Leo
02/02/2022

Abstract

The most promising option for lowering the cost and environmental impact of cement is the use of blended cement. The well-known supplementary cementitious materials such as slag and fly ash are limited in most African countries. An attractive option is to produce LC^3 binders, which consist of ground limestone, calcined kaolinite clay, and cement. In this study, the suitability of kaolinite clays for use in LC^3 binders from selected deposits in South Africa and Tanzania was assessed. Four samples of clays were selected for the experimental work. The selection was based on the kaolinite content of the clay. Further, LC^3 mixes with clinker content in the range of 40% to 70% were designed using the mixture design 3-factors approach. The compressive strength of mortar with a water/binder ratio of 0.4 was used as the performance parameter for optimising proportions. Two reference mixes were considered: a mix with 100% CEM II/A-L 52.5 N, and a recommended mix for South African marine environments with 50% cement replaced by ground-granulated blast-furnace slag. In general, the results suggest that, for optimum performance, regardless of the type of clay, the lowest practical clinker content is 55%, at which the amount of calcined clay is 35% and the amount of limestone is 10%. However, on the knowledge that high compressive strength does not automatically represent concrete with excellent durability, two other LC^3 proportions were also considered for the concrete work: one with 65% clinker, 25% calcined clay and 10% limestone and the other with 45% clinker, 40% calcined clay and 15% limestone. The performance properties of the concrete mixes considered were workability, strength development, durability indexes, chloride diffusion characteristics, electrical resistivity, carbonation resistance, shrinkage, and potential for early age cracking. Overall, it can be concluded that the selected LC^3 concrete mixes perform similarly or better than the reference mixes. The results indicate that, apart from kaolinite content, factors that influence the performance of the system include other minerals present in the clay, the filler effect, pozzolanic reaction, formation of carboaluminate phases, stabilisation of the ettringite phase, and the internal surface area of the clay.

Summary

One of the fundamental challenges in the cement industry is mitigating its contribution to climate change. It is anticipated that emissions of greenhouse gases such as CO_2 will be tightly regulated in the future. Moreover, there is the high cost of cement production due to energy consumption. These challenges drive researchers to look for improved ways to reduce the cost and the net CO_2 emissions from the production and use of cement. Globally, the trend is to reduce the clinker factor to 0.6 or less without adversely affecting the performance of the system. The most promising option for lowering cost and environmental impact of cement is the use of blended cement. The well-known supplementary cementitious materials (SCMs), such as ground-granulated blast-furnace slag (GGBS) and fly ash, are limited in most African countries. In contrast, Africa has abundant reserves of kaolinite clays, which when calcined produce exceptionally good SCMs. The high alumina content of calcined kaolinite clays makes them particularly suitable for co-substitution with ground limestone to replace clinker in concrete. This ternary combination is called a Limestone Calcined Clay Cement (LC^3) system.

Several LC^3 studies have already been conducted, especially in Switzerland and India, but because these materials differ all over the world, there is no consensus concerning the required characteristics of superplasticisers, particle sizes and optimum proportions of these materials in connection with the quality of the raw materials for good workability, strength development and durability performance of concrete. In view of this, the suitability of each source of material needs to be examined and evaluated. Therefore, the main objective of this research was to use a performance-based approach in the development of low-clinker concrete (i.e., partially replacing clinker with calcined clay and ground limestone) for structural and non-structural applications.

The compressive strength of mortar (from 50 mm cubes) with a water/binder ratio of 0.4 was used as the performance parameter for optimization of proportions. Two reference mixes were considered: a mix with 100% CEM II/A-L 52.5 N, and a recommended mix for South African marine environments with 50% cement replaced with GGBS. LC^3 mixes with kaolinite clays from selected deposits in South Africa and Tanzania, and clinker

contents in the range of 40% to 70%, were selected using the mixture design 3-factors approach. In general, the results suggest that for best performance, regardless of the difference in the compressive strength values obtained for each of the LC^3 mixes with different calcined clays (CC), the lowest practical clinker factor is 0.55, at which the CC factor is 0.35 and the limestone (LS) factor is 0.1. However, since high compressive strength does not necessarily relate to concrete of high durability, two other proportions of binder were also considered: one with 65% clinker, 25% CC and 10% LS, and the other with 45% clinker, 40% CC and 15% LS.

The performance properties of the concretes considered were limited to workability, strength development, durability indexes, chloride diffusion characteristics, electrical resistivity, carbonation resistance, shrinkage, and potential for early age cracking. All clays selected had kaolinite contents of at least 40% but with different internal surface areas (ISAs) and Na_2O_{eq} contents. Overall, it can be concluded that the selected LC^3 concrete mixes perform similarly or better than the reference mixes with 100% cement or 50% replacement of cement by GGBS. In general, the increase in compressive strength and resistance to ingress of aggressive substances of the LC^3 systems is linked to the porosity refinement produced by the pozzolanic reaction and formation of carboaluminate and ettringite phases. Further, apart from the filler effect, the ISA of the clay and the amount of alkalis present in the clay also influence the performance of the system.

Acknowledgments

A lot happened during my PhD Journey, most of which was beyond my control. I thank the Almighty God, for giving me strength, courage, and ability to work hard throughout the entire duration of this research at the University of Cape Town (UCT). Further, I would very much like to express my appreciation and sincere gratitude to the following:

My supervisor, Professor Mark Alexander, for trusting and believing in me, his excellent discussions, encouragement, advice, and tireless support throughout this work. Thank you so much for being a fantastic mentor and for guiding me on the right path.

My co-supervisor, Professor Hans Beushausen, for his support, encouragement, insightful comments, contributions, and efforts to bring this work to a good ending. Professor Karen Scrivener of EPFL, Switzerland, is also gratefully acknowledged for her helpful advice on the research programme from time to time.

The Head of Department, Professor Pilate Moyo, and all staff in the department of civil engineering and the Concrete Materials and Structural Integrity Research Unit (CoMSIRU) for their extensive support and assistance throughout the entire duration of this research.

Also:

The University of Dar es Salaam (UDSM), AfriSam (SA), PPC Ltd, CCSA, Chryso (SA), Sika (SA) Pty Ltd, and the Water Research Commission (WRC) for the financial support over the period of this work.

Kaolin-group (SA), Serina Trading (SA), Dr. Mohsen Ben Haha, HeidelbergCement (TZ), Mr. Pieter Nel, and Mr. Robert Damian for supplying/assisting in obtaining samples of kaolinite clay from different deposits in South Africa and Tanzania.

Civil and Chemical Engineering laboratory staff, Nooredien Hassen, Taahir Mukaddam, Charles May, Christopher Caesar, Elvino Witbooi, Leonard Adams, Portia Johnston, Keshree Pillay, Rachel Cupido, Lorraine Nkemba, Sandeeran Govender, Russell Geland, and Shene Klink; My fellow CoMSIRU students, Ichebadu Amadi, Alice Bakera, Saarthak

Surana, Joanitta Ndawula, Nicholas Jarrat, and Bukhosi Nyoni, to mention a few, who shared their time, friendship, advice, and assistance during the seminars and in the laboratories.

My wife Elizabeth, my son Ethan, my daughters, Emilyn, Ernalyn and Emmalyn, my mother Veneranda Qambalo, my father Leo Blasi Akonaay, my mother-in-law Vicky Komba, my father-in-law Professor Lucian Msambichaka, my sisters, Felister, Irene, and their families, and my uncles Wille Qambalo, Dr. Herbert Hambati and their families for their prayers, love, understanding, support, and sacrifice throughout the duration of my studies.

Table of Contents

List of figures

List of tables

List of abbreviations

PC	Plain Portland Cement
w/b	Water to binder ratio
SCM	Supplementary Cementitious Material
CC	Calcined Clay
MK	Pure metakaolin
CK	Calcined kaolinite
LS	Limestone
LS-K5	Limestone Kulubrite 5
GGBS	Ground Granulated Blast Furnace Slag
FA	Fly ash
SF	Silica Fume
FA30	PC with 30%FA
B-Clay	Sample of clay from Bronkhorstspruit deposit in Gauteng, South Africa
G-Clay	Sample of clay from Grahamstown deposit in Eastern Cape, South Africa
H-Clay	Sample of clay from Hopefield deposit in Western Cape, South Africa
PH-Clay	Sample of clay from Pugu deposit (Hard clay), Tanzania
PS-Clay	Sample of clay from Pugu deposit (Soft clay), Tanzania
HC-Clay	Sample of clay from HeidelbergCement plant area in Dar es Salaam, Tanzania
LC^3	Limestone Calcined Clay Cement
LC^3-X	LC^3 mix with X% clinker content (X = 45, 50, 55, or 65)
LC^3 (Y)	LC^3 mix with Y-Clay (Y = B-Clay, H-Clay, PH-Clay, or HC-Clay)
LC^3-X (Y)	LC^3 mix with X% clinker content and Y-Clay
LC^3 (Y:CC/LS)	LC^3 mix with Y-Clay and CC/LS ratio
LC^3-X(CC/LS)	LC^3 mix with X% clinker content and CC/LS ratio
LC^3-X(Y:CC/LS)	LC^3 mix with X% clinker content, Y-Clay, and CC/LS ratio
HoH	Heat of Hydration
RC	Reinforced Concrete
RH	Relative Humidity
RD	Relative Density
FM	Fineness Modulus
SP	Superplasticiser
PSD	Particle Size Distribution
ISA	Internal Surface Area
d_{90}	Particles with diameter small than d is 90%
d_{50}	Particles with diameter small than d is 50%
d_{10}	Particles with diameter small than d is 10%
BET	Brunauer Emmet Teller
TGA	Thermogravimetric Analysis
DTG	Derivative Thermogravimetric
XRD	X-Ray Diffraction

SEM	Scanning Electron Microscopy
CIPM	Compaction Interaction Packing Model
MAAM	Modified Andreasen and Andersen Model
EMMA	Elkem Materials-Mixture Analyser
CCSA	Cement and Concrete South Africa
C_s	Surface chloride concentration
D_a	Apparent chloride diffusion coefficient

Cement chemistry notations

A	Alumina (Al_2O_3)
C	Calcium oxide (CaO)
F	Irone oxide (Fe_2O_3)
H	Water (H_2O)
S	Silica (SiO_2)
$C\bar{C}$	Calcite ($CaCO_3$)
CH	Calcium hydroxide ($Ca(OH)_2$)
$\bar{S}$	Sulphate (SO_3)
AS_2H_2	Kaolinite
AS_2	Matakaolin
C_2S	Dicalcium silicate ($2CaO{\cdot}SiO_2$)
C_3S	Tricalcium silicate ($3CaO{\cdot}SiO_2$)
C_3A	Tricalcium aluminate ($3CaO{\cdot}Al_2O_3$)
C_4AF	Tetracalcium aluminoferite ($4CaO{\cdot}Al_2O_3{\cdot}Fe_2O_3$)
C-S-H	Calcium silicate hydrate
C-A-S-H	Calcium aluminosilicate hydrate
$C_6A\bar{S}_3H_{32}$	Calcium monosulphate
$C_6A\bar{S}_3H_{32}$	Ettrigite (Ettr)
C_2ASH_8	Strätlingite (Strät)
$C_4A\bar{S}H_{12}$	Monosulfoaluminate (Ms)
$C_4A\bar{C}_{0.5}H_{12}$	Hemicarboaluminate (Hc)
$C_4A\bar{C}H_{11}$	Monocarboaluminate (Mc)

Chapter 1 Introduction

1.1 Background

An essential component of concrete is cement which reacts with water to form hydrate phases that bind all other constituents of concrete together. Plain Portland cement (PC), which conventionally contains more than 90% clinker, is made from raw materials that are available in many places around the world.

The cement production process involves grinding and calcining a mixture of limestone (greater than 60% as a source of calcium) and clay (as a source of silica and alumina) at about 1450°C to form clinker. This process generates about 900 kg of carbon dioxide (CO_2) per ton of clinker (Klee et al., 2011). Fossil fuel combustion is responsible for about 40% of the total CO_2 emission while decomposition of limestone (LS) is responsible for the rest (Van Den Heede and De Belie, 2012). CO_2 is one of the gases that leads to global warming, therefore, for environmental reasons, calcination of LS must be minimised to reduce CO_2 emissions.

Cement is the one of the most widely used materials on earth. As shown in Figure 1.1, the amount of cement produced worldwide between 1950 and 2014 increased by more than 2.5 times that of steel, and more than 10 times compared to the worldwide population increase in the same period. In 2015, the total mass of cement produced worldwide was 4.6 billion tons, equivalent to about 630 kg/capita, a value that was noted to be higher than the amount of human food consumption (Scrivener, John and Gartner, 2018).

Currently, it is estimated that the manufacture of cement contributes about 8% of global anthropogenic CO_2 emissions (Müller and Harnisch, 2008; Olivier, Schure and Peters, 2017; Andrew, 2018). Almost 25% of cement that is produced globally is used to make reinforced concrete (Scrivener, John and Gartner, 2018). It is therefore important to integrate sustainable processes into all aspects of the concrete production industry to ensure sustainable development in the coming decades.

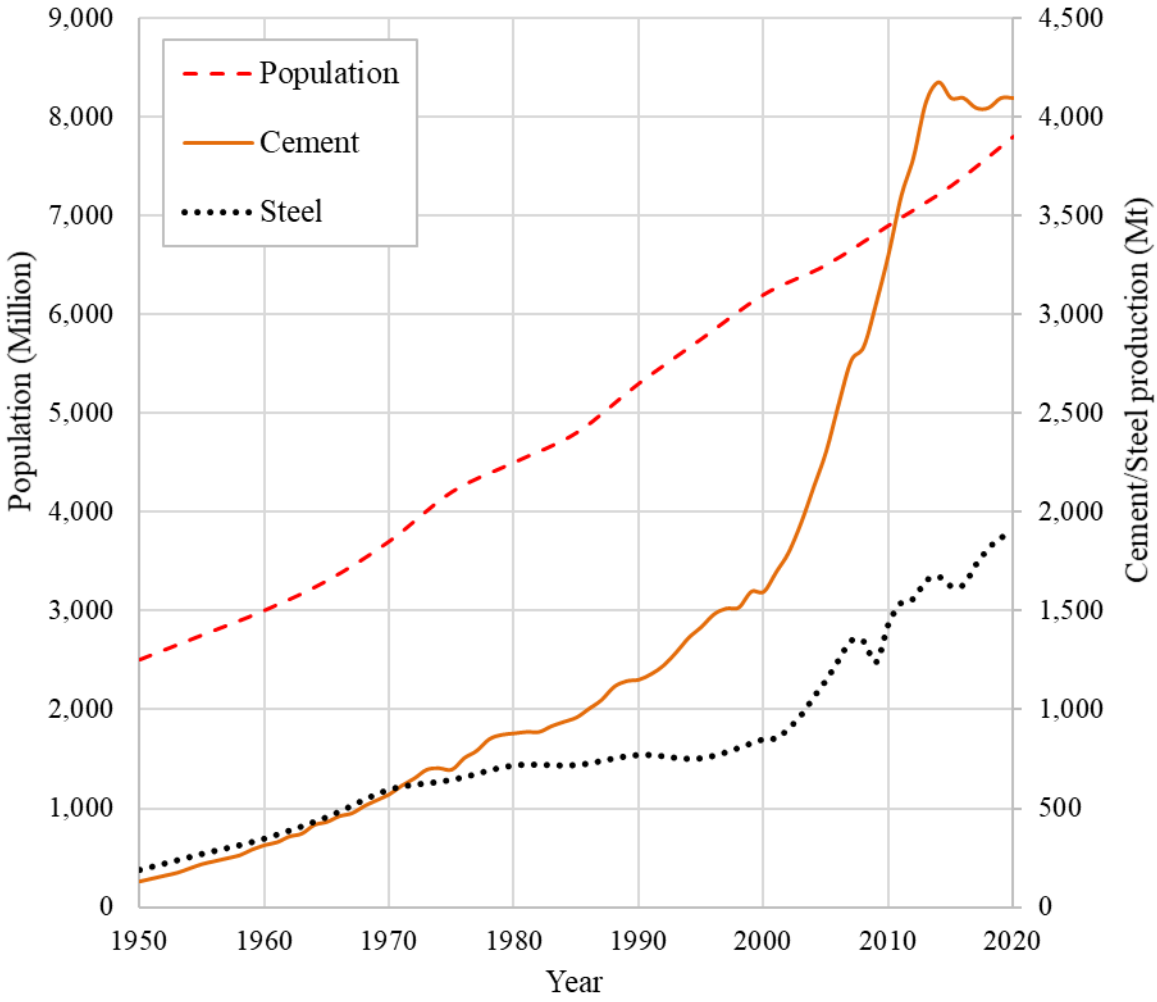

Figure 1.1: Global comparison of cement (U.S. Geological Survey, 2021) and steel (World Steel Association, 2020, 2021) production with the development in global population numbers (UN, 2019)

1.1.1 Anticipated demand of concrete and CO_2 emissions

According to the United Nations (UN, 2014), the overall growth of the world's population is projected to add 2.5 billion people to the urban population by 2050, with almost 90% of the increase concentrating in Asia and Africa. At the same time, the proportion of the world's population living in urban areas is expected to reach 66%. For Africa, the proportion is estimated to reach 56% by 2050. Overall, South Africa and Tanzania are among the top 10 contributors to population increase in Africa (UN, 2016). This will result in an immense demand for urban infrastructure including housing, sewage networks, marine infrastructure such as ports, and transport infrastructure such as roads and bridges. Most of these structures are made of concrete as it is a relatively low-cost construction

material with very good mechanical properties. Compared to other construction materials, concrete is characterised by an intrinsically low environmental impact. However, due to the anticipated increasing demand for concrete, it will increasingly contribute to global CO_2 emissions. Therefore, Africa has a role in ensuring a significant reduction in global CO_2 emissions through the use of low-clinker concrete. Figure 1.2 shows the trend of cement production in Tanzania and South Africa between the years 1990 and 2019.

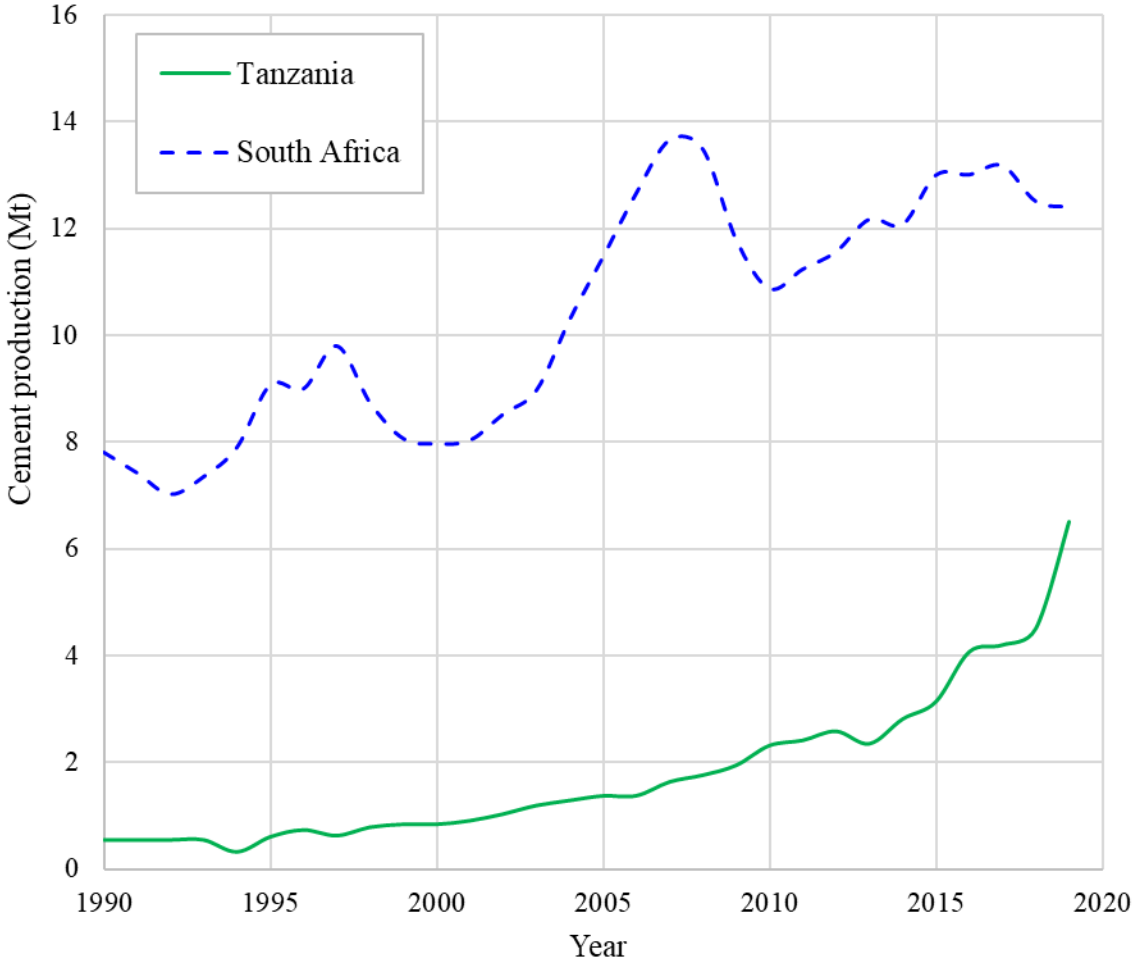

Figure 1.2: Cement production in Tanzania and South Africa
(U.S. Geological Survey, 2021)

It is believed that PC will continue to dominate the cement industry in the coming decades due to (Scrivener, John and Gartner, 2018): i) the economies of scale which result in low cost cement; ii) the widespread availability of raw materials; iii) ease of use enabled by the "open time" before setting and iv) confidence in long-term durability based on prolonged

usage of these cements. In view of this, there is a need to reduce CO_2 emissions from the production of PC. Efforts to reduce the energy-related emissions involves reducing dependence on fossil fuels whereas LS-related emissions involve substituting some of the PC clinker with supplementary cementitious materials abbreviated as SCMs (Habert et al., 2010; Schneider et al., 2011; Scrivener, 2014; Scrivener, John and Gartner, 2018)

1.1.2 Availability of SCMs

The most widely used SCMs, ground granulated blast furnace slag (GGBS) and fly ash (FA), are limited worldwide, especially in most African countries (Klee et al., 2011; Snellings, 2016; Scrivener, John and Gartner, 2018). In Tanzania, there are no sources of FA or slag, although there are certain volcanic ashes available in Mbeya, Moshi and Arusha regions, which are of poor quality for use as SCMs (Lema and Lweikiza, 2014). In South Africa, especially the north-eastern side of the country, large amounts of FA are generated in coal-fired power stations. However, the burning of coal to produce electricity is also considered worldwide as the largest source of CO_2 emissions (Pretorius et al., 2015; Scrivener, John and Gartner, 2018), so in the long term the availability of FA in South Africa is also in question. Also, the Saldanha steel plant ceased to operate in 2020, which means that Corex slag is no longer available in the Western Cape region. Figure 1.3 shows the estimated availability and usage of common SCMs in concrete mixes.

In contrast to the shortage of some of the more common SCMs, Africa has abundant reserves of clays, which when calcined make exceptionally good SCMs (Castillo et al., 2010; Scrivener, 2014; Almenares et al., 2017) and are most likely to exist within 5 metres below the top surface. This is shown in Figure 1.4, in regions coloured in yellow (Ultisols), pale green (Alfisols) and pink (Oxisols) on the world soil map. The main difference between these clays is their pH and type of minerals present in the clay, but all contain kaolinite minerals. Alfisols have a higher concentration of nutrients (Ca^{2+}, Mg^{2+}, K^{+} and Na^{+}) than Ultisols and Oxisols, Ultisols are more acidic i.e., higher concentration of H^{+} and Al^{3+}, and the dominant mineral is kaolinite, while Oxisols have higher concentration of Iron and Aluminium oxides. Section 2.7 provides more discussion about the clay minerals and their pozzolanic activity. There are several kaolinite clays deposits in Africa,

summarised in Heckroodt (1991) and Ekosse (2010). Most of them are small, the potential ones in South Africa (SA) and Tanzania (TZ), based on the estimated amount at the deposits, are given in Table 1.1. The Pugu deposit in Tanzania is believed to be the largest in Africa (Akwilapo and Wiik, 2004).

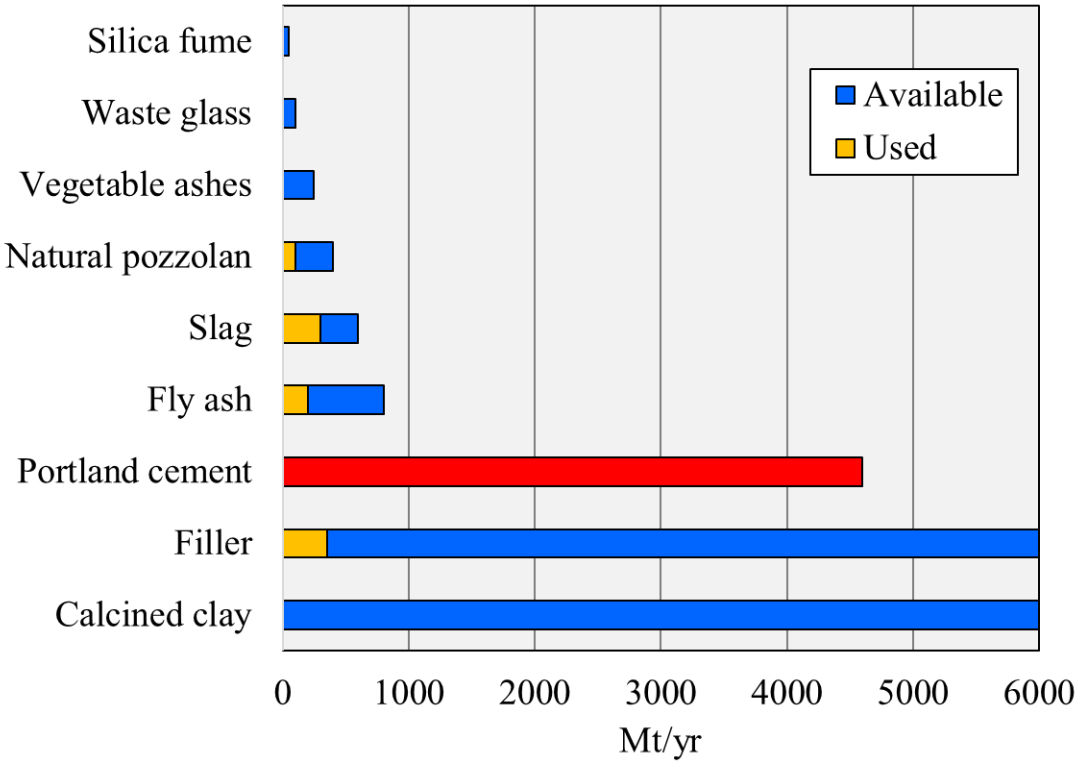

Figure 1.3: Estimated availability of possible SCMs versus amount of cement produced (Scrivener, John and Gartner, 2018)

Table 1.1: Potential of a limited selection of kaolinite clay deposits in South Africa and Tanzania

Country	**Deposit - Location**	**Estimated amount**
South Africa (Hosterman, Patterson and Good, 1978; Ekosse, 2010; Cole, Ngcofe and Halenyane, 2014)	Hopefield – Western Cape	1 Billion tons
	Grahamstown – Eastern Cape	60 Million tons
	Bronkhorstspruit - Gauteng	> 35 Million tons
Tanzania (Ministry of energy and minerals, 2008; Ekosse, 2010)	Pugu - Kisarawe Coast Region	2 Billion tons
	Matamba - Makete Njombe Region	56 Million tons
	Malangali - Mufindi Iringa Region	Unknown

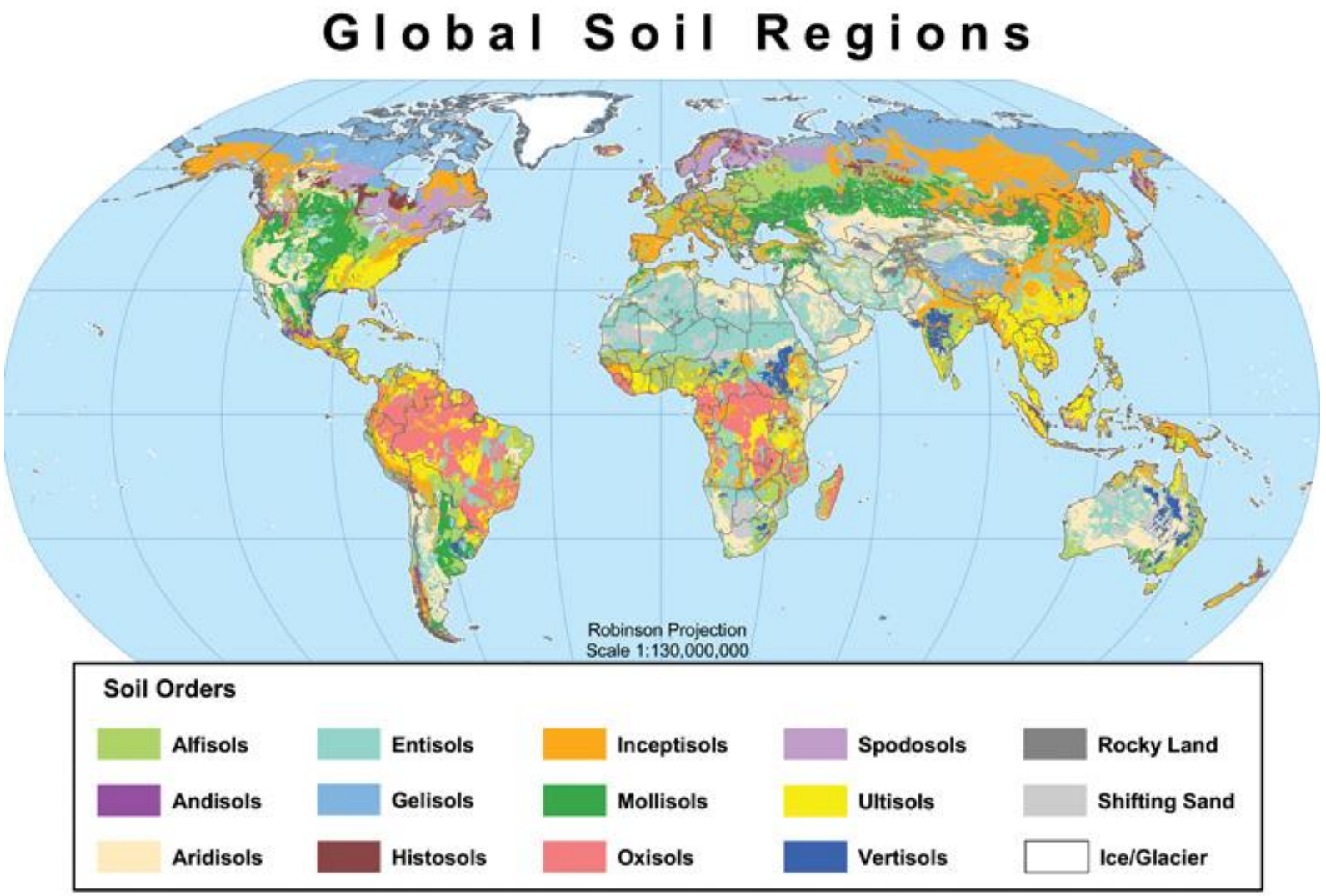

Figure 1.4: World Soil Map (United States Department of Agriculture, 2005)

1.1.3 Why calcined kaolinite clay for clinker replacement?

Kaolinite clays produce reactive minerals when calcined at a temperature of around 800°C (Fernandez, Martirena and Scrivener, 2011). The use of calcined kaolinite clay in concrete reduces the amount of energy used in the production of clinker, and CO_2 emissions. Energy saving occurs because the calcination temperature of clays is lower than that of clinker and they are also easier to grind. Further, a great quantity of CO_2 is emitted in the decomposition of LS during clinker production, whereas calcination of kaolinitic clays emits water vapor. Moreover, the high alumina content of calcined kaolinitic clays makes them particularly suitable for co-substitution with LS to replace clinker in concrete (Antoni et al., 2012). This means that with this combination, it is possible to have a more sustainable and durable concrete for future projects. In addition, the grade of kaolinite clay required for clinker replacement is much lower than pure kaolinite clays required in ceramic or paper industries, therefore would not compete with demand for resources by such industries. Also, some international standards have already started to allow the use of this system (ASTM C595/C595M, 2021; BS EN 197-5, 2021). Therefore, the aim of this work is to develop low-clinker concrete or LC^3 concrete (i.e., partially replacing PC with calcined kaolinite clay and LS) for structural applications such as construction of buildings and civil infrastructure, and for semi-structural applications such as blocks, paving and roof tiles.

1.1.4 LC^3 system and sustainability

In this research, with the new type of binder system (LC^3) in concrete, sustainability means obtaining concrete that has the required durability performance and a relatively low impact on energy consumption and carbon footprint. Figure 1.5 shows the estimated CO_2 emission per unit volume of LC^3-concrete compared to FA30 and PC-concrete, based on a study by Gettu et al. (2018) in India. In their study, two RC structures were considered, a bridge pier with a strength of 35 MPa and a bridge girder with a strength of 50 MPa. In both cases, materials were proportioned using different binder systems and different water/binder (w/b) ratios to attain the targeted strengths. For the case of the pier (35 MPa), two LC^3-concrete mixes, LC^3-1, and LC^3-2, were designed such that the strength of LC^3-1 is similar to PC and FA30 concretes, and the mixing proportion of LC^3-2 is similar to FA30 concrete.

In their calculations for emissions and energy consumption, all factors from extraction of raw materials to their end use were taken into account. From the results (Figure 1.5), in both cases, PC-concrete was shown to have the highest environmental impact and LC^3-concrete the lowest impact. The trend is largely related to the amount of clinker in the concrete mixes investigated. This also confirms that it is possible to have a more sustainable and durable LC^3-concrete for future projects.

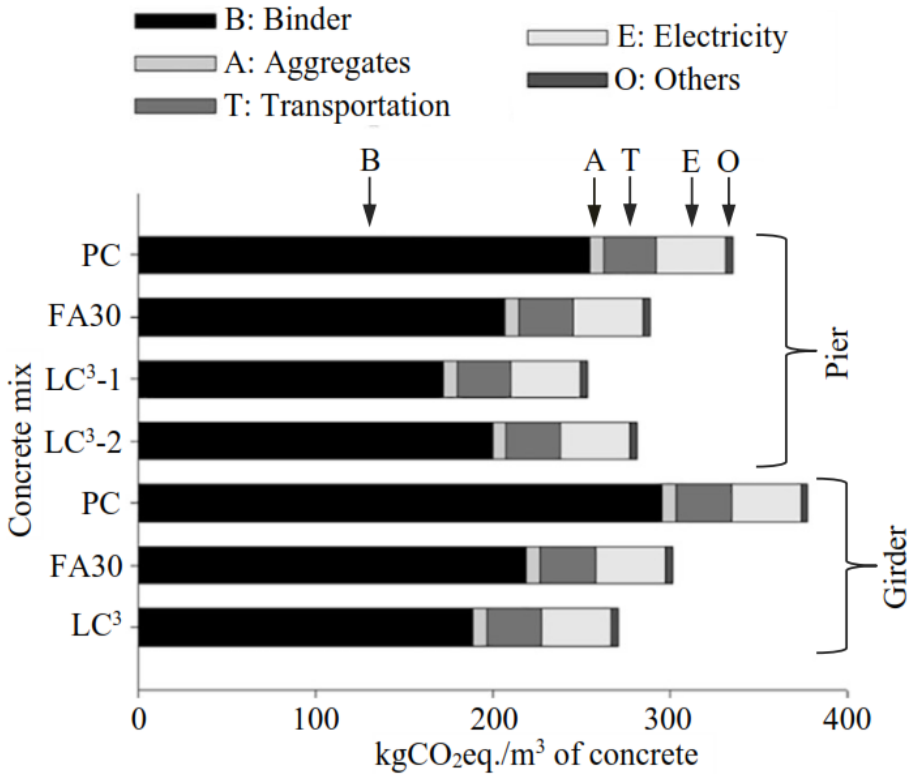

Figure 1.5: CO_2 emissions per unit volume of concrete, based on an Indian study (Gettu et al., 2018)

1.1.5 Prescriptive approach versus performance-based approach

Design and specification approaches for concrete durability are divided into prescriptive and performance-based approaches (Beushausen, 2014; Beushausen, Torrent and Alexander, 2019; Alexander, 2021). Concrete specifications as provided in standards such as EN 206-1 2000 are prescriptive in nature as they limit cement contents, w/b ratios, strength for different exposure classes, and also the amount and types of SCMs that can be added to the concrete mixes. The performance measure most often used is compressive strength, which does not necessarily directly relate to the durability of a structure (Aïtcin,

2000; Neville, 2001; Bentur and Mitchell, 2008). In contrast, the performance-based approach is based on quantitative measures and predictions of durability from prevailing exposure conditions and measured material parameters. In this approach, no (unnecessary) restrictions are put on the materials used in making the concrete provided that the required performance is met (Lobo, Lemay and Obla, 2005; Beushausen, Torrent and Alexander, 2019). This encourages the use of higher proportions of SCMs to replace clinker in the cement (Mehta, 2001); the use of admixtures to reduce water content with a corresponding reduction of cement content (Aïtcin, 2000); and a reduction of the cement content in a concrete mix while maintaining the performance of a mix (Wassermann, Katz and Bentur, 2009; Proske et al., 2013). In view of this, this research considers the performance-based approach in the reduction of clinker content in concrete with a specific emphasis on durability.

1.2 Objectives of the study

Apart from construction processes and workmanship, the overall performance of concrete for a specific environment depends on the type, quality, and proportion of constituent materials in achieving the intended fresh and hardened properties of concrete. Globally, the trend is to reduce the clinker factor to 0.6 or less without adversely affecting the performance of the system (Scrivener, John and Gartner, 2018; WBCSD and IEA, 2018). Studies related to the performance of mixes with PC partially replaced by calcined clay (CC) and LS have been conducted especially in Switzerland (e.g., at EPFL) and in India (e.g., at IIT Madras). However, because the properties of these materials differ all over the world, there is no consensus concerning the required characteristics of superplasticisers, particle sizes, and optimum proportions of these materials in connection with the quality of the raw materials for good workability, strength development and durability performance. In view of this, the suitability of each source of these materials needs to be examined and evaluated.

South Africa and Tanzania are among the top ten contributors to population increase in Africa. Some of these top ten contributing countries are situated along the Indian ocean. Due to the increase of economic activities and job opportunities, more infrastructure is

likely to be built in these regions in the future. If this projected infrastructure development is to have minimal negative environmental impact in terms of concrete usage in Africa, there is a need to develop low-clinker systems for future structural and non-structural applications using abundantly available raw materials. Therefore, the main objective of this study is to use a performance-based approach in the development of low-clinker concrete (i.e., partially replacing PC by CC combined with LS) while reasonably maintaining the required properties of workability, compressive strength, and durability for structural and non-structural applications. Hence, the aim is to create knowledge on the suitability of African clay resources for production of LC^3 cement and concrete, and aid industry in developing and manufacturing more sustainable cementitious binders and concrete mixes for the future.

To attain this main objective, the study aimed at:

i) Summarising existing knowledge on the materials and performance of LC^3 systems
ii) Characterising the selected materials for chemical and mineralogical composition
iii) Optimising system chemistry and mineralogy to achieve synergistic effects with all constituents, for the selected sources of clays from the two countries.
iv) Optimising proportions of concrete materials to further reduce the powder content in the concrete.
v) Assessing the performance of the selected low-clinker mixes, including but not exclusively, in comparison with the recommended concrete mixes for marine concrete structures in South Africa.

1.3 Key research questions

The key research questions in this study are:

i) What proportions of CC and LS (at a given amount of clinker) will produce the optimum properties of LC^3 concrete?
ii) What is the limiting percentage of clinker that can be replaced by CC/LS ratio while maintaining the required performance of the concrete?
iii) To what extent can the optimisation of a mixture of concrete materials contribute to reduce clinker content in the concrete, subject to adequate workability and concrete performance?

iv) Based on the performance of reference mixes, what are the required performance levels (i.e., workability, compressive strength, and durability) of the low-clinker mixes for marine concrete structures?

1.4 Scope and limitations of the study

This study aimed at evaluating the effects of reducing clinker content in concrete for structural and non-structural applications. The materials considered are cement, LS and kaolinite clay, ground separately and mixed to form the cementitious binder for use in concrete production. To minimize variables in the experimental work, certain limitations regarding the cement type, admixture type and water/binder ratio (w/b) were considered. Cement used was CEM II/A-L 52.5 N sourced from a local cement manufacturer, AfriSam (SA), LS was Kulubrite 5 with 97% calcium carbonate ($C\overline{C}$) purity from Idwala Carbonates (SA), and four samples of kaolinite clay from South Africa and Tanzania (two from each country). It important to note that there are numerous kaolinite clays deposits in Africa (Heckroodt, 1991; Ekosse, 2010). However, in this research the suitability of samples of clay from six potential sources, namely Hopefield, Grahamstown and Bronkhorstspruit deposits in South Africa, and Pugu kaolin deposit (hard and soft clay) and a deposit from the HeidelbergCement plant area in Tanzania was evaluated. Based on the kaolinite content, four sources were selected. The study incorporated the use of polycarboxylate ether superplasticizer to improve the packing density of the materials in the mix.

The performance properties of the concrete considered were limited to workability, setting time, shrinkage, potential for early age cracking, strength development, durability indexes, bulk diffusion, electrical resistivity, and carbonation resistance. Studies were also done using microstructural characterization techniques i.e., X-ray diffraction (XRD), thermogravimetric analysis (TGA), Bruner Emmett Teller (BET) surface area, and scanning electron microscopy (SEM) to get scientific understanding of the selected samples of clay as well as hydration products of the pastes at various ages. All samples were prepared, conditioned, and tested in the laboratory.

1.5 Research significance

This research will contribute to the ongoing development of economical and practical concrete construction solutions appropriate for Africa, in view of the environmental impact of concrete construction and the importance of constructing durable structures.

Africa has abundant reserves of kaolinite clays and LS. The high alumina content of calcined kaolinite clay makes them particularly suitable for co-substitution with LS. The importance of this research lies in mitigating climate change by developing low-clinker concretes (partially replacing clinker in concrete by the combined addition of calcined kaolinite clay and LS). Therefore, this research contributes to the ongoing strategies of minimizing CO_2 emissions associated with the immense development of infrastructure which is anticipated to occur in Africa in the coming decades, and therefore to the sustainability of the local cement industries and their continued contributions to society.

Regarding knowledge contribution, this study contributes to expanding the current limited knowledge, particularly in Eastern and Southern Africa, on concrete mixes prepared using the combined addition of calcined kaolinite clay, LS, and PC, aiming at reducing CO_2 emission with good performance in use. To meet this challenge, it was necessary to identify potential kaolinite clay deposits in these regions, test for their performance and build up knowledge which can be obtained from microstructural studies and the factors controlling the reaction of the materials, the products formed and how they fill space in the cement matrix.

1.6 Layout of thesis document

This work consists of six chapters, organized as follow:

Chapter 1 gives the background and a brief overview of the research area. The objectives, key questions of the project, scope and the significance of the study are also presented.

Chapter 2 provides a review of literature on the proposed strategies for CO_2 reduction in the cement industry, required performance of concrete in marine environments, the use of SCMs in concrete, clay minerals and their pozzolanic activity, suitability of kaolinite clays

for clinker replacement, and previous studies done on the performance of LC^3 systems. The interaction effects of concrete materials and methods of particle packing are also reviewed.

Chapter 3 present a detailed description of the research methodology, types and characteristics of materials used in this study.

Chapter 4 provides details about the chemical and mineralogical properties of the selected clays (before and after calcination) and their suitability for clinker replacement in concrete.

Chapter 5 begins with an overview of the approach used in reducing the clinker factor. It goes on to present results and discussion about the optimal proportions (i.e., chemistry) of cementitious materials for best performance using compressive strength results of LC^3 mortars, also results and discussion about the hydration products of the selected LC^3 pastes aiming to gain a better understanding on the influence of hydrates on the strength and durability performance of concrete, then further reduction of clinker/powder in concrete by optimising proportions of concrete materials.

Chapter 6 present results and discussion from testing for fresh and hardened properties of the selected LC^3 concrete mixes versus references mixes. Tests that were carried out included workability, free shrinkage, restrained shrinkage cracking (ring), compressive strength of the concrete at 1, 3, 7, 28 and 90 days, durability indexes, electrical resistivity, bulk diffusion, and accelerated carbonation test.

Chapter 7 gives the general discussions, conclusions and recommendations based on the findings and discussions presented in the previous chapters.

Chapter 2 Literature review

2.1 Introduction

Concrete is one of the most consumed materials on Earth. An essential component of concrete is cement. Figure 2.1 shows cement use in Brazil (similar to South Africa), about 60% of cement that is produced is used to make concrete and other cementitious products such as blocks, pavers, and roof tiles.

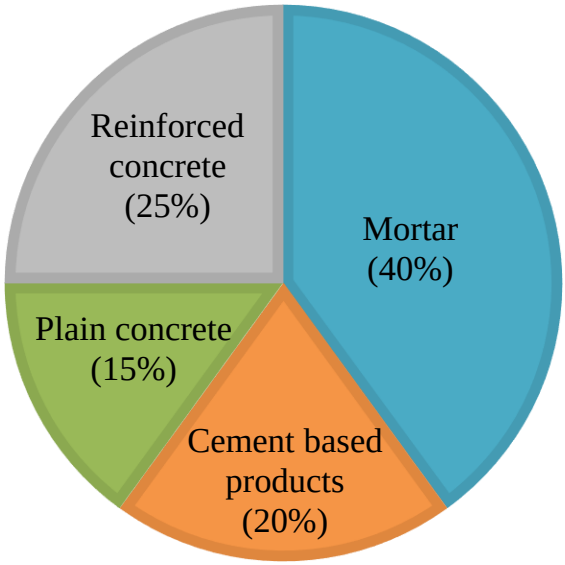

Figure 2.1: Cement use in Brazil, similar to South Africa
(Scrivener, John and Gartner, 2018)

Currently, cement manufacturing contributes about 8% of global CO_2 emissions (Müller and Harnisch, 2008; Olivier, Schure and Peters, 2017; Andrew, 2018) and CO_2 is one of the gases that leads to global warming. Due to the anticipated high demand in Africa for concrete and other cementitious products in the coming decades, this will contribute more to global CO_2 emissions under 'business-as-usual' practices. Therefore, Africa has a role in ensuring a significant reduction in global CO_2 emissions through the use of low-clinker systems in structural and non-structural applications. This chapter provides a review of literature on the strategies for CO_2 reduction from the cement industry, the required performance of concrete in marine environments, the use of SCMs in concrete, and methods for packing of concrete materials to achieve maximum packing density. Focus is

given to previous studies done on LC^3 systems and why this system is of interest for the reduction of the CO_2 emissions in Africa, at the same time achieving a durable concrete.

2.2 Strategies for reduction of carbon dioxide emissions from the cement industry

In 2009, the Cement Technology Roadmap of the International Energy Agency for carbon emissions reduction up to 2050 (WBCSD and IEA, 2009) proposed mitigation strategies for CO_2 emission from cement industries, grouped under the headings of Fuels; Energy efficiency; Clinker substitutes; and Carbon Capture and Storage (CCS). i) The use of alternative fuels is likely to be a major sustainable approach to reducing CO_2, as there are still many opportunities to expand the use of fuels produced from renewable resources worldwide; ii) Major efforts to increase the energy efficiency involve improvement of the production process to make it less energy intensive. In general, this strategy has been in place for the past few decades, and thus new cement plants are coming up with new technologies and old ones are being upgraded. However, this strategy has been noted to require a significant capital investment but in the long run may result in low-cost cement since it reduces energy costs; iii) The use of clinker substitutes has the advantages of reducing energy consumption and CO_2 emission per ton of cement as well as increasing production of cement without requiring new kilns; iv) the use of CCS has been observed to have a great possibility of reducing a large percentage of CO_2 emission, but it will have a major impact on the cost of cement production as it can increase power consumption up to more than 100%. Among these four strategies, civil engineers can contribute to the reduction of CO_2 emission through the use of clinker substitutes or SCMs.

The most common SCMs are reactive by-products from other industries which includes GGBS, a by-product of iron production in blast furnaces; silica fume (SF), a by-product of producing silicon metal or ferrosilicon alloys in electric arc furnaces; and FA, generated by burning coal to produce electricity. Kaolinite clays also make extremely good SCMs when calcined (Castillo et al., 2010; Scrivener, 2014; Almenares et al., 2017). LS can be regarded as a ‘semi-SCM’ as it can react with the available alumina in the mix (Matschei, Lothenbach and Glasser, 2007; Lothenbach et al., 2008; Scrivener, John and Gartner, 2016). These SCMs can be used in binary, ternary, or quaternary mixes. A good review of different binders involving LS additions is given by Dhandapani et al. (2021).

Other approaches aimed at reducing CO_2 emission include the use of cements made from alternative cement clinkers and the use of alkali-activated cements or geopolymers (Gartner and Sui, 2016; Scrivener, John and Gartner, 2018). The most feasible alternative class of hydraulic clinkers are belite-ye'elimite-ferrite (BYF) clinkers and Carbonatable Calcium Silicate (CCSC) clinkers which can reduce substantial percentage of CO_2 emission. However, these approaches have higher raw materials costs than using SCMs and are limited to factory-made products. In this view, these approaches are unlikely to have a major global CO_2 impact as the facility to cast cementitious materials on-site is fundamental to their use in construction. The use of alkali-activated cements may also reduce global CO_2 emission. However, many current alikali-activated materials technologies require the use of limited globally available GGBS to give acceptable performance. In general, it is difficult to adapt use of these alternative binders in the near future until they are made more practical for use in construction (Scrivener, John and Gartner, 2018).

In 2016, the UNEP report on eco-efficient cements identified two key areas with the greatest potential for reducing CO_2 emission over the next few decades (Scrivener, John and Gartner, 2018). One area is replacing clinker in cement by the combined addition of CC and LS. The potential of this ternary system, which is also called Limestone Calcined Clay Cement (LC^3), has been shown to give good mechanical and durability performance with only 50% clinker (Antoni et al., 2012; Alujas et al., 2015; Dhandapani et al., 2018) and can help to reduce CO_2 emissions by almost 30% compared to a reference PC (Berriel et al., 2016; Pillai et al., 2019). Moreover, industrial trials have already been carried out with success in Cuba and India (Bishnoi et al., 2014; Vizcaíno-Andrés et al., 2015; Emmanuel et al., 2016). A good review of research work done on LC^3 systems for the past 6 to 10 years is given by Dhandapani et al. (2020) and Sharma et al. (2021). The second area is making more efficient use of PC clinker in concretes and mortars. This involves optimisation of packing of concrete materials coupled with the use of dispersants and fillers to reduce clinker content while maintaining the required performance of concrete, use of high strength concrete to reduce overall consumption of materials, and also industrialising

production of concrete and mortars to avoid wastage of materials from poorly controlled in-situ mixing.

The focus of this research is on the development of LC^3 concrete for marine concrete structures by considering two approaches i) replacing clinker by the optimal proportion of calcined kaolinite clay and LS ii) and further reduce clinker/powder in the system by optimising proportion of concrete materials. The performance of SCMs in concrete is discussed in the next section.

2.3 The performance of SCMs in concrete

The main processes that take place in the hydration of PC are well described by Taylor (1997). The understanding of the reaction kinetics in blended systems is complicated by the fact that the hydration of the PC and SCM occur simultaneously and may also influence the reactivity of each other (Lothenbach, Scrivener and Hooton, 2011; Roussel, 2012). Therefore, it is difficult to measure the degree of reaction of these two materials independently (Roussel, 2012). In addition, hydration of PC does not behave exactly as the simple superposition of the hydration of each phase of cement considered independently (Roussel, 2012). However, the kinetics of the SCM reaction depends on the chemical composition, the fineness, the amount of reactive phases of the SCM as well as the composition of the interacting solution (Lothenbach, Scrivener and Hooton, 2011).

SCMs are generally characterized by lower calcium content and higher alumina and silica than PC (Lothenbach, Scrivener and Hooton, 2011). The reactivity of SCMs is generally negligible in the first day or so, because the reactivity depends highly on the alkalinity of the solution which builds up over the first few days of the mix. However, the presence of SCM in the mix can enhance the reaction of the clinker phases by what is called ‘the fine filler effect’ (Lothenbach, Scrivener and Hooton, 2011; Roussel, 2012). The term “filler effect” describes the effect of adding a material which initially does not react, but the extra surface provided by the material acts as nucleation sites for the hydration products of the clinker phases and as the filler does not produce hydrates at the same water to solids ratio, the water to clinker ratio becomes higher and therefore more space is available for the hydration products of the clinker phases to form in the mixture.

In addition to the pozzolanic reaction and the filler effect, other secondary hydration reactions which enhance the mechanical and durability performance even at a low clinker factor exist in blended systems. Chemical reactions of SCM occur when it reacts with CH which is formed after the hydration of the calcium silicate compounds (C_3S and C_2S) in PC, Equations 2.1 and 2.2 (Thomas, 2013). Hydration of PC provides both the alkalinity (CH) and the Calcium Silicate Hydrate (C-S-H) in the mix. The reaction of CH with the silica (S) component of a pozzolan can be represented by Equation 2.3 (Helmuth, 1987 cited in Thomas 2013). In the blended system, less clinker is present which results in lower amount of CH and formation of C-S-H of lower C/S ratio compared to C-S-H formed in PC without pozzolan. The ratio varies depending on the age, type, and amount of pozzolan (Thomas, 2013). A C-S-H of a lower Ca/Si ratio has higher capacity to incorporate alumina (Richardson and Groves, 1993).

$$2C_3S + 11H \rightarrow C_3S_2H_8 + 3CH \quad (2.1)$$

$$2C_2S + 9H \rightarrow C_3S_2H_8 + CH \quad (2.2)$$

$$xCH + yS + zH \rightarrow C_xS_yH_z \quad (2.3)$$

The alumina present in pozzolans will also react with the CH from PC and may produce a variety of phases, the principal ones being strätlingite (C_2ASH_8) and hydrogarnet (C_3AH_6), others being calcium aluminate hydrate (C_4AH_{13}), ettringite ($C_6A\bar{S}_3H_{32}$), calcium monosulfoaluminate ($C_4A\bar{S}H_{12}$) and calcium monocarboaluminate ($C_4A\bar{C}H_{11}$). Whether the dominant type of the aluminate ferrite monosulphate (AFm) phase is monosulphate, hemicarbonate or monocarbonate will depend on the availability of sulphate, carbonate, alumina or calcium in the solution (Matschei, Lothenbach and Glasser, 2007; Thomas, 2013; Zajac et al., 2014). The incorporation of alumina in C-S-H, often referred as C-A-S-H, increases with increasing alumina concentration in the solution (Pardal, Pochard and Nonat, 2009; L'Hôpital et al., 2015; Avet and Scrivener, 2018) and with decreasing Ca/Si ratio of the C-S-H (Richardson and Groves, 1993). For example when metakaolin (AS_2) reacts with CH, it produces mainly C-S-H and strätlingite as shown in Equation 2.4 (Helmuth, 1987 cited in Thomas 2013). Figure 2.2 shows schematically the chemical

composition of SCMs and the hydrate phases formed in the $CaO\text{-}SiO_2\text{-}Al_2O_3$ ternary system.

$$AS_2 + 3CH + zH \rightarrow CSH_{z\text{-}5} + C_2ASH_8 \quad (2.4)$$

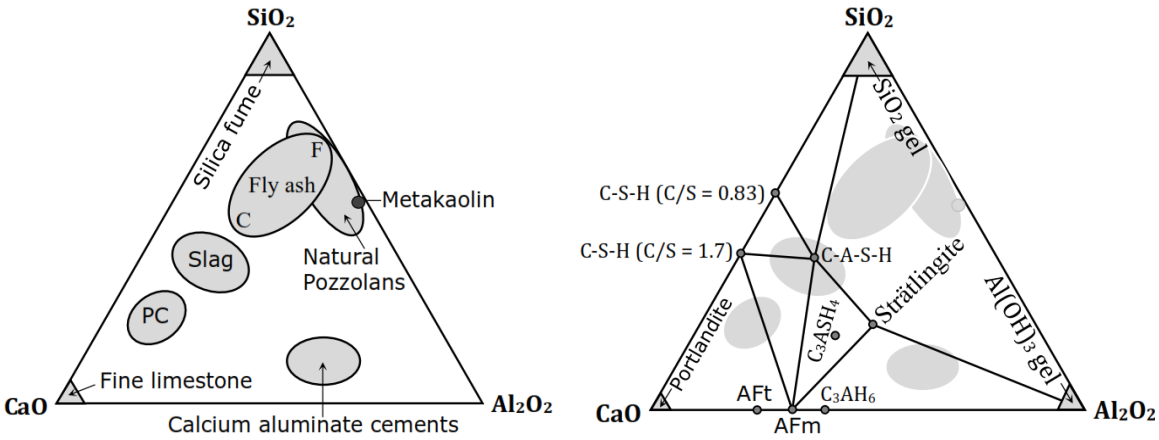

Figure 2.2: Chemical composition of SCMs and hydrate phases (Scrivener and Nonat, 2011)

The considerable variation in the properties of different SCMs means that they have different reactivity, and thererefore different requirements for their use in concrete (Thomas, 2013). The physical properties of the SCMs that influence the concrete properties are fineness, particle size distribution (PSD) and particle shape (Arvaniti et al., 2015; Alderete et al., 2016; Briki et al., 2021). Both SF and FA tend to have spherical particles. Slag, metakaolin (MK), and LS require grinding to make them suitable for use in concrete and this produces irregular particles, and their fineness depends on the extent of grinding.

In general, the pozzolanic activity of a SCM depends on the total amount of CH in the mix and the rate at which the reaction with CH occurs. The total amount of CH with which a pozzolan can combine depends on (Massazza 1998 cited in Thomas 2013): i) Nature of the reactive phases in the pozzolan; ii) Content of these phases; iii) SiO_2 content; iv) CH/pozzolan ratio of the mix; and iv) Duration of curing. On the other hand, the rate of the reaction of a pozzolan with CH depends on (Thomas, 2013): i) the fineness of the pozzolan; ii) Water/solid ratio of the mix; iii) Temperature; and iv) Composition of the PC, in particular its alkali content. The following section reviews the effect of SCMs on cracking of early age concrete

2.4 Effect of SCMs on cracking of early-age concrete

Although SCMs offer several advantages as explained in the previous sections, they may also cause adverse effects on concrete properties, especially during the first few days after casting (Pillai, Gettu and Santhanam, 2020). In general, cracking of early-age concrete largely depends on the degree of restraint, extent of shrinkage, creep, elastic modulus, and tensile strength of early-age concrete as discussed by Safiuddin et al. (2018). Substitution of cement by SCMs slows down the gain of tensile strength of concrete at an early age (Megat Johari et al., 2011; Ji, Kanstad and Bjøntegaard, 2018). The lower early age strength provides less resistance to restrained shrinkage-induced stresses which might result in early cracking of concrete (Akkaya, Ouyang and Shah, 2007; Sirajuddin and Gettu, 2018) which then affects durability performance by permitting ingress of harmful agents such as chloride ions or carbon dioxide (Song et al., 2006; Park, Kwon and Jung, 2012). This problem can be minimised by understanding the influence of the SCMs on the strength gain, shrinkage of concrete, creep, and associated relaxation (Khan et al., 2020).

In this research, in addition to the free shrinkage test, the early age surface cracking of LC^3 concrete (in comparison with the reference mixes) is also investigated using the restrained ring test (ASTM C1581-18a). The principle of this test involves casting a concrete ring around the restrained core and the concrete ring is allowed to shrink against it. Tensile stresses will develop in the concrete ring leading to cracking if the stresses are sufficiently greater than the tensile strength of the concrete. The performance is evaluated based on appearance and quantification of cracks in terms of time of occurrence, number, and average width of cracks. So far, no one has reported the performance of LC^3 mix using this test, however, the test has been used with success to evaluate the possibility of early-age cracking of different concrete due to restrained shrinkage (Akkaya, Ouyang and Shah, 2007; Dittmer and Beushausen, 2014; Nguyen et al., 2019; Khan et al., 2020). The required performance of concrete in a marine environment is discussed in the next section.

2.5 Concrete for marine environments

The primary concern in the design and specification for concrete structures in marine environments is durability, strength being a secondary concern (Alexander, 2016).

Chloride-induced corrosion of reinforcing steel bars is the main durability concern of RC structures. This is a result of the penetration of chloride ions from the environment through the porous structure of the concrete cover (or chloride ions may be added during concrete mixing) which eventually causes cracking, delamination and spalling of the concrete. Figure 2.3 shows a schematic representation of the corrosion process in RC. Carbonation can also induce corrosion, as it decreases the pH of the pore solution in concrete and destroy the stability of a passive oxide layer which is only stable at high pH condition. In contrast, chloride ions when reaches a critical level of concentration leads to depassivation of reinforcing bars even when the pH is high. In view of this, durability design largely covers prevention of reinforcement corrosion for the intended service life of the structure.

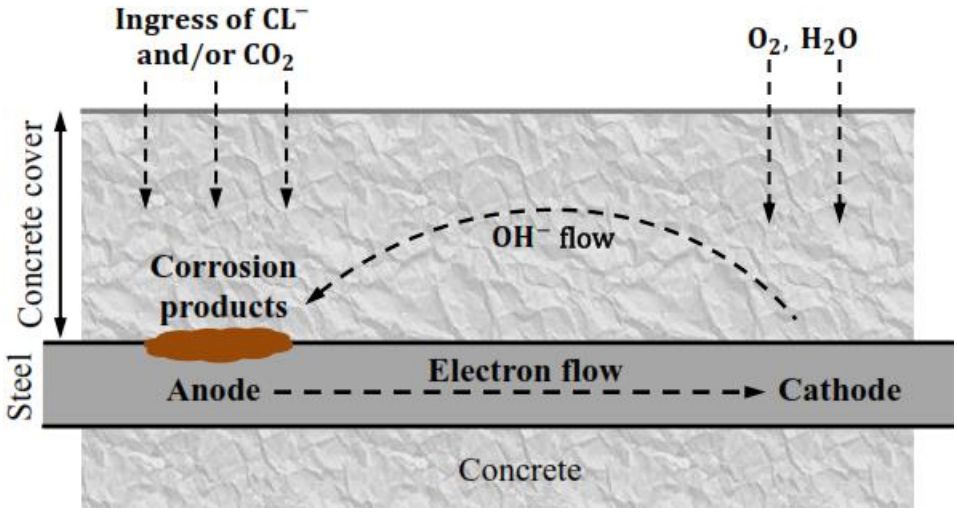

Figure 2.3: Schematic representation of corrosion process in RC (Mackechnie, 2001)

2.5.1 Marine exposure environments

Design standards generally provide requirements for marine concrete structures in relation to exposure conditions. Recommended cement types, minimum 28-day strength, minimum binder content, maximum w/b ratio and minimum concrete cover are given for each environment. CEM I (or PC) has poor chloride resisting properties, and therefore is not appropriate for concrete structures in marine environments unless blended with suitable proportions of SCM (Alexander, 2016). BS EN 450-1:2012 and BS EN 15167-1:2006 prescribe the quality of FA and GGBS for blending with CEM I at the batching plant, respectively. In the case of reinforcement corrosion, tidal and splash zones are considered

as the most aggressive zone in marine environments as the concrete is subjected to wetting and drying cycles (i.e. chloride deposition and crystallization) of seawater (Broomfield, 2007; Alexander, 2016). The severity of this zone also depends on the climatic condition, for instance warm climates favour more rapid chloride penetration and reinforcement corrosion as the rate of both increases with temperature. Table 2.1 shows exposure classes for risk of corrosion induced by chloride ions from sea water (EN 206, 2013). However, as pointed out by (Beushausen et al., 2021), the airborne chloride exposure zone may be as aggressive as the splash and spray zone depending on the prevailing environmental and topographical conditions. Conversely, the tidal zone may be less aggressive compared to the splash and spray zone, especially in terms of reinforcement corrosion (not chloride ingress), depending on the permeability and cover depth of concrete.

Table 2.1: Exposure classes for chloride-induced corrosion (EN 206, 2013)

Class designation	**Description of the environment**	**Informative example where exposure may occur**
XS1	Exposed to airborne salt but not in direct contact with sea water	Structures near to or on the coast
XS2	Permanently submerged	Parts of marine structures
XS3	Tidal, splash and spray zones	Parts of marine structures

2.5.2 Prevention of steel reinforcement corrosion

Penetrability and cover depth of concrete are considered the most important RC parameters that have influence on the time to reinforcement corrosion initiation and its propagation. Concrete penetrability is influenced by binder type, w/b ratio, compaction, and curing. Use of low w/b ratio together with SCM can minimise chloride penetrability and heat of hydration in concrete (Alexander, 2016).

Studies done at IIT Madras (India) have shown that a ternary LC^3 system can give mechanical properties, depending on age, similar to or better than the reference PC system (Figure 2.4) and at the same time provides better resistance to chloride ingress than a system with only PC or a binary system with 30% fly ash (FA30). All mixes had the same binder content (360 kg/m^3) and w/b ratio (0.45). The resistance to chloride penetration was evaluated using the Rapid Chloride Penetration Test (Figure 2.5) and Accelerated Chloride

Migration Test (Figure 2.6). The increased penetration resistance is mainly due to a refinement in the pore structure as well as chloride-binding capacity of the LC^3 system (Dhandapani and Santhanam, 2017; Avet and Scrivener, 2018; Dhandapani et al., 2018; Sui et al., 2019).

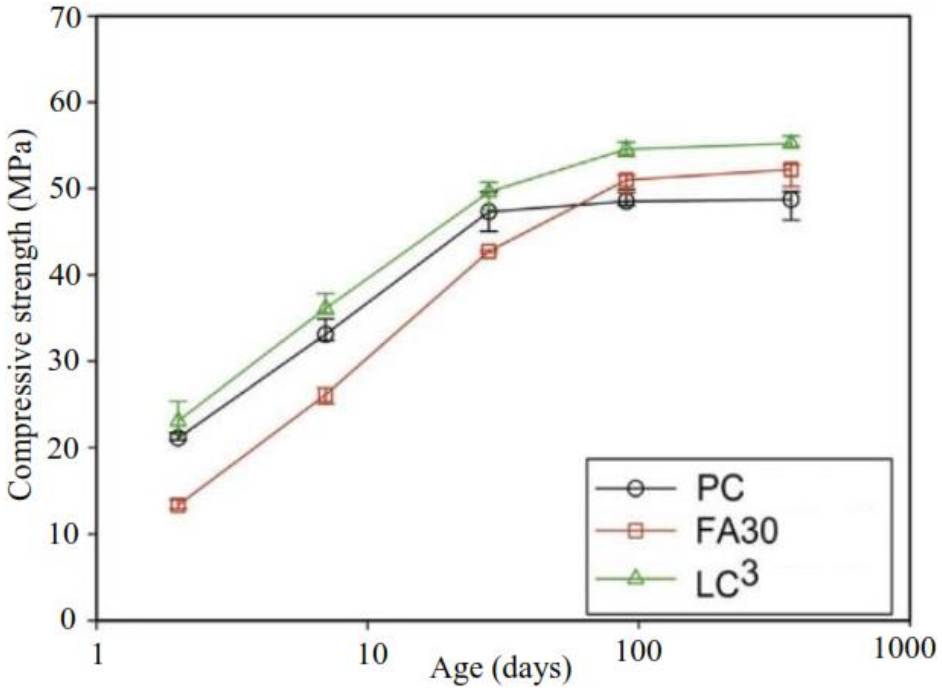

Figure 2.4: Compressive strength development: LC^3 versus PC and FA concrete (Dhandapani et al., 2018)

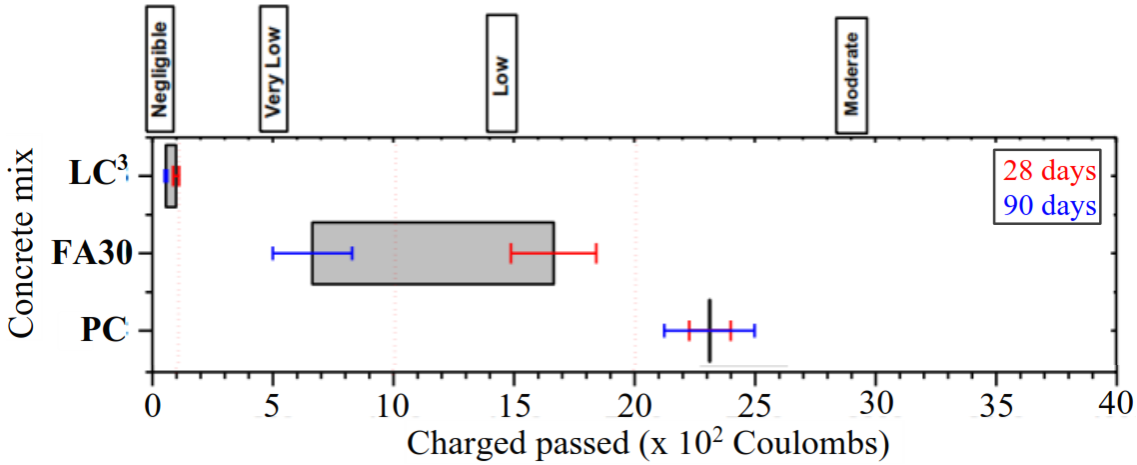

Figure 2.5: Total charge passed in the concrete (Dhandapani et al., 2018)

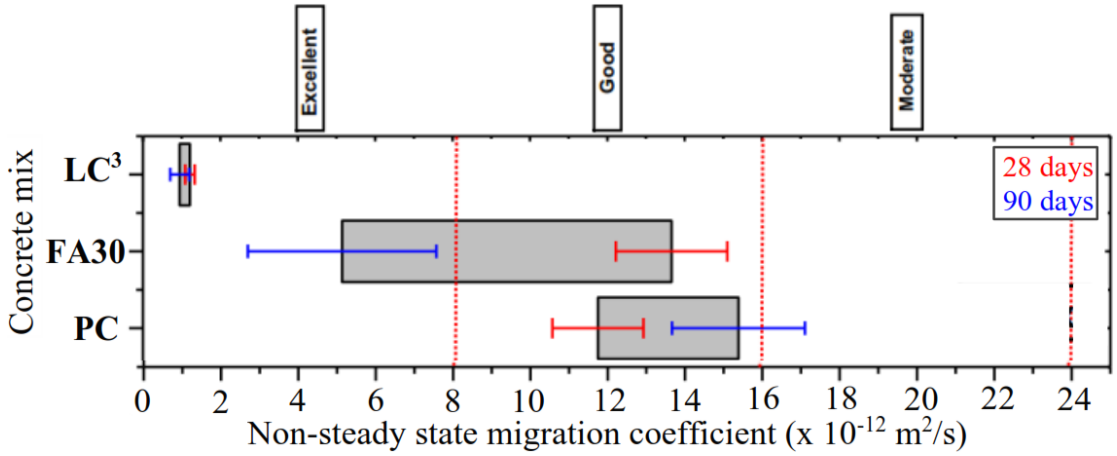

Figure 2.6: Chloride migration coefficient in the concrete (Dhandapani et al., 2018)

Replacement of cement in concrete with SCMs alters the physical and chemical properties of a concrete mix, which influence the hydration reactions, rate at which they occur and the products formed (Lothenbach, Scrivener and Hooton, 2011). The changes in chemical properties occur due to pozzolanic reaction with portlandite or calcium hydroxide (CH), which is formed from the hydration of the calcium silicate compounds in PC. The following section review different methods to assess reactivity of SCMs.

2.6 Assessment of SCM reactivity

The reactivity of SCM can be obtained by either of the following approaches (Snellings and Scrivener, 2016): i) Correlating SCM composition and reactivity; ii) Comparison of compressive strength of mortars containing SCM with a reference mix that has no SCM; iii) measuring CH related to the pozzolanic reaction of the SCM; and iv) monitoring the reaction of the SCM.

The first approach involves correlating the reactivity of SCM to its chemical compositions obtained by X-Ray Fluorescence (XRF). ASTM C618 standard prescribes that for SCM to be reactive ($SiO_2 + Al_2O_3 + Fe_2O_3$) $\geq$ 70%. Considering this summation as an indicator for calcined kaolinite clays may not be appropriate as these clays contain secondary minerals such as quartz and carbonate which may have additional effects on the reactivity of the clay. Moreover, the reactivity also depends on the fineness of the SCM (Obla et al., 2003; Gudissa and Dinku, 2010; Thomas, 2013).

The compressive strength approach involves running compressive strength tests on mortars composed of lime and SCM. This approach is specified in Indian standard IS 1727 - 1967 and Brazilian standard NBR 5751. However, this approach is not consistent when using different SCMs (Avet, 2017). Moreover, the system is likely to run out of lime for highly reactive SCMs such as calcined kaolinite clays.

Test methods that use CH consumption approach are: i) the Chapelle test; ii) a modified version of Chapelle test (NF P18-513); and iii) the Frattini pozzolanicity test (EN 196-5). However, these standard reactivity testing methods have been noted to have shortcomings, particularly in terms of reproducibility, duration of test and correlation to strength development of cements (Snellings and Scrivener, 2016). However, some researchers claims that the Frattini test can give an accurate estimation of CH consumption (Mohammed, 2017). Other techniques that can be used to quantify CH consumption in a system include TGA (Payá et al., 2003; Tironi et al., 2013) and XRD (Antoni et al., 2012; Ramezanianpour and Bahrami Jovein, 2012). The main disadvantage of using TGA is that a sample must be dried using solvent exchange for some days whereas for XRD, it is not essential. However, for XRD, reliable results depend on sample preparation and operator skills (Avet, 2017).

Methods that can be used to monitor continuously the reactivity of SCMs include the use of isothermal calorimetry to measure heat release during hydration, and the chemical shrinkage method. In both methods, the reactivity of SCM is evaluated by comparing a system with PC partially replaced by SCM and a reference mix with 100% PC.

Recently, the so called ‘‘R^3 method” has been developed, initially for assessing pozzolanic reactivity of CC and synergistic reaction between CC and LS (Avet et al., 2016). R^3 stands for Rapid (i.e., shorter time), Reliable (i.e., giving reproducible results) and Relevant (i.e., giving results correlating to strength in standard mortars). The test involves preparing R^3 paste which contain SCM, CH powder and water. Small amounts of sulphate and alkali are also added to the mixture to simulate the conditions occurring in blended cement. The aim of using CH, sulphate, and alkali instead of cement is to avoid interference of clinker hydration reactions in the system. The test is accelerated by continuously heating the R^3 paste at 40°C either in isothermal calorimetry (for measuring cumulative heat release at 7

days) or in the oven (for determination of bound water at 7 days). This test, in comparison with other tests, has been observed to have a very good correlation to a reference 28-day relative strength of standard mortar (Li et al., 2018; Parashar and Bishnoi, 2020). In view of this, this test was used to evaluate the reactivity of the selected clays. The aim was to find the optimum calcination temperature of the clays.

2.7 Clay minerals and their pozzolanic activity

Clay minerals are divided into two groups of minerals, 1-1 or 2-1-group of minerals, based on the number of tetrahedral and octahedral sheets in the layer structure. The tetrahedral sheet is made up of SiO_4 tetrahedra with three of the four O^{2-} ions of each tetrahedron shared with the adjacent tetrahedra while the octahedral sheet consists of Al_2O_3 octahedra arranged such that each OH^- is shared between two adjacent octahedra. Figure 2.7 shows separately a polyhedral model of tetrahedron and octahedron.

Figure 2.7: A polyhedral model of (a) tetrahedron and (b) octahedron (Schulze, 2005)

The most common clay minerals include kaolinite, montmorillonite and illite, Figure 2.8. They are usually found mixed with each other and contain other minerals such as quartz, feldspars, carbonates, and micas. The main difference between kaolinite and other clay minerals is the Si/Al ratio; its layer is formed of two sheets: one octahedral aluminate sheet and one tetrahedral silicate sheet, and therefore belongs to 1:1 group of minerals, while montmorillonite and illite belong to 2:1 group of minerals. Kaolinite clay is characterized as a non-swelling clay because its adjacent layers are linked by hydrogen bonding which prevents penetration of water into the interlayer space (Schreiner and Wypych, 2002).

Uncalcined kaolinite clay has two forms of water, physically bound and chemically bound water. Both can be estimated from the TGA and DTG curve, from which the removal of physical bound water (dehydration) corresponds to a mass loss on the TGA curve (or an endothermic peak on the DTG curve) when heating the clay from above 20°C to 200°C

while for the case of chemically bound water (dehydroxylation) the same happens between 400°C and 600°C.

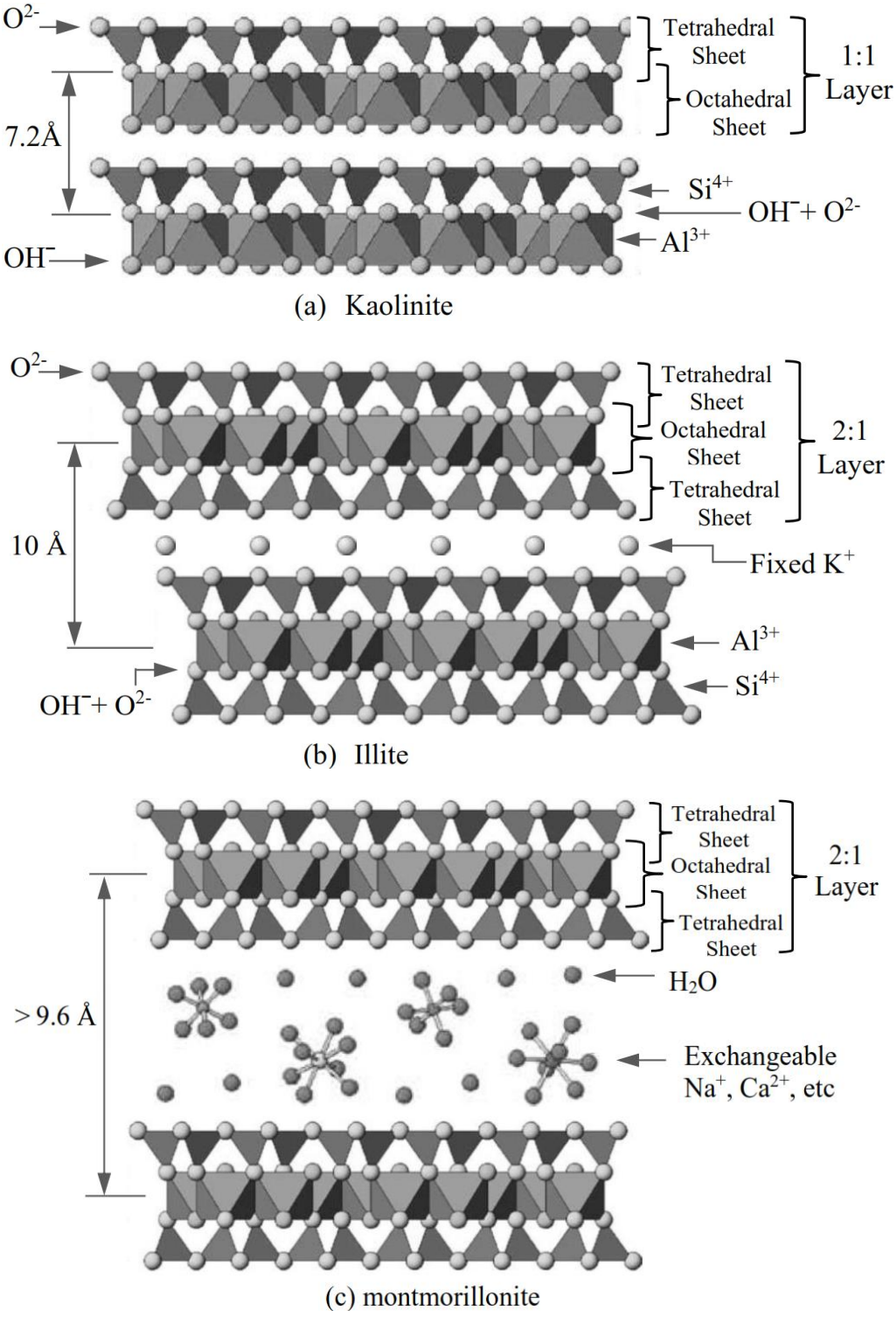

Figure 2.8: Structure of common clay minerals (Schulze, 2005)

For the kaolinite to break down and produce an amorphous material for pozzolanic reactivity, calcination between 600 and 850°C is necessary (Fernandez, Martirena and Scrivener, 2011). Studies using ^{27}Al-Nuclear Magnetic Resonance (^{27}Al-NMR) on the dehydroxylation of kaolinite, montmorillonite and illite at 600 and 800°C (Lambert, Millman and Fripiat, 1989; Fernandez, Martirena and Scrivener, 2011) revealed that, for illite and montmorillonite, thermal treatment causes a change of the coordination number of Al from $Al^{(VI)}$ to $Al^{(IV)}$, while for kaolinite clay, the change is from $Al^{(VI)}$ to $Al^{(IV)}$ and $Al^{(V)}$ as shown in Figure 2.9. The extra pozzolanic activity of calcined kaolinite clay compared to other clays is related to the appearance of $Al^{(V)}$ after calcination (Ambroise, Murat and Péra, 1985; Fernandez, Martirena and Scrivener, 2011). As can be seen in Figure 2.9, the intensity of $Al^{(V)}$ increases as temperature increases from 600°C to 800°C. Too high temperature (> 850°C) reduces reactivity due to increase of particle sizes due to agglomeration and sintering and then re-crystallization (Fabbri, Gualtieri and Leonardi, 2013). Table 2.2 shows the effect of calcining on the structure change of kaolinite clay (He, Osbaeck and Makovicky, 1995; Heller-Kallai, 2006; Fernandez, Martirena and Scrivener, 2011; Bernal et al., 2017).

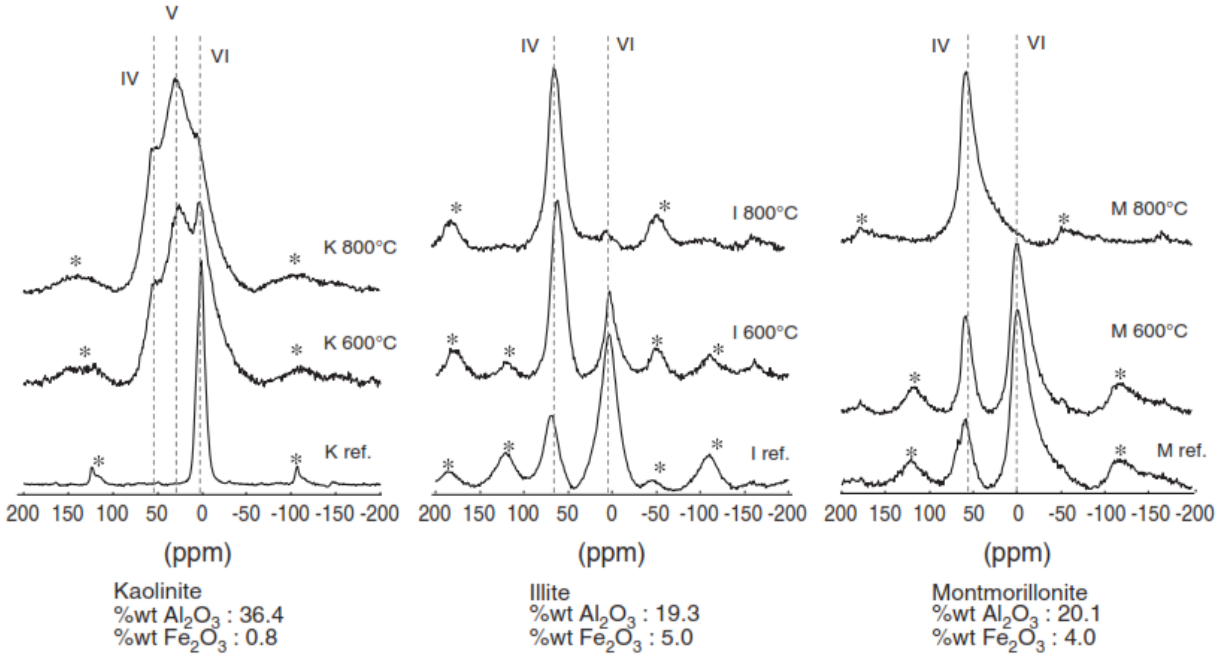

Figure 2.9: ^{27}Al NMR spectra of raw clays and clays calcined at 600°C and 800°C (Fernandez, Martirena and Scrivener, 2011)

Table 2.2: Effect of calcining kaolinite clay

Stages	Temperature (°C)	Effect of calcination
Stage 1	< 200	Loss of surface and adsorbed water (Dehydration)
Stage 2	400 – 600	Removal of OH^- group (Dehydroxylation)
Stage 3	600 - 800	Rupture of bonds and collapse of layer structure resulting in the formation of amorphous product (enhances reactivity)
Stage 4	800 - 950	loss of surface area and agglomeration of particles (Reactivity decreases)
Stage 5	> 950	Re-crystallization, formation of mullite (Reactivity decreases)

2.7.1 Suitability of kaolinite clay for clinker replacement

It has been indicated that a suitable clay for clinker replacement is one with a kaolinite content of at least 40% and that secondary minerals have less influence on the reactivity of the clay (Alujas et al., 2015; Avet et al., 2016; Avet, 2017; Maraghechi et al., 2018). This means that kaolinite content is an important indicator for clay suitability. Chemical composition of clay, usually obtained by X-Ray Fluorescence (XRF), can give an indication if a clay is of kaolinite type. For kaolinite clay, a Si/Al ratio is approximately equal to 1 while other clays have more silica and less alumina in the ratio of approximate 2:1. Based on the XRF results, it has been suggested that a suitable clay for the LC^3 binder is the one with Al > 18%, Si/Al > 0.3 and LOI > 7% (A. A. Díaz et al., 2018). However, presence of other minerals in the clay may affect the results of chemical analyses. Therefore, to get conclusive results, TGA coupled with XRD must be conducted to determine the kaolinite content in the clay (Shvarzman et al., 2003; Alujas et al., 2015). With TGA, Equation 2.5 can be used to determine kaolinite content ($m\%_{kaol}$) in the raw clay (Avet, 2017),

$$m\%_{kaol} = m\%_{(kaol-OH)} \times \frac{M_{kaol}}{2M_{water}} \quad (2.5)$$

where $m\%_{(kaol-OH)}$, M_{kaol} and M_{water} stand for mass loss over kaolinite-dehydroxylation interval (400 – 600°C), the molecular mass of kaolinite (258.26 g/mol) and molecular mass of water (18.015 g/mol), respectively. $m\%_{(kaol-OH)}$ can also be estimated using Equation 2.6,

$$m\%_{(kaol-OH)} = \frac{m_{400°C} - m_{600°C}}{m_{200°C} - m} \times 100 \quad (2.6)$$

where m stand for the mass of crucible, $m_{200°C}$, $m_{400°C}$, and $m_{600°C}$ stand for the combined mass of clay and crucible calcined at 200°C, 400°C and 600°C for one hour. All these parameters can simply be obtained using only an oven and a balance.

Minor errors in the results may be due to presence of secondary minerals such as illite and montmorillonite which partly dehydroxylate in the same temperature range (Fernandez, Martirena and Scrivener, 2011). As shown in Figure 2.10, Illite also dehydroxylates between 450°C and 700°C and montmorillonite between 550°C and 750°C (Fernandez and Scrivener, 2009; Avet, 2017).

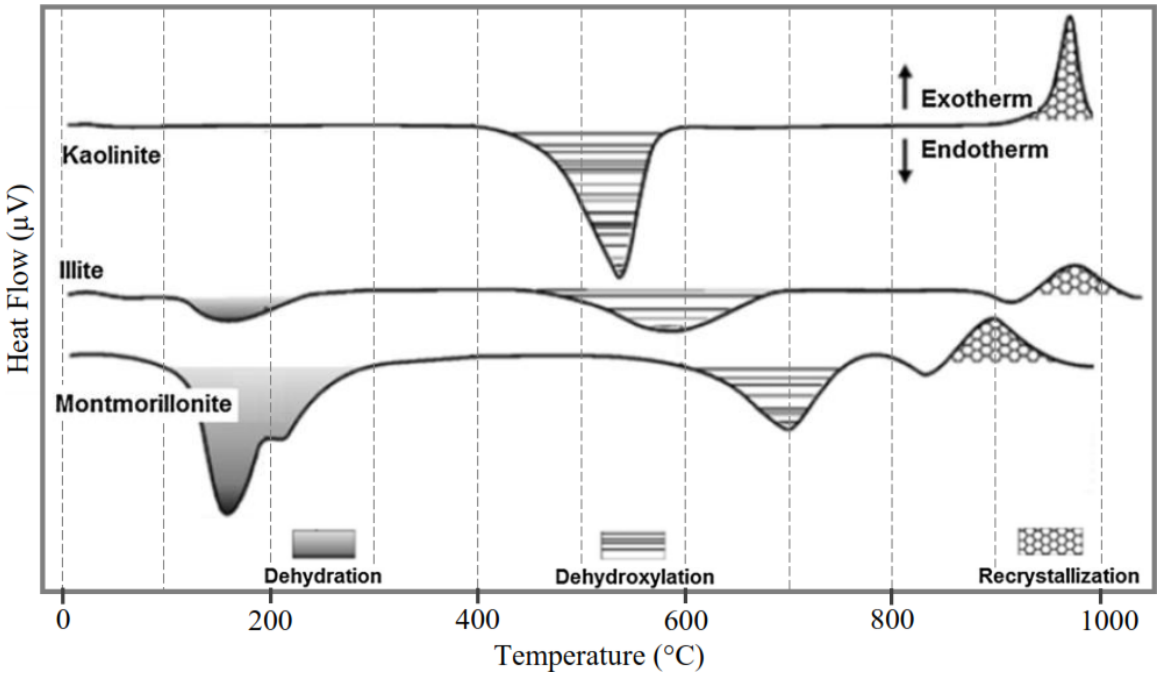

Figure 2.10: Differential thermal analysis of common clay minerals
(Snellings, Mertens and Elsen, 2012; Bernal et al., 2017)

2.8 LC^3 system

2.8.1 Overview

Africa has abundant reserves of kaolinite clay and LS. These materials can be used in binary or ternary mixes as SCM and obtain cement or concrete at a reasonable cost (Cancio

Díaz et al., 2017; Scrivener, John and Gartner, 2018). The main limitations that arise with most systems of binary mixes are slow development of strength and the need for proper curing to attain higher long-term strength and reduced penetrability (Bijen, 1996; Nehdi, 2001; Bentz, 2010). This often restricts the effective application of low-clinker binary systems in construction. To overcome these limitations, ternary systems such as LC^3 have been developed which incorporate the use of two SCMs combined with PC clinker. For instance a ternary mix of MK, LS and PC appeared to react faster in the system than in the binary mix of MK and PC or LS and PC (Antoni et al., 2012).

However, this system requires adjustment of sulphate and alkali content. Sulphate content is adjusted due to the filler effect of the SCMs which accelerates the reaction of C_3S and C_3A (Zunino and Scrivener, 2019, 2020a). As the rate of precipitation of C-S-H is increased more sulphate gets adsorbed by the C-S-H. Adjustment is done by ensuring that the aluminate reaction occurs shortly after the silicate reaction peak to get full benefit of the reaction of both silicate and aluminate phases, otherwise the silicate reaction will be reduced. Excess gypsum can combine with CH and the alumina component of the CC to form ettringite and therefore reduce the amount of CH available to react with CC and LS (Krishnan, Emmanuel and Bishnoi, 2019). Alkali content is adjusted (to an optimum amount) to increase early age strength (i.e., increasing rate of hydration of the silicate and aluminate) but at the same time ensuring that the long-term performance of the mix is not affected (Krishnan, Singh and Bishnoi, 2021).

2.8.2 The synergy of the system

In addition to the filler effect, both calcined kaolinite (CK) (from CC) and $C\overline{C}$ (from LS) also react chemically during hydration. CK reacts as pozzolan during cement hydration to form C-A-S-H. The aluminate component of the clay reacts with $C\overline{C}$ and enhances the formation of carboaluminate phases which results in a decrease of porosity and thus an increase of compressive strength. As shown in Figure 2.11, $C\overline{C}$ reacts with C_3A (from the clinker) to form carboaluminate phases as shown in Equations 2.7 (Kevin and Kenneth, 1991; Bonavetti, Rahhal and Irassar, 2001), it also reacts with monosulphate to form monocarboaluminate phase and leads to the stabilisation of ettringite phase as shown in Equations 2.8 (Klemm and Adams, 1990). In the presence of calcined kaolinite clay

(Equation 2.9), the alumina component of the CC also reacts with $C\overline{C}$ from LS and enhances the formation of hemicarboaluminate phase (Krishnan, Emmanuel and Bishnoi, 2019) and largely occurs during the fourth hydration peak which is after the silicate and aluminate peaks (Zunino and Scrivener, 2021b). C_4AF can also react to form carboaluminate phases as well as ettringite but at a lower rate than C_3A (Black et al., 2006; Dilnesa et al., 2011; Radwan and El Hemaly, 2011).

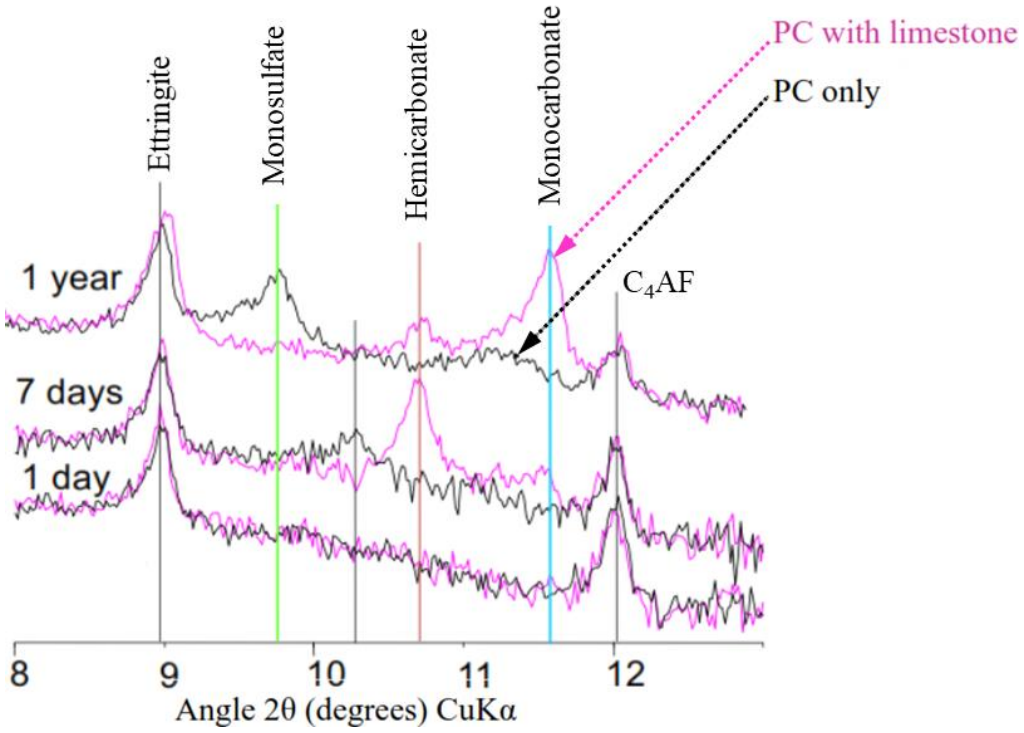

Figure 2.11: XRD patterns of PC versus PC with 4% limestone (Lothenbach et al., 2008)

$$\left.\begin{aligned} C_3A + \underbrace{C\overline{C}}_{\text{Calcium carbonate}} + 11H &\rightarrow \underbrace{C_4A\overline{C}H_{11}}_{\text{Monocarboaluminate}} \\ C_3A + 0.5C\overline{C} + 0.5CH + 11.5H &\rightarrow \underbrace{C_4A\overline{C}_{0.5}H_{12}}_{\text{Hemicarboaluminate}} \end{aligned}\right\} \quad (2.7)$$

$$\left.\begin{aligned} 3\underbrace{C\overline{S}H_2}_{\text{Gypsum}} + C_3A + 26H &\rightarrow \underbrace{C_6A\overline{S}_3H_{32}}_{\text{Ettringite}} \\ \underbrace{C_6A\overline{S}_3H_{32}}_{\text{Ettringite}} + 2C_3A + 4H &\rightarrow 3\underbrace{C_6A\overline{S}_3H_{32}}_{\text{Calcium monosulphate}} \\ 3\underbrace{C_6A\overline{S}_3H_{32}}_{\text{Calcium monosulphate}} + 2C\overline{C} + 18H &\rightarrow \underbrace{C_6A\overline{S}_3H_{32}}_{\text{Ettringite}} + 2\underbrace{C_4A\overline{C}H_{11}}_{\text{Monocarboaluminate}} \end{aligned}\right\} \quad (2.8)$$

$$A_{(\text{From CC})} + 0.5C\overline{C} + 3.5CH + 8.5H \rightarrow \underbrace{C_4A\overline{C}_{0.5}H_{12}}_{\text{Hemicarboaluminate}} \quad (2.9)$$

For comparison, a study was done using XRD (Figure 2.12) on four different systems: 100% PC, PC partially replaced by LS (LS15), PC partially replaced by metakaolin (MK30), and PC partially replaced by LS combined with metakaolin (MK-B45). From the results (Figure 2.12), all systems show the formation of ettringite (Ettr) and portlandite (CH). The PC system shows formation of monosulfoaluminate (Ms) especially after 7 days. Systems with metakaolin (MK30 and MK-B45) show formation of stratlingite (Strat) and Ms from about 7 days. All systems with LS (LS15 and MK-45) show formation of hemicarboaluminate (Hc) at early ages and later monocarboaluminate (Mc) instead of Ms.

It is clear that, unlike all other systems, the LC^3 system which in this case is the MK-B45 system gets benefits from both, the pozzolanic reaction as well as the reaction between alumina (from MK) and calcium carbonate (from LS) to form significant amount of carboaluminate phases. However, as shown in Figure 2.13, the formation and the amount of carboaluminate phases in the system also depends on the amount of kaolinite minerals in the clay, but also this needs enough amount of CH (from PC) to react with MK (from the CC).

It is also been reported that the low amount or absence of CH in the system causes C-S-H to carbonate extensively which increases concrete porosity (Shah and Bishnoi, 2018a), however, it is also important to note that the formation and amount of all the phases and therefore the required performance of the LC^3 system will obviously depend on the reactivity and proportion of all the minerals in the system (Alujas et al., 2015; Maraghechi et al., 2018; Krishnan, Dhoopadahalli and Bishnoi, 2020; Rodriguez and Tobon, 2020).

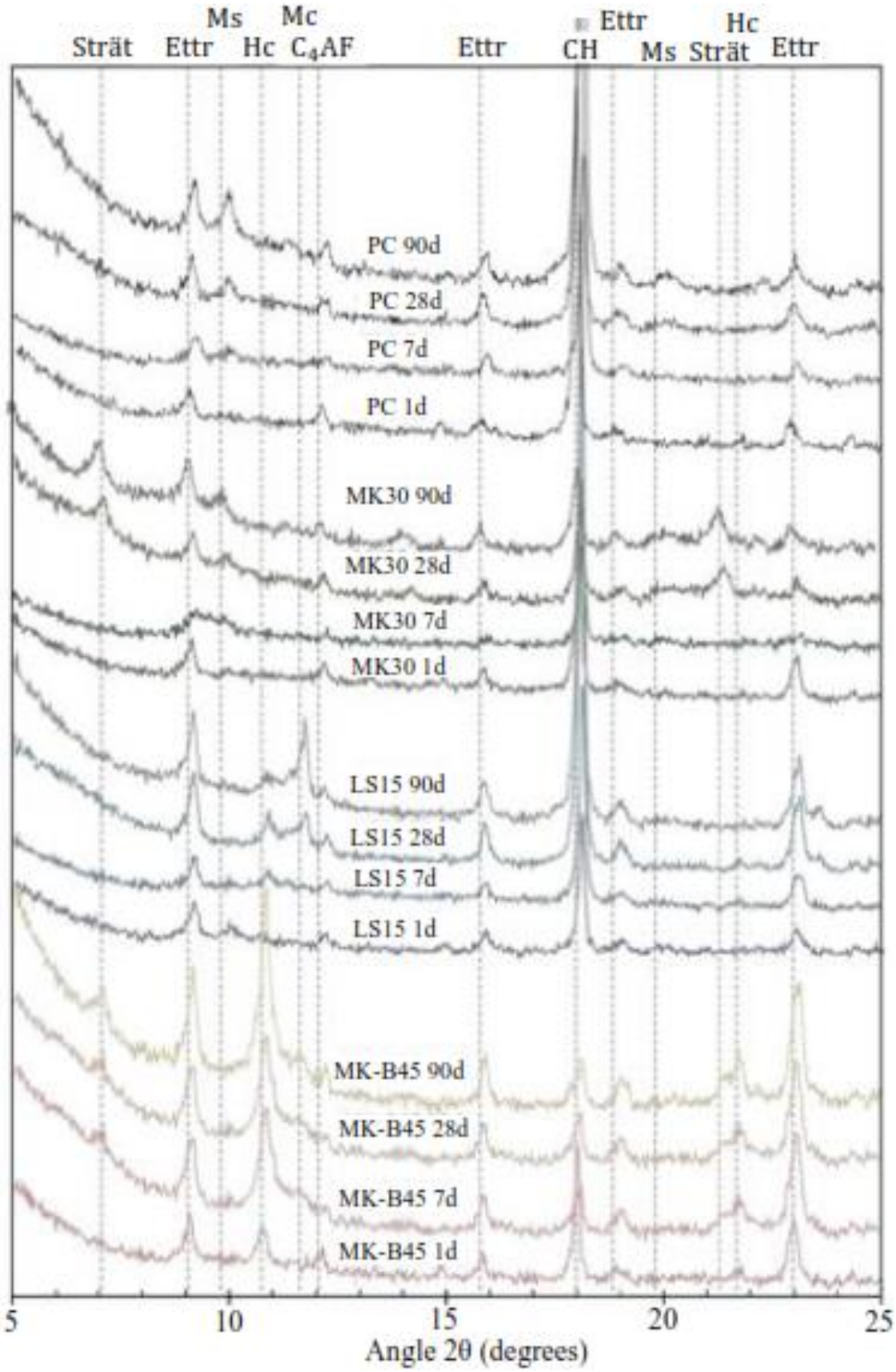

Figure 2.12: XRD patterns of PC, LS15, MK30 and MK-B45 at different ages (Antoni et al., 2012)

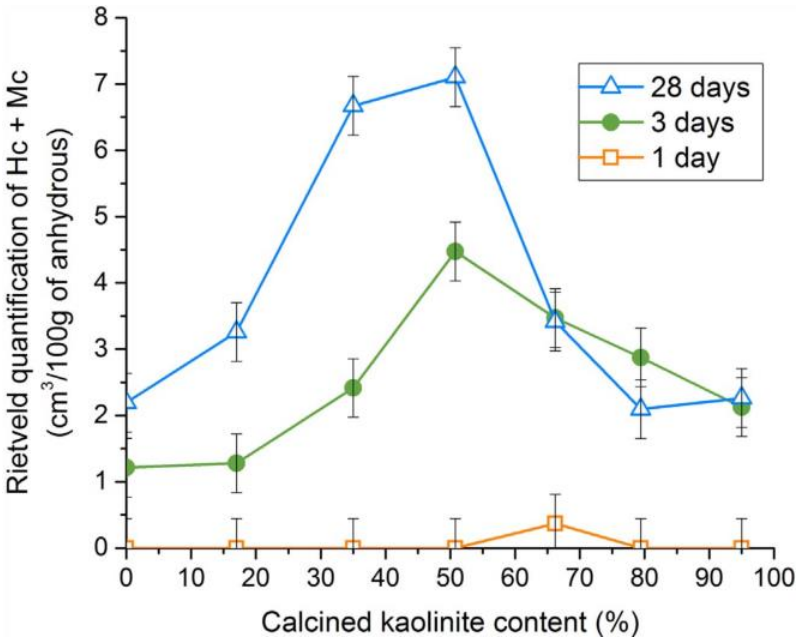

Figure 2.13: Amount of carboaluminate phases at 1, 3 and 28 days in relation to kaolinite content in the clay (Avet and Scrivener, 2018)

2.8.3 Grinding

Grinding of cementitious materials increases the specific surface area and thus reactivity. A required level of fineness of the LC^3 constituents is essential in achieving the required performance of the system (Pérez et al., 2015, 2018). Blended cement can be produced by either inter-grinding the constituents or separate grinding and blending. With the inter-grinding process, all the constituents are ground together leading to a homogenized mixture. In the case of LC^3 systems, clinker is harder to grind than CC and LS and at the same time, during grinding, CC particles (as they get finer) tend to agglomerates and stick on the grinding medium which in turn prevent further grinding of clinker (Justnes and De Weerdt, 2007). As a result, CC and LS will be ground finer (compared to clinker) and may increase the water demand of the system (Ferreiro et al., 2019). However, it has been reported that the agglomeration and sticking of CC particles during grinding can be reduced by using grinding aids (Rajendran Nair and Paramasivam, 1999; Vargas et al., 2020; Zunino and Scrivener, 2021a). With separate grinding and blending, the particle sizes of the individual materials can be efficiently optimised. In this research, all materials were ground separately and blended.

2.8.4 Mechanical performance

2.8.4.1 Compressive strength

Studies done at EPFL (Switzerland) on mortars with clinker content fixed at 50% (Figure 2.14) indicates that, for maximum strength, the optimum proportion of pure MK and LS is about 2:1. From Figure 2.14, comparing the compressive strength of LC^3 mortars relative to 100% PC mortar it is clear that even a system with 3:1 ratio of MK and LS at 50% clinker is better than the 100% PC system.

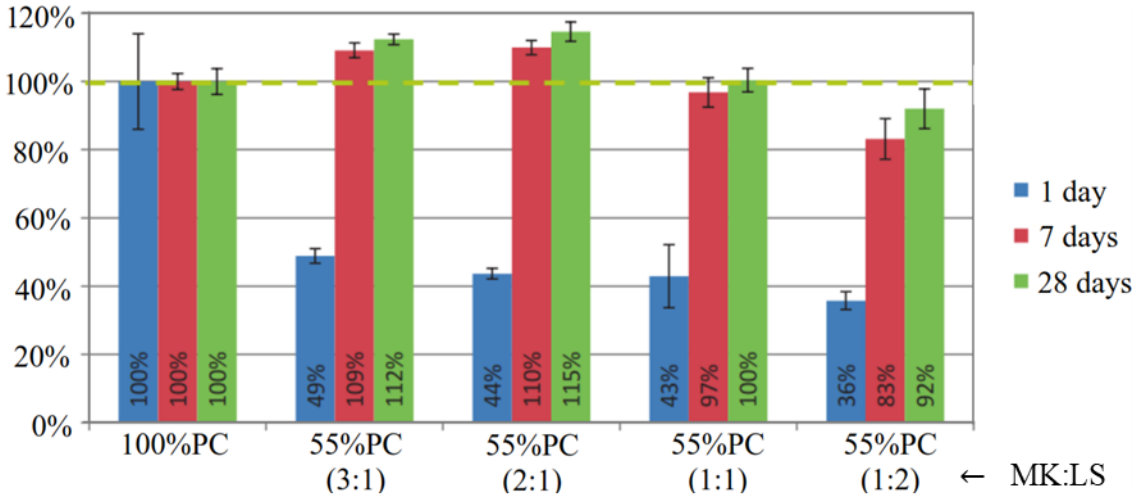

Figure 2.14: Compressive strength of LC^3 mortars relative to PC mortar (Antoni et al., 2012)

In another study by Sui et al. (2019), seven mortar mixtures with different replacement levels of PC and combinations as shown in Table 2.3 were compared. In all binary systems, PC was replaced by 30% while in ternary mixes extra LS was added to replace more PC by 15%. For systems containing CC, 1.96% of gypsum was added to control aluminate reactions. The kaolinite clay was calcined at 800°C and had a kaolinite content of 48%. In general, results (Figure 2.15) show that the compressive strength of PC system is high at early ages compared to other systems, however, after 4 days, the rate of increase of strength is high for samples with SCMs. At 7 days, samples with CC have the highest compressive strength while after 28 days samples with FA and slag takes the lead. Looking at the strength results of the ternary systems, their strengths are similar or slightly lower than binary systems even though they contain 15% less PC. From all the three ternary systems,

a system with CC and LS (LC^3 mix) gain strength faster compared to other two systems especially up to 28 days.

Table 2.3: Proportions of binders for mortar samples used by Sui et al. (2019)

#	Name	PC (g)	LS (g)	CC (g)	Slag (g)	FA (g)	Added Gypsum (g)	SP (g)	Water (g)
1	PC	100.0	-	-	-	-	-	-	50
2	CC	68.6	-	29.4	-	-	1.96	0.283	50
3	CC + LS	53.9	14.7	29.4	-	-	1.96	0.283	50
4	Slag	70.0	-	-	30	-	-	-	50
5	Slag + LS	55.0	15	-	30	-	-	-	50
6	FA	70.0	-	-	-	30	-	-	50
7	FA + LS	55.0	15	-	-	30	-	-	50

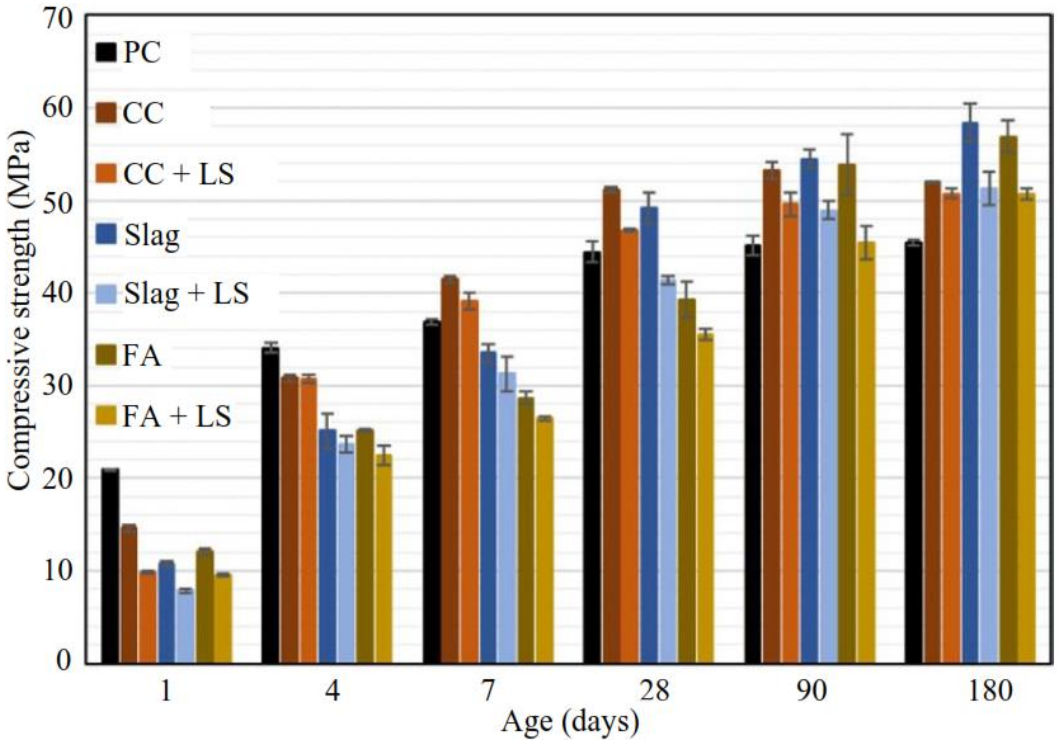

Figure 2.15: Compressive strength of different binary and ternary mixes (Sui et al., 2019)

A study done on concrete by Avet, Sofia and Scrivener (2019), compared the performance of a LC^3-50 (with 2:1 ratio of CC and LS) system with 100% PC, a blend of 50% PC and GGBS (GGBS50), and a blend of 10% PC replaced by SF (SF10). Two cases with different targets (i.e., slump and compressive strength) were studied. For the first case (Case A), the

total binder content was 375 kg/m^3, a w/b ratio of 0.43, and the targeted slump and compressive strength at 28 days were 40 mm and 50 MPa, respectively. For Case B, the total binder content was 500 kg/m^3 with a w/b ratio of 0.34 and maximum aggregate size of 16 mm, and the target was to have a mix with self-placing properties and a compressive strength of 70 MPa at 28 days. Figure 2.16 shows the compressive strength results at 2, 7 and 28 days measured in cylindrical specimens. In general, at all ages, results show that the LC^3-50 system performs better or similar than the 100% PC system, better than GGBS 50, and slightly lower than SF10. Dhandapani et al. (2018) also observed a similar performance of the LC^3-50 concrete system compared to a system with 100% PC and a system with 30% PC replaced by FA. However, Nguyen, Khan and Castel (2018) in their studies observed low performance of a LC^3-50 system compared to a similar system with 100% PC, but most likely because the mix was prepared without optimising sulphate and alkali content in the LC^3 system.

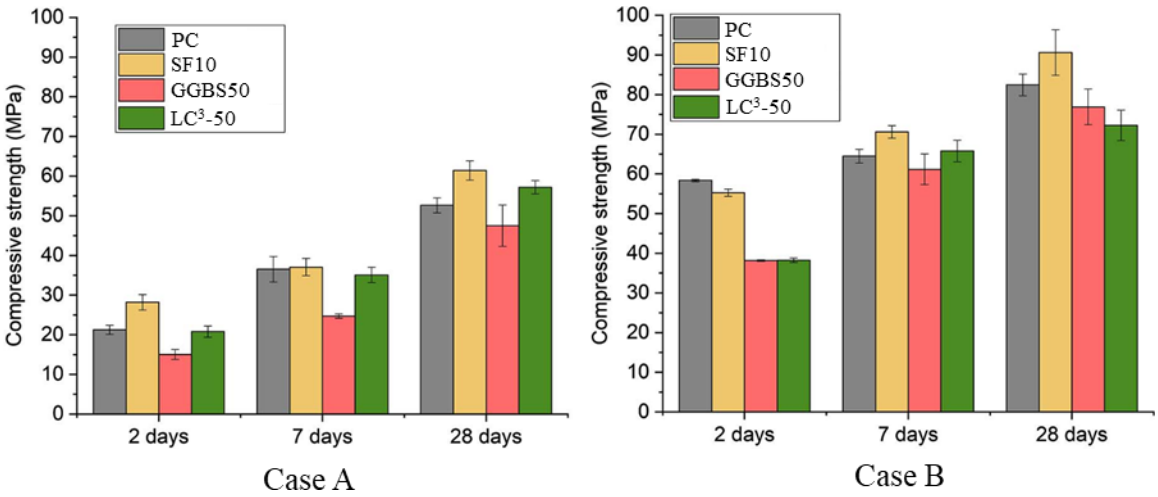

Figure 2.16: Compressive strength of LC^3-50 versus PC, SF10 and GGBS50 concrete (Avet, Sofia and Scrivener, 2019)

It has been noted that the strength performance of the LC^3 system also depends on the fineness of PC clinker and CC (Krishnan, Emmanuel and Bishnoi, 2019). The LC^3 system with finer PC clinker will have higher strength at the early age (which is a result of faster silicate and aluminate hydration) and no loss of long-term performance. On the other hand, a system with finer CC will have higher strength at the early age but the long-term performance of the system will be reduced. In both cases, the system will be affected by

higher water demand. In view of this, there is a need to find a balance between all these factors to arrive at a reasonable performance of the LC^3 system by controlling grinding and blending of these materials.

2.8.4.2 Shrinkage

Drying shrinkage causes cracking of concrete due to loss of moisture from the cement paste. Factors influencing drying shrinkage include w/b ratio, volume of paste, RH and specimen size (Bissonnette, Pierre and Pigeon, 1999; ACI Committee 209, 2005). Figure 2.17 shows development of shrinkage strain for three different concrete mixes, PC, FA30 and LC^3 mix. Each mix had the same binder content (360 kg/m^3) and w/b ratio (0.45). The test was carried out as per ASTM C 157. Results indicate that all the three systems have comparable measured total shrinkage strain. The authors (Dhandapani et al., 2018) noted that it is the w/b ratio (not the binder system) that controls shrinkage development in the concrete. However, it is important to note that this also depends on the aggregate to cement ratio in the system.

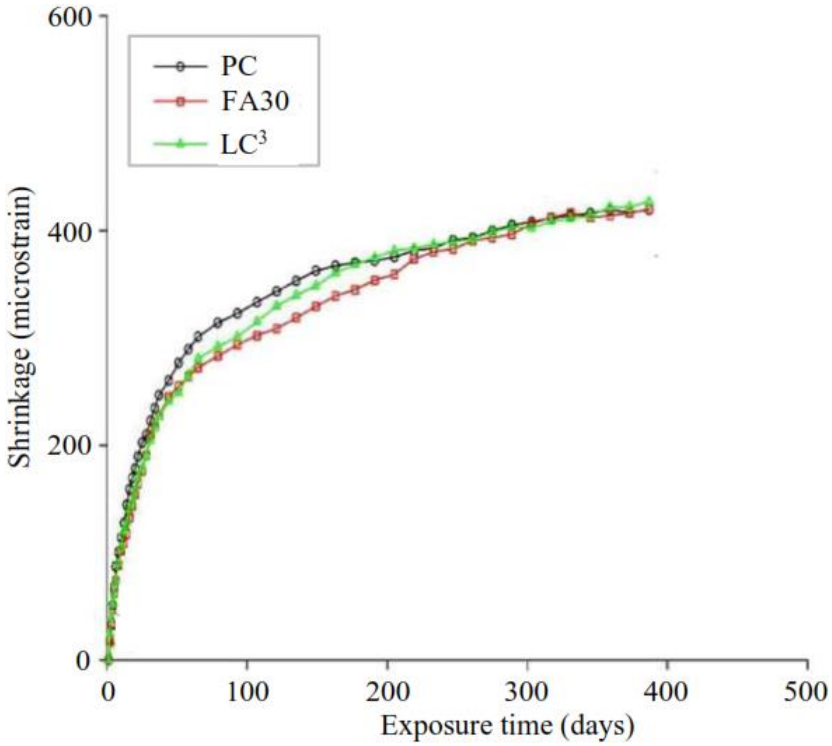

Figure 2.17: Shrinkage strain: LC^3 versus PC and FA concrete (Dhandapani et al., 2018)

2.8.5 Durability performance

2.8.5.1 Chloride resistance

In general, the increased penetration resistance of the LC^3 system is linked to the porosity refinement produced by the pozzolanic reaction and formation of carboaluminate phases as well as chloride-binding capacity. Figure 2.18 shows the chloride profiles of different mortar samples after 1-year exposure in 0.5 M NaCl solution. The replacement levels of PC and combinations for each sample are shown in Table 2.3. From the results, samples with CC, both in binary and ternary systems, show better resistance to penetration of chloride ions than all other mixes. Interestingly, the LC^3 mix (CC + LS) exhibits the best resistance to chloride penetration than all the binary mixes even though there is less PC in the system.

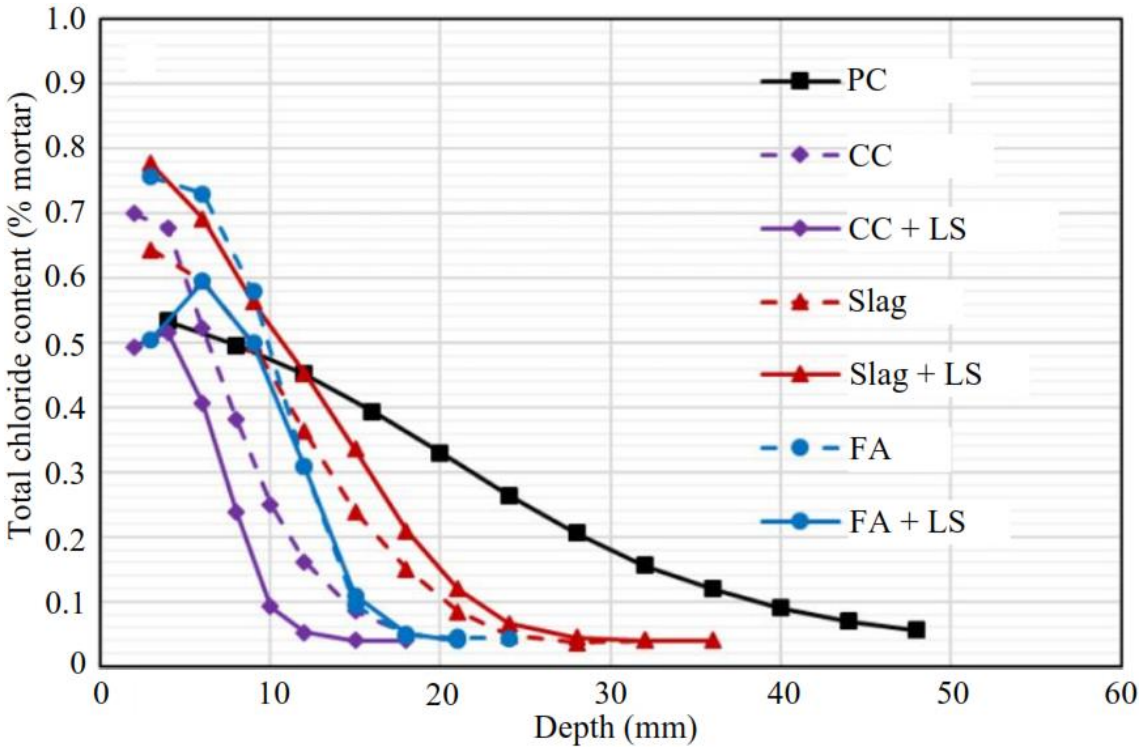

Figure 2.18: Chloride profile of different binary and ternary mixes (Sui et al., 2019)

The binding of chloride ions in the hydrates, especially carboaluminate AFm phases and C-A-S-H, slows down the ingress of chloride ions in the concrete (Maraghechi et al., 2018). In the presence of chloride ions, carboaluminate phases and ettringite convert to Friedel's salt. Figure 2.19 shows distribution of bound chloride between C-A-S-H and Friedel's salt

for 100% PC system and LC^3-50 blends (with different kaolinite content) after being exposed to 2 M NaCl solution. Results show that in LC^3-blends more chloride ions are bound by Friedel's salt, whereas for the PC system more ions are adsorbed on C-A-S-H hydrate. It is also clear from Figure 2.19 that the binding of chloride ions also varies with calcined kaolinite content in the LC^3-50 blends.

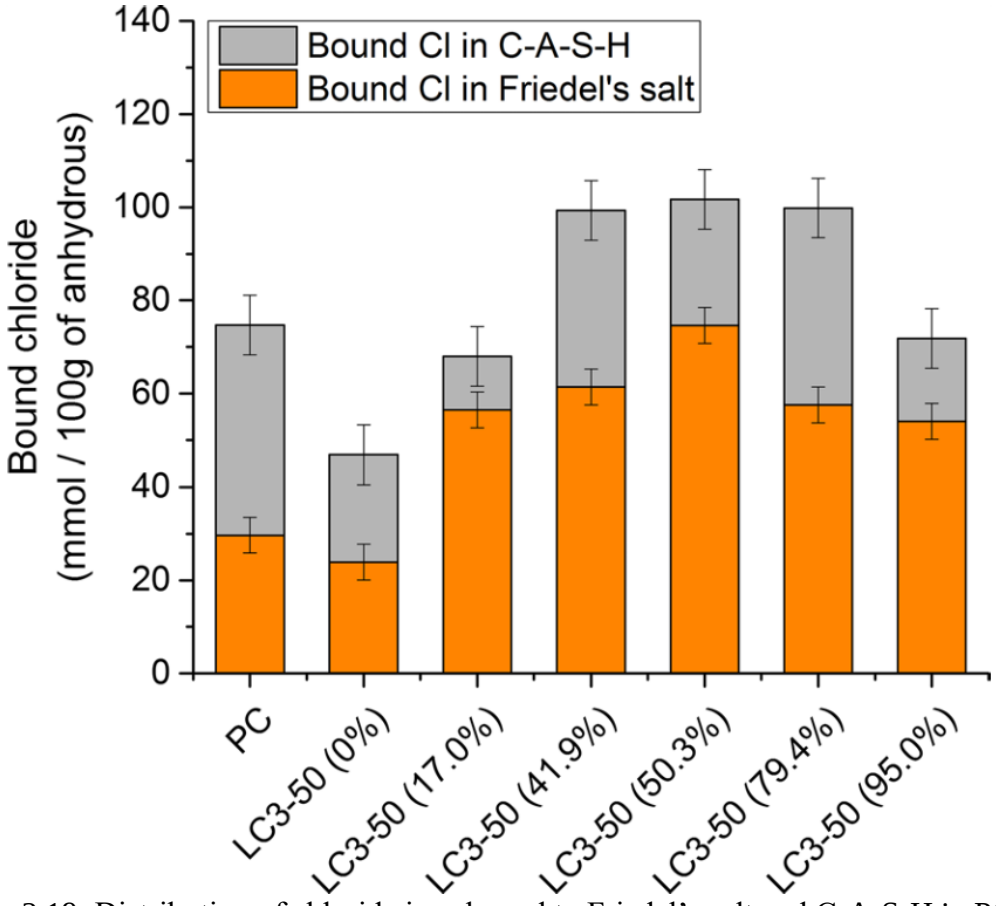

Figure 2.19: Distribution of chloride ions bound to Friedel's salt and C-A-S-H in PC and LC^3-pastes (Maraghechi et al., 2018)

2.8.5.2 Carbonation resistance

Carbonation of concrete can induce corrosion in RC structures, as it decreases the pH of the pore solution in concrete and destroys the stability of a passive oxide layer which is only stable at high pH condition. With low-clinker systems such as LC^3 system, you already have low CH in the system which will also be consumed by the pozzolanic reaction making the available CH to be quite low for protecting the system against carbonation. The carbonation resistance of concrete can be predicted using the results of the Oxygen

Permeability Index (OPI) test (Mackechnie and Alexander, 2002; Salvoldi, Beushausen and Alexander, 2015) .

Figure 2.20 shows OPI test results for PC, FA30 and LC^3 concrete mix from a study done in India. Each mix had the same binder content (360 kg/m^3) and w/b ratio (0.45). Results indicate that all the three systems have OPI values greater than 10 (log scale). The three mixes fall into "excellent" durability class as suggested by Alexander, Mackechnie and Ballim (1999) which implies high resistance to carbonation. Results indicate that the LC^3 system has higher penetration resistance of CO_2 than PC system but lower than FA30 system, probably this also depends on the type of cement, amount of clinker and/or kaolinite content in the LC^3 system. It is important to note that most of the cements that are used in India have low alite, high belite clinker in which the amount of CH produced in these kind of cements is usually lower than cements with high alite, low-belite clinker.

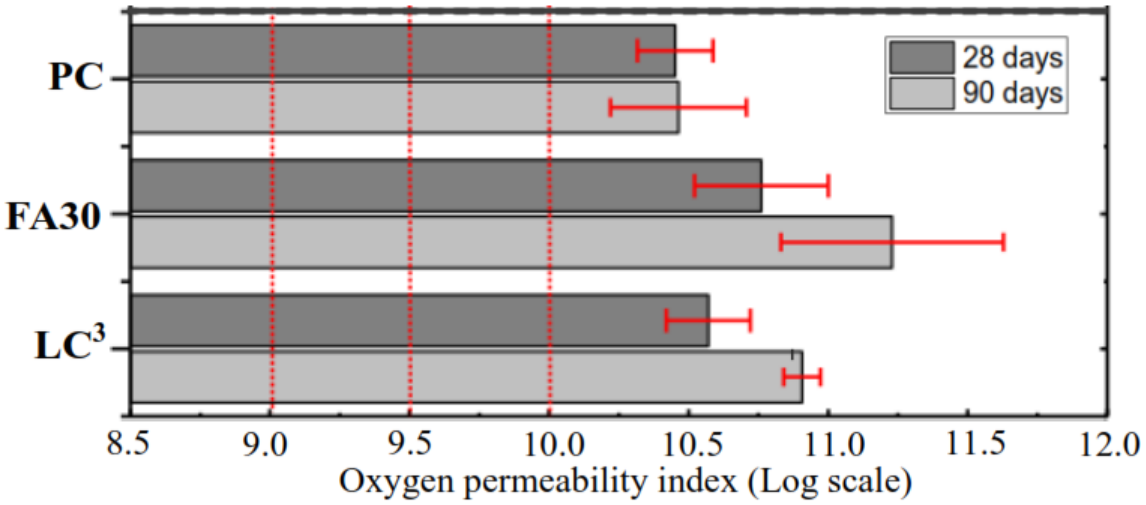

Figure 2.20: Gas permeability: LC^3 versus PC and FA concrete (Dhandapani et al., 2018)

2.9 Interaction effects in a mixture of concrete materials

Interactions of concrete materials influence the way in which materials pack together. The interaction effect is influenced by the degree of compaction effort applied, water content and the use of dispersant admixtures.

Solid particles in concrete mix can be classified as aggregates particles when only mechanical interactions exist; and cementitious particles when particle surface forces exist

(Mehdipour and Khayat, 2018). In general, the interaction effect can be divided into two broad categories (Fennis, 2010; Knop and Peled, 2016): one category is that of geometric interaction and another category is due to interparticle forces.

Two geometric particle interactions that have become widely acknowledged are defined as ‘wall’ and ‘loosening’ effects (Stovall, De Larrard and Buil, 1986; Goltermann, Johansen and Palbøl, 1997; De Larrard, 1999; Fennis, 2010; Mehdipour and Khayat, 2018). The two effects are illustrated in Figure 2.21 below.

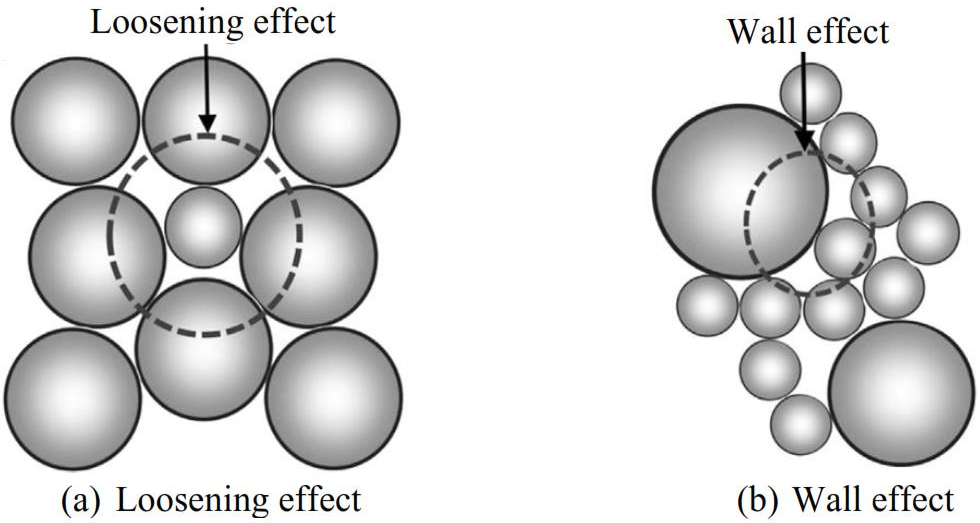

Figure 2.21: Schematic representation of particle interactions (Mehdipour and Khayat, 2018)

The loosening effect occurs when the coarse particles are dominant, and the fine particles are not sufficiently small to fit into voids among coarse particles without disturbing the skeleton of the coarse particles (Mehdipour and Khayat, 2018). In this case the squeezing of the fine particles into the voids among coarse particles tends to loosen the frame of coarse particles, thus lowering the packing density of the granular skeleton (De Larrard, 1999). In contrast, the wall effect occurs when fine particles are dominant and the regular packing of the fine particles is interrupted by the wall boundaries induced by coarse particles (Mehdipour and Khayat, 2018). This results in the formation of additional voids in the vicinity of coarse particle surfaces (De Larrard, 1999) and is one of the causes of the formation of the interfacial transition zone (ITZ) in concrete (Alexander and Mindess, 2005). The degree of loosening and wall effects depends on the ratio of fine to coarse

particle sizes (d_1/d_2). The smaller particle size ratio minimizes the loosening and wall effects (Mehdipour and Khayat, 2018).

For optimal packing, particles must be distributed apart from each other due to the action of either gravitational-shear forces, Figure 2.22a, or repulsive inter-particle forces, Figure 2.22b (Mehdipour and Khayat, 2018). However, as the size of particles decreases, there is a vast increase in the surface area to volume ratio and the influence of gravitational and shear forces on packing is substantially reduced. Instead, interparticle surface forces begin to govern the interaction and increase the tendency of particles to be agglomerated and form interconnected flocs, rather than dispersed as shown in Figure 2.22c (Fennis, 2010; Mehdipour and Khayat, 2018). Interparticle forces that exist when packing cementitious materials are the attractive Van der Waals's forces, electrostatic charges and chemical bonding (Fennis, 2010).

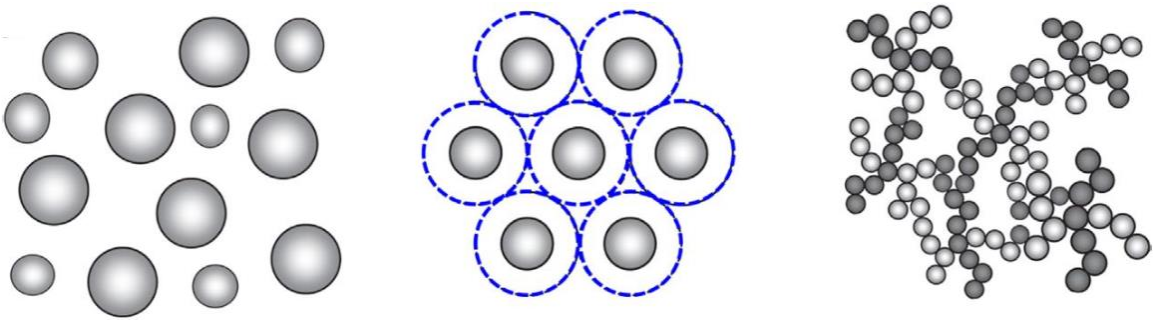

(a) (b) (c)

Figure 2.22: Schematic representation of: (a) distributed aggregate particles, (b) dispersed cementitious particles (dashed lines represent repulsive forces which keep particles separated), and (c) agglomerated cementitious particles (Mehdipour and Khayat, 2018)

The formation of agglomerates significantly reduces the packing density of cementitious particles due to the following reasons (Damineli, Pillegi and John, 2017): i) the agglomerates act as large particles and therefore hinders the mobility of smaller particles; ii) generates voids within themselves thus increasing water consumption; and iii) decreases the efficiency of the binders because the surface area available for pozzolanic and hydration reactions is decreased. To ensure total dispersion of the fine particles, dispersing admixtures such as polycarboxylate ether (PCE) are normally added in the mixture to

enhance the packing of the materials (Collepardi, 1998; Flatt and Houst, 2001; Flatt, 2004; Zingg, Holzer, et al., 2008; Zingg, Winnefeld, et al., 2008). High dosage of SP is usually required for the LC^3 system compared to conventional systems, primarily because of the high surface area of the clay (Ferreiro, Herfort and Damtoft, 2017; Dhandapani et al., 2018; Muzenda et al., 2020; Nair et al., 2020).

2.10 Concrete mix design approaches

When carrying out a concrete mix design, it is always desirable to compose the materials to form as dense a matrix as possible. The intention is usually to produce a concrete mix which is workable, strong, durable, and economical. The proportioning of materials is influenced by morphological characteristics of particles such as shape, angularity, surface texture, and PSD which are collectively reflected in the context of packing density.

Various researchers have tried to optimise the packing of concrete materials (Fennis, 2010; Yu, Spiesz and Brouwers, 2013; Proske et al., 2014). It has been observed that with an increased packing density of constituent materials, porosity is minimised and therefore the compressive strength and impenetrability of concrete is improved. It has also been noted that increasing packing density may affect the workability and compactability of fresh concrete due to its influence on water demand (Johansen and Andersen 1991, Fennis and Walraven 2011), and also there is a challenge of agglomeration of fine particles due to interparticle forces (Fennis, Walraven and Den Uijl, 2013). In general, it is not possible to optimise all concrete properties simultaneously as the optimisation of one property affects other properties.

There are several standards and methods that have been developed to optimise proportions of concrete materials, however, all these approaches eventually follow the same basic trial and error principles. In this work, optimisation of concrete materials aimed at further reducing clinker content in concrete to an extent that fresh concrete properties are not adversely affected.

2.10.1 Particle packing models

Studies on particle packing involve selection of appropriate sizes and proportions of materials to get a suitable combination for optimal packing. The aim of these packing models is to come up with the right amount of different particle sizes in the system. This will help to make sure that the voids between larger particles are filled by the smaller particles thereby reducing the volume of voids or increasing the packing density.

Several packing models have been developed to predict the packing density of materials. In majority of these models, the particles are idealized as spherical particles. The accuracy of the prediction depends on the particle size ratio (i.e. fine to coarse particle size ratio) such that, as the size ratio increases, the particle interaction effects become more significant (De Larrard, 1999). In general, polydisperse packing systems can be divided into two classes (Funk and Dinger, 1994; Kumar, S. and Santhanam, 2003): i) The packing of several discretely sized particles (or discrete models); ii) The packing of continuous PSDs where all particle sizes between a maximum and minimum particle size are represented (continuous models).

Figure 2.23 presents an overview of some of these packing models developed between year 1931 and 2000, the term "Compaction effect" refers to the ability of the model to account for the influence of applied compaction on the resulting packing density.

2.10.1.1 Discrete models

Discrete models consider two or more discrete class sizes of particles with coarse particles forming the base skeleton and the voids are filled by smaller particles (Kumar, S. and Santhanam, 2003). The fundamental assumption is that each class of particles will pack to its maximum density in the available volume (Funk and Dinger, 1994). The input parameters are PSD and packing density of each material in the mixture. The output parameter is the theoretical PD of the mixture. To optimise a mixture, the approach involves determination of PD of different combination of materials until a combination which gives maximum packing density is achieved. The accuracy of the result depends on the interaction functions describing the wall and loosening effects and consideration of compaction effort.

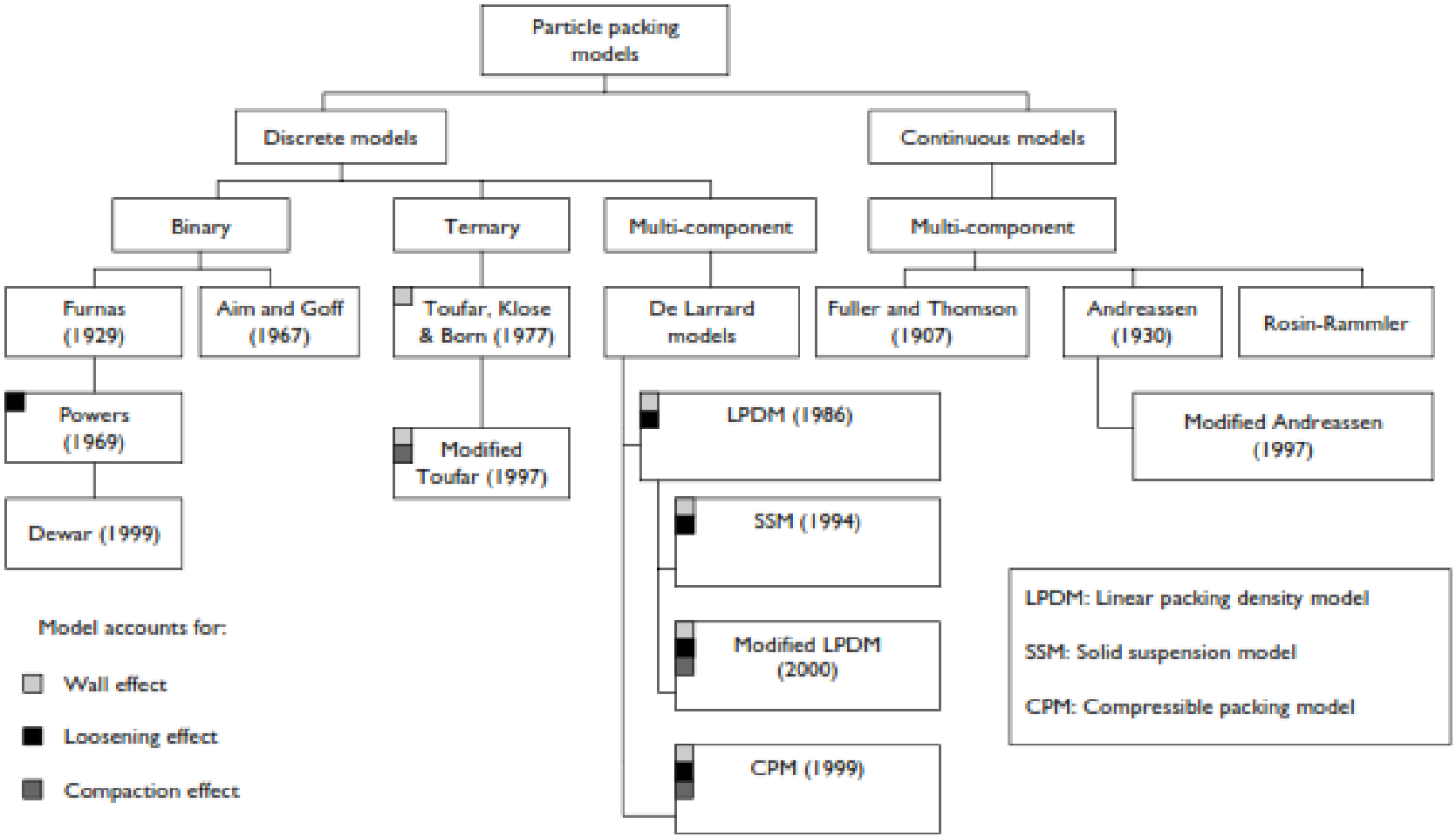

Figure 2.23: Overview of existing packing models (Alexander and Mindess, 2005)

The CPM which is a refined version of the LPDM has been noted to accurately predict the packing density of materials relative to other models (Jones, Zheng and Newlands, 2002; Lecomte, Mechling and Diliberto, 2009; Fennis, 2010; Knop and Peled, 2016; Moutassem, 2016; Van Der Putten et al., 2017). However, the CPM considers only the size ratio of the interacting particles and not the size of particles. Fennis, Walraven & Den Uijl 2013 developed the compaction interaction packing model (CIPM) which considers the theoretical concepts of the CPM with consideration of size of particles. In general, the CIPM improves the CPM by incorporating the effects of particle surface forces into the equations and therefore considers the packing of fine particles. Fine particles in the CIPM are defined as those with a particle size of less than 125 μm.

2.10.1.2 Continuous models

Continuous models require only the PSD of the available materials to optimise a mixture with the assumption that all possible sizes are present in the particle distribution system which represent real distribution of particles compared to the theory of discrete distributions of particles (Funk and Dinger, 1994). The approach involves the use of grading curves to optimise mixes and obtain the maximum packing density whereby particles are combined so that the total PSD of the mixture is nearest to the optimum curve. However, these models do not take into account the effect of particle surface forces and the influence of compaction effort on packing of particles as in the case of discrete models (Fennis, 2010; Damineli, Pillegi and John, 2017).

As shown in Figure 2.23, several continuous models have been developed to achieve optimal packing of materials. However, of all the models, the modified Andreasen and Andersen (MAAM), Equation 2.11, has received considerable attention in the literature (Snehal and Das, 2020). Although it does not directly account for the particle interaction effects and influence of compaction effort on packing of particles, it has been successfully employed to optimise different concrete types (Brouwers and Radix, 2005; Hüsken and Brouwers, 2008; Yu, Spiesz and Brouwers, 2013, 2014, 2015; Khayat and Libre, 2014; Mueller, Wallevik and Khayat, 2014; Khayat and Mehdipour, 2015), therefore, there is potential for its application in optimising the selection of concrete materials to obtain the highest packing density. It is easy to use and requires few input parameters, for example

when PSD modulus (q) is fixed, only the PSD and/or quantity of materials can be adjusted to optimise a concrete mixture. In addition, a commercial software named Elkem Materials-Mixture Analyser or EMMA (Hanssen, 2012) which uses MAAM to optimise packing of materials is available for free on Elkem website.

$$CPFT_{tar}(D_i) = \frac{D_i^q - D_{min}^q}{D_{max}^q - D_{min}^q} \cdot 100 \qquad D_i \in [D_{min}, D_{max}] \tag{2.11}$$

Where :

$CPFT_{tar}$ - Cumulative percent finer than D_i for the target grading curve

D_{max} - the maximum particle size of distribution

D_{min} - the minimum particle size of distribution

D_i - the particle size (diameter)

q - the PSD modulus

For optimum packing, the PSD modulus can be varied between 0.21 and 0.37 depending on workability requirements and method of compaction (Funk and Dinger, 1994). In general, the amount of fine materials in the mix increases as you decrease the value of q. For high performance and conventional concrete, the recommended q value is between 0.25 and 0.3 (Kumar and Santhanam, 2003).

2.10.2 Methods given in the standards

Almost every country or region has its own approved standardised concrete mix design method. These methods involve use of, charts, tables, graphs, and/or empirical relations developed/approved based on experience, experiments, and investigations of locally available materials. Some of the prevalent methods includes American Concrete Institute Standards Method ACI 211.1-1991, British standards BS 8500-1:2006 and Indian Standard method IS 10260: 2009. The South African approach, named the Cement and Concrete SA (CCSA) method (previously named the Concrete Institute (TCI) method or the C&CI method), is derived from ACI 211.1-1991, with some refinement to accommodate local practice which involves use of crushed fine aggregate and gap-graded mixtures. Although the CCSA method does not consider interaction effects of particles or match an ideal grading curve to maximise packing density, it has been successfully employed to design different concrete mixes in South Africa. It is likely that the estimation of stone content based on the fineness modulus (FM) of sand, dry Compacted Bulk Density (CBD) of stone

and a factor (which depends on the required workability and maximum size of stone) helps in maximising packing density. The employment of a gap-graded mixture helps to reduce internal friction of angular particles and enable satisfactorily workable mixtures.

2.10.3 Selected approach

A study done at the University of Cape Town integrated CIPM and MAAM to optimise packing of concrete materials (Holmes, 2018). The CIPM was used to optimise packing of powder materials and MAAM was used to optimise the entire range of concrete materials (including powder optimised from CIPM). The reference mixture was designed using the CCSA method. The CIPM, which incorporates the effect of surface forces, did not predict the trend in PD with consistent accuracy. Good results obtained were mainly because of MAAM. However, although the CCSA method is not intended to obtain grading of materials to match an ideal grading curve, the overall grading curve obtained reasonably matches the MAAM grading curve. In view of this, in this research the CCSA method coupled with MAAM (using the EMMA software) were used as a starting step in obtaining proportions of concrete materials, and the clinker/powder content further reduced by adjusting proportions of other materials but maintaining w/b ratio. However, it is important to note that both methods do not take into account the effectiveness of admixtures, therefore, some modification to the admixture dosage to get the required workability was necessary when making up the concrete mix.

2.11 Summary of literature review

A fundamental challenge being faced by the cement industry is climate change. It is anticipated that emissions of greenhouse gases such as CO_2 will be more tightly regulated in the future. At the moment, in South Africa, carbon tax on cement stands at R120 per ton of CO_2 (Republic of South Africa, 2019). Moreover, more than 60% of the cost of cement production is related to energy consumption including electricity (Gartner, 2004). This drives researchers to look for improved ways to reduce the cost and the net CO_2 emissions from the production and use of cement.

In general, the clinker content of concrete can be greatly reduced by the use of SCMs, which also generally improves the durability of the concrete mainly due to the porosity

refinement produced by the pozzolanic reaction, formation of carboaluminate phases and stabilization of ettringite. The current approach of using SCMs such as GGBS and FA is reaching its limits due to lack of sufficient and sustainable sources of these materials. Thus, alternative low-CO_2 and low-cost approaches such as the use of LC^3 mixes are being investigated. However, improper use of these materials may result in obtaining a concrete with poorer durability properties than a conventional concrete (Alexander, 2016). Furthermore, It has also been noted that the usage of SCMs may result in low carbonation resistance of concrete due to the increased penetrability at early ages (caused by the dilution effect of clinker) and the lower amount of CH in concrete (Papadakis, Fardis and Vayenas, 1992; Papadakis, 2000; Ashraf, 2016). Therefore, it is important to understand the way in which these materials can be used to achieve a required durability performance.

Despite the higher clinker substitution rate of the LC^3 system, this system has superior quality because the alumina phase (from clay) reacts strongly during the first few days, thus overcoming the main problem of binary mixes which is the slow gain of strength at early ages. As for the case of SCM in the first days of the mix, the presence of LS in the mix also enhances the initial hydration reaction of the clinker components by the filler effect. The extra LS provided in the system can further contribute to the hydration of clinker phases of cement. This shows that, apart from the filler effect, there is a strong synergistic chemical effect when CC is combined with LS to replace cement in making concrete. Therefore, with careful choice of compositions, it is possible to reduce PC clinker content while maintaining the product performance. In this case, factors such as type and quality of LS, clinker factor, alkali content and grade of kaolinite clay can be optimised to produce LC^3 systems with acceptable mechanical and durability properties. Impacting factors and properties of LC^3 systems are well summarised by Scrivener et al. (2019).

The recent revision of the European standard (BS EN 197-5, 2021) limits the clinker factor to no less than 0.5, and limestone purity at no less than 75% but not the CC/LS ratio. On the contrary, the (ASTM C595/C595M, 2021) limits limestone purity at no less than 70% and the amount of limestone and pozzolan at less than 15% and 40% (by mass of the blended cement), respectively, but not the CC/LS ratio.

The objective of this study is to develop low-clinker concrete for structural and non-structural applications (including a focus on marine concretes), aiming at minimizing CO_2 emission associated with the immense development of infrastructure which is anticipated to occur in Africa in the coming decades. Studies related to the performance of mixes with PC partially replaced by calcined kaolinite clay and LS have been conducted, especially at EPFL (Switzerland) and IIT Madras (India), but there is no clear conclusion concerning the optimum proportion of these materials for marine environments in connection with the quality of the materials used. The following has been noted from the literature survey:

i) From a concrete materials perspective, the carbon footprint of concrete is closely related to the amount of PC clinker in concrete. Notably, about 40% of cement that is produced worldwide is used to make concrete.

ii) Kaolinite content is an important indicator for clay suitability. A suitable clay for clinker replacement is that with a kaolinite content of at least 40%. Secondary minerals such as quartz and illite have less influence on the reactivity of the clay.

iii) For a kaolinite clay to break down and produce an amorphous material for pozzolanic reactivity, calcination to about 800°C is necessary. During calcination, the dehydroxylation of kaolinite leads to the formation of a highly disordered structure (with the presence of $Al^{(V)}$) which increases the reactivity of the CC.

iv) Substitution of PC by CC and LS requires adjustment of sulphate and alkali content. Sulphate content is adjusted to ensure alumina reaction occurs shortly after the silicate reaction peak to get full benefit of both reactions. Alkali content is adjusted to ensure continuous gain of strength.

v) In addition to the filler effect, both CK (from CC) and $C\overline{C}$ (from LS) also react chemically during hydration. CK reacts as a pozzolan during hydration. The aluminate component of the clay reacts with $C\overline{C}$ and enhances the formation of carboaluminate phases which reduce porosity and therefore increase compressive strength.

vi) Inter-grinding of the LC^3 system is not ideal because clinker is harder to grind than CC and LS. LS and CC will be ground finer than clinker. Separate grinding would be more efficient but is less economically feasible. It is better to inter-grind LC^2 separately from clinker and then blend.

vii) There can be problems in the LC^3 system when increasing the fineness of CC. Grinding aids can improve inter-grinding by preventing agglomeration of particles.

viii) For RC exposed to a marine environment, chloride-induced corrosion of the embedded steel bars is the primary durability concern. The principal performance test is to measure chloride-ion resistance of concrete using, for example, the chloride conductivity test (SANS 3001-CO3-3:2015) and bulk-diffusion test (ASTM C1556).

ix) The reduction of chloride ion penetration in concrete relates to reducing ingress by refinement and reduction of porosity and enhancing the chloride binding capacity of the cementitious system. This can be achieved with low w/b ratios together with the correct proportion of SCM in the system.

x) It has also been reported that the use of SCMs results in low carbonation resistance of concrete due the lesser amount of CH in the binder matrix. This means that it is important to check for carbonation resistance of concrete when SCM is used in the development of a new mix. However, it is important to note that carbonation generally increases the strength of concrete and has no generally negative effect on the properties of the concrete. Carbonation is only problematic to the reinforced steel in the concrete, not the concrete itself.

xi) Early age cracking of concrete is related to use of extremely low w/b ratios and high amount of SCM. Therefore, it is important to check shrinkage characteristics and the potential for early age cracking of a new mix composition.

Overall, the review of the literature indicates that more research needs to be done to convince engineers and other decision makers regarding the use of LC^3 mixes in construction. In particular, the following needs to be addressed:

i) The suitability of kaolinite clay sources in Africa.

ii) Limiting percentage of clinker that can be replaced by CC/LS ratio while maintaining the required performance of the concrete.

iii) Best proportions of CC and LS (at a given amount of clinker) that will produce the optimum properties of concrete for structural and non-structural applications

iv) Assessment of the performance of the LC^3 mixes in comparison with the recommended mixes for marine concrete structures.

Chapter 3 Materials and methods, material properties

3.1 Introduction

The aim of this research is to develop low-clinker concrete by partially replacing cement with CC and LS for structural and non-structural applications. The target is to minimize CO_2 emissions associated with the immense development of infrastructure which is anticipated to occur in Africa in the near future. This research work is grouped into three phases, shown in Figure 3.1, which describes schematically the approach and scope of the work carried out. This chapter also gives details about the selected materials and their properties, preparation of specimens as well as tests undertaken to study the performance of the LC^3 systems (i.e., LC^3-pastes for hydration products, LC^3-mortars for proportion optimisation, and LC^3-concretes for the mechanical and durability performance).

3.2 Selected cementitious materials

The cementitious materials used in this study are kaolinite clay, LS, and cement. The selected deposits for the clay were, for South Africa, Hopefield (H-Clay) in the Western Cape, Grahamstown (G-Clay) in the Eastern Cape and Bronkhorstspruit (B-Clay) in Gauteng provinces, and for Tanzania, Pugu (P-Clay) and HeidelbergCement (HC-Clay). CEM II/A-L 52.5 N was sourced from a local cement manufacturer, AfriSam (SA), from their Ulco factory, and the limestone 'Kulubrite 5', (LS-K5) with 97% $C\overline{C}$ purity, from Idwala Carbonates (SA). Both fine and coarse aggregates were locally sourced and available in the concrete laboratory at UCT.

3.2.1 CEM II/A-L 52.5 N from AfriSam

Two samples of CEM II/A-L 52.5 N, from different batches, were received at UCT. A first batch ('Old-CEM II') was received in May 2019 from AfriSam Ulco factory. However, due to limiting factors beyond control, it was not possible to utilize this cement within a reasonable period and so there was concern that its quality might have deteriorated. The factors included delays in receiving, grinding, and calcining kaolinite clay samples and the prominent lockdown due to the outbreak of Covid-19 in 2020. In view of this, new bags ('New-CEM II') were requested from the same factory and received in October 2020. The old CEM II had about 7% LS and the New CEM II had about 4% LS (Appendix I compares

the two cements). The old CEM II was only used for preliminary checks (presented in Section 5.2.1.1) and the New CEM II was used for the rest of the work.

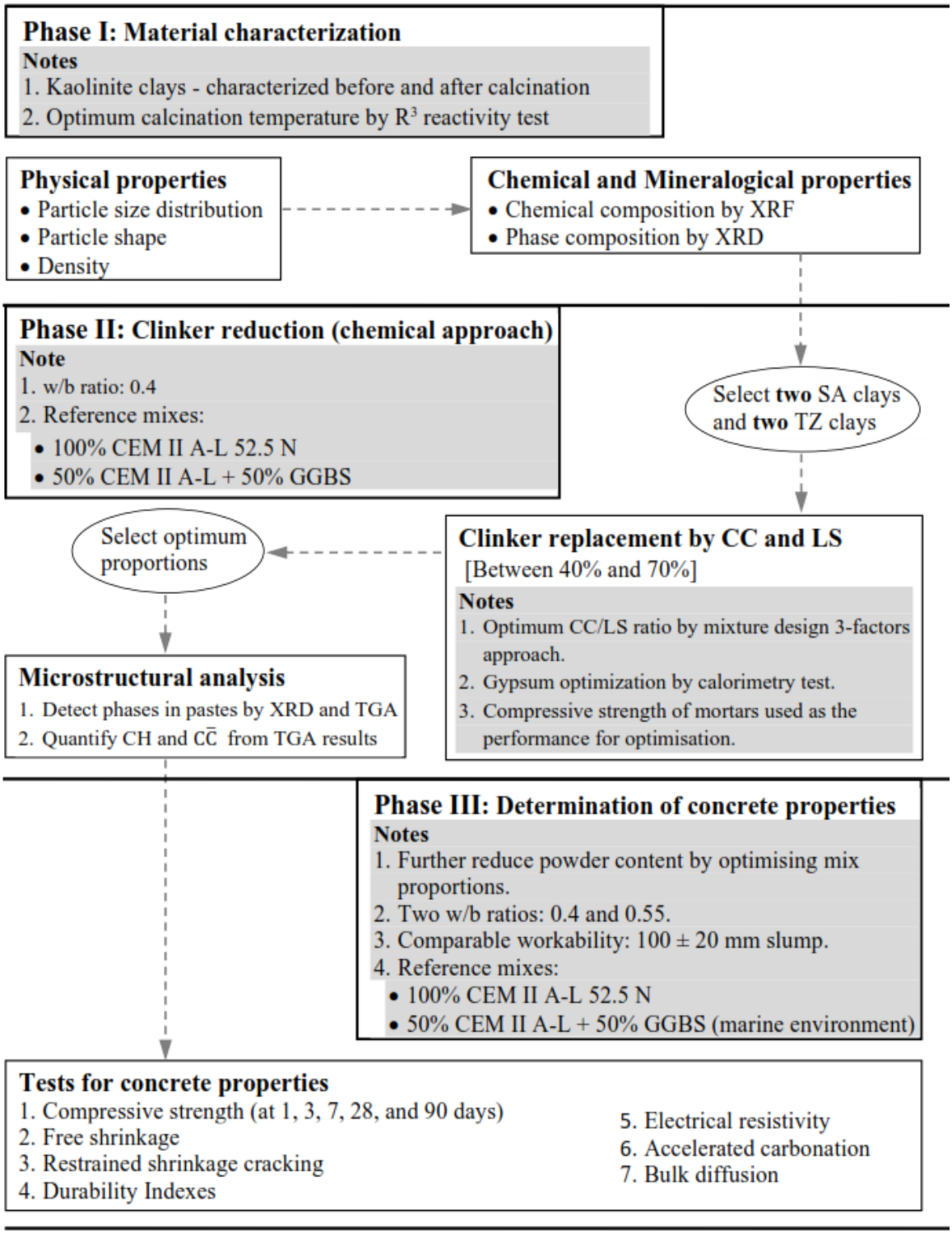

Figure 3.1: Schematic of experimental research methodology

3.2.2 Samples of clay

A beneficiated sample of G-Clay, graded as Kaolin A, was supplied to the University of Cape Town (UCT) by Serina Trading, a sample of B-Clay was supplied by the owner of the deposit, a beneficiated sample of H-Clay by Kaolin-group, and HC-Clay by HeidelbergCement Tanzania.

There are two types of kaolinite clay at the Pugu deposits, Hard clay (PH-Clay) and Soft clay (PS-Clay), and both were sourced directly from the deposit.

G-Clay was beneficiated (by Serina Trading) to produce a clean, off-white, low iron, and high alkali product and H-Clay was beneficiated to increase kaolinite content.

For preliminary checks, small samples of uncalcined and flash-calcined H-Clay (Old H-Clay) produced on a laboratory scale were delivered to UCT. About 18 months later, samples of uncalcined and flash-calcined H-Clay (New H-Clay) produced on an industrial scale were delivered to UCT for further work.

The Tanzania clays were hammer-crushed to get particle sizes less than 1 mm for transportation to Cape Town, and at UCT a few grams were sieved through a 45 µm sieve for the R^3 reactivity test (Avet et al., 2016; Li et al., 2018) and micronised for chemical analysis.

Figure 3.2 shows photos of the samples of uncalcined clays.

3.2.3 Fine and coarse aggregates

Two types of fine aggregates (i.e., Philippi dune sand and crushed granite sand), and one coarse granite aggregate with nominal size of 19 mm, were used. However, for the restrained shrinkage test, a 13 mm granite stone (instead of 19 mm size) was used as recommended by ASTM C 1581-18a (2009).

The granite aggregates were obtained from AfriSam and sourced from their Malmesbury Rheebok quarry; dune sand was sourced from Cape Flats area in the Cape Peninsula. The characteristics of these aggregates are presented in Table 3.2

B-Clay
Light brown

PH-Clay
Pearl

H-Clay
White

PS-Clay
Pearlish white

G-Clay
Pinkish white

HC-Clay
Red

Figure 3.2: Photos of the samples of uncalcined clays

3.3 Grinding of clays

After determining the suitability of each clay for clinker replacement (Section 4.2), four clays were selected for further work: B-Clay and H-Clay from South Africa, and PH-Clay and HC-Clay from Tanzania (details in Chapter 4). Milling of these clays was undertaken at Cermalab Materials Testing Laboratory in Pretoria. Dry milling was carried out in a 400 mm diameter polypropylene mill jar using alumina balls (< 40 mm diameter) at a rotational

speed of 40 rpm. 5 kg of sample was milled at a time. With the B-Clay, it was possible to obtain particle sizes with d_{90} = 16.5 µm and d_{50} = 5.9 µm after dry milling for one hour. It was then decided to grind HC-Clay and PH-Clay to get particle sizes similar to B-Clay. But because of the high amount of quartz in HC-Clay and PH-Clay compared to B-Clay, it was only possible to archive d_{90} < 30 µm and d_{50} < 10 µm after 2 hours dry milling and 4 hours wet milling, respectively. H-Clay was used as received from the supplier. The PSD curves are shown in Figure 3.4.

3.4 Calcination of clays

As pointed out in Section 2.7, calcination of kaolinite clays is important to make them reactive. All samples of clay were found to be most reactive when calcined at 800°C for one hour using an electric kiln (Figure 3.3) for firing commercial ceramics (more details in Section 3.5.1). The H-Clay received from Kaolin group had already been flash-calcined at 850°C. However, reactivity test results showed that the flash-calcined H-Clay sample and H-Clay sample calcined at 800°C using electric kiln have approximately the same reactivity (see Section 4.3). This similarity was also noted by Salvador (1995) and Scrivener et al. (2019). In view of this, it was decided to calcine all selected clay samples at 800°C using an electric kiln. The electric kiln (Figure 3.3) could calcine about 20 kg of clay at a time. Clay bowls were used to contain the clay samples during calcination as shown in Figure 3.3.

Figure 3.3: Kiln used to calcine sample of clays, also showing the clay bowls containing the clays to be calcined.

3.5 Material characterisation

Characterisation of materials was done to determine their physical and chemical properties and evaluate their influence on the properties of both fresh and hardened concrete. All samples of clay were milled as described in Section 3.3 except H-Clays which were used as received from the supplier. At all times, samples were stored in water-vapour-tight containers. Before carrying out measurements, all samples of clay were dried at 200°C for 24 hours to remove moisture. Kaolinite clays were characterised before and after calcination in order to evaluate the changes in properties resulting from calcination.

3.5.1 Reactivity test

As described in Section 2.7, for the kaolinite clay to be reactive to break down and produce an amorphous material for pozzolanic reactivity, calcination between 700 and 850°C is necessary (Fernandez, Martirena and Scrivener, 2011). The aim of the reactivity test was to find the optimum calcination temperature of each clay. In view of this, it was decided to test the reactivity of the samples of clay (particle size d_{90} < 45 µm) calcined at 750, 800 and 850°C. Reactivity was assessed using the R^3 bound water test (described in Section 2.6). The bound water (%) in the R^3 paste was calculated based on the mass loss of sample heated between 105°C and 350°C (Li et al., 2018). Table 3.1 presents the materials used for this test and their proportion.

Table 3.1: Material used for the R^3 bound water test

Material	CC	CH[a]	Deionised Water	KOH[a]	K_2SO_4[a]	LS-K5
Mass (g)	11.11	33.33	60.00	0.24	1.2	5.56
[a] Lab grade						

3.5.2 Particle size distribution of materials

The particle size distribution (PSD) of the cementitious materials was determined by laser diffraction analysis using Malvern Mastersizer 2000. For the aggregates, sieve analysis was used as per (SANS 201:2008). With the Malvern Mastersizer 2000, cement was dispersed in ethanol, whereas clays and LS-K5 were dispersed in distilled water. Since Mastersizer uses Mie theory to calculate particle size, the test involves defining optical properties of the material i.e., refractive index and absorption index. Refractive indexes chosen for the

clays, LS, GGBS and cement, were 1.55, 1.60, 1.64 and 1.68, respectively and the absorption values chosen were 0 for the clays and 0.1 for the cement, GGBS and LS (Instruments, 2000, 2007; Jewell and Rathbone, 2009). To reduce agglomeration of particles, for the clays and LS-K5, samples were first mixed with Sodium Hexa-metaphosphate (about 1:10 ratio) then added to the dispersion tank until the obscuration level was within the recommended range (10 – 20%). A good fit between the measured data and calculated data was indicated by a residual value below 1%. The PSD curves are shown in Figure 3.4. PSD values (d_{10}, d_{50}, and d_{90}) of all the cementitious materials and the fineness modulus (FM) of aggregates are presented in Table 3.2.

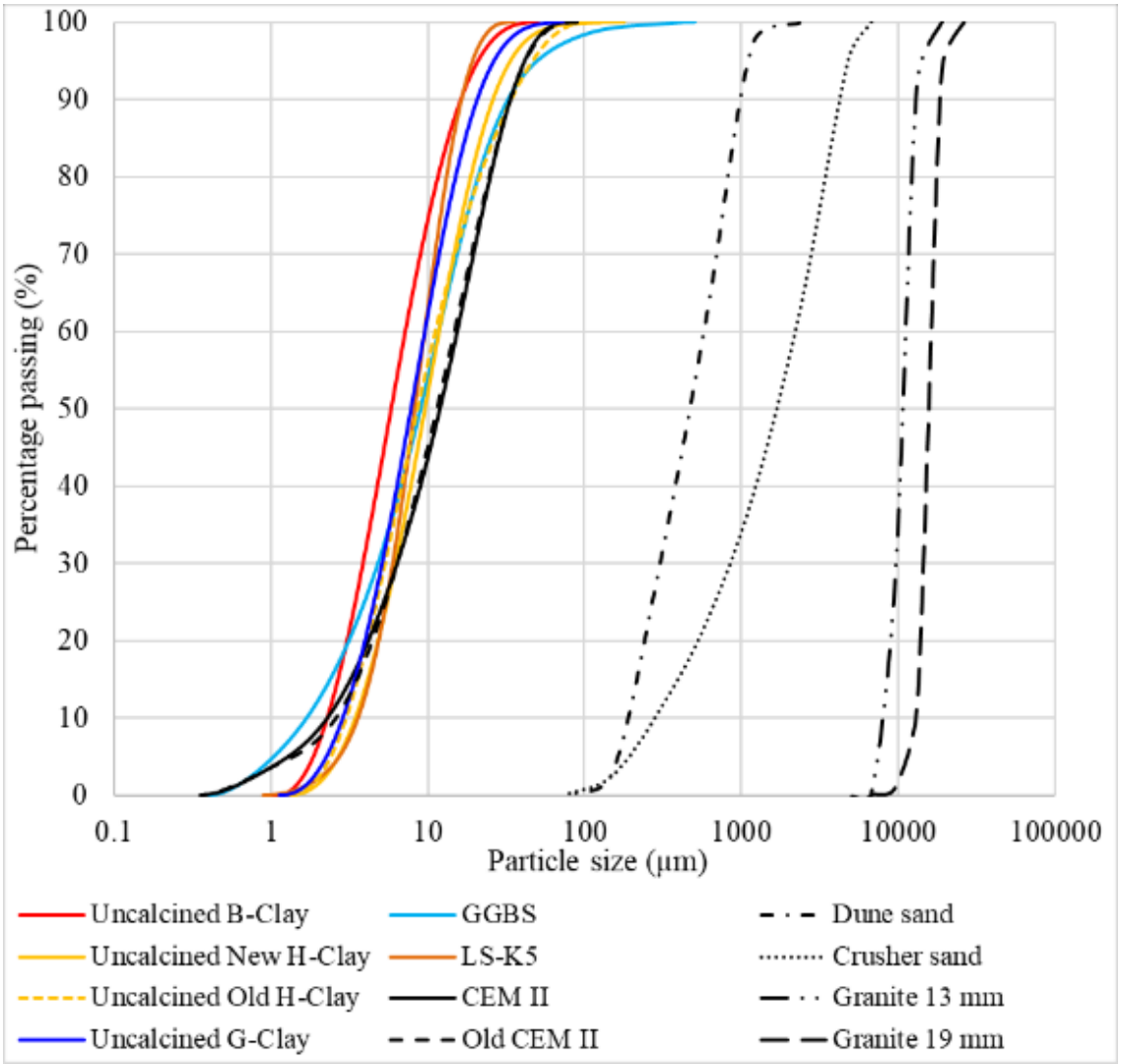

Figure 3.4: PSD curves of uncalcined clays, cement, GGBS, LS-K5, and aggregates (See also Table 3.2)

3.5.3 Densities of materials

The relative density (RD) of the clays, GGBS and LS-K5 were determined as per BS 1377-2: 1990. The compacted bulk density (CBD) of aggregates was determined following the procedure given in SANS 5845:2006. The results are presented in Table 3.2.

Table 3.2: Characteristics of materials received at UCT

Material name	RD	d_{10} (µm)	d_{50} (µm)	d_{90} (µm)	FM	CBD (kg/m^3)
Uncalcined B-Clay	2.61	2.3	5.9	16.5	-	-
Uncalcined Old H-Clay	2.67	3.0	8.9	33.9	-	-
Uncalcined New H-Clay	2.67	3.5	9.6	26.0	-	-
Uncalcined G-Clay	2.66	2.9	7.8	20.7	-	-
Uncalcined PH-Clay	2.66	Crushed in Tanzania to				
Uncalcined PS-Clay	2.64	get particle sizes < 1 mm			-	-
Uncalcined HC-Clay	2.73	for transportation				
LK-K5	2.70	3.6	8.2	16.4	-	-
GGBS	2.90	1.7	9.0	32.3	-	-
Old-CEM II	2.96	2.6	11.4	33.5	-	-
New-CEM II	2.96	2.3	11.9	33.5	-	-
Dune sand	2.64	-	-	-	2.09	-
Crushed sand (granite)	2.65	-	-	-	3.67	-
Granite 13 mm	2.65	-	-	-	7.80	1540
Granite 19 mm	2.65	-	-	-	8.93	1560

3.5.4 BET Surface area of the selected clays

The surface area of the clays was estimated by the nitrogen adsorption/desorption method using an automated gas adsorption analyser (TriStar II 3020) at -196°C. The surface area is estimated based on the N_2 adsorbed on the surface of the clay including the ISA of the clay. About 0.5 g of each sample was loaded into a glass tube with a small bulb at the end to hold the sample. Before measurement, all samples were degassed overnight at 200°C to completely remove moisture and any adsorbed gas present in the sample that would otherwise interfere with the analysis. The surface area of the samples was estimated using the Brunauer-Emmet-Teller (BET) equation in the relative pressure (P/P_o) range of 0.05 to 0.2 kPa where P is the equilibrium gas pressure and Po is the saturated pressure. The BET surface area indicates the magnitude of the ISA of one clay relative to the other, especially if the clays have similar particle size distributions (Heller-Kallai, 2006). The results of the selected clays are summarised in Table 3.3. From the results, HC-Clay has the highest ISA

compared to other clays and H-Clay has the lowest ISA. So, in this case, it was expected that a mix with HC-Clay to demand more water or more SP to get similar workability.

Table 3.3: BET surface area of the selected clays before calcination

Sample Name	BET Surface area (m^2/g)
Uncalcined B-Clay	12.6
Uncalcined H-Clay	5.4
Uncalcined PH-Clay	14.4
Uncalcined HC-Clay	45.8

In general, kaolinite clays differ worldwide, and two or more clays may have similar PSDs and mineralogical composition but different ISAs. The reason might be the crystal quality of the kaolinite particles, those that are well crystallized have smaller surface area than the poorly crystallized kaolinite clays as reported by Murra and Lyons (1960). For instance, one of the clays presented in Tironi et al. (2015) and Nguyen, Afroz and Castel (2020) had PSD similar or slightly coarser compared to the H-Clay presented in this work but their BET surface areas are higher compared to that of H-Clay. Likewise, the clays presented by Anil, Mohan Misra and Misra (2018) had similar PSD but different BET surface areas or sometimes those with coarser PSD have higher BET surface area compared to those with finer PSD, as in Akindahunsi, Avet and Scrivener (2020). The physical properties of the clays, before and after calcination, are presented and discussed in Section 4.4.

3.5.5 Chemical composition of cementitious materials

Chemical compositions of all the cementitious materials were obtained using a Panalytical Axios wavelength dispersive XRF spectrometer. Major oxides (except H_2O and LOI) were measured on fused discs prepared from ignited powders. H_2O- represents mass loss upon heating the sample at 110°C for 12 hours. The Loss on ignition (LOI) was determined by heating samples to 800°C for 4 hours. The results for the cementitious materials are presented in Table 3.4 and Table 3.5. As described in Section 2.7.1, XRF results can give an indication if a clay is suitable for producing LC^3 binders (A. A. Díaz et al., 2018). This is discussed in Section 4.2.1. In addition, the changes in the chemical composition brought by the calcination are presented and discussed in Section 4.4.1.3.

Table 3.4: Chemical composition of uncalcined clays

Oxides (%)	Uncalcined clays						
	B-Clay	Old H-Clay	New H-Clay	G-Clay	PH-Clay	PS-Clay	HC-Clay
SiO_2	51.52	62.63	60.30	68.53	65.98	70.11	60.94
TiO_2	1.57	1.35	0.97	0.77	0.98	0.39	0.93
Al_2O_3	31.59	20.95	24.21	20.58	22.60	19.79	21.41
Fe_2O_3	1.14	1.60	1.67	0.52	0.71	0.65	7.39
MnO	0.07	0.01	0.01	0.00	0.01	0.01	0.16
MgO	0.46	0.83	0.90	0.27	0.27	< 0.01	0.17
CaO	1.64	0.03	0.02	< 0.01	0.03	< 0.01	0.27
Na_2O	0.25	1.21	0.73	0.38	0.17	0.37	0.23
K_2O	0.35	2.35	2.54	2.74	0.06	0.20	0.55
P_2O_5	0.12	0.03	0.02	0.02	0.01	0.02	0.02
SO_3	0.06	0.01	< 0.01	< 0.01	<0.01	0.01	< 0.01
Cr_2O_3	0.02	0.01	0.01	0.01	0.01	< 0.01	0.01
NiO	0.01	0.01	0.01	0.01	0.00	< 0.01	0.01
H_2O-	0.08	0.03	0.04	0.06	0.09	0.17	0.02
LOI	11.00	8.25	7.48	5.15	8.63	7.61	7.53
Total	99.87	99.30	98.92	99.01	99.53	99.31	99.62
Na_2O_{eq}.	0.48	2.76	2.41	2.18	0.21	0.50	0.60

Table 3.5: Chemical composition of cement, GGBS, and LS-K5

Oxides (%)	Old-CEM II	New-CEM II	LS-K5	GGBS
SiO_2	19.61	20.49	0.57	35.06
TiO_2	0.21	0.24	0.00	0.68
Al_2O_3	4.03	4.21	0.07	15.59
Fe_2O_3	1.97	2.21	0.00	0.78
MnO	1.48	1.09	0.00	0.70
MgO	2.77	1.99	1.74	8.42
CaO	62.40	63.69	54.61	36.90
Na_2O	< 0.01	< 0.01	< 0.01	0.24
K_2O	0.46	0.42	0.01	0.67
P_2O_5	0.06	0.05	0.01	0.02
SO_3	2.07	2.00	0.02	1.93
Cr_2O_3	< 0.01	0.01	< 0.01	< 0.01
NiO	0.01	0.01	< 0.01	0.01
H_2O-	0.10	0.10	0.02	0.01
LOI	4.43	3.07	43.12	-1.24
Total	99.53	99.44	99.97	99.77
$Na_2O_{eq.}$	0.30	0.27	< 0.01	0.68

3.5.6 Mineralogical composition of the materials

X-Ray Diffraction (XRD) and Thermogravimetric analysis (TGA) were used to determine the mineralogical composition of the cementitious materials.

XRD measurements were obtained using a Bruker D8 Advance Powder Diffractometer with Vantec detector, fixed divergence and receiving slits with Co-Ka radiation in the 2θ range of 5° to 80° at a scan speed of 1 second per step. The phases were identified using Bruker Topas 4.1 software and the relative phase amounts were estimated using the Rietveld method.

An SDT 650 TA instrument was used to investigate thermal behaviour of the clays. Thermogravimetric measurements were taken from room temperature to 1000ºC, at a heating rate of 10 ºC/min, using alumina crucibles with no lids under a 30 ml/min flow of nitrogen gas. The mass change over the kaolinite-dehydroxylation interval (Equation 3.1) was used to estimate the kaolinite content of the clay. The optimum calcination temperature of clays was decided based on the information available in the literature, the TGA results and the results of the R^3 bound water test. In general, all selected clays consist mainly of kaolinite, quartz, and illite with an optimum calcination temperature of 800°C (more details in Chapter 4).

3.6 Optimisation of mix proportions of LC^3 binders

To reduce the amount of materials for the research, the compressive strength of mortars (from cubes of 50 mm size) was used as the performance parameter for optimisation of binder proportions. A w/b ratio of 0.4 was used (same as for the concrete work). A mix with 100% CEM II/A-L 52.5 N was considered as a reference mix. LC^3 mixes with clinker levels in the range of 40 to 70% were decided by considering suitable ratios to combine calcined clay and limestone, obtained using the mixture design 3-factors approach (Cornell, 2002; Lawson and Willden, 2016). In this approach, the simplex shape is a triangle with lower boundaries as described in Figure 3.5. At 70% clinker content, the lower boundaries for calcined clay and limestone (assumed 2:1 ratio) are 20% and 10%, respectively. With these three lower boundaries (i.e., 40% clinker, 20% CC, and 10% LS), the hatched area shown in Figure 3.5 becomes the ‘area of interest’ or the mixture design region (more details in Section 5.2). The corresponding upper boundaries (i.e., 50% CC, and 40% LS)

are also indicated in Figure 3.5. To make sure that the main factors controlling the reactions are clinker, calcined clay and limestone, small amounts of gypsum and NaOH were added to have the same amounts of SO_3 and Na_2O_{eq} in all the mixes as described Section in 3.6.1 (more details in Section 5.2.1).

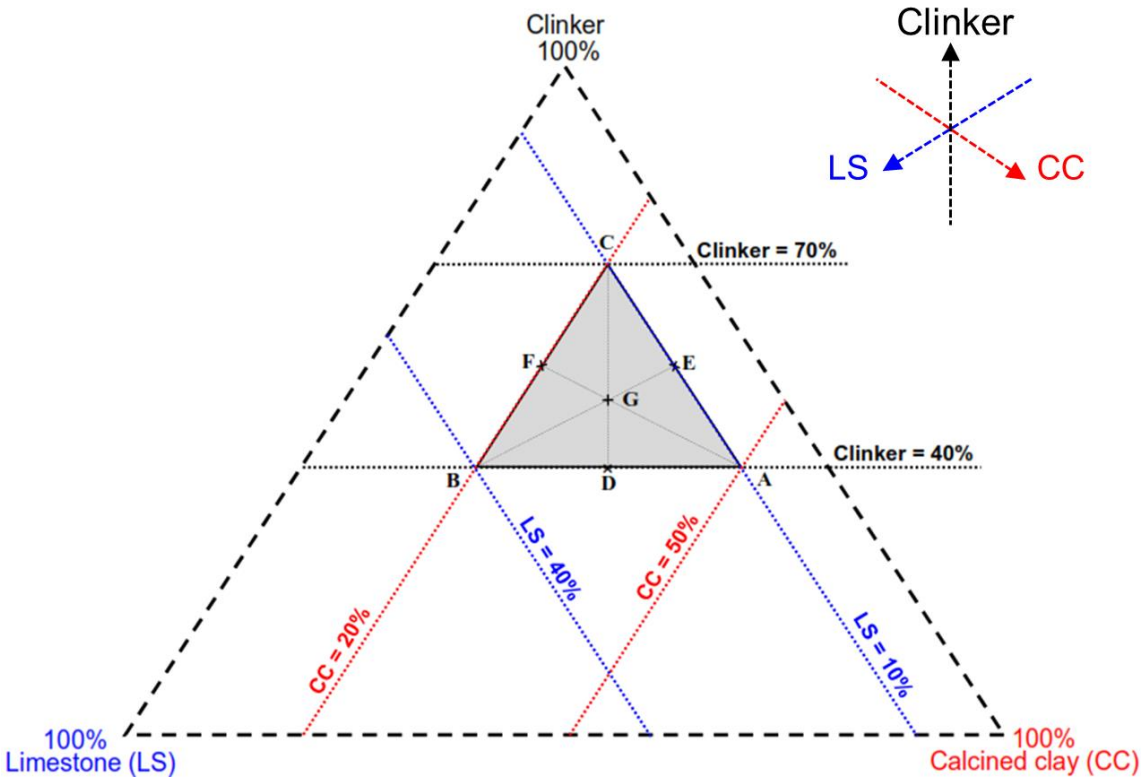

Figure 3.5: Mixture space with boundaries

3.6.1 Sulphate and alkali adjustment

As indicated in Section 2.8.1, LC^3 mixes require adjustment of sulphate and alkali contents. Sulphate content is adjusted due to the filler effect of the added SCMs (i.e., CC and LS) which accelerates silicate and aluminate reactions, and as a result more SO_3 gets adsorbed by C-S-H (Zunino and Scrivener, 2019, 2020a). The target was to ensure that the aluminate reaction peak occurs shortly after the silicate reaction peak and between 13 and 18 hours (window selected for optimisation purposes). In this work, the sulphate was adjusted by studying heat of hydration (HoH) curves of the LC^3 pastes during the first 24 hours of hydration. This was done using an I-Cal 2000 HPC Isothermal calorimeter (2-channels) at 20°C. Pastes were produced with a w/b ratio of 0.4. To ensure comparable workability, superplasticizer (Chryso® optima 175) was added in all the pastes (maximum 0.2 wt.% of

total solid mass). The pastes were mixed using an electric hand mixer for 2 minutes. 20 g of pastes were then poured in vials, sealed, and placed in the calorimeter. The alkali content was adjusted to increase early-age strength. Based on the literature, the required Na_2O_{eq} for the LC^3 mixes is between 0.6 and 0.8% (Antoni, 2013). Consequently, 0.7% was selected.

3.7 Identification and quantification of hydration products

The aim was to study the hydration products of the selected LC^3 mixes (with different CC) at different ages and compare between themselves and with the reference mix 1 (R1). For each clay, the optimum proportion (obtained from the compressive strength optimisation work using mortar cubes) and a w/b ratio of 0.4 was used. Paste discs of approximately 2.5 mm thick and 24 mm diameter were prepared (Figure 3.6). The pastes were then tightly covered with plastic up to 24 hours. To minimize carbonation while in the mould, the pastes were stored in an air-tight plastic vessel filled with saturated solution of calcium hydroxide (CH) (Figure 3.7) until the age of testing.

The hydration products at various ages were characterised using TGA and XRD. At each age (i.e., 1, 3, 7, 28 and 90 days) of the paste, XRD was used to detect different phases in the specimens and TGA was used to quantify CH and $C\overline{C}$ at different ages of the specimens. These techniques have been used in numerous studies to study hydration products of different mixes. Hydration stoppage was done using the solvent exchange approach described in Section 3.7.1. Details on sample preparation, test protocols and precautions are well documented in (Scrivener, Snellings and Lothenbach, 2018) and will thus not be repeated here.

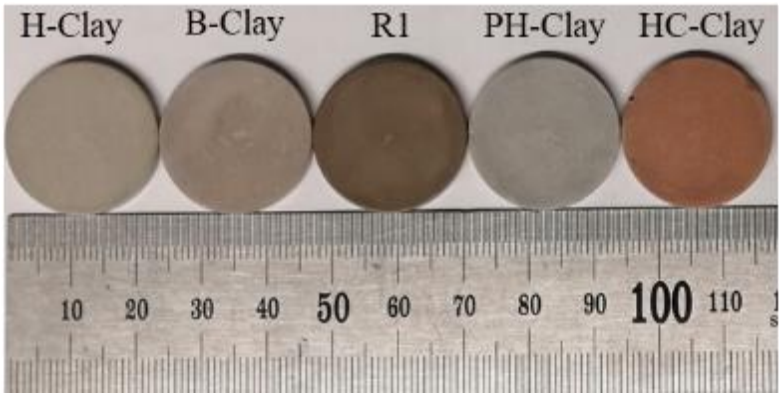

Figure 3.6: Paste discs prepared for TGA and XRD

Figure 3.7: Storage of paste specimens for TGA and XRD

3.7.1 Hydration stoppage

Hydration stoppage for TGA and XRD samples was carried out by a solvent exchange method, following the procedure recommended by Snellings et al. (2018). For TGA, prepared paste discs were gently crushed (at the different ages) to have particles less than 1 mm. For XRD, the smooth faces of the paste discs were scanned. At each age, all samples were immersed in isopropanol (> 95% purity) for 15 minutes, rinsed by diethyl ether (99% purity) to slow down solvent evaporation, dried at 40°C in a ventilated oven for 8 minutes and tested within 30 minutes after oven drying.

3.7.2 Detection and quantification of phases

TGA and XRD were used to detect hydrated phases in the cementitious pastes. This was mainly done to assess and compare the amount and number of phases in the mixes. TGA was specifically used to quantify unreacted CH and $C\overline{C}$ in the mixes; this is because in cementitious systems, it is only these two phases that lose mass at specific ranges of temperature. CH dehydroxylates between 350°C and 500°C whereas $C\overline{C}$ decomposes between 600°C and 800°C due to the release of CO_2. The mass loss of other phases (i.e., C-S-H, AFm and AFt phases) overlap between 50°C and 350°C, which makes quantification of individual phases by TGA difficult.

The mass loss of CH and $C\overline{C}$ was estimated using the tangential method (Scrivener, Snellings and Lothenbach, 2018) as illustrated in Figure 3.8 and Equation 3.1 where 74.09,18.02,100.09 and 44.01 g/mol are the molecular masses of CH, H_2O, $C\overline{C}$ and CO_2 respectively. The tangential method unlike the stepwise method does not include mass loss of C-S-H and other phases which also dehydroxylate slightly after 350°C. Based on the

results obtained, CH was estimated between 400°C and 500°C, $C\overline{C}$ between 650°C and 800°C and the water bound to hydrates (C-S-H, AFm, AFt and CH) was estimated based on the mass change between 105°C and 500°C.

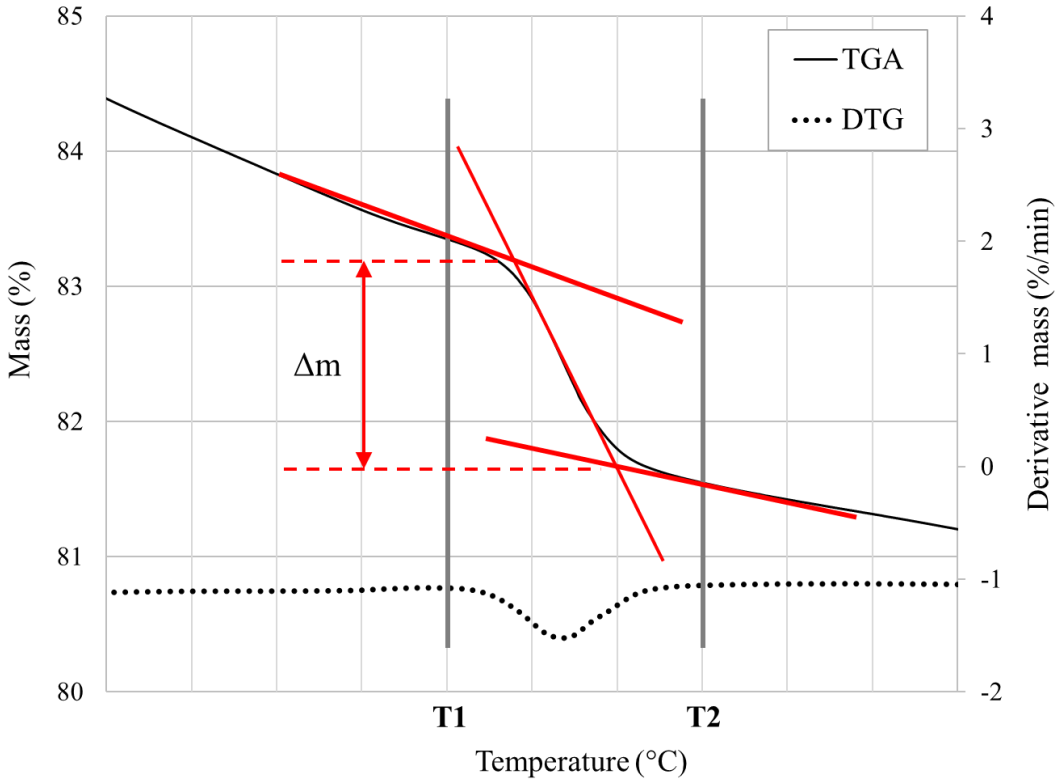

Figure 3.8: Schematic of the tangent method

$$m_{CH} = \Delta m_H \cdot \frac{74.09}{18.02} \quad \text{and} \quad m_{C\overline{C}} = \Delta m_{CO_2} \cdot \frac{100.09}{44.01} \qquad \text{--- (3.1)}$$

Where; m_{CH} = mass of CH in the paste

$m_{C\overline{C}}$ = mass of $C\overline{C}$ in the paste

Δm_{CO_2} = Change of mass due to the decomposition of $C\overline{C}$

Δm_H = Change of mass due to the dehydroxylation of CH

3.8 Determination of fresh and hardened properties of concrete

Using the selected replacement levels and proportion of materials obtained from Phase II (see Chapter 4), concrete mixes were prepared to determine their fresh and hardened properties. Initially, a commercial software named Elkem Materials-Mixture Analyser

(EMMA) (Hanssen, 2012) was used to optimise packing of materials. All mixes were optimized by adjusting the quantity of the materials while maintaining the required proportions of binders and w/b ratios. The obtained proportions were then adjusted based on trial mixes, and the target was to get a comparable workability with a slump of 100 ± 20 mm and a superplasticizer (Chryso@ Optima 175) dosage limit of 1.5%.

Two reference mixes were considered: A mix with 100% CEM II/A-L 52.5 N, and a recommended mix for South African marine environments with 50% cement replaced by GGBS. For each clay, three LC^3 proportions were selected (see Section 5.2.2.4). Two water/binder (w/b) ratios of 0.4 and 0.55 were selected, 0.4 to represent a relatively high-performance concrete for marine environment class XS3 (EN 206, 2013) and 0.55 on selected mixes to represent medium quality concrete which can be used in common construction projects.

Tests that were carried out included workability, free shrinkage, restrained shrinkage cracking, compressive strength at 1, 3, 7, 28 and 90 days, Durability Indices, bulk diffusion, and accelerated carbonation. In addition, electrical resistivity measurements were conducted to assess and compare the risk of corrosion damage. For each test, the results are reported as an average of the result of three samples/specimens tested and, in all cases, the results of LC^3 mixes are presented in comparison with the results of the reference mixes.

3.8.1 Workability

For concrete, a slump test as per SANS 5862-1:2006 was used whereas for mortar, a flow test as per SANS 5862-2:2006 was used. To ensure comparable workability, superplasticizer (Chryso® optima 175) was added in all the mixes (maximum 1.5 wt.% of total mass of cementitious materials) to maintain a slump of 100 ± 20 mm for the concrete and a flow of 145 ± 15 mm for mortars.

3.8.2 Free shrinkage test

The test was conducted following the procedure given in ASTM C 157. The size of the mould used was slightly different from the one specified in the standard. This test was conducted on 75 mm x 75 mm x 280 mm concrete prism specimens instead of 75 mm x 75 mm x 285 mm size given in the standard, which is considered to have no influence on the

test results. At all times, all specimens were cured for 28 days in lime-saturated water and then exposed in an environmental room maintained at 23 ± 2.0°C and relative humidity of 50 ± 4%, Figure 3.9. Measurements (i.e., change in length) were taken using a length comparator (Figure 3.10). For each specimen, the initial reading was taken after 28 days of curing. Further readings were taken up to 224 days after curing. During each measurement, the masses of the specimens were also recorded.

Figure 3.9: Free shrinkage specimens

Figure 3.10: Shrinkage measurement using the length comparator

3.8.3 Ring test (restrained shrinkage)

The restrained shrinkage test was performed in order to evaluate and compare the potential for shrinkage-induced early-age cracking of the LC^3 mixes versus the reference mixes. Early-age cracking offers access for aggressive agents which may affect the durability and service life of the structure. The specimens were prepared using the principles given in ASTM C1581-18a (2018). The mould used (Figure 3.11) and testing procedure differ slightly from the one specified in the standard. In this case, the outer diameter of the ring was 400 mm, and the inner diameter was 323.8 mm, slightly different compared to the outer diameter of 402 mm and inner diameter of 327 mm specified by the standard. Also, instead of strain gauges and data acquisition systems, a crack meter and/or crack ruler were used to estimate the crack width on the surface of the concrete.

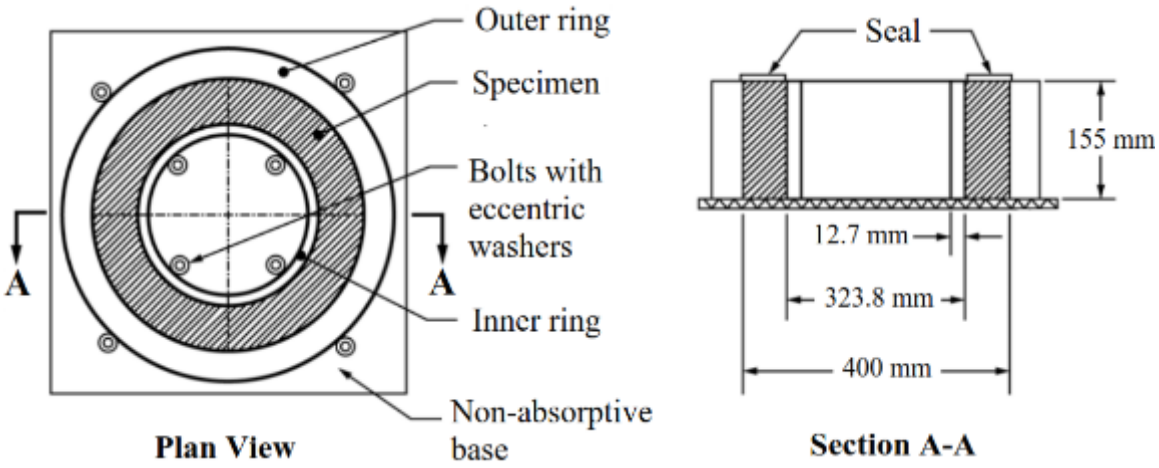

Figure 3.11: Ring test specimen mould (from ASTM C1581-18a (2018))

After casting, the specimens were covered with plastic sheets and left in their mold for the first 24 hours. After 24 hours, the outer wall of the mold was removed, and the specimens were further covered with wet burlaps for 6 more days. To ensure proper curing, the burlaps were wetted after every 12 hours during the curing periods. After curing, the top surface of the specimens was then covered with paraffin wax so that drying happened only on the outer circumferential surface. The specimens were then monitored (with the help of a magnifying glass) for the occurrence of the first crack after every 12 hours.

Figure 3.12 shows the photo of the concrete ring specimens placed in an environmental room maintained at 23 ± 2.0°C and relative humidity of 50 ± 4%. The age at cracking was

recorded to the nearest day. The specimens were then monitored for the appearance of the second crack and the increase of the crack width was measured up to the age of 90 days. The crack widths were estimated as an average of the three-crack width measured near the top, mid-height and at the bottom of the cracks.

Figure 3.12: Concrete ring specimens

3.8.4 Compressive strength test

For each mix, concrete cubes were prepared for assessing the development of compressive strength. Concrete cubes of 100 mm size and a maximum aggregate size of 19 mm were used. However, to reduce the amount of materials for the research, mortar cubes of 50 mm size and a 50:50 blend of granite crusher sand (maximum size 4.75 mm) and dune sand were used for LC^3 proportion optimisation purposes. After casting, all specimens were cured in a water tank until tested at 1, 3, 7, 28 and 90 days. The concrete cubes were tested as per SANS 5863 (2006) using an INSTRON 1000RD-E4-H2 hydraulic dynamic testing machine whereas the mortar cubes were tested following guidelines given in ASTM

C109/C109M-20b (2020) using the same machine. Specimens were loaded without shock until failure at a uniform rate of 0.3 MPa/s for concrete cubes and 0.36 MPa/s for mortar cubes. The results are reported as an average of the result of three specimens tested.

3.8.5 Static elastic modulus test

The static elastic modulus test was conducted according to the principles of BS 1881 (1983) using an INSTRON 1000RD-E4-H2 testing machine. For each mix, three concrete cylinders of 200 mm height and 100 mm diameter were prepared. After casting, all specimens were cured in a water tank until tested at 7, 28 and 90 days. Each specimen was centrally positioned between the compressive test machine platens. Loads cycles (at a uniform rate) up to 10 MPa were applied to each specimen, and stress-strain curves were obtained from which the modulus of elasticity was determined.

3.8.6 Durability index tests

The three durability index tests i.e., Oxygen Permeability Index (OPI), Water Sorptivity Index (WSI), and Chloride Conductivity Index (CCI), as well as a porosity test were done to assess and compare the resistance of LC^3 specimens versus reference specimens to penetration of gases, liquid, and ions. Specimens were prepared and tested following procedure and testing conditions given in SANS 3001-CO3-1:2015, SANS 3001-CO3-2:2015 and UCT DI Manual (Alexander & Otieno, 2018). Eight concrete specimens, each 70 mm diameter and 30 mm thickness were prepared for each mix, four specimens for the CCI test and four other specimens for the OPI, WSI and porosity test.

The CCI test assesses the resistance of concrete to penetration of ions based on electrical conductivity. A CCI value less than 1.0 mS/cm is generally considered to represent good to excellent resistance to ingress of chloride ions. The OPI test involves measuring pressure decay of oxygen passing through the specimen of 30 mm thick. Typical OPI values, on a log scale, range between 8 to 11 where a higher OPI value indicates lower permeability implying higher resistance to penetration of deleterious gases such as CO_2. Following the OPI test and subsequent sample preconditioning, the same specimens were tested for WSI and porosity. The WSI measures the rate of absorption of water through the specimen when only one face is exposed to water. Sorptivity values typically range from 5 mm/√hr to 15 mm/√hr, with lower values indicating better quality concrete. Water-penetrable porosity is

measured after the WSI test whereby specimens are soaked in water and vacuum-saturated for 18 hours to obtain the saturated mass of the specimen. Typical concrete porosity values vary from 8% to 15%, with lower values reflecting a denser pore structure and hence better-quality concrete.

3.8.7 Bulk diffusion test

This test was done to assess and compare chloride diffusivity in LC^3 concrete specimens versus reference concrete specimens. The test was carried out as per (ASTM C1556, 2016). The test involved having 100 mm cubes cured for 28 days, then cut into two slices, 20 mm, and 75 mm depth. The 20 mm slices were used to obtain initial chloride ion in the specimens. The remaining 75 mm pieces were then coated with epoxy (Sikadur@-32N) so that only one face was exposed to a 2.8 M NaCl solution at 23 ± 2.0°C and RH of 50 ± 4% for 180 days. This is done to allow natural transport of the chloride ions through the saturated exposed face of the specimen. After the exposure period, the specimens were sliced to have 6 concrete discs each of approximate 2 mm thick from the exposed face. The discs were then pulverized, and the powder obtained at each depth was used for estimation of chloride ion concentration at that particular depth as per the procedure given in ASTM C1152 (2020) and using Mettler Toledo auto titrator (Figure 3.13).

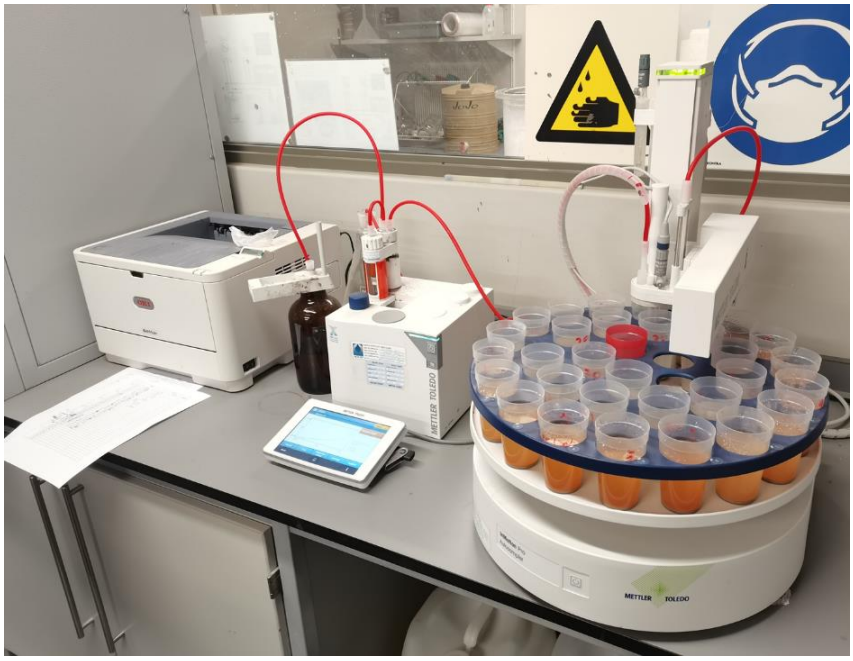

Figure 3.13: Mettler Toledo auto titrator used for chloride analysis

3.8.8 Resistivity measurement

This test was conducted to evaluate and compare the ability of the concrete specimens to resist penetration of chloride ions through measuring the resistance of concrete against the flow of electrical current (Tanesi and Ardani, 2012; Sengul, 2014; Ghosh and Tran, 2015; Lim et al., 2016). In general, this test reflects the interconnectivity of pores inside the concrete and is further influenced by pore chemistry and water saturation levels. Three cylindrical concrete specimens, 100 mm diameter and 200 mm height, were prepared for each mix. Measurements were done after 28, 56 and 90 days using Resipod 4-point Wenner probe resistivity meter from Proceq with fixed probes equally spaced 50 mm apart. For each specimen, measurements were taken at three different locations equally spaced around the circumference of the specimens and an average taken.

3.8.9 Accelerated carbonation test

In general, use of SCMs in concrete leads to a lesser amount of CH in the system which in turn lowers the carbonation resistance of concrete. However, it is important to note that this also depends on the resistance of the concrete to penetration of CO_2, which is influenced by the density of its microstructure and its permeability to gases. Two 100 mm concrete cube specimens were prepared for each mix. Testing was conducted as recommended by RILEM (1994).

To minimise the influence of the internal RH of the concrete on the rate of carbonation, specimens were wet cured for 28 days, and then dried in a room controlled at 20 ± 2.0°C and 50 ± 4% RH, until the rate of mass change per week was 0.1% or less. Specimens were then coated with epoxy (Sikadur$^{@}$-32N) leaving two opposite cast faces exposed to CO_2 ingress and left overnight to dry. Thereafter, specimens were placed in a carbonation chamber (Figure 3.14) controlled at (20 ± 2.0°C and 65 ± 4% RH) for 14 days before applying CO_2.

After preconditioning, while the specimens were still in the carbonation chamber, CO_2 was applied at a concentration of 2% as recommended by the fib Model Code for Service-life Design (2006). The carbonation depth was then assessed by spraying phenolphthalein indicator on the freshly cut surfaces of the concrete pieces (20 mm thick) sliced from the 100 mm concrete cubes specimens. The solution detects loss of alkalinity on the concrete

associated with carbonation by turning the non-carbonated concrete surface pink while carbonated surfaces remain colourless. The carbonated depth was measured on the cut surfaces using a Vernier calliper (to the nearest mm) after 24 hours from when the indicator solution was applied on the surface of the concrete. Results were obtained at 12 and 24 weeks after exposure to CO_2. Concrete cutting was done with the help of a sawing machine. To avoid redistribution of CH on the surface of the cut face, minimal water was applied during cutting.

Figure 3.14: Carbonation chamber

3.8.10 Summary

A detailed description of the research methodology and materials used in this study was presented in this chapter. The chapter began by giving details about the types of the selected materials, as well as their physical and chemical properties. The chemical approach used to optimise proportions of LC^3 mixes for best performance, including adjustment of sulphate and alkali content, was then presented. The chapter concludes by presenting the approach used to optimise a mixture of concrete materials, preparation of specimens as well as tests undertaken to study the performance of the mixes.

Chapter 4 Studies on selected clays

4.1 Introduction

Potential deposits of kaolinite clay in South Africa and Tanzania are given in Table 1.1. The selected samples of clay were sourced and supplied to UCT as reported in Section 3.2. Before undertaking the concrete work, it was important to assess the suitability of the clay samples for clinker replacement. This was done by determining and quantifying phases present in the clay samples and determining their reactivity. The changes in properties of the clay samples after calcination are also presented and discussed in this chapter. Before measurements, all samples of the clays were dried at 200°C for 24 hours to remove moisture.

4.2 Suitability of selected clays for clinker replacement

As indicated in Section 2.7.1, a suitable clay for clinker replacement is one with kaolinite content of 40% and above (Alujas et al., 2015; Avet et al., 2016; Avet, 2017; Maraghechi et al., 2018). The kaolinite content of the clay can be estimated from the results of TGA and by Quantitative-XRD measurements. Table 4.1 and Table 4.2 summarise the results from TGA and XRD measurements. The TGA and XRD curves are presented in Figure 4.1 and Figure 4.2, respectively.

The TGA curves show that there is a very little mass loss between room temperature and 200°C due to dehydration. The mass change between 400 and 600°C corresponds to the dehydroxylation of kaolinite and the formation of metakaolin as shown in Equation 4.1 (Shvarzman et al., 2003; Fernandez, Martirena and Scrivener, 2011; Snellings, Mertens and Elsen, 2012; Alujas et al., 2015). From these mass losses and the molecular weights of kaolinite and water, the percentage of kaolinite was estimated using Equation 2.5, and results are summarised in Table 4.3 (a typical example is shown in Appendix II). Loss of mass after 600°C is mainly related to the dehydroxylation of illite (Fernandez, Martirena and Scrivener, 2011). The mass gain after 850°C as seen on the TGA curve corresponds to the transformation of metakaolin to form spinel (Brown et al., 1985).

$$\underbrace{AS_2H_2}_{\text{Kaolinite}} \overset{400°C-\,600°C}{\rightleftharpoons} \underbrace{AS_2}_{\text{Metakaolin}} + 2H\uparrow \qquad \text{----} \qquad (4.1)$$

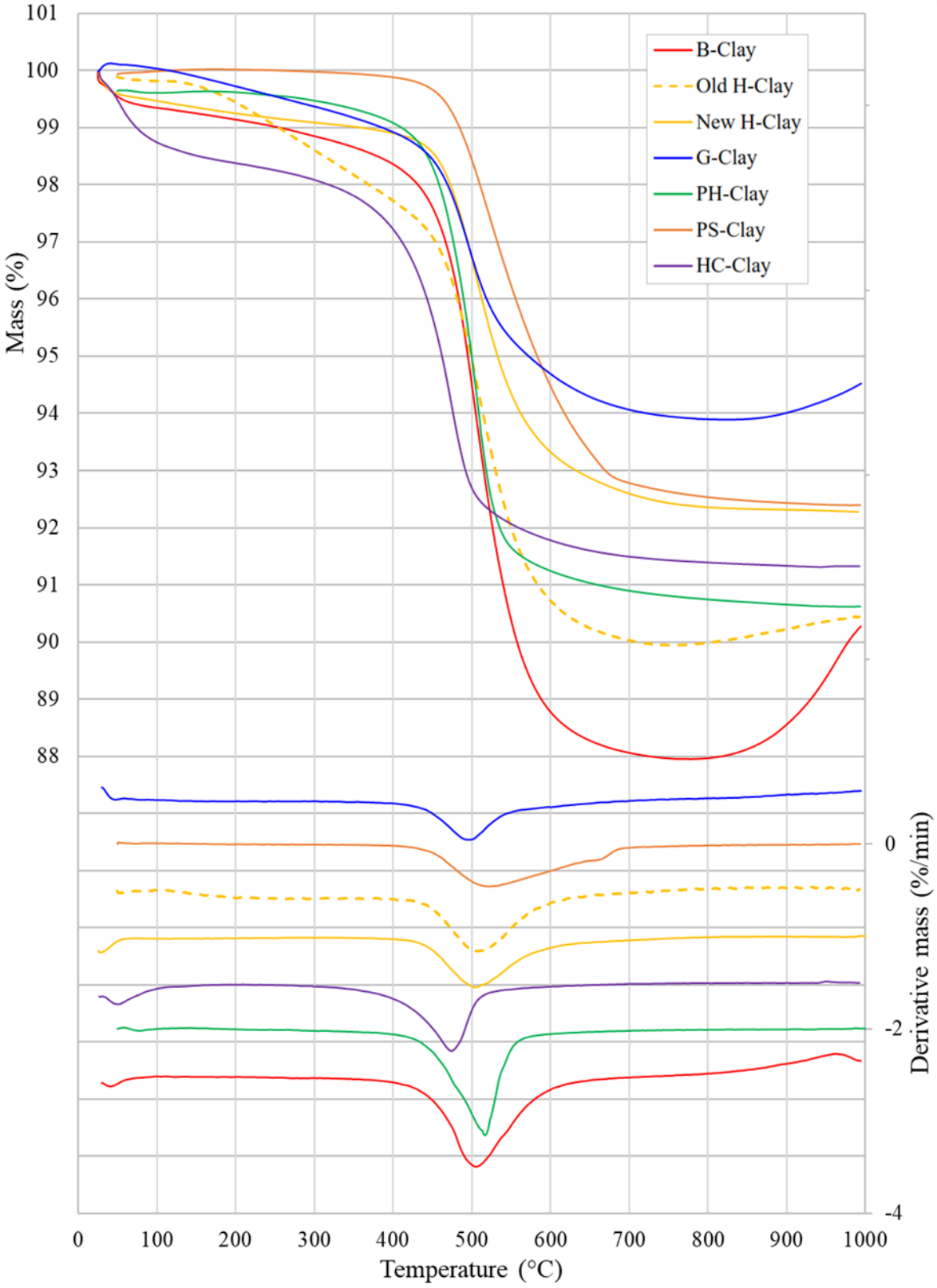

Figure 4.1: TGA curves of the samples of uncalcined clays

Table 4.1: Estimated amount of kaolinite from the TGA curves using the tangent method

Uncalcined sample	Mass change between 400°C and 600°C (%)	Kaolinite [calculated using Equation 2.5] (%)
B-Clay	9.0	64.5
Old H-Clay	6.0	43.0
New H-Clay	5.3	38.0
G-Clay	4.1	29.4
PH-Clay	7.2	51.6
PS-Clay	5.7	40.9
HC-Clay	5.4	38.7

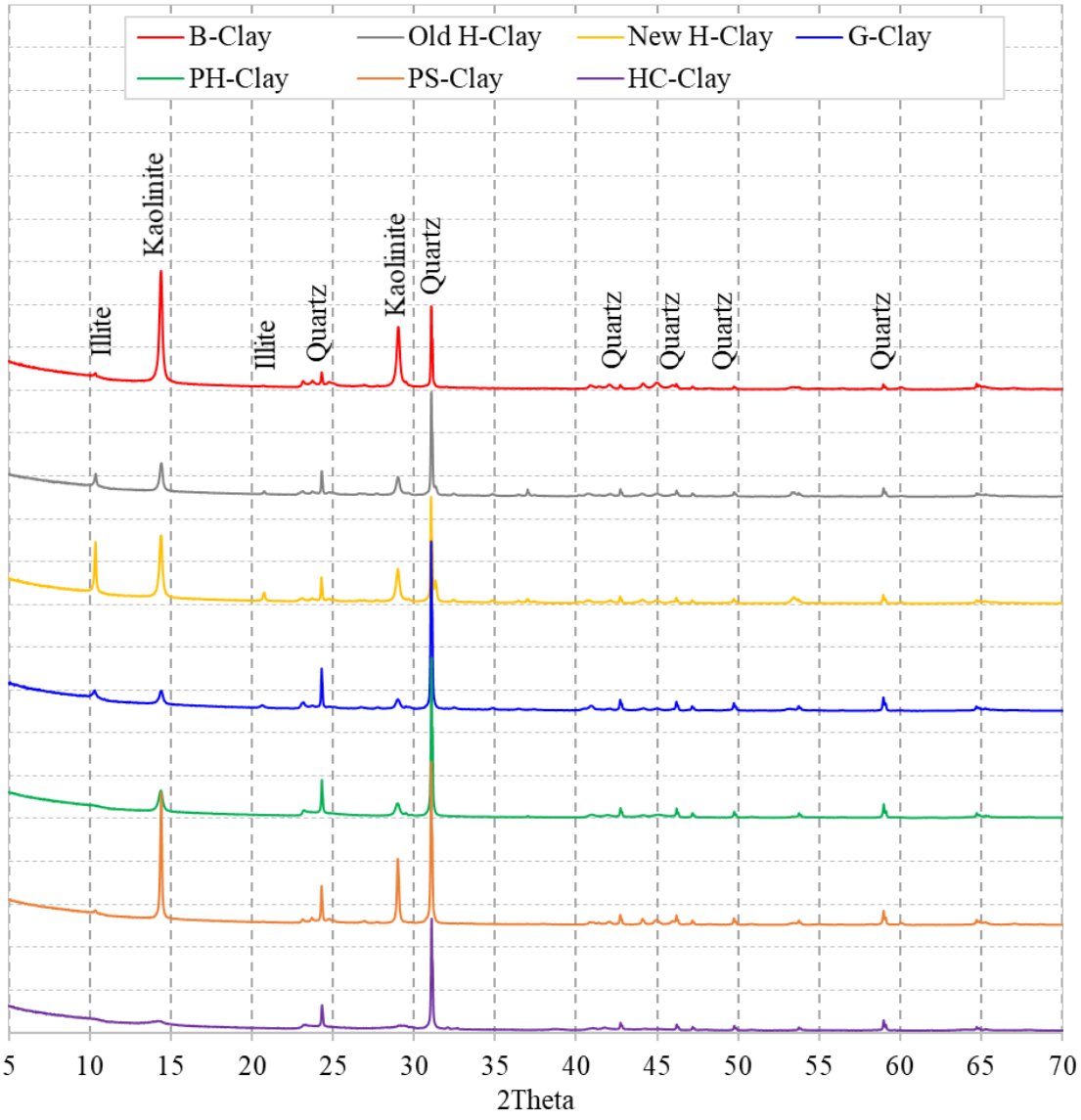

Figure 4.2: XRD pattern of the samples of uncalcined clays

Table 4.2: Estimated percentage of minerals in the uncalcined clays from the XRD scans

	Kaolinite (%)	Illite (%)	Quartz (%)	Feldspar (%)	Magnetite (%)
B-Clay	72.6	8.0	18.3	-	-
Old H-Clay	44.0	20.0	35.0	2.0	-
New H-Clay	46.3	6.5	44.0	3.2	-
G-Clay	24.9	29.2	45.9	3.2	-
PH-Clay	49.2	3.1	47.7	-	-
PS-Clay	48.7	1.2	50.1	-	-
HC-Clay	45.7	8.7	41.7	2.5	1.2

4.2.1 Discussion

From the results, all clays are composed mainly of kaolinite, quartz, and muscovite/illite. It has been pointed out that a suitable clay for clinker replacement is one with kaolinite content of at least 40%. In general, the XRF results (Table 3.4) are in good agreement with the mineralogical composition obtained by XRD and TGA. This is summarised in Table 4.3 (Data compiled from Table 3.4, Table 4.1, and Table 4.2).

Table 4.3: Summary of XRF, TGA and XRD results

	Al_2O_3 (%)	Al_2O_3/SiO_2	LOI (%)	**Kaolinite (%)**		Comment
				TGA	**XRD**	
Suitable clay	> 18	> 0.3	> 7	**> 40%**		
	(A. A. Díaz et al., 2018)			(Alujas et al., 2015)		
B-Clay	31.59	0.61	11.00	64.5	72.6	OK
Old H-Clay	20.95	0.33	8.25	43.0	44.0	OK
New H-Clay	24.21	0.40	7.48	38.0	46.3	OK
G-Clay	20.58	0.30	5.15	29.4	24.9	Marginal
PH-Clay	22.60	0.34	8.63	51.6	49.2	OK
PS-Clay	19.79	0.28	7.61	40.9	48.7	OK
HC-Clay	21.41	0.35	7.53	38.7	45.7	OK

The difference between TGA and XRD results for kaolinite content depends largely on the amounts of other phases present in the samples. With XRD, phases in small amounts will

go undetected, and consequently the main phases will tend to be overestimated. With TGA, the illite phase also dehydroxylates partly within the kaolinite-dehydroxylation interval (400°C to 600°C) which, if present in the sample in significant amounts, also affects the estimation of kaolinite content.

In this case, all the clays (except G-Clay) have at least 40% kaolinite content, making them potentially suitable to be used in cement and concrete. The G-Clay has about 30% kaolinite content from TGA and 25% from XRD results, and therefore is not suitable, without beneficiation, for use in cement and concrete.

4.3 Reactivity of the clays and optimal calcination temperature

As described in Section 2.6, for the kaolinite clay to be reactive, by being altered to produce an amorphous material for pozzolanic reactivity, calcination between 700°C and 850°C is necessary (Fernandez, Martirena and Scrivener, 2011). In view of this, it was decided to test the reactivity of the samples of clay calcined at three temperatures: 750, 800 and 850°C. The received flash-calcined samples of H-Clay were also tested and compared with the uncalcined sample that was calcined at 800°C.

Reactivity was assessed using the R^3 bound water test (described in Section 2.6). The bound water (%) in the R^3 paste was calculated based on the mass loss of the sample heated between 105°C and 350°C (Li et al., 2018). The aim was to find the optimum calcination temperature of each clay. The results are presented in Table 4.4 as an average of three samples tested for each clay (more details on Appendix III).

It is clear in Table 4.4 that B-Clay is the most reactive clay and G-Clay is the least reactive clay, mainly related to the amount of kaolinite in the samples. The results also indicate that all samples are more reactive when calcined at 800°C. As indicated in the literature (Li et al., 2018), for a calcined clay with amorphous content of about 70% (similar to B-Clay), the R^3 bound water value is 7.49 ± 1.6%. As shown in Table 4.4, the bound water value for B-Clay calcined at 800°C is 8.65% which is within the range. Unfortunately, it is not clear in the literature why the standard deviation is high, but it could be because of particle sizes of the materials and/or quality of the chemicals used.

Table 4.4: R^3 bound water test results (optimum temperature in bold)

Calcined sample	Temperature (°C)	Bound water (105°C – 350°C)	
		Average (%)	SD
B-Clay	850	8.32	0.13
	800	**8.65**	0.10
	750	8.43	0.10
Old H-Clay	Received flashed calcined at 850	6.08	0.10
	850	5.46	0.10
	800	**6.13**	0.11
	750	6.05	0.12
New H-Clay	Received flashed calcined at 850	5.09	0.02
G-Clay	850	3.80	0.06
	800	4.02	0.12
	750	**4.19**	0.13
PH-Clay	850	4.08	0.01
	800	**5.17**	0.02
	750	4.65	0.03
PS-Clay	850	4.59	0.11
	800	**5.04**	0.12
	750	4.60	0.05
HC-Clay	850	5.05	0.09
	800	**6.15**	0.05
	750	6.00	0.04

4.4 Changes in the properties of clay after calcination

4.4.1 Physical and chemical composition

Figure 4.3 shows photos of the selected clays before and after calcination. The chemical composition of the selected samples of calcined and uncalcined clays, their PSD parameters, SD, and BET surface areas are presented in Table 4.5. The aim was to evaluate changes in the properties of the clays brought about by calcination. In general, all samples calcined at 800°C have somewhat larger particle sizes with slightly lower density and lower BET surface area (except PH-Clay) compared to uncalcined samples. This is because of the changes in the chemical properties of the clay and the fact that particles tend to agglomerate as temperature increases.

4.4.1.1 The colour of the clay after calcination

As shown in Figure 4.3, the colour of the clay also changes during calcination. In this case, the B-Clay changes from darkish-brown to lighter-brown, H-Clay from white to yellow, PH-Clay from pearlish-white to pinkish-white, and HC-Clay from darkish-red to bright red. This colour change depends on the oxidation and reduction of iron, titanium and manganese present in the clay during calcination (Gámiz et al., 2005; Chandrasekhar and Ramaswamy, 2006). The change of colour can be controlled or modified during calcination (Chotoli et al., 2015; Martirena et al., 2020). For instance, a reddish-clay can be made dark gray if calcined in an anoxic environment (Martirena et al., 2020).

Figure 4.3: Photos of the samples of clays, before (left) and after (right) calcination

4.4.1.2 Particle sizes

Figure 4.4 shows PSD results of the selected clays before and after calcination. The PSD values are presented in Table 4.5. Grinding was done before calcination and the target was to achieve d_{50} < 10 um and d_{90} < 30 um. However, during calcination the particles tend to agglomerate (Alujas et al., 2015) as evidenced by the SEM images in Figure 4.5 to Figure 4.8 and the reduction in the BET surface areas presented in Table 4.5. Only the BET surface area of the PH-Clay remained almost the same after calcination. It is also clear from the images that the agglomerated particles are not the same, hence it is likely that the clays have different agglomeration behaviour during calcination. This needs further work.

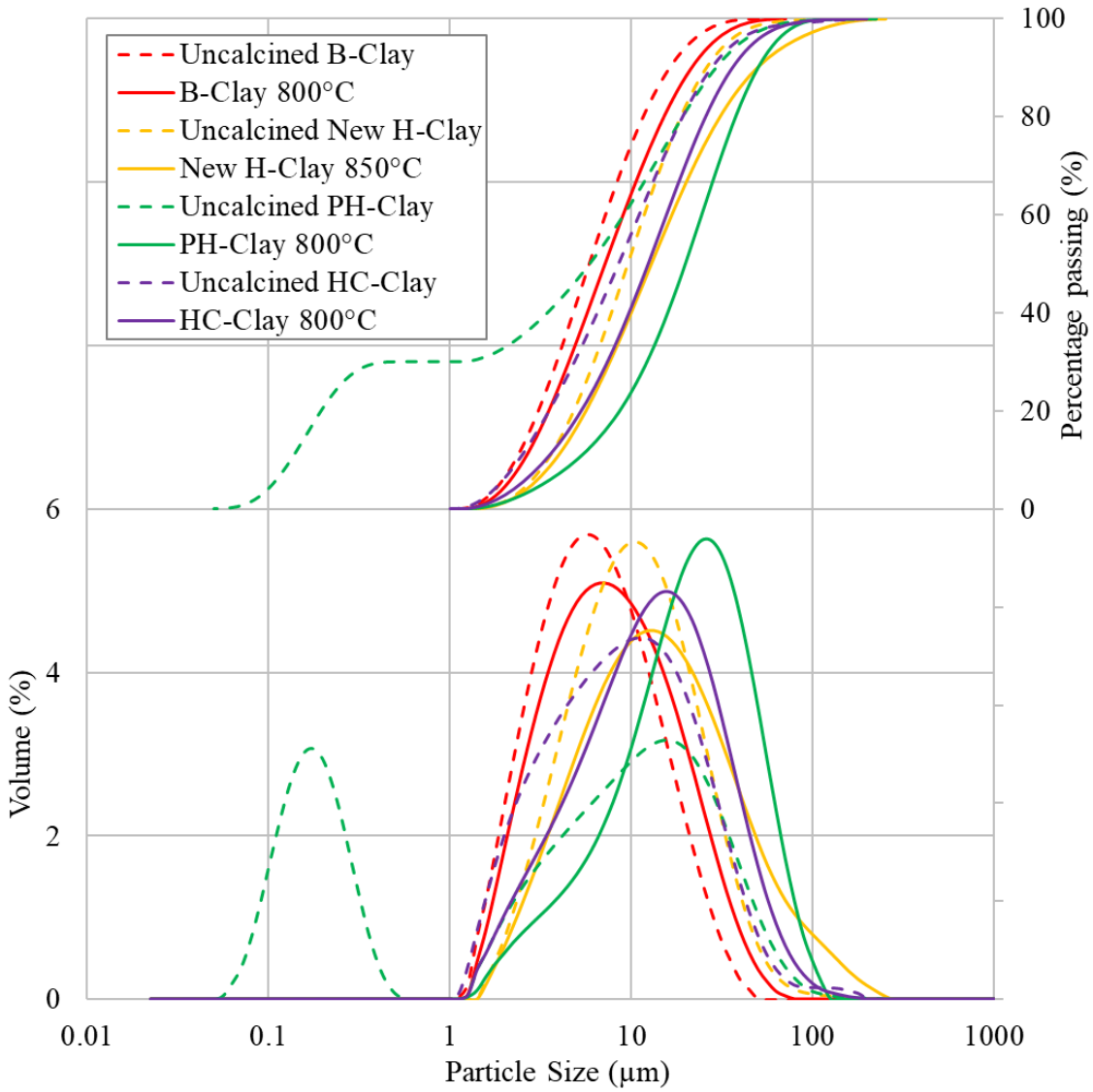

Figure 4.4: PSD curves of uncalcined and calcined samples of clay

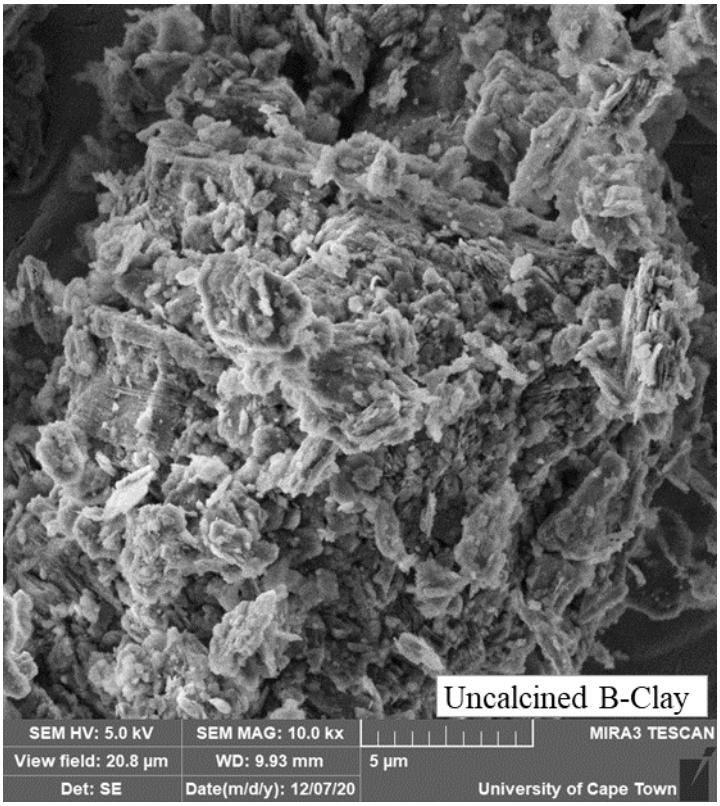

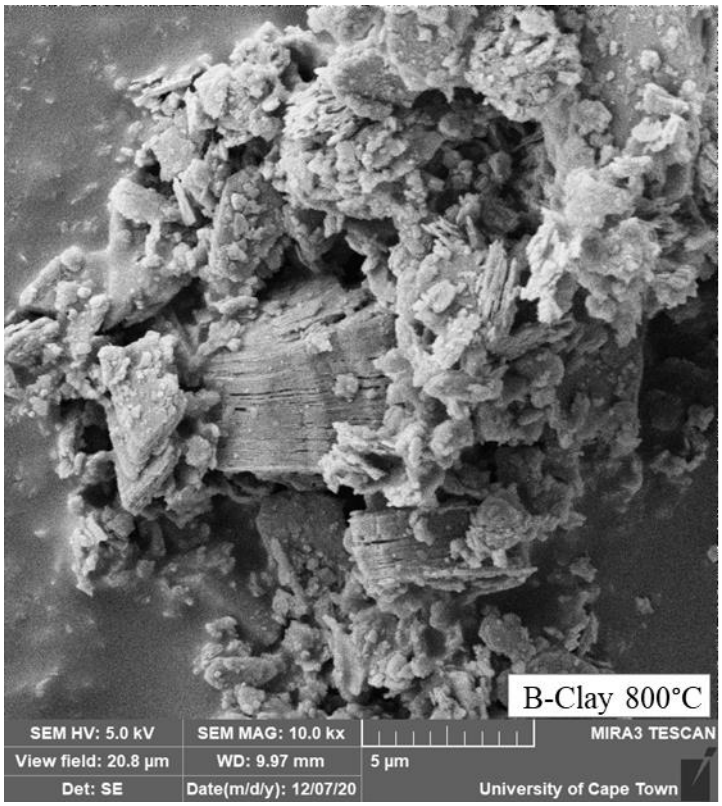

Figure 4.5: SEM Images of the sample of B-Clay, before and after calcination

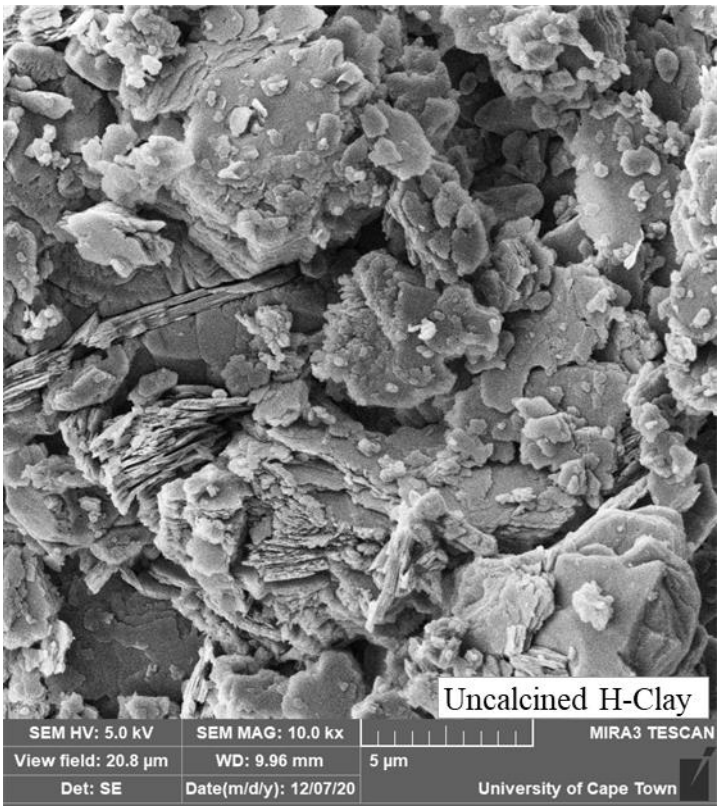

Figure 4.6: SEM Images of the sample of H-Clay, before and after calcination

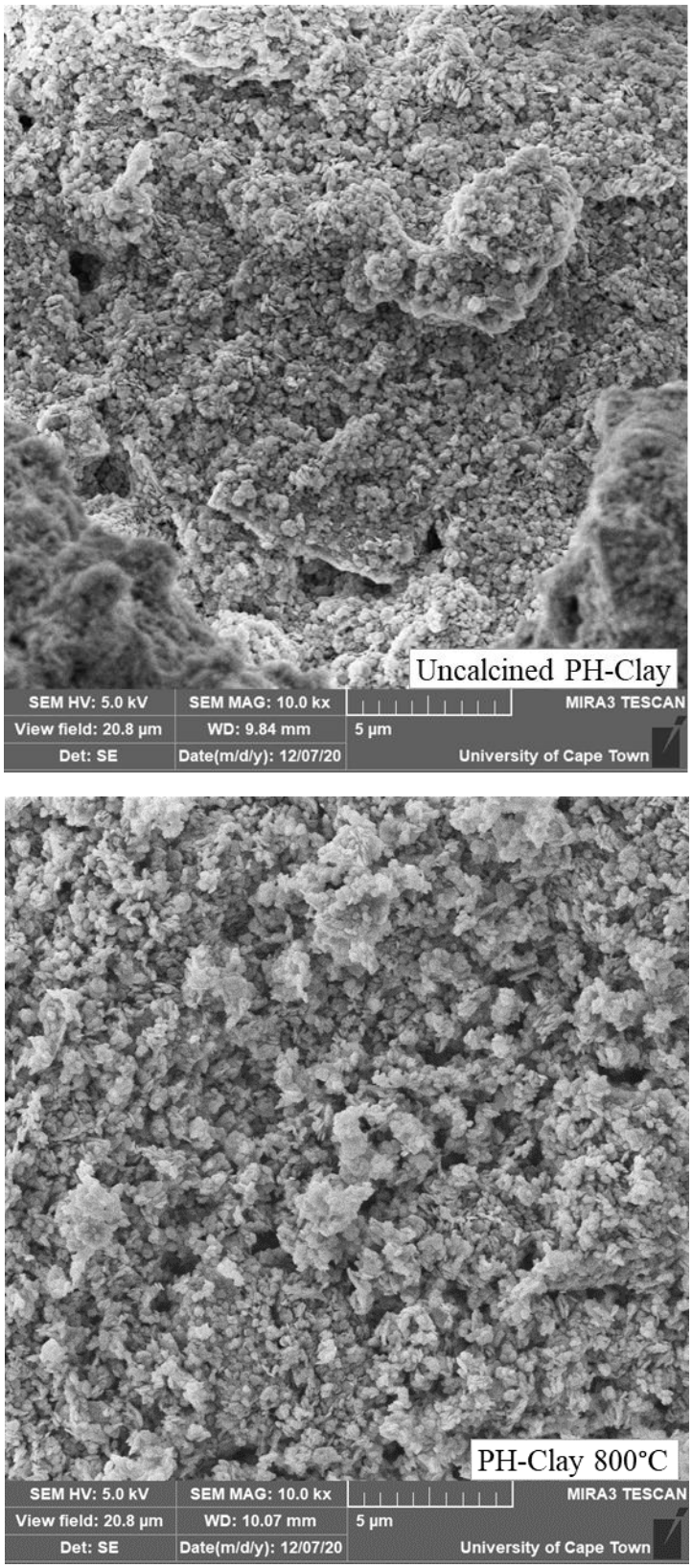

Figure 4.7: SEM images of the sample of PH-Clay, before and after calcination

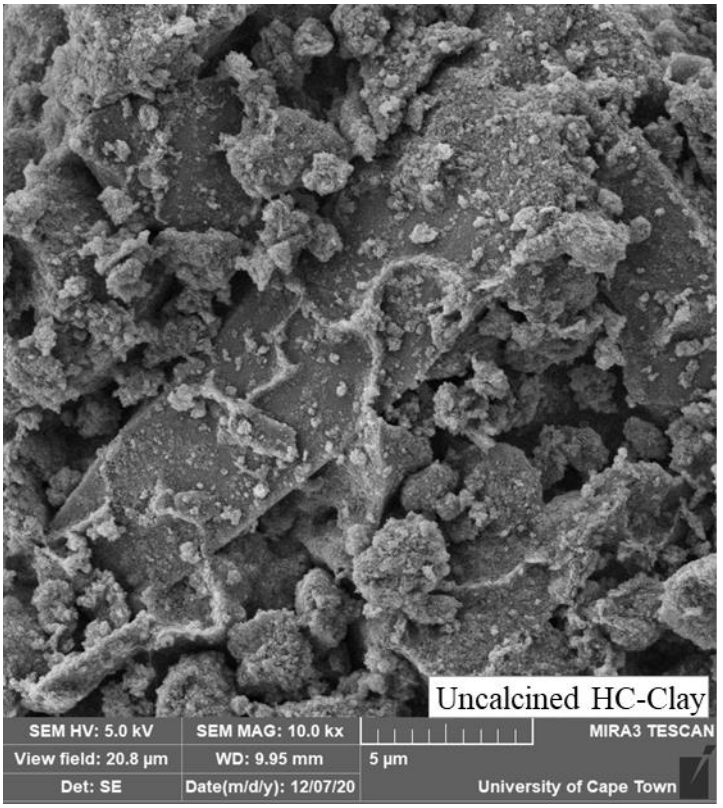

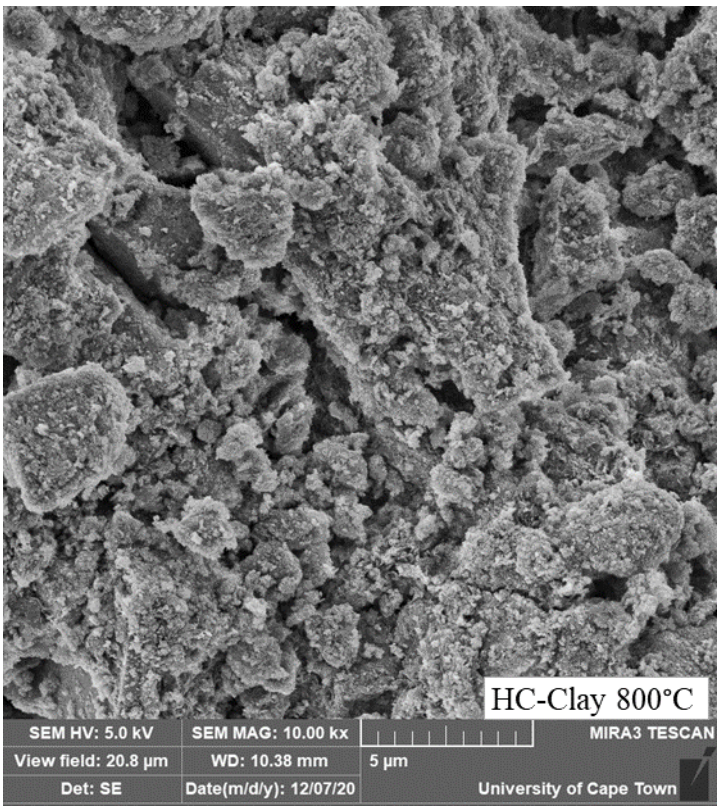

Figure 4.8: SEM Images of the sample of HC-Clay, before and after calcination

4.4.1.3 Chemical composition

The difference in the relative percentages of oxides between uncalcined and calcined samples of clay, especially in the amounts of Al_2O_3 and SiO_2, as can be seen in Table 4.5, comes from the loss of free and chemically bound water (as indicated by the difference in the LOI values) as well as transformation of kaolinite to metakaolin during calcination.

Table 4.5: XRF results and characteristics of uncalcined versus calcined samples of clay

Oxides	B-Clay		New H-Clay		PH-Clay		HC-Clay	
	Raw	800°C	Raw	850°C	Raw	800°C	Raw	800°C
SiO_2	51.52	57.33	60.30	68.08	65.98	71.81	60.94	63.86
TiO_2	1.57	1.76	0.97	1.43	0.98	1.05	0.93	1.06
Al_2O_3	31.59	35.08	24.21	23.08	22.60	25.14	21.41	24.20
Fe_2O_3	1.14	1.34	1.67	1.74	0.71	0.81	7.39	8.38
MnO	0.07	0.07	0.01	0.01	0.01	0.01	0.16	0.18
MgO	0.46	0.51	0.90	0.86	0.27	0.34	0.17	0.03
CaO	1.64	1.83	0.02	0.01	0.03	0.05	0.27	0.31
Na_2O	0.25	0.22	0.73	1.15	0.17	0.27	0.23	0.20
K_2O	0.35	0.39	2.54	2.60	0.06	0.07	0.55	0.61
P_2O_5	0.12	0.12	0.02	0.04	0.01	0.02	0.02	0.05
SO_3	0.06	0.04	< 0.01	0.01	< 0.01	< 0.01	< 0.01	< 0.01
Cr_2O_3	0.02	0.02	0.01	0.01	0.01	0.01	0.01	0.01
NiO	0.01	< 0.01	0.01	0.01	0.00	0.01	0.01	0.01
H_2O-	0.08	0.28	0.04	0.04	0.09	0.02	0.02	0.05
LOI	11.00	0.47	7.48	0.42	8.63	0.36	7.53	0.63
Total	99.87	99.47	98.92	99.50	99.53	99.98	99.62	99.55
Na_2O_{eq}	0.48	0.48	2.41	2.88	0.21	0.32	0.60	0.60
RD	2.61	2.60	2.67	2.59	2.66	2.64	2.73	2.70
BET (m^2/g)	12.6	11.1	5.4	4.6	14.4	14.5	45.8	37.0
d_{10} (μm)	2.3	2.6	3.5	3.8	< 1.0	5.0	2.4	3.4
d_{50} (μm)	5.9	7.1	9.6	12.9	5.9	19.7	8.5	12.3
d_{90} (μm)	16.5	21.4	26.0	49.2	29.2	49.5	27.7	35.9

4.4.2 Mineralogical composition

Table 4.6 presents the estimated percentage of phases in the clay before and after calcination. Figure 4.9 shows XRD patterns of the selected clays before and after calcination. It is clear from the figure that all kaolinite peaks present before are not seen at 800°C and there is no presence of spinel or mullite in the samples. This indicates that all kaolinite minerals present in the clay were transformed into the amorphous phase (i.e., metakaolin). The amount of amorphous phases was estimated by the Rietveld method

based on the XRD pattern of calcined clay (2 g) mixed and micronized with 20% amount of Fluorite (De La Torre, Bruque and Aranda, 2001; Walenta and Füllmann, 2004).

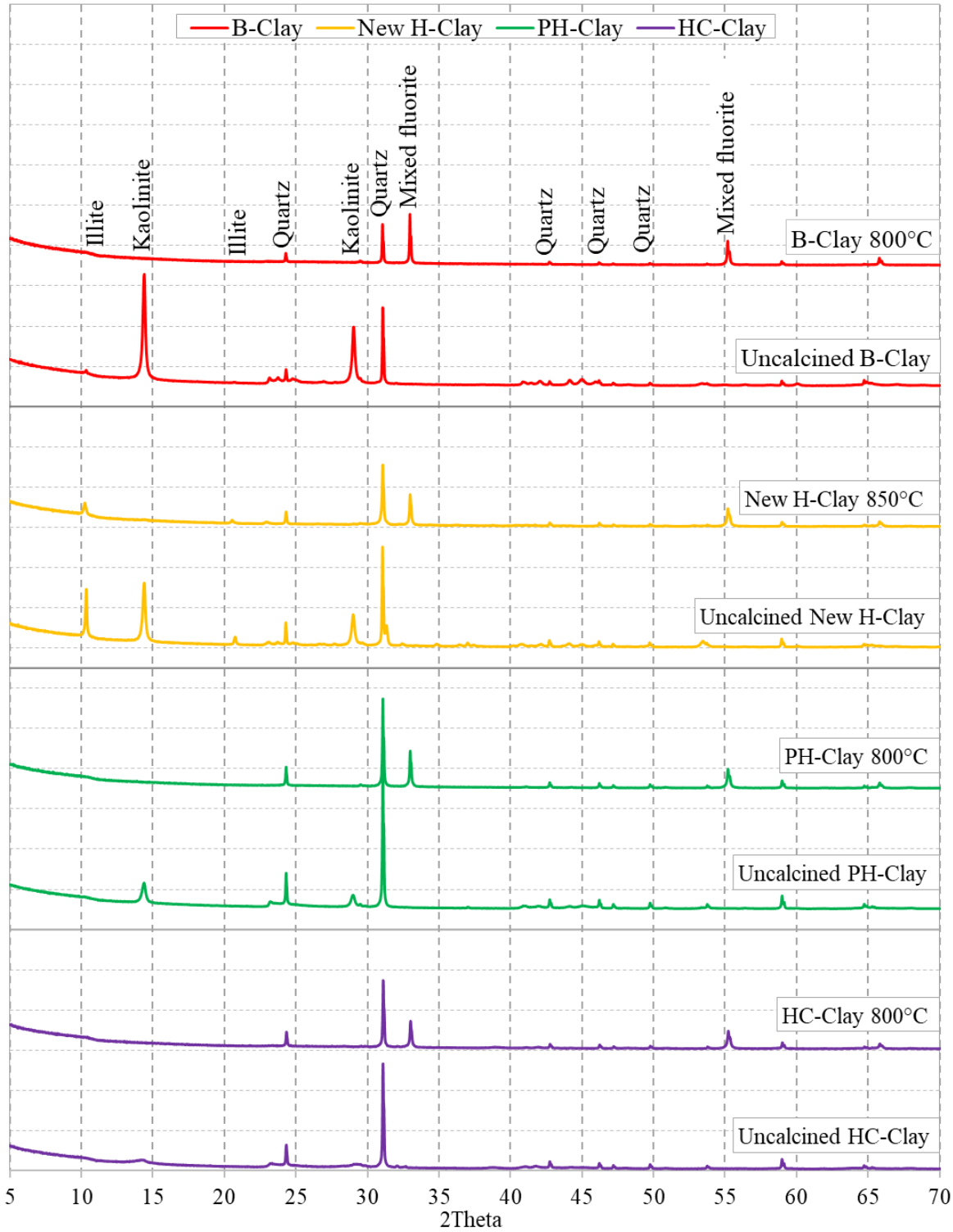

Figure 4.9: XRD pattern of the selected clays, before and after calcination

Table 4.6: Estimated percentage of phases in the selected clays before and after calcination

Phases (%)	B-Clay		New H-Clay		PH-Clay		HC-Clay	
	Un-calcined	800 °C	Un-calcined	850 °C	Un-calcined	800 °C	Un-calcined	800 °C
Kaolinite	72.6	0.0	46.3	5.1	49.2	0.0	45.7	0.0
Illite	8.0	7.3	6.5	3.5	3.1	1.3	8.7	3.4
Quartz	18.3	18.9	44.0	38.3	47.7	48.3	41.7	42.1
Feldspar	-	<1.0	3.2	1.1	-	-	2.5	<1.0
Magnetite	-	-	-	-	-	-	1.2	<1.0
Amorphous	-	73.5	-	52.0	-	50.4	0	54.5

4.5 Summary and general discussion

In this chapter, all selected clays were studied for their potential application in the production of cement and concrete. According to the results, all the selected clays are composed mainly of quartz, kaolinite, and illite in varying proportions. In general, most kaolinite clay sources in other parts of the world (as stated in the literature) contain quartz in large amounts, small amounts of illite in many cases, and other minerals in smaller or larger amounts in limited cases. For example, the kaolinite clays found in Mukurweini, Kenya (Ez-zaki et al., 2021), some areas in Nigeria (Akindahunsi, Avet and Scrivener, 2020), Zonouz in the northwest of Iran (Souri et al., 2015), Zettlitz in the Czech Republic (Souri et al., 2015), Guangdong province in the south of China (Huang et al., 2020), Pontezuela deposit in Cuba (Vizcaíno-Andrés et al., 2015) and different locations in Argentina (Tironi et al., 2012), also contain the same main phases but with different proportions, and in some cases no evidence of illite. The kaolinite clays from Carranchola-LaMoza deposit in Cuba (Alujas et al., 2015), Jeolla-Do area in South Korea (Lin et al., 2019), a deposit in Colombia (Rodriguez and Tobon, 2020), Chile (Zunino and Scrivener, 2020b) and some areas in Nigeria (Akindahunsi, Avet and Scrivener, 2020), were also naturally mixed with montmorillonite and/or muscovite in noticeable amounts, and again in some cases, no evidence of illite. The clays in some areas of China (Zunino, Boehm-Courjault and Scrivener, 2020) and India (Chandrasekhar and Ramaswamy, 2002; Anil, Mohan Misra and Misra, 2018; Krishnan and Bishnoi, 2018) also naturally contain anatase in noticeable amounts and in some areas no signs of illite. Some deposits in Italy also contain cristobalite in large amounts but no signs of illite (Dondi et al., 2001).

Furthermore, in some areas of the world such as Yaguajay in Cuba (Escobar, Díaz and Pérez, 2020), Kütahya in Turkey (Aras et al., 2007) and Terra Alta in Spain (Garcia-Valles et al., 2020), kaolinite clays are found naturally mixed with calcite, which negatively influences the reactivity of the clay during calcination (Zunino, Boehm-Courjault and Scrivener, 2020). Calcite decomposes between 600°C and 800°C into free lime and CO_2, and if present in the clay, some decomposition may occur during the calcination process leading to the formation of a calcium-rich phase with the metakaolin particles which reduces the specific surface area and therefore the reactivity of the calcined clay (Zunino, Boehm-Courjault and Scrivener, 2020). However, this effect can be minimised by calcining the clays at no more than 700°C and having a residence time of not less than 60 minutes (Zunino, Boehm-Courjault and Scrivener, 2020).

The XRF results are in good agreement with the mineralogical composition estimated by XRD and TGA. A summary of XRF, TGA and XRD results is given in Table 4.3. The difference between TGA and XRD results is mainly due to the presence of other phases present in the samples. In this case, all the selected clays have illite phases which also partly dehydroxylate between 400°C to 600°C. Consequently, the kaolinite content may be overestimated with TGA results. The differences are most likely also because of other secondary phases that are present in a very small amounts and therefore not detected by XRD.

The optimum calcination temperature of each clay was also investigated using the R^3 reactivity test. Samples of each clay calcined at 750, 800 and 850°C were tested for reactivity. Results indicate that all clays are most reactive when calcined at around 800°C. This finding agrees well with the literature (He, Osbaeck and Makovicky, 1995; Heller-Kallai, 2006; Fernandez, Martirena and Scrivener, 2011; Bernal et al., 2017) which is that, while dehydroxylation of chemically bound water occurs between 400°C and 600°C, the kaolinite clay becomes more reactive when calcined between 600°C and 850°C which is mainly related to change of the coordination number of Al from $Al^{(VI)}$ to $Al^{(IV)}$ and $Al^{(V)}$, as presented in Figure 2.9.

The chapter also presents a comparison of the physical, chemical, and mineralogical properties of the selected clays before and after calcination. The difference comes mainly from agglomeration (physical) due to calcination, and loss of free and chemically bound water, as indicated by the difference in the LOI values (Chemical and mineralogical). All samples of clays changed colour after calcination. The change in colour is caused by the oxidation of iron, titanium and manganese ions present in the clays which can be controlled during calcination, for example by calcining clay in an oxygen-free environment. However, Chotoli et al. (2015) observed that the change of colour, or the general colour of the clay have little influence on its performance.

Grinding was done before calcination with a target of achieving $d_{50} < 10$ um and $d_{90} < 30$ um. After calcination, a slight increase of particle sizes (due to agglomeration of particles) was consistently noted for all the clays, based on the results of the PSD analysis. The PSD results of the selected clays (before and after calcination) agree well with the BET surface areas of the clays (except PH-Clay) obtained by the nitrogen adsorption/desorption method, and supported by the SEM images presented in Figure 4.5 to Figure 4.8. Although PSD results indicate a large change in the PSD values of the PH-Clay compared to other clays, the BET surface area of this clay remained almost the same after calcination, which needs further investigation for a deeper understanding on the behaviour of this clay.

Chapter 5 Optimisation of proportion of binders

5.1 Introduction

The underlying aim of this research was to develop LC^3 concrete for structural and non-structural applications, aiming at minimising CO_2 emissions associated with the immense development of infrastructure which is anticipated to occur in Africa in the near future. Based on the amount of kaolinite in the clays, the decision was made to proceed with B-Clay, New H-Clay, PH-Clay, and HC-Clay for the optimisation and concrete work. The so-called mixture design 3-factors approach was used for optimisation of LC^3 proportions. The chemical composition and characteristics of all the selected materials are presented in Table 5.1. The PSD curves of the calcined samples of the clays, cement, and LS-K5 are shown in Figure 5.1.

Table 5.1: Chemical composition and characteristics of selected materials

Oxides	Calcined clay				CEM II /A-L 52.5 N		LS-K5	GGBS
	B-Clay	New H-Clay	PH-Clay	HC-Clay	Old-CEM II	New-CEM II		
SiO_2	57.33	68.08	71.81	63.86	19.61	20.49	0.57	35.06
TiO_2	1.76	1.43	1.05	1.06	0.21	0.24	0.00	0.68
Al_2O_3	35.08	23.08	25.14	24.20	4.03	4.21	0.07	15.59
Fe_2O_3	1.34	1.74	0.81	8.38	1.97	2.21	0.00	0.78
MnO	0.07	0.01	0.01	0.18	1.48	1.09	0.00	0.70
MgO	0.51	0.86	0.34	0.03	2.77	1.99	1.74	8.42
CaO	1.83	0.01	0.05	0.31	62.40	63.69	54.61	36.90
Na_2O	0.22	1.15	0.27	0.20	<0.01	< 0.01	<0.01	0.24
K_2O	0.39	2.60	0.07	0.61	0.46	0.42	0.01	0.67
P_2O_5	0.12	0.04	0.02	0.05	0.06	0.05	0.01	0.02
SO_3	0.04	0.01	<0.01	<0.01	2.07	2.00	0.02	1.93
Cr_2O_3	0.02	0.01	0.01	0.01	<0.01	0.01	<0.01	<0.01
NiO	<0.01	0.01	0.01	0.01	0.01	0.01	<0.01	0.01
H_2O-	0.28	0.04	0.02	0.05	0.10	0.10	0.02	0.01
LOI	0.47	0.42	0.36	0.63	4.43	3.07	43.12	-1.24
Total	99.47	99.50	99.98	99.55	99.53	99.44	99.97	99.77
Na_2O_{eq}	0.48	2.88	0.32	0.60	0.30	0.27	0.01	0.68
RD	2.60	2.59	2.64	2.70	2.96	2.96	2.70	2.90
BET(m^2/g)	11.1	4.6	14.5	37.0	-	-	-	-
d_{10} (μm)	2.6	3.8	5.0	3.4	2.6	2.3	3.6	1.7
d_{50} (μm)	7.1	12.9	19.7	12.3	11.4	11.9	8.2	9.0
d_{90} (μm)	21.4	49.2	49.5	35.9	33.5	33.5	16.4	32.3

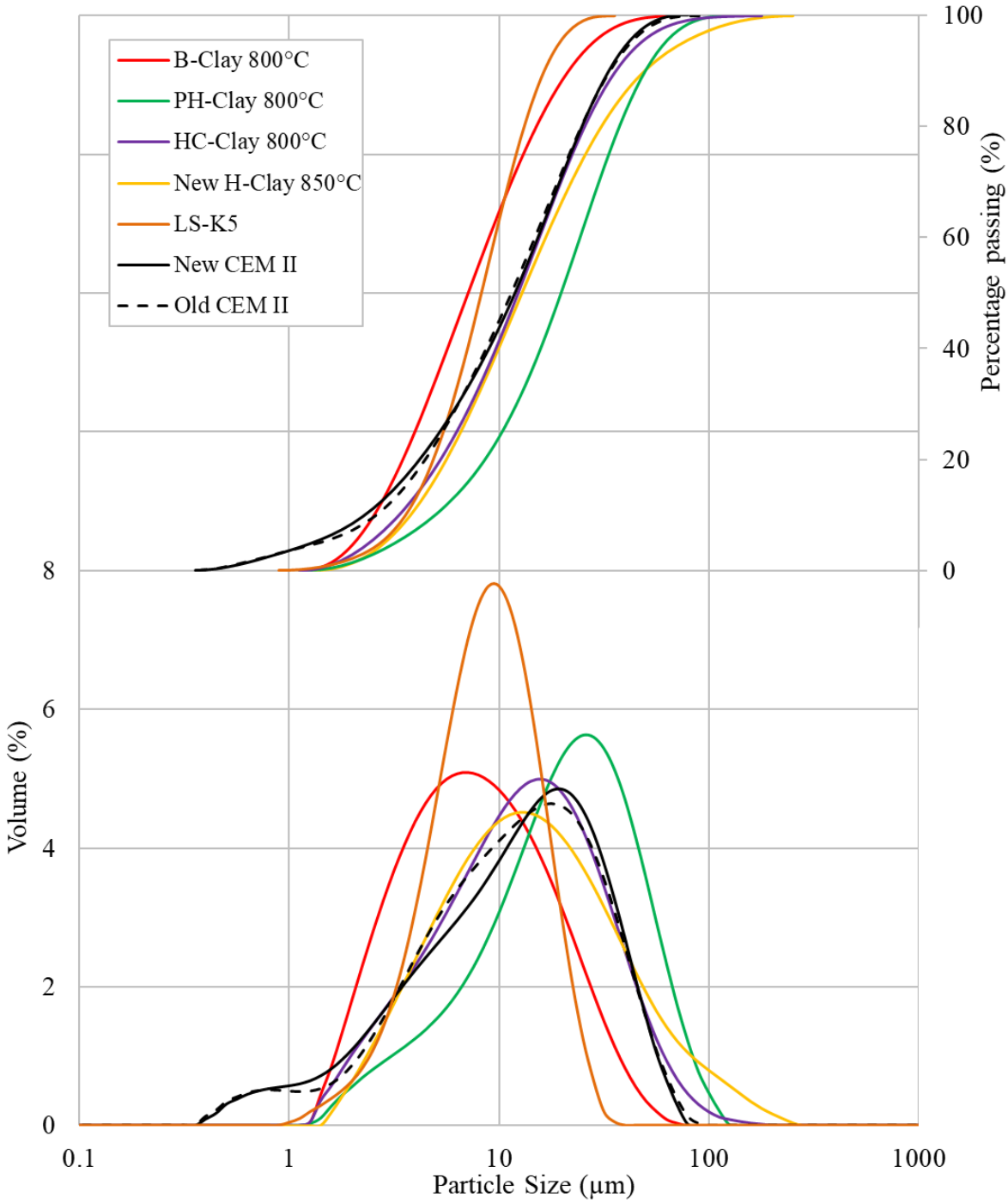

Figure 5.1: PSD curves of calcined clays, cement, and LS-K5

Two approaches were considered for reducing amount of clinker, i.e., approaches based on chemical and physical material properties. The compressive strength of mortar at a w/b ratio of 0.4 was used as the reference performance for optimisation. The chemical approach involved replacing clinker with optimal proportions of calcined kaolinite clay and LS,

whereas the physical approach involved further reduction of clinker/powder in the system by optimising proportions of concrete materials. The former was done using the mixture design 3-factors approach, described in Section 3.6. The latter was initially done using the CCSA method coupled with the commercial software, Elkem Materials-Mixture Analyser (EMMA), which uses MAAM (Equation 2.11) to optimise the packing of materials (details are provided in Appendix V). The obtained proportions were then adjusted based on developing and testing trial concrete mixes.

The focus of this chapter is on the first approach, which also includes sulphate and alkali adjustments, identification of hydrates formed, and quantification of CH, $C\overline{C}$, and bound water at different ages for the selected proportions.

5.2 Optimisation of CC/LS ratio at a given clinker content

As described in Section 3.6, it was important to obtain optimum limestone/calcined clay ratios at clinker replacement levels in the range of 40 to 70% that would give best strength and durability performance. To achieve this, the mixture design 3-factors approach with low boundaries (L_i) at 40% cement, 20% CC and 10% LS as described in Section 3.6 and Figure 3.5 was used. Figure 5.2 shows the required mixture design region i.e., the shaded region from Figure 3.5.

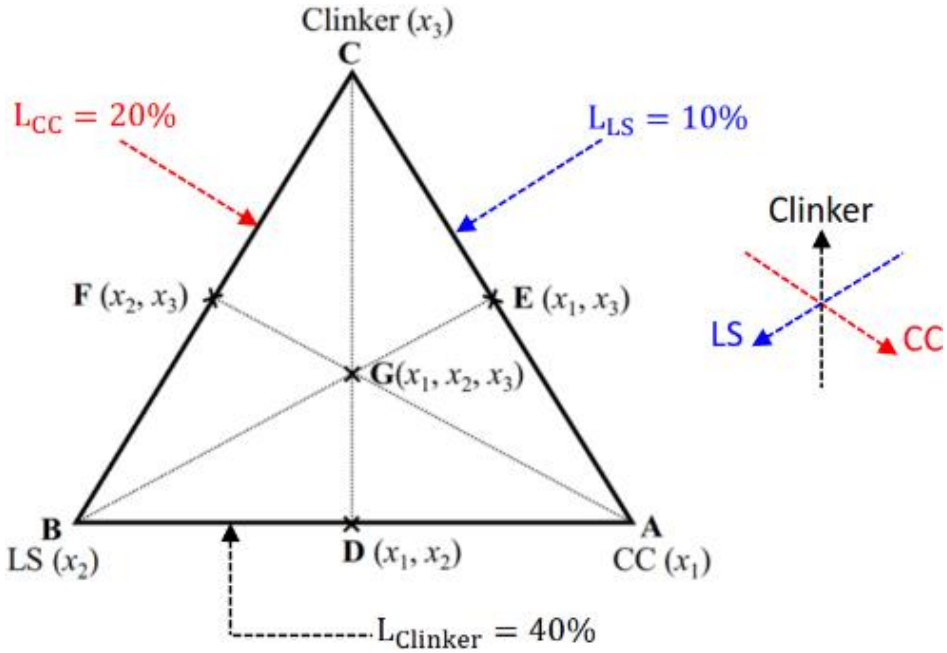

Figure 5.2: Mixture design region

All materials were ground separately and thoroughly mixed to obtain a homogeneous mixture. Table 5.2 presents the required proportions of calcined clay, limestone and clinker at points A to G (marked on Figure 5.2) obtained using Equation 5.1, with the lowest clinker factor at 0.4 and the highest clinker factor at 0.7 as described in Figure 3.5. Equation 5.1 maps the 'pseudo' proportions to real proportions using the lower boundaries and the scaling factor shown in the bracket in the equation (example is given in Appendix VI).

Table 5.2: Required proportions of calcined clay, limestone, and clinker for optimisation

Point	Pseudo proportions (x_i^P)			Σ	Real proportions (x_i^R)			Σ
	CC	LS	Clinker		CC	LS	Clinker	
A	1	0	0	1	0.50	0.10	0.40	1
B	0	1	0	1	0.20	0.40	0.40	1
C	0	0	1	1	0.20	0.10	0.70	1
D	0.5	0.5	0	1	0.35	0.25	0.40	1
E	0.5	0	0.5	1	0.35	0.10	0.55	1
F	0	0.5	0.5	1	0.20	0.25	0.55	1
G	0.33	0.33	0.33	1	0.30	0.20	0.50	1

$$x_i^R = x_i^p \left(1 - \sum_{i=1}^{3} L_i\right) + L_i \qquad -----\qquad (5.1)$$

5.2.1 Sulphate and Alkali adjustments

In this work, as described in Section 3.6.1, sulphate (SO_3) was adjusted by studying HoH of the LC^3 pastes during the first 24 hours of hydration. This was done using an I-Cal 2000 HPC Isothermal calorimeter at 20°C. The target was to make sure that for each LC^3 proportion given in Table 5.2, the aluminate peak appears after the silicate peak and occurs between 13 and 18 hours. On the other hand, a certain amount of alkalinity in the system is also important to enhance early reaction. Literature suggests Na_2O_{eq} between 0.6 and 0.8% (Antoni, 2013), and consequently, 0.7% was selected.

To ensure that the main factors controlling the reactions are clinker, calcined clay, and LS, it was decided to add gypsum and NaOH (as the alkali source) so that all the LC^3 mortar

with binder proportions (shown in Table 5.2), for each clay, have the same amounts of SO_3 and Na_2O_{eq}. Using the SO_3 content (estimated by XRF) for the Portland cement (i.e., 2%) and LS (i.e., ≈ 0%) presented in Table 3.5 and for the calcined clays (all samples ≈ 0%) presented in Table 4.5, the required SO_3 added for each LC^3 proportion was estimated (example is given in Appendix IV) .

5.2.1.1 Preliminary checks

As a check, calcined B-Clay and Old-CEM II were used. Gypsum ($CaSO_4.2H_2O$) with 74% purity supplied by PPC cement company was used to supply the needed sulphate. Table 5.3 presents the chemical composition of the PPC gypsum. As a start, it was decided to add small amounts of PPC gypsum and NaOH in all the LC^3 proportions to maintain SO_3 at 2.07% (as in the Old-CEM II) and Na_2O_{eq} at 0.7%, respectively, so that it is the amounts of calcined B-Clay, LS and clinker that are controlling the reaction.

Table 5.3: Chemical composition of PPC gypsum

Oxide (%)	SiO_2	TiO_2	Al_2O_3	Fe_2O_3	MnO	MgO	CaO	Na_2O	K_2O	P_2O_5
wt.%	8.54	0.05	0.86	0.33	0.02	0.98	31.22	0.27	0.25	0.02

SO_3	Cr_2O_3	NiO	H_2O-	LOI	Sum
34.32	< 0.01	0.02	17.03	4.17	98.06

Figure 5.3 and Figure 5.4 show HoH curves for the LC^3(B) pastes with "no additions" and with SO_3 and alkali additions, respectively. In general, in both cases, the amount of CC and LS in the mix significantly affect the intensity and position of both silicate and aluminate peaks. The dormant period of the LC^3 mixes appears similar to that of the reference mix. The intensities of the peaks are generally lower for mixes with lower clinker factor. In the case of "no addition" (Figure 5.3), in all the LC^3 mixes, the silicate reaction is overlapped by the aluminate reaction, and after the aluminate peak, a sharp drop of the heat rate is observed, which corresponds to suppression of the later part of the silicate reaction leading to low cumulative heat release and reactivity.

In the case of SO_3 and alkali addition (Figure 5.4), the aluminate peaks appear after the silicate peak and are observed to occur between 13 and 18 hours as expected.

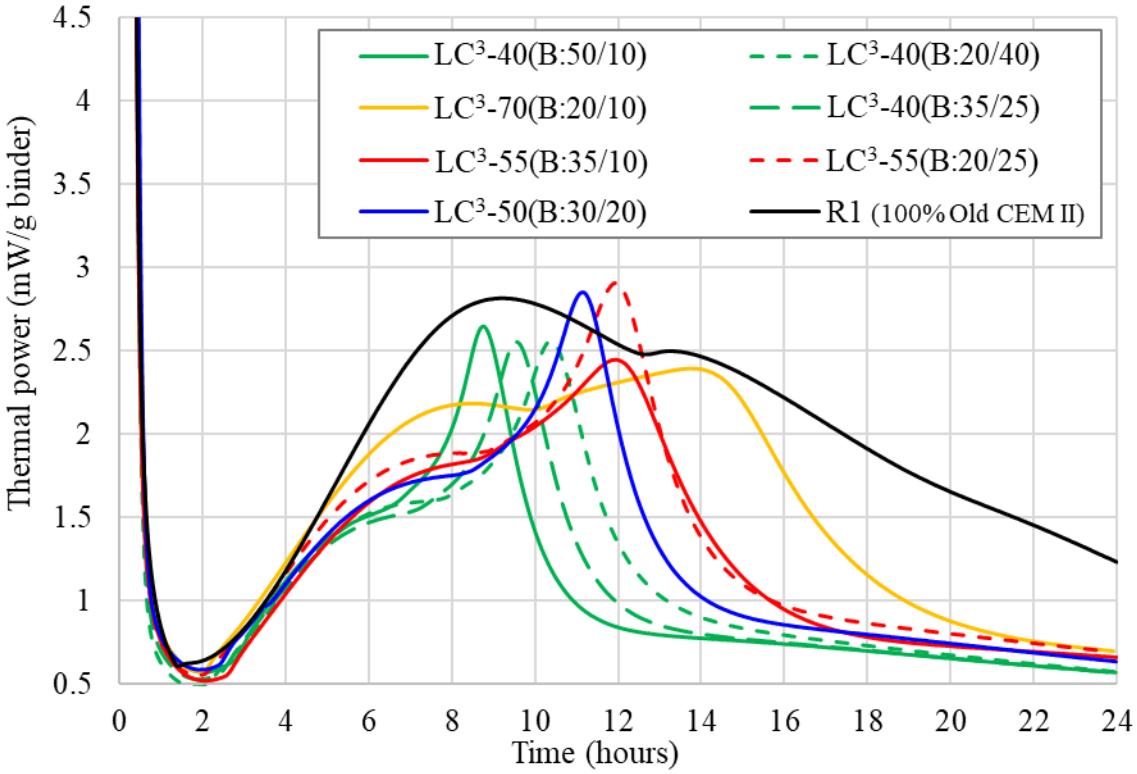

Figure 5.3: HoH curves of LC^3 pastes with B-Clay (No additions)

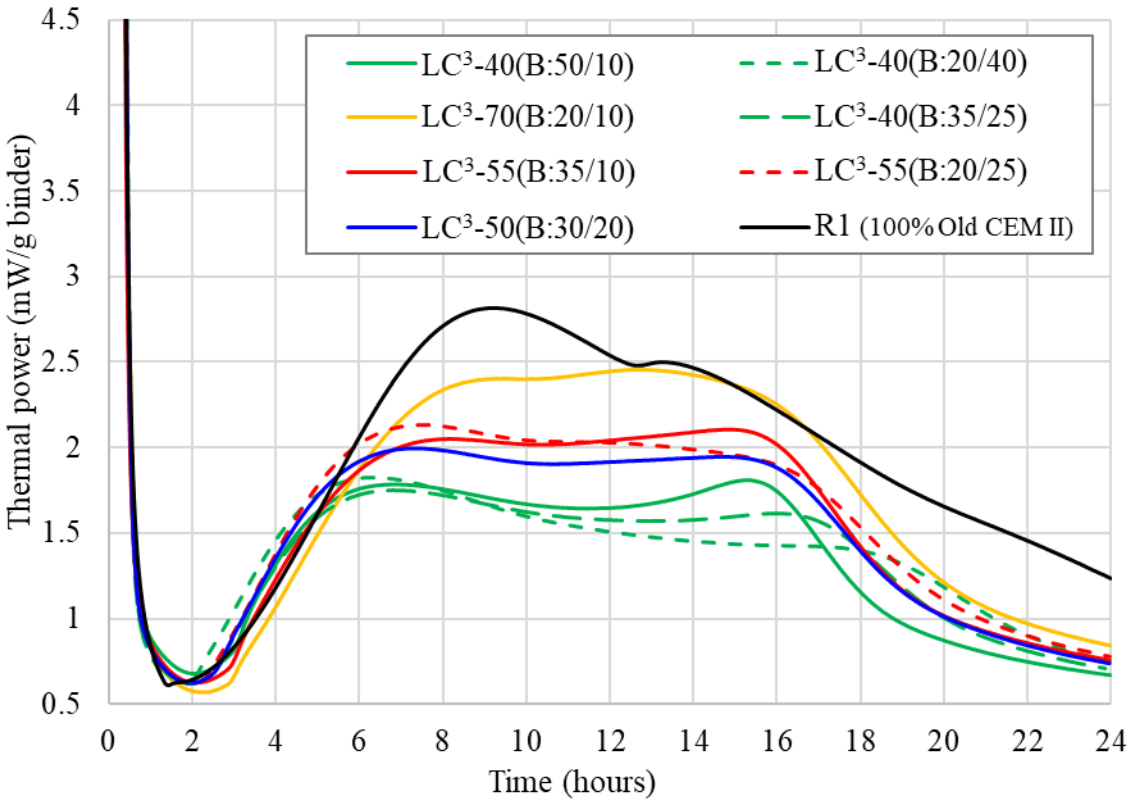

Figure 5.4: HoH curves of LC^3 pastes with B-Clay (2.07% SO_3; 0.7% Na_2O_{eq})

5.2.1.2 Sulphate and alkali requirement for the LC^3 mixes with the selected clays

From Section 5.2.1.1 on preliminary checks, it is clear that:

i) The aluminate peak of the LC^3 proportion with highest amount of LS and the lowest amount of clinker (LC^3-40(20/40)) occurs much later than the aluminate peaks of other proportions

ii) The aluminate peak of the LC^3 proportion with the lowest amount of LS and highest amount of clinker (LC^3-70(20/10)) occurs earlier than the aluminate peaks of other proportions.

iii) The kink of the aluminate peak depends largely on the amount of CC in the system.

Based on the above observations and after several trials (to reduce impurities, a 98% gypsum ($CaSO_4.2H2O$) from KIMIX was used to supply the needed SO_3 in the system at this stage), it was decided to add small amounts of gypsum such that the amount of SO_3 in all the LC^3 mixes with the selected clays (calculated based on the XRF data of cement, LS and CC presented in Table 3.5 and Table 4.5) was as follows (this ensured that the aluminate peak of each LC^3 mix occurs shortly after the silicate peak and between 13 and 18 hours):

i) 1.8% for the LC^3 mixes with B-Clay

ii) 1.2% for the LC^3 mixes with New H-Clay

iii) 2.0% for the LC^3 mixes with PH-Clay and

iv) 2.0% for the LC^3 mixes HC-Clay.

The minimum and maximum time boundaries for each calcined clay were confirmed using LC^3 proportions LC^3-70(20/10) and LC^3-40(20/40), respectively. For the LC^3 mixes with the New H-Clay, it was only possible to adjust to 1.5% SO_3 for the LC^3-70(20/10) (Figure 5.6). Na_2O_{eq} was maintained at 0.7% for all the LC^3 mixes except LC^3 mixes with New H-Clay as the alkalis in this clay were already high at 2.88% Na_2O_{eq}.

Figure 5.5 to Figure 5.8 confirm the appearance of both peaks and their positions. It is clear from the figures that: the aluminate peaks appear after the silicate peaks and between 13 and 18 hours and by adding or reducing a small amount of gypsum the aluminate peaks shift towards right or left, respectively.

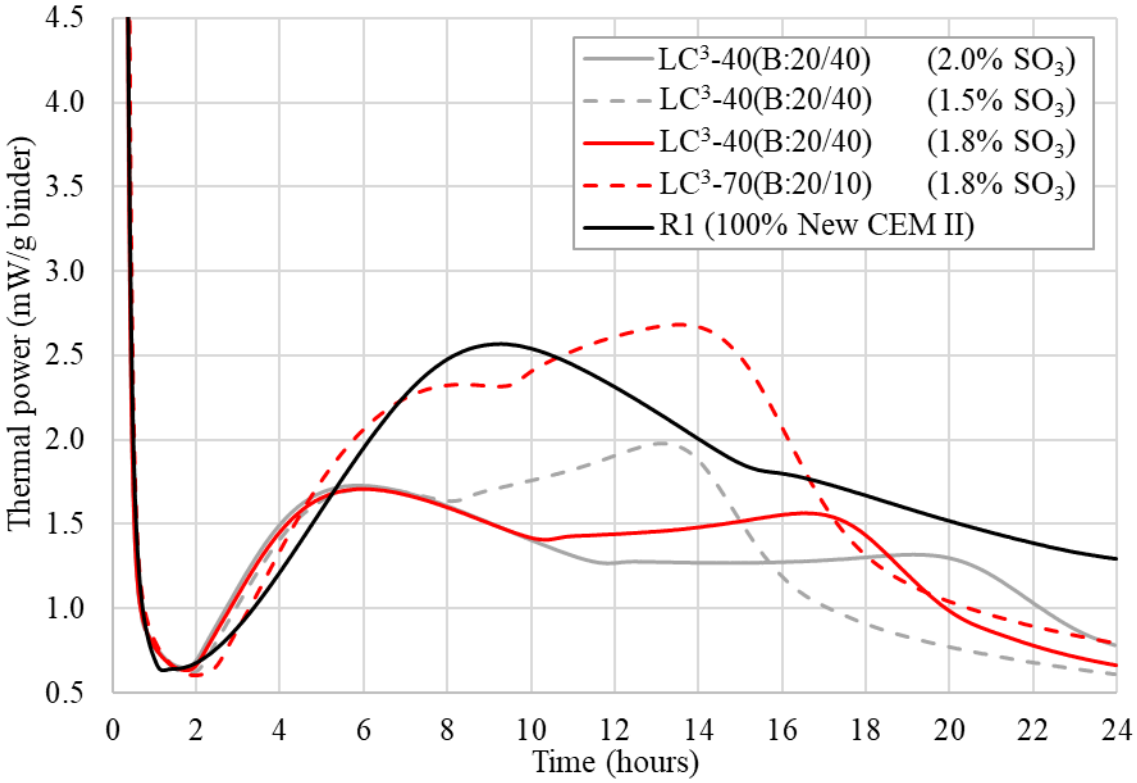

Figure 5.5: HoH curves of LC^3 pastes (Boundary proportions) with B-Clay

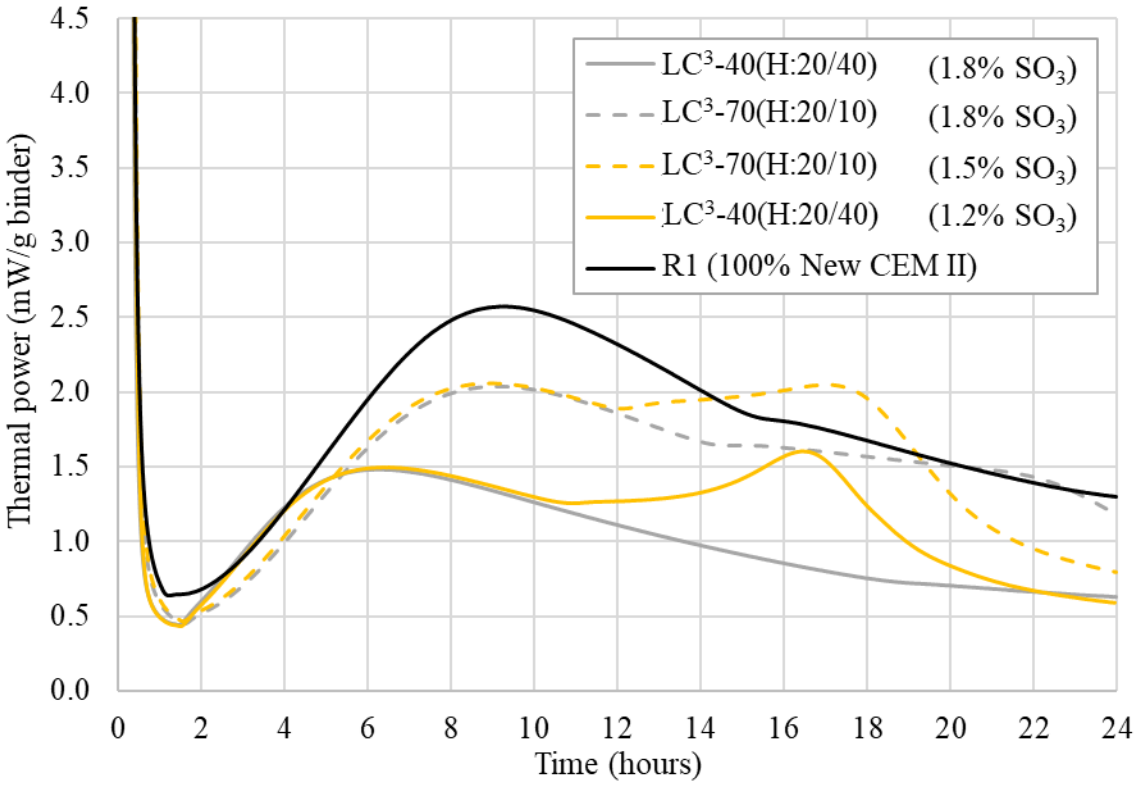

Figure 5.6: HoH curves of LC^3 pastes (Boundary proportions) with New H-Clay

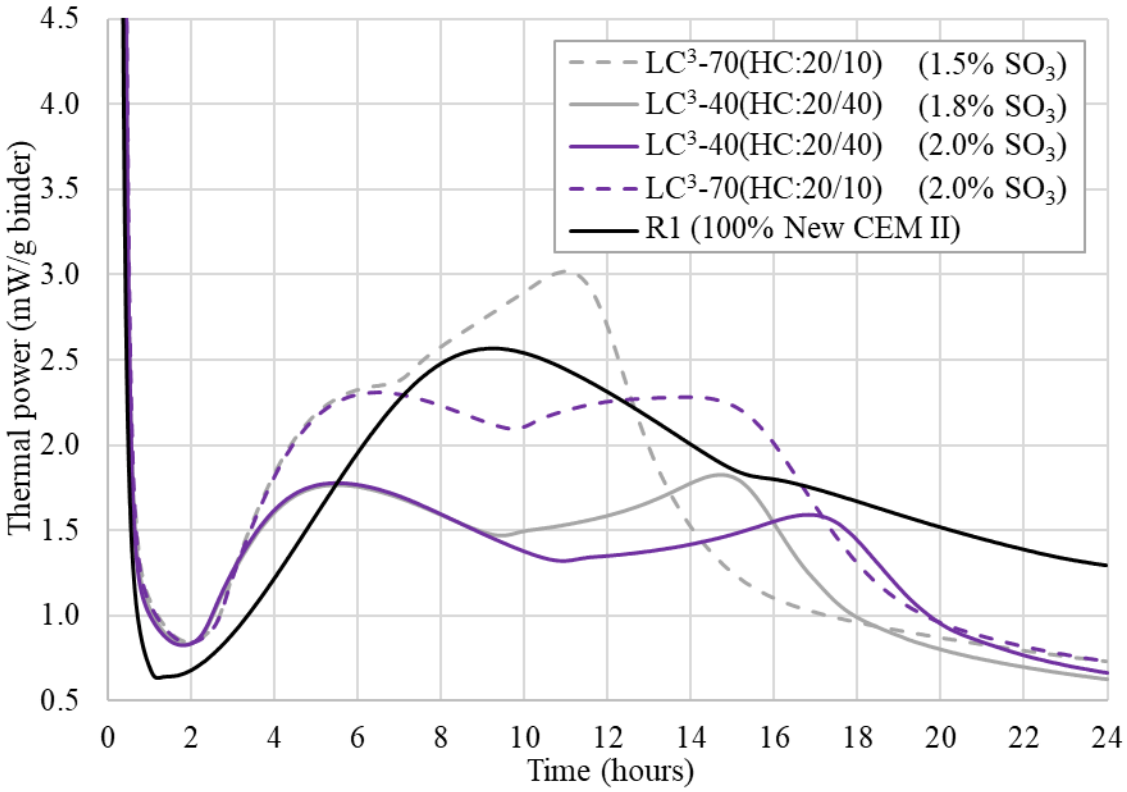

Figure 5.7: HoH curves of LC^3 pastes (Boundary proportions) with HC-Clay

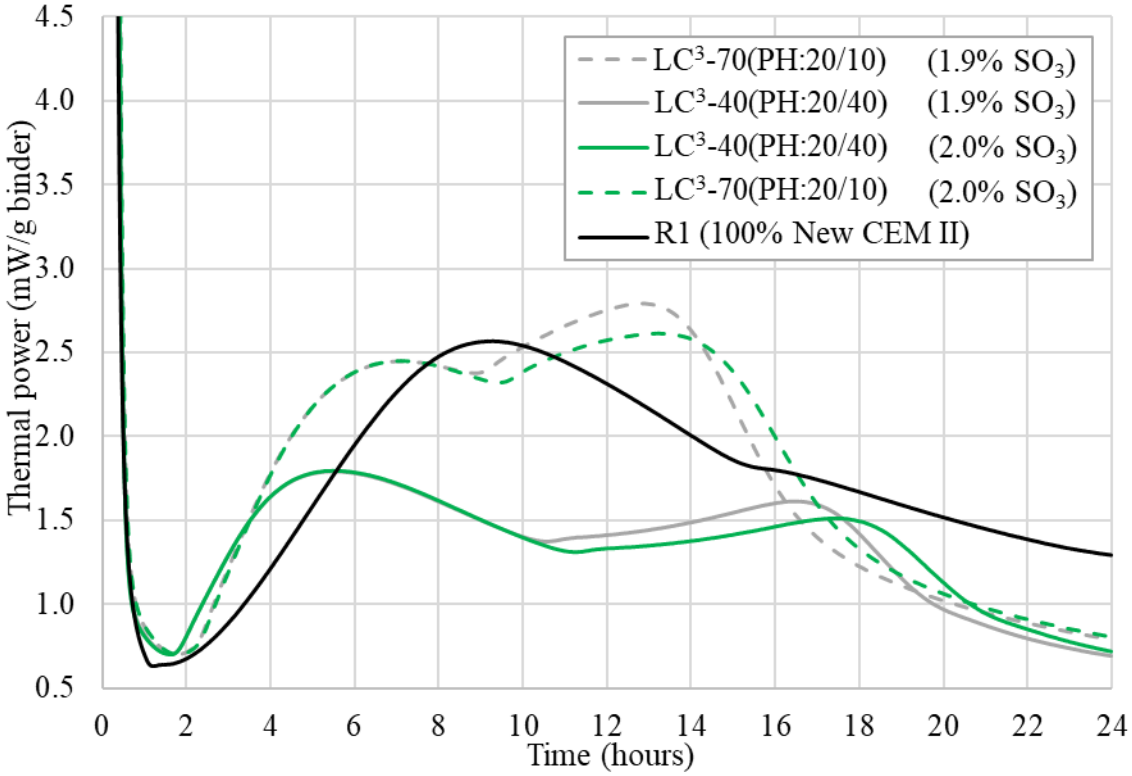

Figure 5.8: HoH curves of LC^3 pastes (Boundary proportions) with PH-Clay

5.2.2 Compressive strength of mortars

As pointed out in the previous sections, in order to reduce the amount of materials for the research, the compressive strength of mortars was used as the performance criterion for optimization of binder proportions. 50 mm cube mortars with binder and sand in the ratio of 1:3 and w/b ratio of 0.4 were prepared. In all mixes, superplasticiser (Chryso® optima 175) was added to maintain a flow of 145 ± 15 mm (SANS 5862-2, 2006) and the limit was 2% of the total weight of binder. With the HC-Clay, it was only possible to achieve a flow of 135 mm at 2% SP dosage for a mix with 20% calcined HC-Clay, 40% LS and 40% Clinker. In view of this, the HC-Clay was excluded from this work and the proportions used for the concrete work was decided based on the results obtained from optimisation of other clays. As expected, results show that the performance of the mixes depends largely on the clinker content. However, as indicated by Antoni et al. (2012), there must be an optimum proportion with performance similar to a reference mix with 100% PC.

5.2.2.1 LC^3 mortars with B-Clay

The results of the compressive strength of the LC^3 mortars (at 1, 3, 7, 28 and 90 days) with B-Clay and Old-CEM II, of each mix proportion (A to G as defined in Table 5.2), are presented in Table 5.4 and plotted in Figure 5.9. Results for the LC^3 mortars with B-Clay and New CEM II are presented in Table 5.5 and plotted in Figure 5.10.

In both cases, results show that the reference mixes R1 with 100% CEM II have the highest strength up to 3 days followed by LC^3-70(B:20/10) and LC^3-55(B:35/10). At 7 days, the strength of both LC^3-70(B:20/10) and LC^3-55(B:35/10) mixes with New-CEM II are higher than the reference mixes R1 but lower with Old-CEM II. The performance is opposite at 28 days but with strength values higher compared to the reference mix R2.

At 3 days and 7 days, both LC^3-70(B:20/10) and LC^3-55(B:35/10) mixes, regardless of the difference in the clinker factor of 15%, have approximately the same strength. At 90 days, the reference mixes have the highest strength followed by LC^3-55(B:35/10) mix. In both cases, all other mix proportions have low strength at all ages compared to LC^3-55(B:35/10), LC^3-70(B:20/10) and R1 mixes, and the LC^3-40(B:20/40) mixes produce the lowest strength at all ages. It is clear from the results that in both cases the optimum mix proportion in terms of strength with the lowest clinker factor is LC^3-55(B:35/10).

Table 5.4: Compressive strength of LC^3 mortars with B-Clay and Old-CEM II

Mix	Compressive strength (MPa)									
	1 day		3 days		7 days		28 days		90 days	
	MPa	%	MPa	%	MPa	%	MPa	%	MPa	%
R1	**32.3**	**100**	**67.3**	**100**	**79.8**	**100**	**89.7**	100	**104.8**	100
LC^3-40(B:50/10)	17.7	55	51.7	77	69.1	87	75.6	84	79.1	76
LC^3-40(B:20/40)	16.6	51	37.7	56	58.0	73	70.4	79	72.8	70
LC^3-70(B:20/10)	31.0	96	58.0	86	77.8	98	93.3	104	95.5	91
LC^3-40(B:35/25)	16.8	52	45.1	67	65.6	82	75.7	84	79.4	76
LC^3-55(B:35/10)	25.6	79	59.1	88	79.9	100	91.0	102	97.2	93
LC^3-55(B:20/25)	24.5	76	48.5	72	69.8	88	78.1	87	84.7	81
LC^3-50(B:30/20)	22.7	70	52.5	78	74.9	94	83.9	94	87.7	84

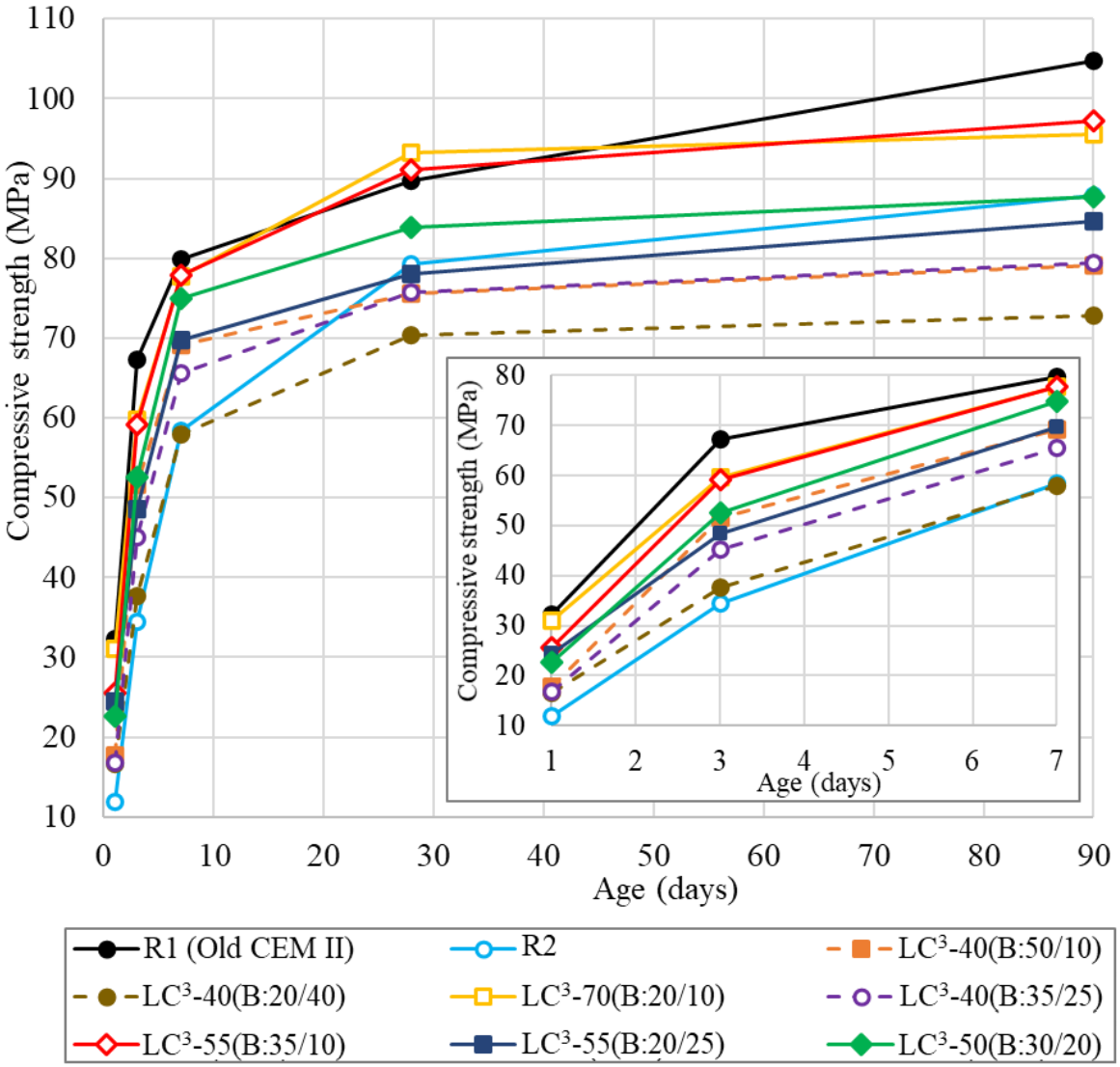

Figure 5.9: Compressive strength of LC^3 mortars with B-Clay and Old-CEM II to 90 days

Table 5.5: Compressive strength of LC^3 mortars with B-Clay and New-CEM II

Mix	Compressive strength (MPa)									
	1 day		3 days		7 days		28 days		90 days	
	MPa	%	MPa	%	MPa	%	MPa	%	MPa	%
R1	**30.0**	100	**64.2**	100	**73.5**	100	**94.1**	100.0	**103.7**	100
LC^3-40(B:50/10)	14.3	48	40.5	63	62.4	85	75.5	80	80.3	77
LC^3-40(B:20/40)	14.3	48	31.3	49	51.6	70	62.3	66	65.4	63
LC^3-70(B:20/10)	26.6	89	48.9	76	76.5	104	90.2	96	95.5	92
LC^3-40(B:35/25)	13.6	45	37.0	58	58.9	80	71.6	76	74.6	72
LC^3-55(B:35/10)	19.4	65	48.9	76	74.9	102	91.3	97	97.2	94
LC^3-55(B:20/25)	20.0	67	41.8	65	62.3	85	75.7	80	77.2	74
LC^3-50(B:30/20)	17.9	60	40.9	64	65.4	89	77.4	82	80.4	78

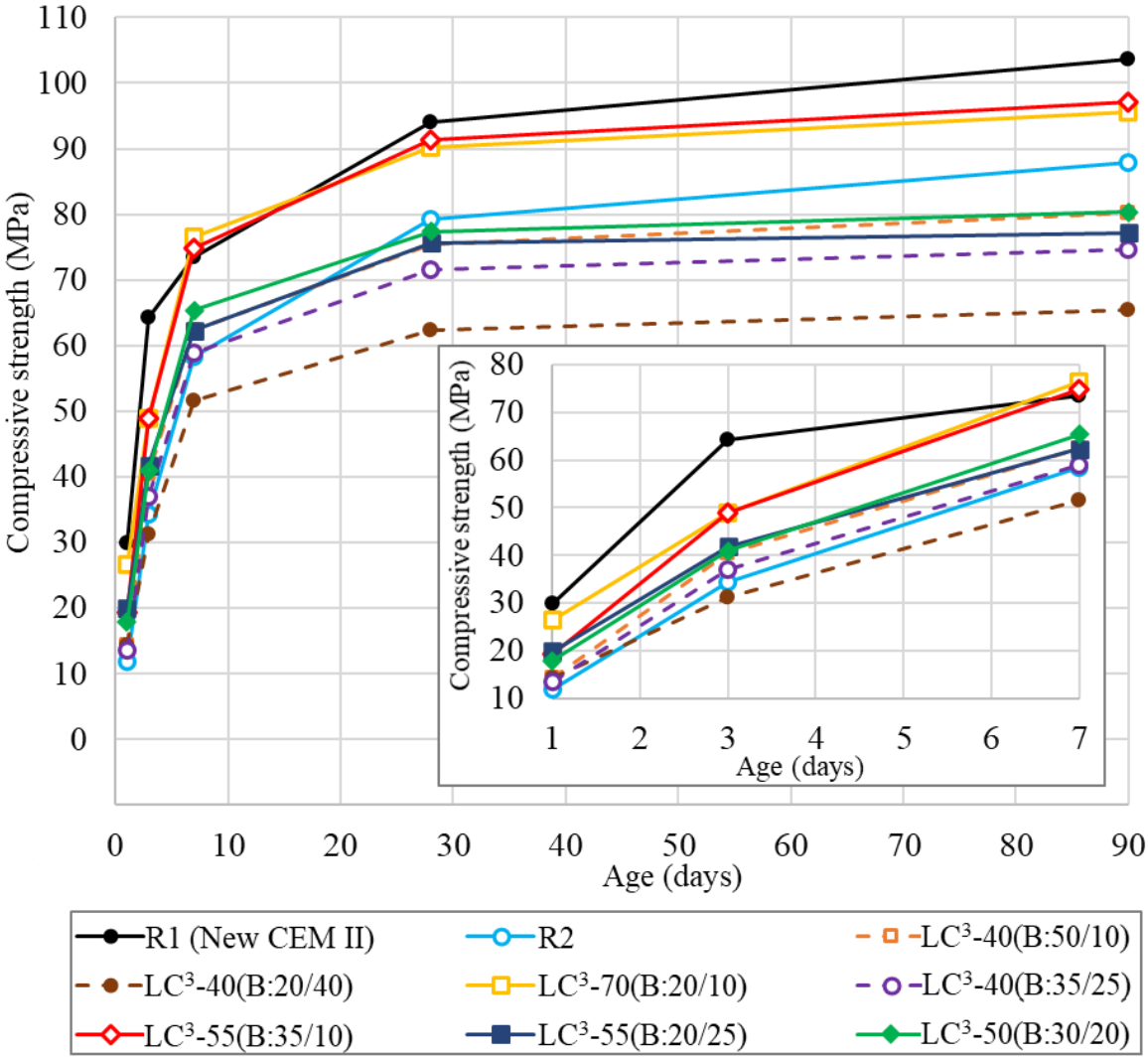

Figure 5.10: Compressive strength of LC^3 mortars with B-Clay and New-CEM II to 90 days

5.2.2.2 LC^3 mortars with New H-Clay

Table 5.6 presents compressive strength results of LC^3 mortars with New H-Clay. The results are plotted in Figure 5.11. In this case, results show that the reference mix R1 has the highest strength at all ages followed by LC^3-70(H:20/10) then LC^3-55(H:35/10).

At all ages, the strength values of all the mix proportions are lower compared to the strength values of the same LC^3 mix proportions with B-Clay. This is mainly because the B-Clay has more kaolinite content than the New H-Clay. It has also high ISA compared to the New H-Clay, so most likely it absorbs more of the available water and therefore reduces the effective water-cement ratio, at the same time the high surface area of the B-Clay made it more reactive than the New H-Clay.

As in the case of LC^3 mortars with B-Clay, all other mix proportions have low strength at all ages compared to LC^3-70(H:20/10), LC^3-55(35/10) and reference mixes, and the LC^3-40(H:20/40) mix produces the lowest strength at all ages.

It is clear from the results that although the LC^3 mortars with New H-Clay produce lower strength than LC^3 mortars with B-Clay, the optimum proportion with the lowest clinker factor is still LC^3-55(H:35/10).

Table 5.6: Compressive strength of LC^3 mortars with New H-Clay and New CEM II

Mix	Compressive strength (MPa)									
	1 day		**3 days**		**7 days**		**28 days**		**90 days**	
	MPa	%	MPa	%	MPa	%	MPa	%	MPa	%
R1	30.0	100	64.2	100	73.5	100	94.1	100	103.7	100
LC^3-40(H:50/10)	10.3	34	23.3	36	47.9	65	69.2	74	70.4	68
LC^3-40(H:20/40)	10.0	33	20.0	31	32.0	44	46.5	49	52.0	50
LC^3-70(H:20/10)	23.1	77	45.6	71	62.0	84	80.0	85	83.4	80
LC^3-40(H:35/25)	10.1	34	21.5	34	39.1	53	60.3	64	65.1	63
LC^3-55(H:35/10)	16.7	56	33.4	52	56.1	76	71.0	76	76.4	74
LC^3-55(H:20/25)	17.1	57	34.9	54	49.0	67	65.2	69	68.0	66
LC^3-50(H:30/20)	14.0	47	29.4	46	47.2	64	62.2	66	65.0	63

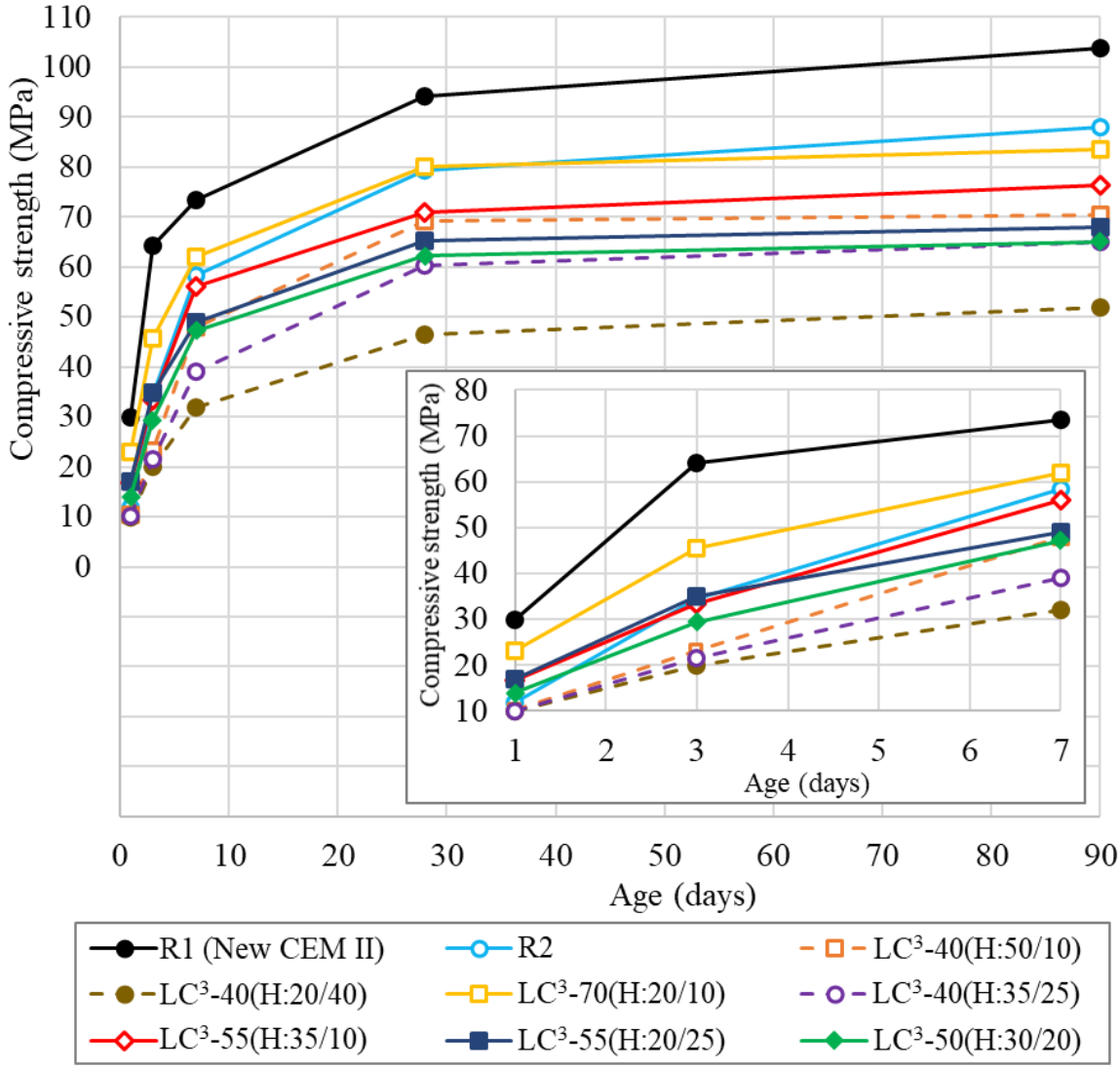

Figure 5.11: Compressive strength of LC^3 mortars with New H-Clay to 90 days

5.2.2.3 LC^3 mortars with PH-Clay

Table 5.7 presents compressive strength results of LC^3 mortars with PH-Clay. The results are also plotted in Figure 5.12. Similar to the results of the LC^3 mortars with B-Clay, the R1 has the highest strength at 1 and 3 days followed by LC^3-70(PH:20/10) and LC^3-55(35/10). At 7 days, the strength of the LC^3-70(PH:20/10) is higher than the strengths of the reference mixes and LC^3-55(PH:35/10). At 28 and 90 days, R1 takes the lead followed by LC^3-70(PH:20/10). All other mix proportions have low strength at all ages compared to LC^3-55(PH:35/10), LC^3-70(PH:20/10), and R1 mixes, and as in the case of LC^3 mixes with B-Clay and New H-Clay, the LC^3-40(PH:20/40) produce the lowest strength at all ages.

Table 5.7: Compressive strength of LC^3 mortars with PH-Clay and New CEM II

Mix	Compressive strength (MPa)									
	1 day		3 days		7 days		28 days		90 days	
	MPa	%	MPa	%	MPa	%	MPa	%	MPa	%
R1	**30.0**	100	**64.2**	100	**73.5**	100	**94.1**	100	**103.7**	100
LC^3-40(PH:50/10)	21.5	72	51.3	80	67.2	91	76.8	82	78.5	76
LC^3-40(PH:20/40)	15.8	53	40.2	63	51.0	69	55.3	59	58.2	56
LC^3-70(PH:20/10)	28.5	95	58.3	91	77.4	105	87.7	93	88.3	85
LC^3-40(PH:35/25)	18.1	60	45.2	70	56.9	77	65.8	70	70.0	68
LC^3-55(PH:35/10)	24.9	83	53.8	84	71.0	97	80.2	85	84.6	82
LC^3-55(PH:20/25)	22.3	74	48.0	75	63.3	86	70.1	75	71.7	69
LC^3-50(PH:30/20)	21.6	72	48.6	76	65.3	89	70.9	75	76.8	74

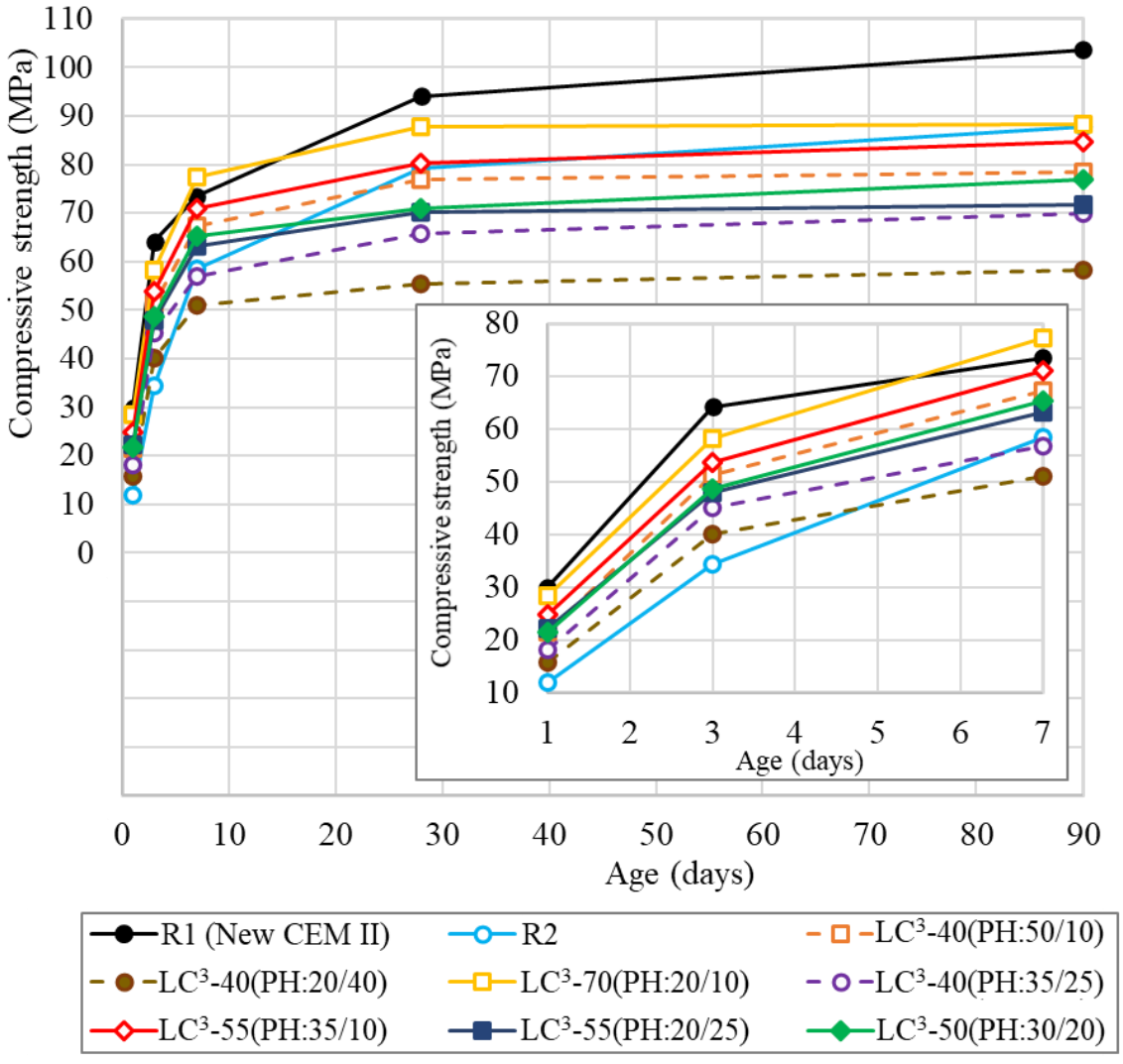

Figure 5.12: Compressive strength of LC^3 mortars with PH-Clay to 90 days

At all ages, the strengths of all the LC^3 mixes are higher compared to the strength values of same LC^3 mix proportions with New H-Clay but lower than most of the LC^3 mixes with B-Clay. This is mainly because of the kaolinite content, the PH-Clay which has high ISA than both B-Clay and New H-Clay, but its kaolinite content is lower than B-Clay and higher than New H-Clay. It is evident from the results that although the LC^3 mortars with PH-Clay produce lower strength than LC^3 mortars with B-Clay, but still the optimum mix with less clinker is LC^3-55(PH:35/10).

5.2.2.4 CC-LS-Clinker ternary plots

Figure 5.14 to Figure 5.17 present the compressive strength results of the LC^3 mortars relative to the results of the reference mix R1 in the CC-LS-Clinker ternary plots at different ages. The plots were drawn with the help of the open source "R Software" using the algorithm shown in Figure 5.13. From the results, it is clear that up to about 24 hours the development of compressive strength is mainly contributed by the hydration of clinker phases whereas from about 3 days the system needs more CC than LS, which suggests that the main contribution comes from the pozzolanic reaction. This is also clear at 7 days but at 28 days the pozzolanic reaction is observed to slow down, which is probably due to the low amounts of CH or CK in the system, and most likely there is still a reaction occurring between alumina (from clay) and $C\overline{C}$ (from LS-K5) to form carboaluminate phases.

Lower boundaries

Compressive strength values at points A to G as noted in Table 5.2

```
orig < - Xvert(nfac = 3, lc = c(0.4, 0.1, 0.2), uc = c(1, 1, 1),
ndm = 1, plot = FALSE)
y < - c (f'c(A), f'c(B), f'c(C), f'c(D), f'c(E), f'c(F), f'c(G))
orig < -cbind(orig[1:7, ], y)
quadm < -lm (y ~ -1 + x1 + x2 + x3 + x1:x2 + x1:x3 + x2:x3 + x1:x2:x3, data = orig)
title < -c ("Actual Component Space", "Pseudo Component Space")
option < -c (FALSE, TRUE)
for (i in 1:2) {
ModelPlot(model = quadm,
dimensions = list (x1 = "x1", x2 = "x2", x3 = "x3"),
main = title[i], lims = c (0.40, 1, 0.10, 1, 0.20, 1),
constraints = TRUE, contour = TRUE, cuts = 7, fill = TRUE,
axislabs = c ("Clinker", "LS", "CC"), cornerlabs = c ("Clinker", "LS", "CC"),
pseudo = option[i])
}
```

Figure 5.13: Algorithm used to draw CC-LS-Clinker ternary plots using R software

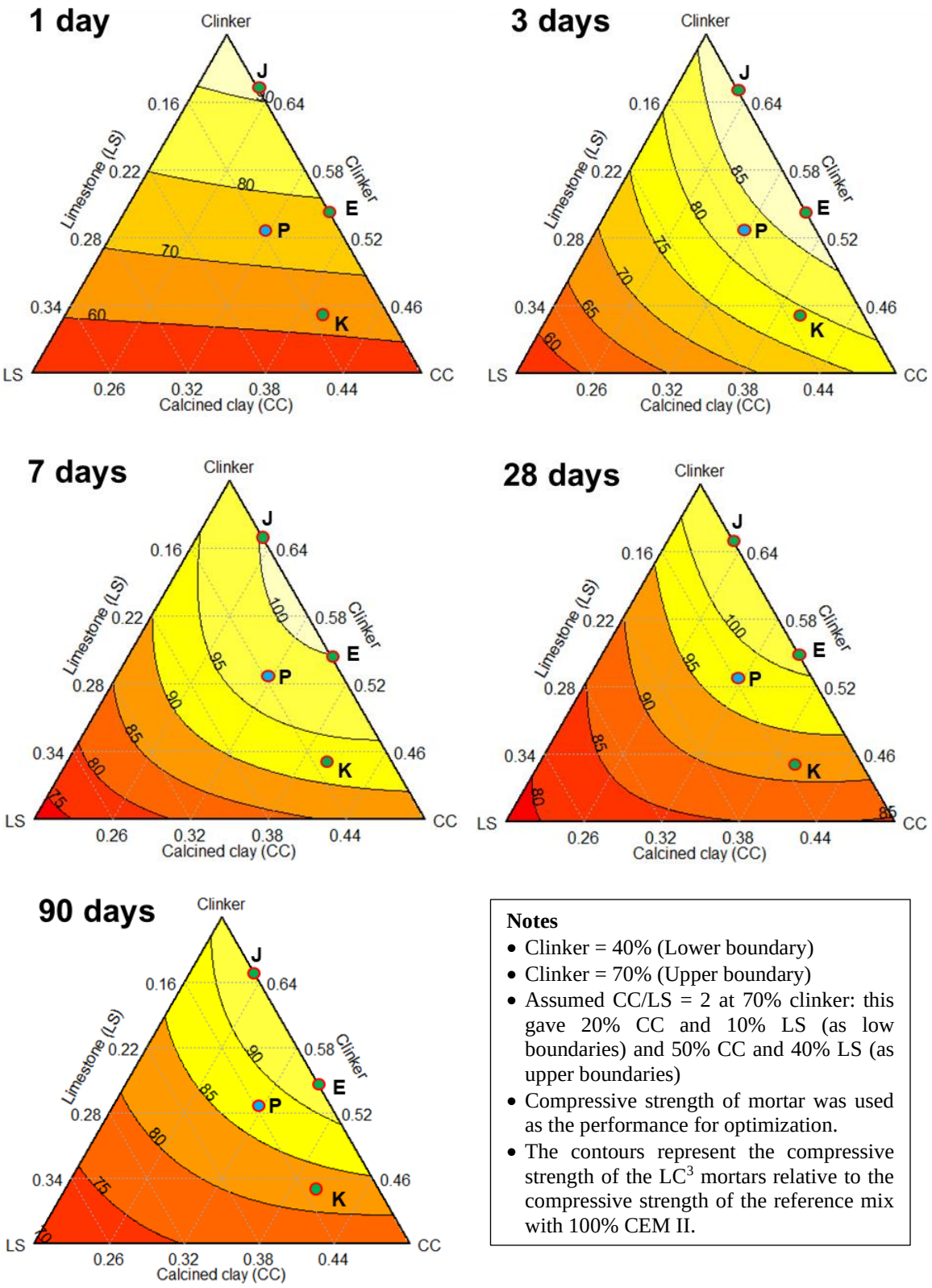

Figure 5.14: CC-LS-Clinker plot of the compressive strength of LC^3 mortars with B-Clay and Old-CEM II

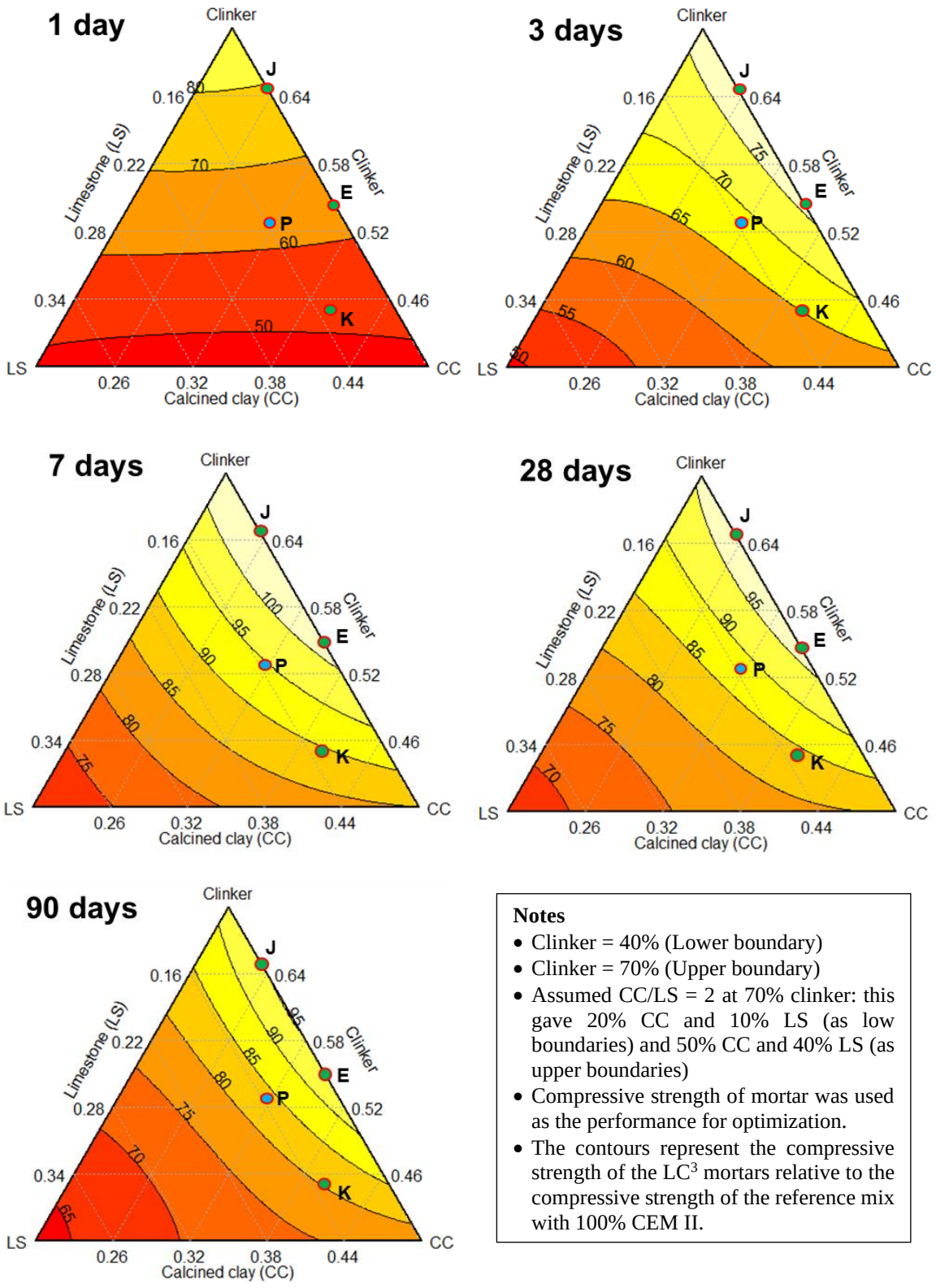

Figure 5.15: CC-LS-Clinker plot of the compressive strength of LC^3 mortars with B-Clay and New-CEM II

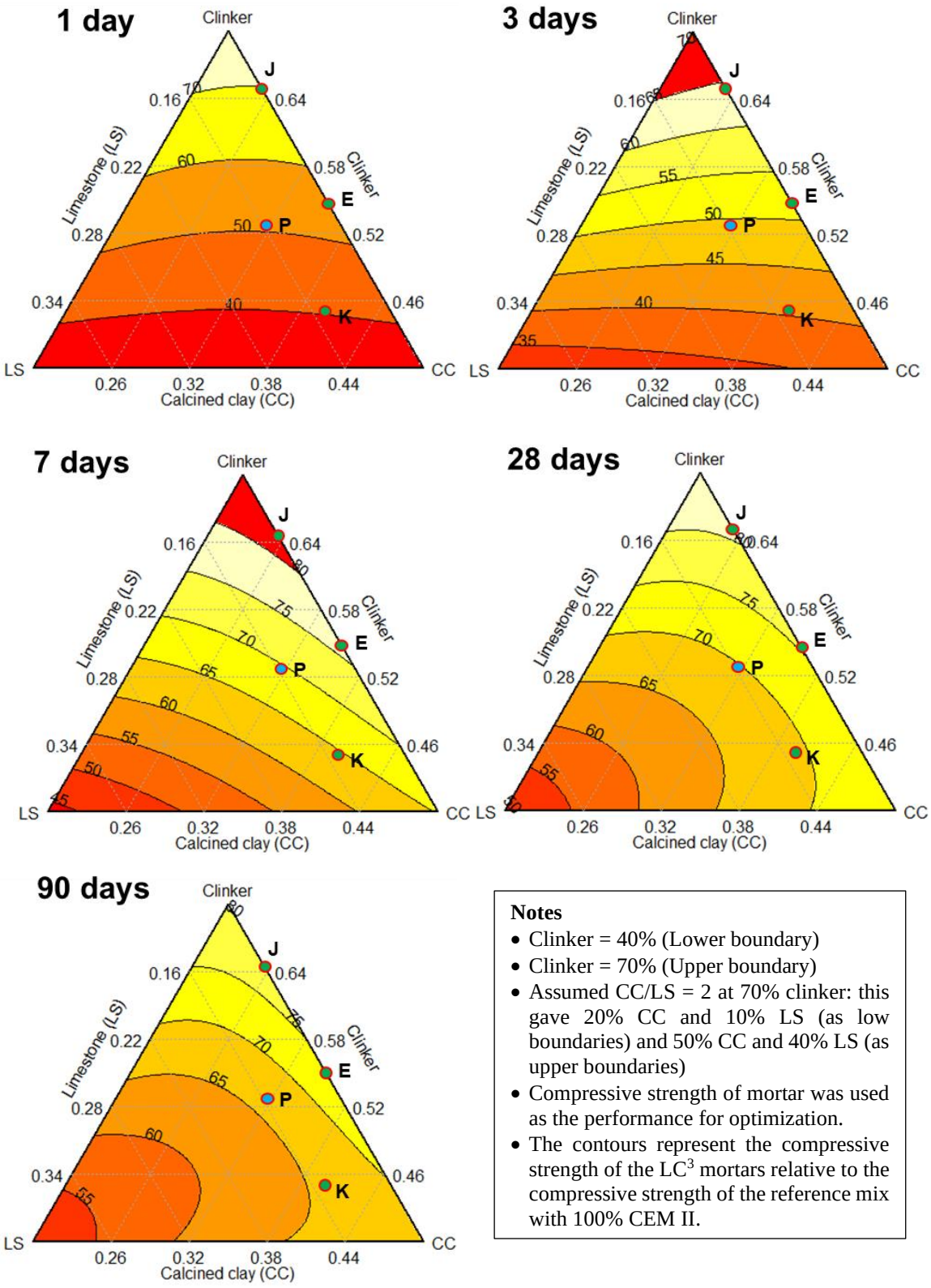

Figure 5.16: CC-LS-Clinker plot of the compressive strength of LC^3 mortars with New H-Clay and New CEM II

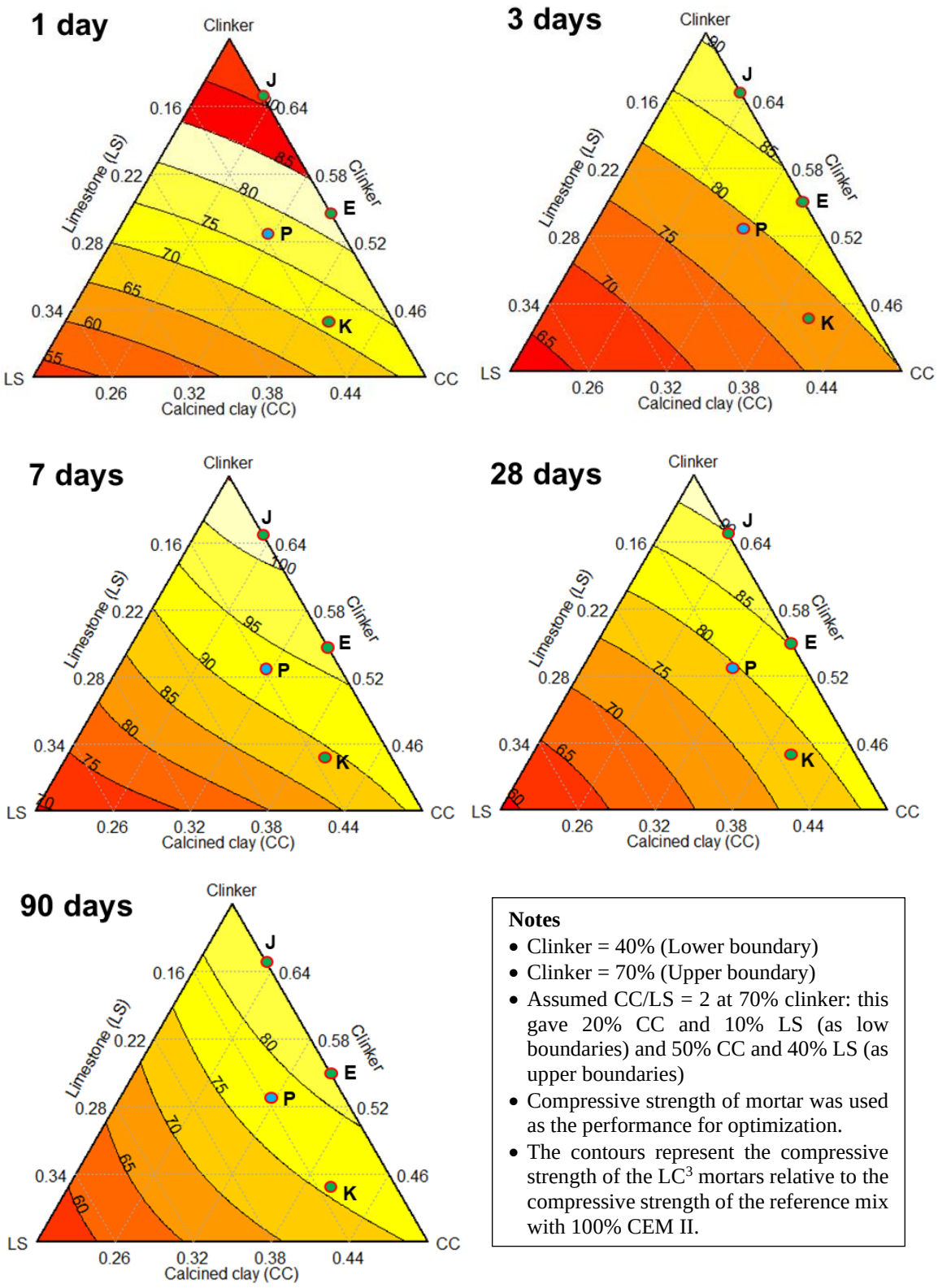

Figure 5.17: CC-LS-Clinker plot of the compressive strength of LC^3 mortars with PH-Clay and New CEM II

5.2.2.5 Discussion

The aim of the work on mortar compressive strength was to obtain the optimum LC^3 proportion with the lowest clinker factor based on the compressive strength results of mortar. In general, the results obtained suggest that, for optimum performance, regardless of the compressive strength values obtained for each LC^3 mix with different CC, the lowest clinker factor is 0.55 (Point E on the CC-LS-Clinker plots), at which the CC factor is 0.35 and the LS factor is 0.1 abbreviated here as LC^3-55.

In the literature, the majority of researchers are reporting the compressive strength performance of the LC^3-50 system (i.e., LC^3 mix with 50% clinker and CC/LS ratio of 2:1 by mass) using either mortar (Bishnoi et al., 2014; Emmanuel et al., 2016; Sui et al., 2019; Shah et al., 2020; Yu et al., 2021) or concrete (Dhandapani et al., 2018; Nguyen, Khan and Castel, 2018; Avet, Sofia and Scrivener, 2019; Shah et al., 2020). This proportion was first reported in 2012 after a study done on mortars with clinker content fixed at 50% (Antoni et al., 2012). On the CC-LS-Clinker plots (Figure 5.14 to Figure 5.17), the LC^3-50 proportion (ignoring the amount of gypsum) is at point P, with about 90% to 95% compressive strength compared to LC^3-55. However, from an economic point of view, the LC^3-50 system with low amounts of clinker and higher amounts of LS would be preferred. In addition, since the reactivity of both CC and LS depends on the availability of CH in the system (Krishnan, Dhoopadahalli and Bishnoi, 2020), it is obvious that the optimal LC^3 proportion would also depend on the reactivity/composition of the clinker (Krishnan and Bishnoi, 2020).

Factors such as purity and fineness of the CC and LS may affect the performance of the system. The European standard (BS EN 197-5, 2021) and American standard (ASTM C595/C595M, 2021) limit the purity of limestone at greater than 75% and 70%, respectively. However, it has been reported that only about 40% kaolinite content in the clay is sufficient for good performance. Likewise, Krishnan and Bishnoi (2018) and Krishnan, Kanaujia, et al. (2018) observed that the purity of LS has minimal effect on the performance of the LC^3 system as only a small fraction of $C\overline{C}$ is required to react with the alumina phases (from the clinker) and MK (from CC) to form carboaluminate phases (Antoni et al., 2012). This concurs well with the XRD scans shown in Figure 5.23 and the

results of $C\overline{C}$ quantification (from TGA results) at different ages presented in Table 5.9 and plotted in Figure 5.25. Regarding fineness, it has been reported that the fineness of both clinker and CC significantly influences the compressive strength performance of the system whereas the fineness of LS only influences the performance of the system at the early age (Anders et al., 2015). In this research, samples of clay were ground to have particle sizes with d_{90} < 30 µm and d_{50} < 10 µm. The CEM II used had particle sizes with d_{90} < 33.5µm and d_{50} < 11.9 µm and LS with d_{90} < 16.4 µm and d_{50} < 8.2 µm as presented in Table 3.2 and Table 4.5.

On the understanding that high compressive strength is not necessarily a proxy for high durability, as elaborated in Alexander (2021) from page 436, two other mixes were also selected together with LC^3-55 for further work: one with 45% clinker, 40% CC and 15% LS, abbreviated as LC^3-45 (point K in the CC-LS-Clinker plots), the other with 65% clinker, 25% CC and 10% LS or LC^3-65 (point J in the CC-LS-Clinker plots).

5.3 HoH and total heat curves of the selected mixes up to 7 days (done on paste)

As indicated in Section 5.2.2.5 above, for each clay only three proportions of binder were considered for the concrete work as shown below. The proportions are within the boundaries used for optimisation. In view of this, the same amount of SO_3 obtained as described in Section 5.2.1.2 (Sulphate and alkali added) were used.

i) 65% clinker, 25% CC and 10% LS (or LC^3-65)
ii) 55% clinker, 35% CC and 10% LS (or LC^3-55)
iii) 45% clinker, 40% CC and 15% LS (or LC^3-45)

and all with a w/b ratio of 0.4.

For a w/b ratio of 0.55, only LC^3-55 mixes were considered. The HoH and total heat curves of all the selected mixes with different clays and w/b ratio of 0.4, together with the reference mixes (R1 and R2), are presented in Figure 5.18, Figure 5.19, and Figure 5.20. The results are normalised per gram of binder. R1 is with 100% CEM II and R2 is with 50% CEM II replaced by GGBS. Figure 5.21 present the HoH and total heat curves for the LC^3-55 mixes with a w/b ratio of 0.55. A detailed HoH curve is given in Figure 5.22 (the case of LC^3-45(B)).

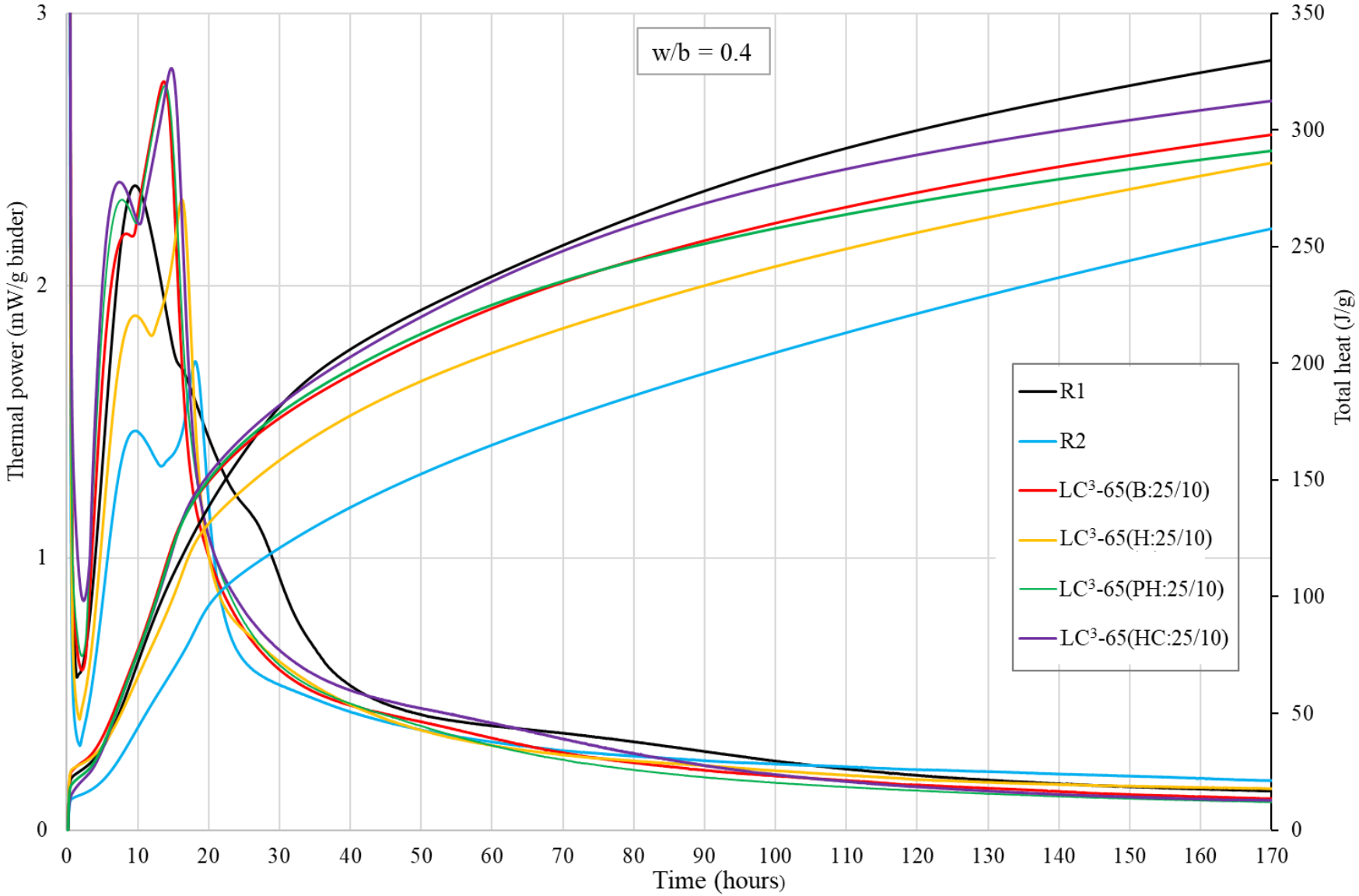

Figure 5.18: HoH and total heat curves of LC^3-65 pastes and reference mixes (w/b = 0.4)

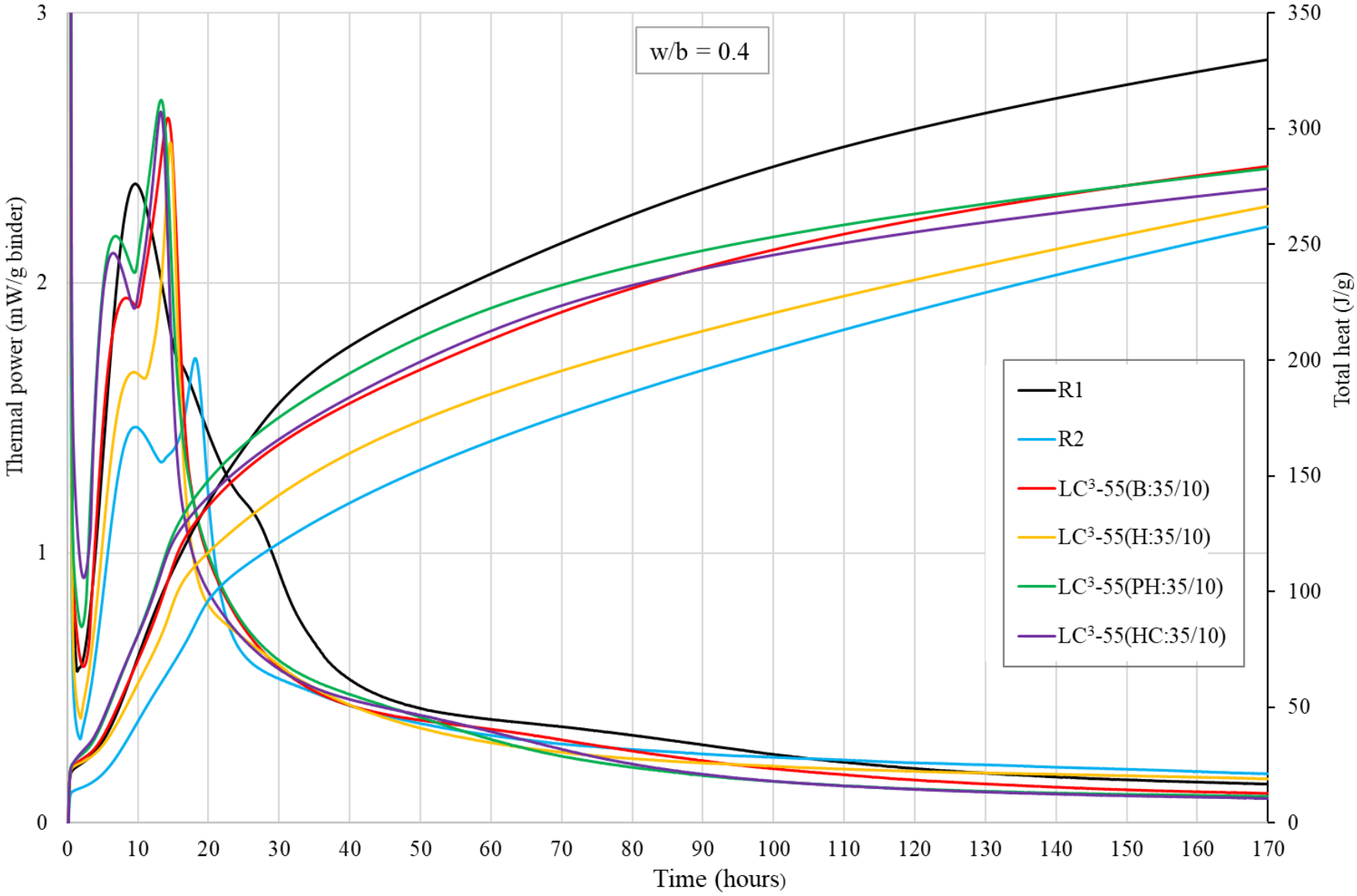

Figure 5.19: HoH and total heat curves of LC^3-55 pastes and reference mixes (w/b = 0.4)

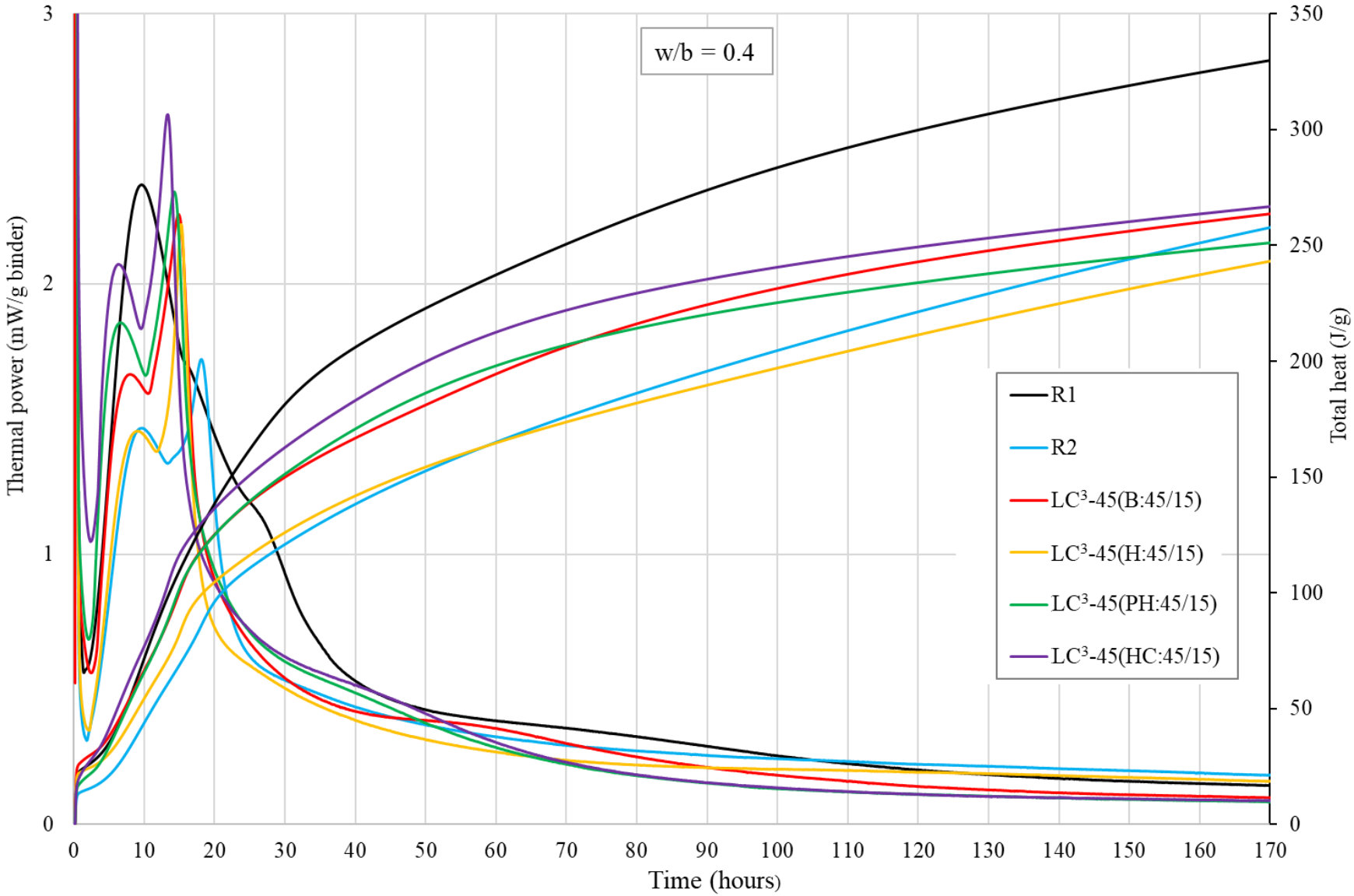

Figure 5.20: HoH and total heat curves of LC^3-45 pastes and reference mixes (w/b = 0.4)

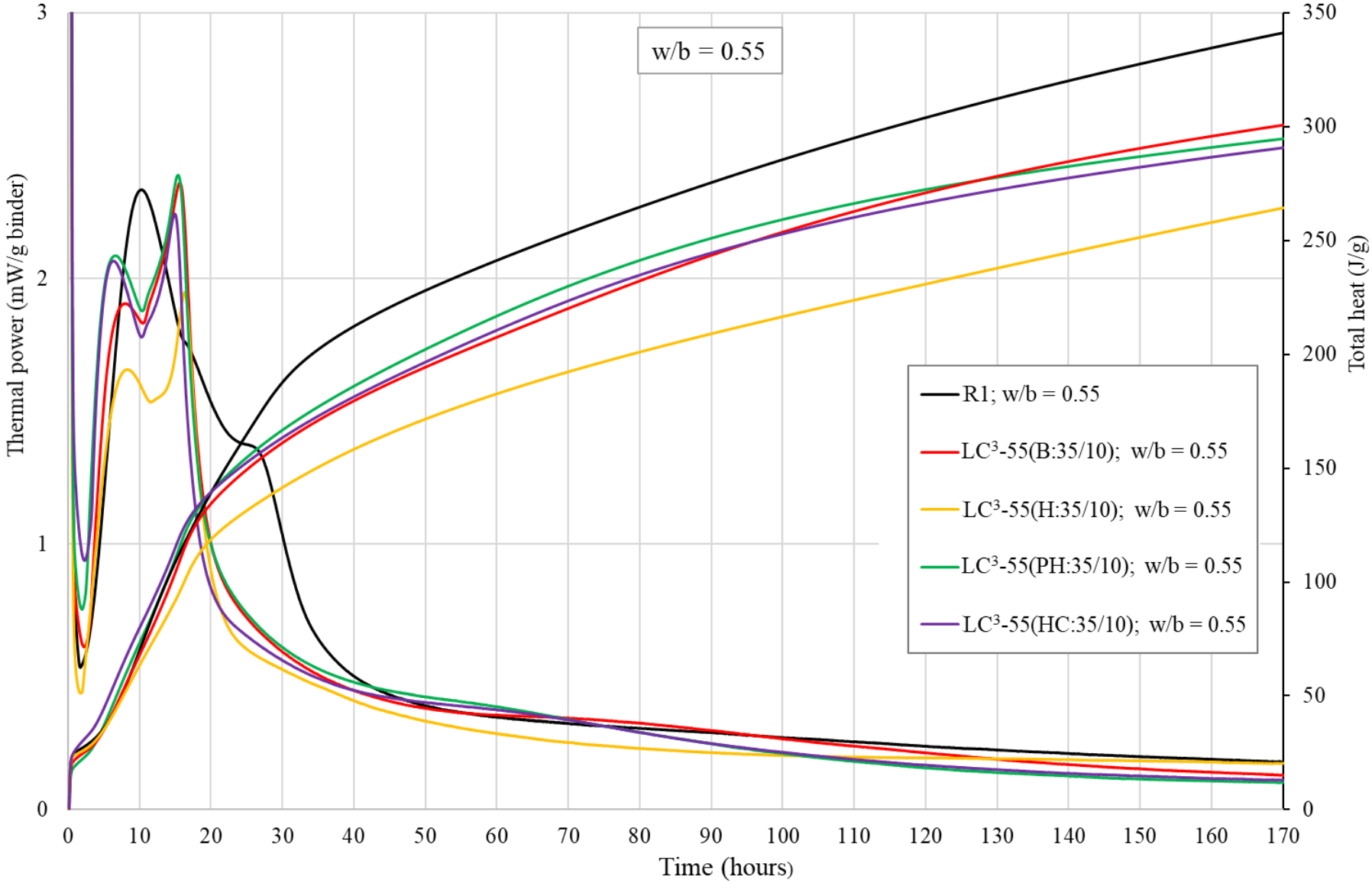

Figure 5.21: HoH and total heat curves of LC^3-55 pastes versus reference mix R1 (w/b = 0.55)

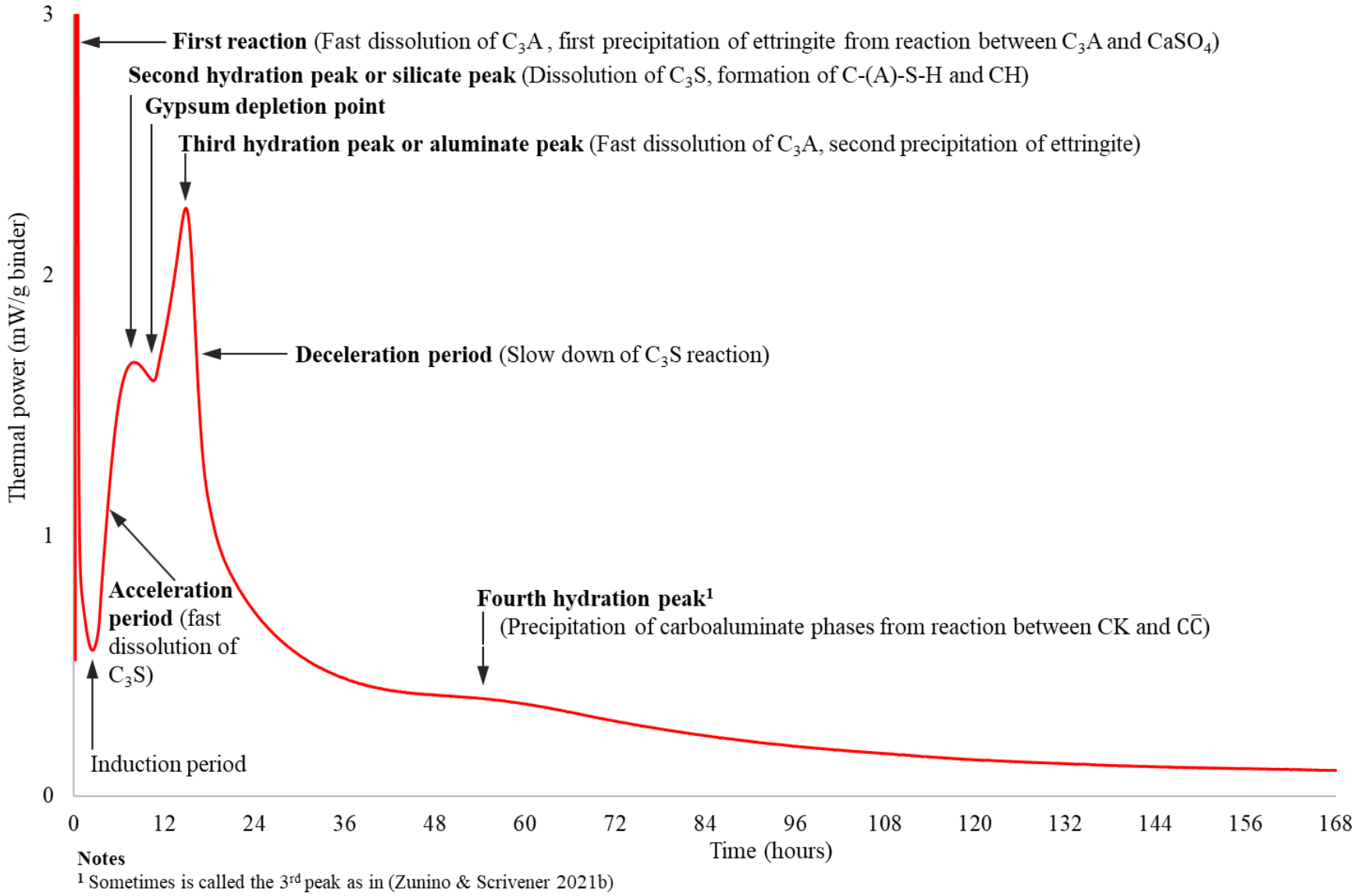

Figure 5.22: Detailed HoH curve, a case of LC^3-45(B)

5.3.1 The induction periods

In all cases, the induction period is about 2 hours. This is when the hydration of silicate phases starts to progress but at a very low rate before gradual increase of heat of hydration until the hydration of C_3S reaches its maximum peak. In general, this period is also controlled by nucleation and precipitation of C-S-H in the system (Taylor, 1997). Looking at the position of the curves during this period, it is clear that the intensities of the curves can be related to the ISAs of the clay. In this case, the intensities of the LC^3 mixes with HC-Clay (which has the highest ISA than all other clays) are high followed by the LC^3 mixes with PH-Clay then LC^3 mixes with B-Clay and the LC^3 mixes with New H-Clay (which has the lowest surface area compared to all other clays) have the lowest intensities.

5.3.2 The second hydration peaks

This second hydration peak (or the silicate peak) is mainly related to the fast dissolution of C_3S and formation of C-(A)-S-H in the system (Pardal, Pochard and Nonat, 2009; L'Hôpital et al., 2015; Avet and Scrivener, 2018). The second hydration peak of all the mixes (including reference mixes) takes place within 12 hours but a bit earlier for the LC^3 mixes compared to reference mixes and earlier for the LC^3 mixes with the highest replacement level of clinker (LC^3-45).

The reference mix R1 has the highest intensity in all cases except in the case of LC^3-65 (Figure 5.18) where the LC^3(HC) has the highest intensity. The peak of the LC^3-65(PH) is also very similar to the reference mix R1. In all other cases, the reference mix R1 has the highest intensity followed by LC^3(PH) in the case of LC^3-55 mixes and LC^3(HC) in the case of LC^3-45 mixes. The reference mix R2 has the lowest intensity compared to all the LC^3 mixes except LC^3-45(New H). In all cases, the LC^3 mixes with the New H-Clay have the lowest intensity compared to all other LC^3 mixes. The trend of the intensities observed in the case of LC^3-55 mixes with a w/b ratio of 0.55 (Figure 5.21) is similar to that of a w/b ratio of 0.4 (Figure 5.19).

In all cases, the pattern of the LC^3 peaks can be largely related to the ISA of the clay, the LC^3 mixes with New H-Clay (which has the lowest ISA than all the other clays) have the

lowest first peak compared to all other LC^3 mixes whereas the LC^3 mixes with HC-Clay (which has the highest ISA than all the other clays) have the highest first peak except in the case of LC^3-55 (both w/b ratios) and the LC^3 mixes with PH-Clay have the highest peak but very close to the LC^3 mixes with HC-Clay.

5.3.3 The third hydration peaks

The third hydration peak (or the aluminate peak) is largely related to the fast dissolution of aluminates and formation of ettringite instead of monosulphate as in case of 100% cement without LS (Quennoz and Scrivener, 2013; Zunino and Scrivener, 2019). It is clear from the HoH curves that the intensities of the third hydration peaks of the LC^3 mixes and reference mix R2 are very high compared the first hydration peaks of the same mixes and the second peak of reference mix R1. This is because of more alumina in the system coming from CC in the case of LC^3 systems, or GGBS in the case of reference mix R2. It is also clear that all the second hydration peaks appear well after the first peaks and between 13 and 18 hours as expected. This confirms that the adjustment of SO_3 was properly done and met the target. The intensities of the third peaks of the LC^3 mixes have a similar trend as the second peaks of the same mixes as described in Section 5.3.2 above.

5.3.4 The fourth hydration peaks

The fourth peak is largely related to the precipitation of carboaluminate phases when CK reacts with $C\overline{C}$, and its position depends highly on the amount of CK in the system (Zunino and Scrivener, 2021b). From the results, the intensities of the fourth peaks of the LC^3 mixes are lower, broader and occur much later (after 48 hours) than the third peak of the reference mix R1. It is difficult to directly compare the pattern (intensity and position) of the fourth LC^3 peaks as the intensities are very low and not sharp.

5.3.5 The total heat curves

In all cases, the total heat curves indicate more rapid early hydration in the LC^3 mixes compared to the reference mix R2. The reference mix R1 produced the highest total heat than all other mixes from about 24 hours. In the case of LC^3-65 mixes, the total heat of all the LC^3 mixes except the LC^3(New H) is higher than the reference mix R1 up to 24 hours. The reference mix R2 produced the lowest total heat in all cases except in the case of LC^3-

45 where its total heat is higher than the LC^3(New H) from about 60 hours and higher than the LC^3(PH) from about 150 hours.

Considering only the LC^3 mixes, it is clear that the LC^3 mixes with HC-Clay (which has the highest ISA than all other clays) produced the highest heat compared with the LC^3 mixes with more kaolinite content than HC-Clay (B-Clay and PH-Clay), especially in the case of LC^3-65 and LC^3-45. This could also be another sign of the importance of the ISA of the clay as it affects the effective water to cement ratio and therefore the total heat produced. In addition, the high surface area also increases the rate of chemical reaction.

In the case of LC^3-55, the LC^3(PH) produced the highest total heat up to about 150 hours in the case of the 0.4 w/b ratio and up to 125 hours in the case of the 0.55 w/b ratio. The LC^3 mixes with B-Clay are observed to produce the highest total heat from between 72 hours and 96 hours in the case of the 0.4 w/b ratio and between 96 hours and 132 hours in the case of the 0.55 w/b ratio. The slowing down with time of the LC^3 mixes with PH-Clay and HC-Clay in the total heat produced relative to the LC^3 mixes with B-Clay is largely related to the low amount of kaolinite in these clays compared to B-Clay. In all cases, the LC^3 mixes with New H-Clay produced the lowest total heat up to 7 days and this is because this clay has the lowest ISA and low amount of kaolinite than other clays.

5.4 Hydration products (evaluated on paste samples)

The aim in this part of the research was to identify and quantify the hydration products of the selected LC^3 mixes with different clays and compare these with those of the reference mix (R1). As discussed in Section 5.2.2.5, it is clear from the results that, with these materials, for best strength performance, the lowest clinker factor is 0.55, at which the calcined clay factor is 0.35 and the limestone factor is 0.1. Using these proportions and a w/b ratio of 0.4, LC^3 pastes with different clays were prepared, conditioned, and tested as described in Section 3.7 i.e., paste discs of 2.5 mm thick by 24 mm diameter, stored in an air-tight plastic vessel filled with CH until testing, and hydration products characterised using TGA and XRD.

The hydration products at various ages were characterised, as mentioned, using TGA and XRD. At each age (i.e., 1, 3, 7, 28 and 90 days) of the paste, XRD was used to detect

different phases in the specimens and TGA was specifically used to quantify CH, $C\overline{C}$ and bound water at different ages of the specimens. Based on the results obtained, CH was estimated between 400°C and 500°C, $C\overline{C}$ between 600°C and 800°C and the water bound to hydrates (C-S-H, AFm, Aft and CH) was estimated based on the mass change between 105°C and 500°C.

5.4.1 Phases identified from XRD scans

Figure 5.23 presents XRD scans of LC^3-55 pastes with different clays versus R1 up to 90 days. From the scans, all mixes (including reference R1) show the presence of ettringite, CH and calcite (or $C\overline{C}$) at 1 day. All mixes show no formation of monosulphate and stratlingite at all ages. This also supports the idea that the presence of calcite stabilizes formation of ettringite, otherwise ettringite would get converted to monosulphate (Klemm and Adams, 1990; Antoni et al., 2012). Stratlingite is usually stable when CH or carbonate ions are not available in the system (Okoronkwo and Glasser, 2016; Krishnan, Kanaujia, et al., 2018; Krishnan, Emmanuel and Bishnoi, 2019). Avet and Scrivener (2018) also observed no evidence of this phase even at 90 days. However, the XRD scans for the LC^3 mixes presented by Antoni et al. (2012) show evidence of this phase from 7 days onwards which counter observations by Okoronkwo and Glasser (2016), Krishnan, Kanaujia, et al. (2018), and Krishnan, Emmanuel and Bishnoi (2019).

The intensities of CH are observed to decrease as mixes age in all the LC^3 mixes (except the LC^3(New H)) which indicates progress of pozzolanic reaction. Most likely the low intensities of CH phase in the LC^3-55(New H) are due to slow consumption of CH by the New H-Clay.

The intensities of $C\overline{C}$ are observed to decrease with time, which is related to the formation of carboaluminate phases, but at a low rate compared to CH, indicating slow consumption of $C\overline{C}$ by the LC^3 mixes. It is clear at 90 days that most of this phase remains unreacted in the system.

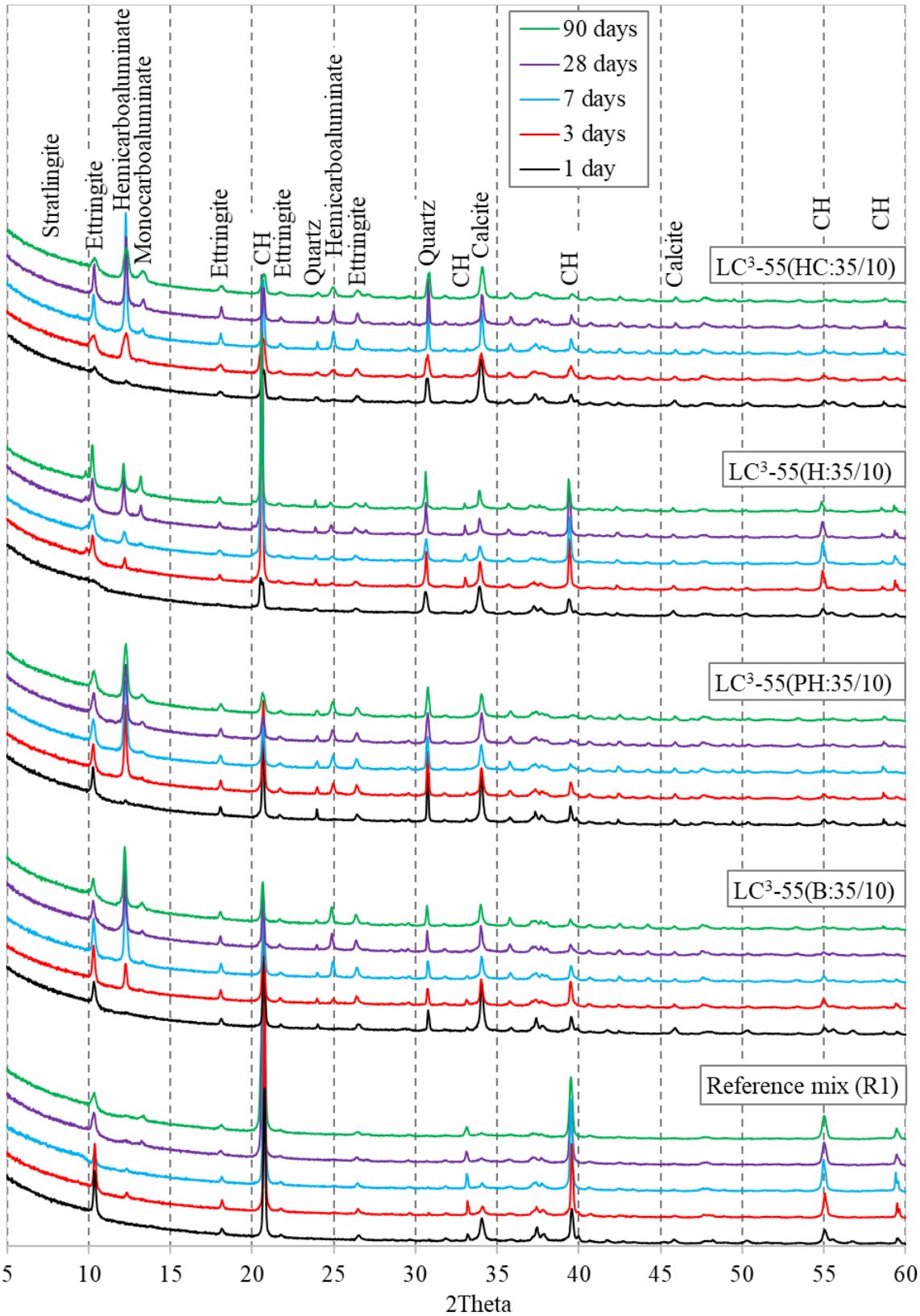

Figure 5.23: XRD scans of LC^3-55 pastes with different clays versus R1 up to 90 days

The LC^3 mixes with PH-Clay (LC^3-55(PH)) and HC-Clay (LC^3-55(HC)) have noticeable hemicarboaluminate peaks from 1 day whereas the reference R1 and LC^3 mixes with B-Clay (LC^3-55(B)), and New H-Clay (LC^3-55(New H)) show visible hemicarboaluminate peaks from 3 days. A study by Antoni et al. (2012) showed formation of hemicarboaluminate from 1 day whereas another study conducted by Avet and Scrivener (2018) showed no formation of hemicarboaluminate at 1 day. This could indicate that the porous nature of the clay affects system performance. As shown in Equations 2.7 and 2.9, the formation of hemicarboaluminate also depends on the availability of water and CH in the system. In this case, since HC-Clay and PH-Clay have high ISA compared to B-Clay and New H-Clay, they absorb more of the available water and therefore reduce the effective water-cement ratio which in turn affects the availability of water and/or CH in the system to react with $C\overline{C}$ and aluminates. However, further research is required to fully understand what is happening.

The monocarboaluminate peak starts to appear at 7 days for all the LC^3 mixes. Both Antoni et al. (2012) and Avet and Scrivener (2018) reported low amount of this phase in the LC^3-50 paste (with clay containing more than 50% kaolinite content) up to 90 days. In the case of reference mix R1, it can be seen that the intensity of the hemicarboaluminate phase is reduced moving from 7 days to 28 days. On the other hand, the peak of the monocarboaluminate phase is observed to appear at 28 days. This indicates that some of the hemicarboaluminate was converted to monocarboaluminate phase during this period, most likely due to the absence of CC in the system (Ipavec et al., 2011; Krishnan, Emmanuel and Bishnoi, 2019).

As expected, the XRD scans of the LC^3 mixes show presence of quartz in the system at all ages. This is the amount of quartz originally present in the calcined clays. The intensities of the quartz are observed to remain unchanged at all ages. This was expected as quartz does not react in the system.

5.4.2 Phases quantified from TGA results

Figure 5.27 to Figure 5.31 present TGA and DTG curves of the R1 paste and LC^3-55 pastes with different calcined clays at different ages up to 90 days. Table 5.8 to Table 5.10

presents amount of CH, $C\overline{C}$, and bound water estimated as described in Section 3.7.2. The amounts are also plotted in Figure 5.24, Figure 5.25, and Figure 5.26, respectively. In general, as discussed in Section 2.8.2, the performance of LC^3 system depends on the chemical effect (i.e., pozzolanic reaction, stabilisation of ettringite, and formation of carboaluminate phases) as well as the filler effect of the added SCMs (i.e., CC and LS). The latter can be ignored in this case as all clays were ground to have similar particle size. The estimated amount of CH, $C\overline{C}$, and water bound to hydrates obtained from the TGA curves are discussed next.

5.4.2.1 Estimated amount of CH at different ages

As expected, the results in Table 5.8 (also plotted in Figure 5.24) show that for the reference mix R1 the amount of CH increases with time (Equations 2.1 and 2.2) while for the LC^3 mixes the amount of CH generally decreases with time as it is reacting with SCMs to produce C-A-S-H and hemicarboaluminate phases as shown in Equations 2.4, 2.7 and 2.9.

Table 5.8: Estimated amount of CH from the TGA curves of the LC^3-55 at different ages

Paste	Estimated amount of CH (%)				
	1 day	**3 days**	**7 days**	**28 days**	**90 days**
Reference R1	7.4	9.9	11.1	12.7	13.2
LC^3-55(B:35/10)	4.7	4.9	3.7	2.5	1.9
LC^3-55(H:35/10)	5.1	6.6	6.2	3.3	3.1
LC3-55(PH:35/10)	4.2	4.3	3.1	2.3	1.6
LC3-55(HC:35/10)	3.3	3.7	3.1	2.5	2.1

Also, as expected, since the amount of clinker in the R1 is high, the amount of CH at 1 day is also high compared to the LC^3 mixes. This is also clear from the XRD scans (Figure 5.23). Looking at the amount of CH for the LC^3 mixes, results show that at 1 day the amount of CH for the LC^3-55(H) is high followed by the LC^3-55(B) then LC^3-55(PH), and LC^3-55(HC) produce the lowest amount of CH. It is evident from the results that, to a large extent, the amount of CH at 1 day depends on the ISA of the clay. The New H-Clay which in this case absorbs less water and therefore makes more water available to react with cement to produce more CH.

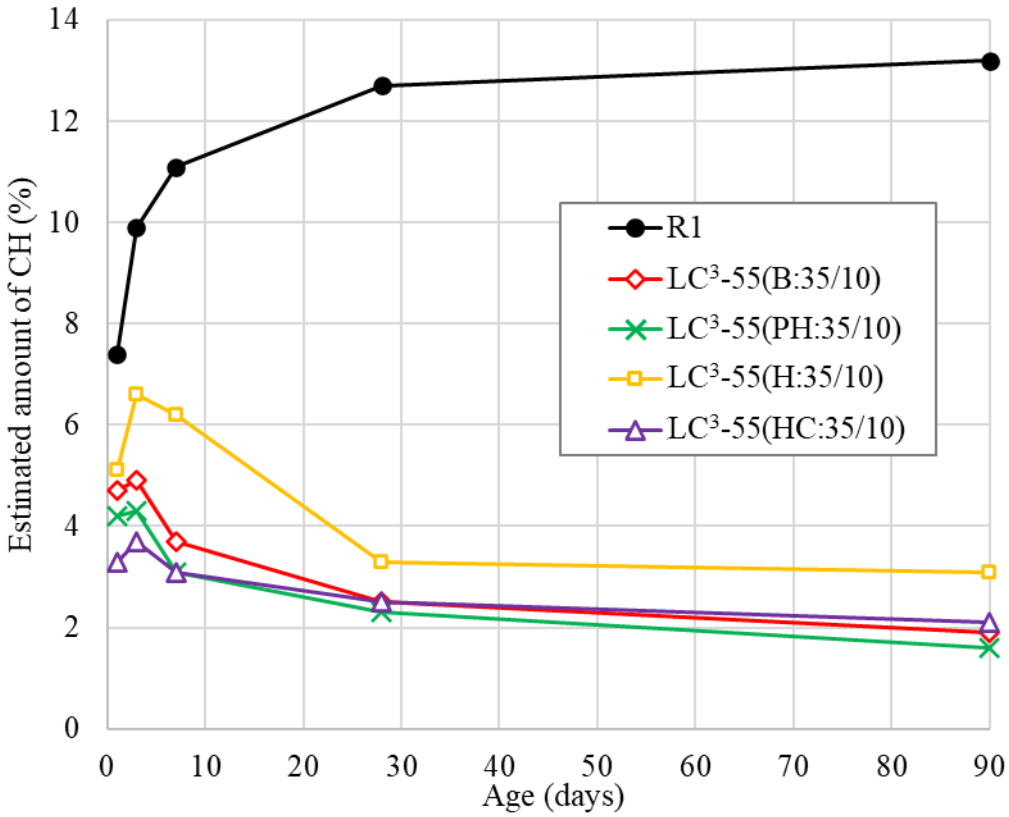

Figure 5.24: Estimated amount of CH from the TGA curves of the LC^3-55 up to 90 days

Between 1 and 3 days, the amount of CH produced is high compared to the amount of CH consumed by SCMs, which explains why there is net increase of CH. From 3 days onwards, there is generally a reduction in the amount of CH for all the LC^3 mixes as some of the CH is consumed by the pozzolanic reaction and formation of carboaluminate and ettringite phases, as seen also from the XRD scans in Figure 5.23.

At 90 days, the remaining amount of CH is high for the LC^3-55(New H) with about 61% of what was available at 1 day, followed by LC^3-55(HC) with about 64%, then LC^3-55(B) with about 40%, and LC^3-55(PH) with about 38% of what was available at 1 day.

In general, results indicate that the remaining amount of CH at any age depends on the amount of CH produced initially, how much is being consumed by the pozzolanic reaction, and formation of carboaluminate and ettringite phases. However, as expected, with low amount of clinker in the LC^3 mixes, there is already a low CH in the system, which is also consumed by the pozzolanic reaction, making the available CH to be significantly lower compared to the 100% CEM II system.

5.4.2.2 Estimated amount of unreacted $C\overline{C}$ at different ages

From the results (Table 5.9 and plotted in Figure 5.25), it is clear that in all the mixes (including R1), the amount of $C\overline{C}$ decreases with time as it is reacting to produce carboaluminate and ettringite phases (Equations 2.7, 2.8 and 2.9). As described in Section 2.8.2, $C\overline{C}$ reacts with C_3A (from the clinker) to form carboaluminate phases (Kevin and Kenneth, 1991; Bonavetti, Rahhal and Irassar, 2001). It also reacts with monosulphate to form monocarboaluminate phase and leads to the stabilisation of ettringite phase (Klemm and Adams, 1990). In the presence of calcined kaolinite clay, the alumina component of the CC also reacts with $C\overline{C}$ (from LS) and enhances the formation of hemicarboaluminate phase (Krishnan, Emmanuel and Bishnoi, 2019).

Table 5.9: Estimated unreacted $C\overline{C}$ from the TGA curves of the LC^3-55 at different ages

Paste	Estimated amount of unreacted $C\overline{C}$ (%)				
	1 day	**3 days**	**7 days**	**28 days**	**90 days**
Reference R1	3.3	3.1	2.8	2.4	1.5
LC^3-55(B:35/10)	6.5	6.1	5.7	5.1	4.9
LC^3-55(H:35/10)	7.0	6.6	5.9	5.3	4.9
LC3-55(PH:35/10)	6.5	5.9	5.8	5.7	5.6
LC3-55(HC:35/10)	6.9	5.8	5.8	5.7	5.5

Results show that at 1 day the amount of $C\overline{C}$ estimated for the LC^3-55(New H) is similar to LC^3-55(HC) whereas for the LC^3(B) the amount estimated is similar to the LC^3-55(PH). The amount is observed to drop at a higher rate between 1 day and 3 days for the LC^3-55(HC) and LC^3-55(PH) and between 1 day and 7 days for the LC^3-55(B) and LC^3-55(New H). After 3 days, the rate of reduction for the LC^3-55(HC) and LC^3-55(PH) is very low and for the LC^3-55(B) and LC^3-55(New H) the rate is low after 7 days. This trend can also be related to the ISA of the respective clay and amount of CH formed to react with $C\overline{C}$.

At 90 days, the remaining amount is high for the LC^3-55(HC) and LC^3-55(PH) with about 80% and 86% of what was available at 1 day, respectively, followed by LC^3-55(B) and LC^3-55(New H) with about 75% and 70% of what was available at 1 day, respectively. As also observed from the XRD scans (Figure 5.23), this indicates that only a small amount of LS reacts in the LC^3 system. This finding agrees well with the observations by (Antoni

et al., 2012; Krishnan, Emmanuel, et al., 2018; Krishnan, Kanaujia, et al., 2018). As per the reactions shown in Equations 2.4, 2.7 and 2.9, the remaining amount at any age depends on the available amount of CH and CK to react with $C\overline{C}$ to produce carboaluminate and ettringite phases.

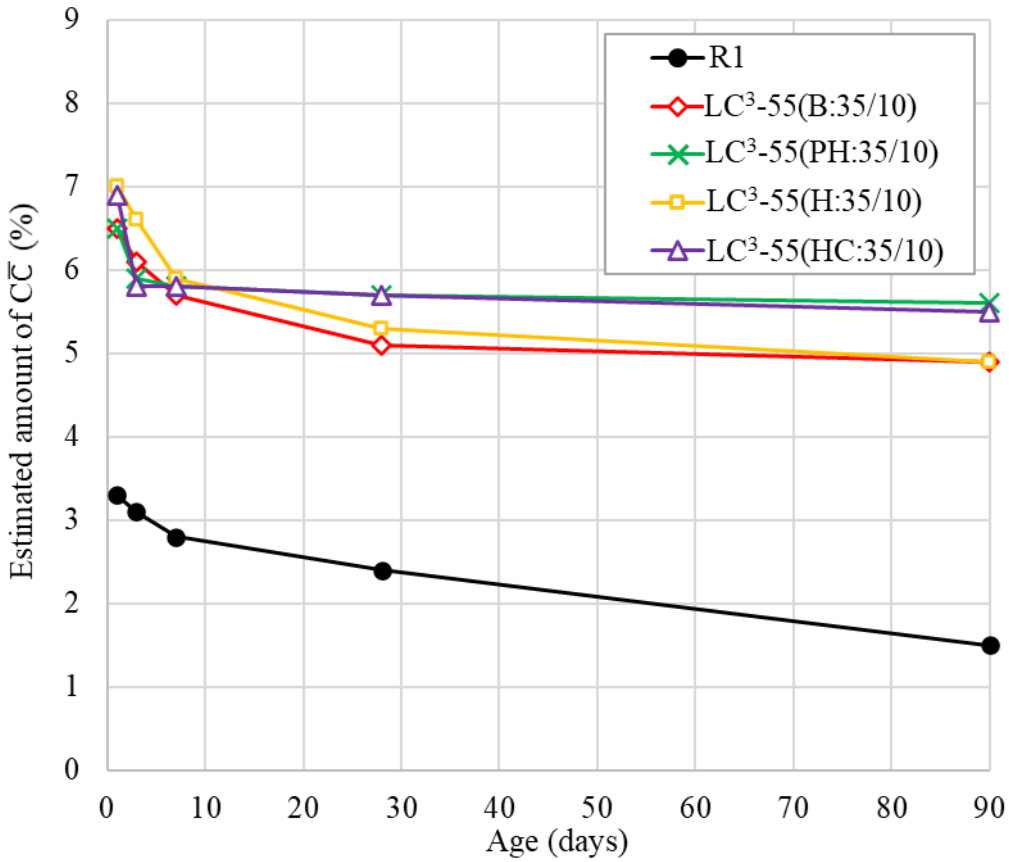

Figure 5.25: Estimated amount of $C\overline{C}$ from the TGA curves of the LC^3-55 up to 90 days

5.4.2.3 Estimated amount of bound water at different ages

As expected, the amount of water bound to hydrates (C-S-H, AFm, AFt, and CH) also increases with time as shown in Table 5.10 and Figure 5.26.

The amount of bound water at 1 day is high for the reference mix. At 3 days, the amount is high for the LC^3-55(PH) compared to all other LC^3 mixes but similar to the reference mix R1. Followed by the LC^3-55(HC) and LC^3-55(B) then LC^3-55(New H).

After 3 days the reference R1 takes the lead followed by the LC^3-55(PH) then LC^3-55(B). This is because of the high amount of CH in the reference mix R1. The LC^3-55(New H) has the lowest bound water at all ages.

Table 5.10: Estimated bound water from the TGA curves of the LC^3-55 at different ages

Paste	Estimated amount of bound water (%)				
	1 day	**3 days**	**7 days**	**28 days**	**90 days**
Reference R1	7.4	10.8	13.8	17.8	19.2
LC^3-55(B:35/10)	6.2	8.6	10.6	14.7	17.8
LC^3-55(H:35/10)	5.2	7.6	9.6	13.5	14.9
LC^3-55(PH:35/10)	6.7	10.7	11.5	17.0	18.3
LC^3-55(HC:35/10)	6.4	9.2	11.5	15.6	15.8

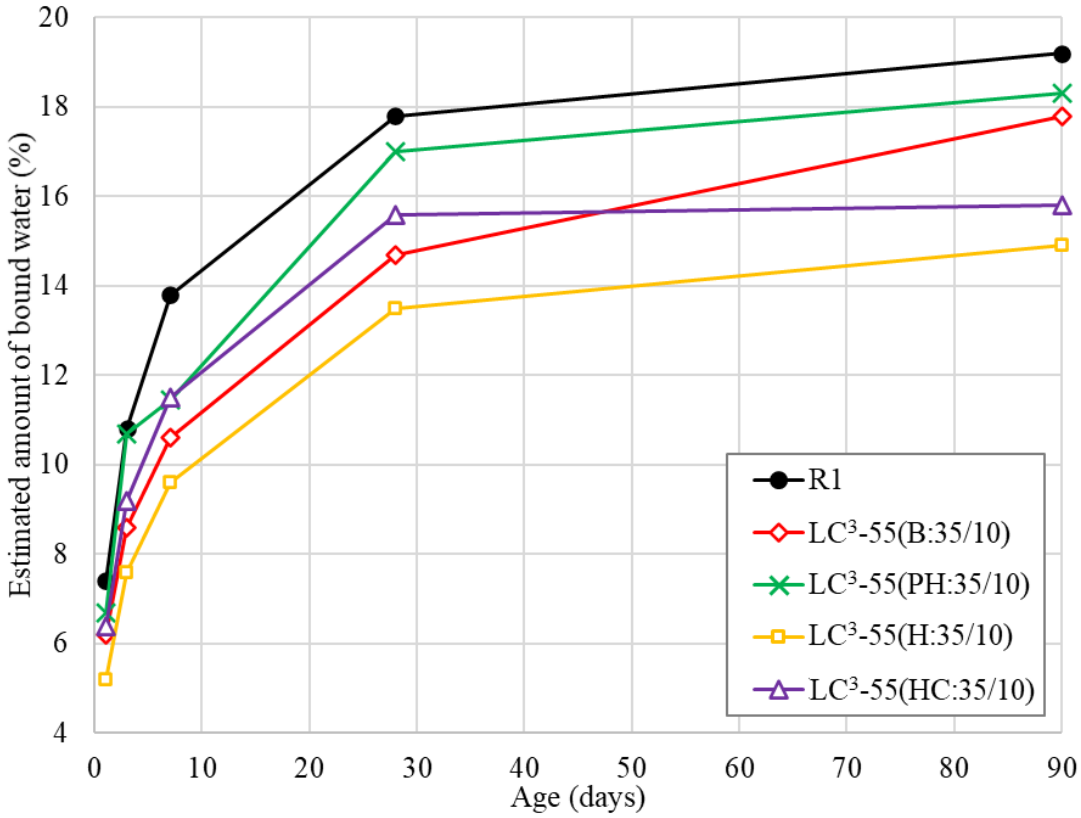

Figure 5.26: Estimated bound water from the TGA curves of the LC^3-55 up to 90 days

In general, results show good agreement with the results of compressive strength. The trend can also be related to the internal surface area (ISA) of the respective clay and the available amount of CK to react with the available CH. In this case, it is most certainly that the amount of bound water is high for the LC^3-55(PH) because of the PH-Clay which has high ISA than B-Clay and H-Clay but with more kaolinite content than HC-Clay. And in the case of LC^3-55(New H), the amount is low because the H-Clay has the lowest ISA and low kaolinite content compared to all other clays.

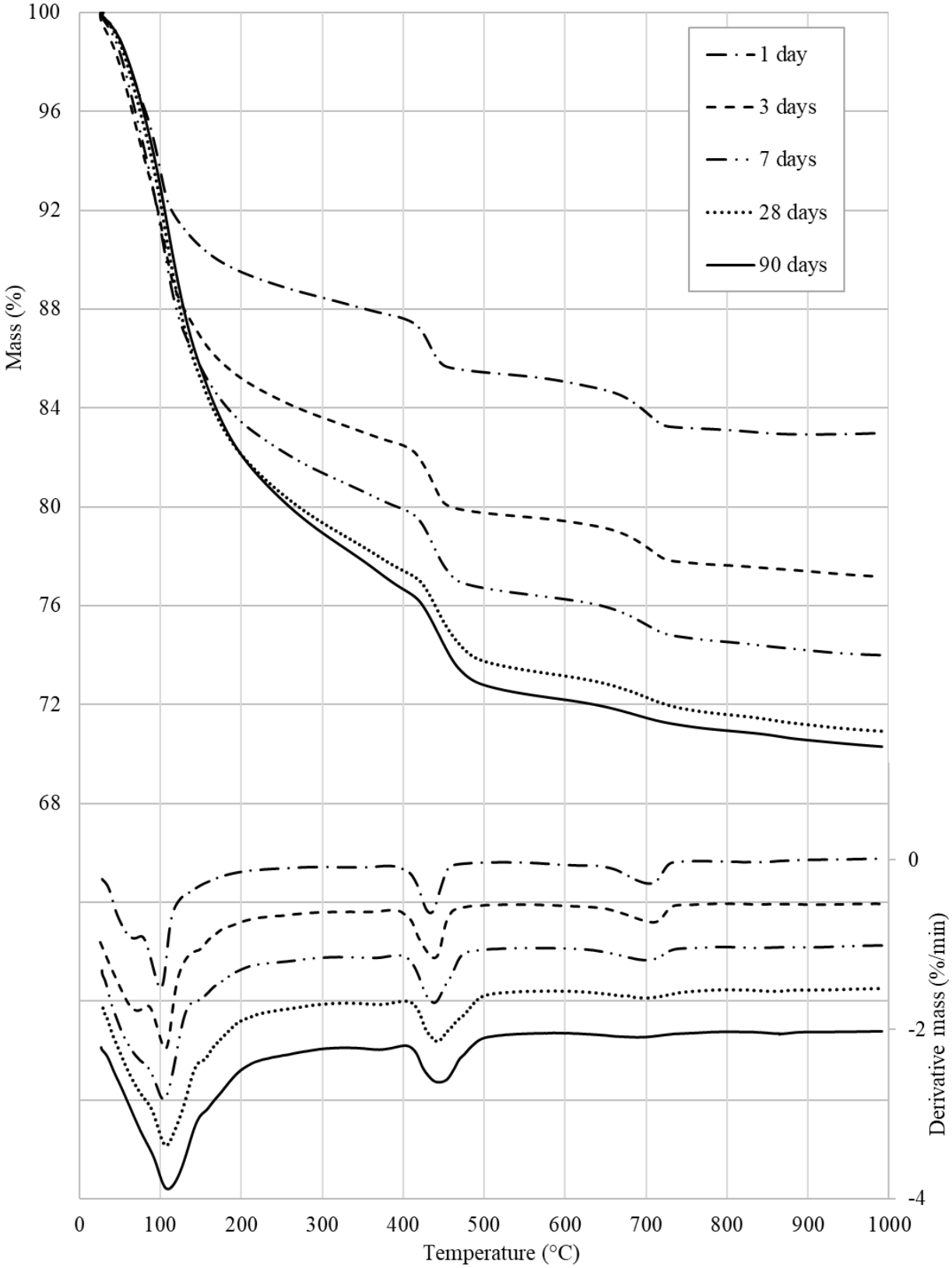

Figure 5.27: TGA and DTG curves of the reference (R1) paste up to 90 days

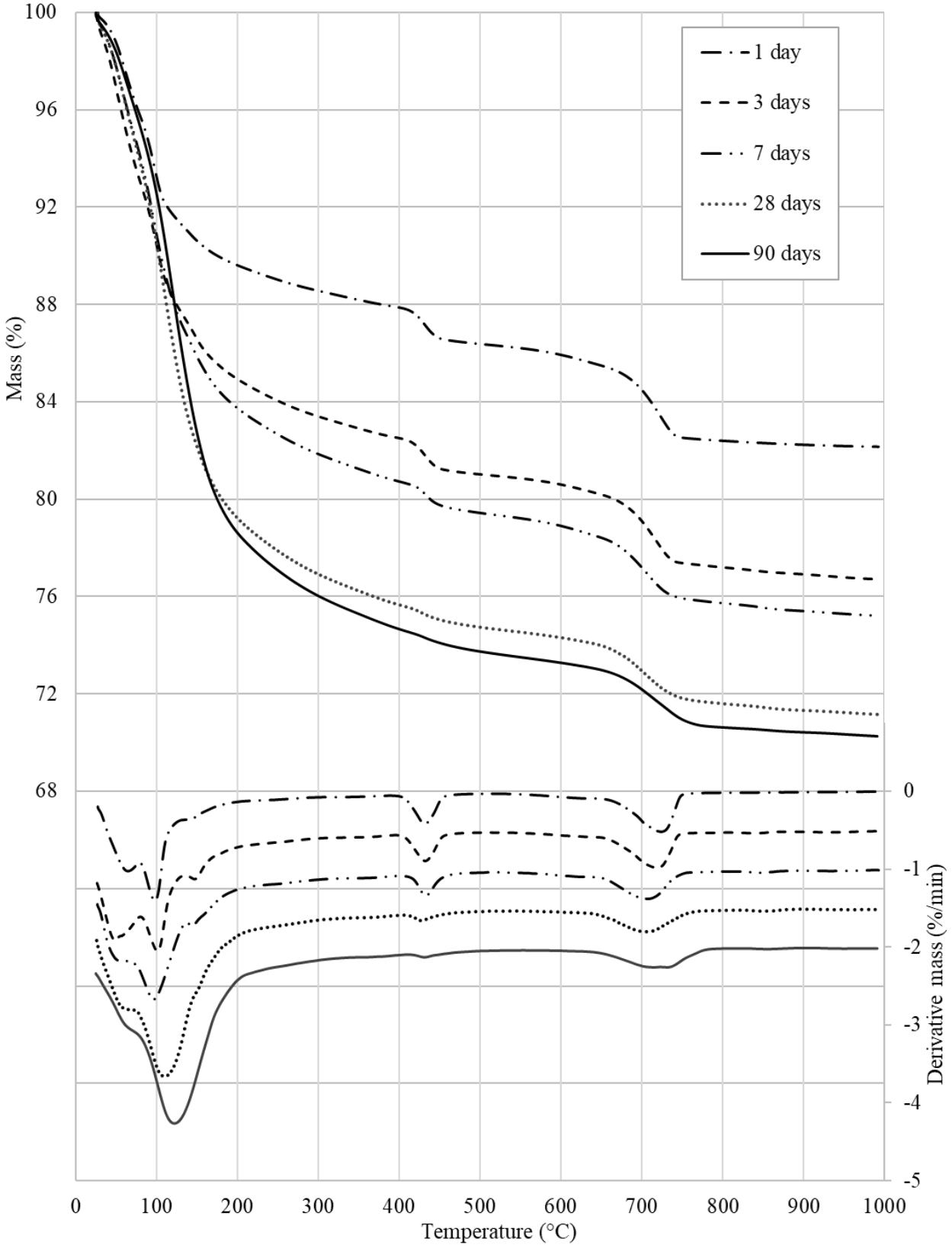

Figure 5.28: TGA and DTG curves of the LC^3-55(B:35/10) paste up to 90 days

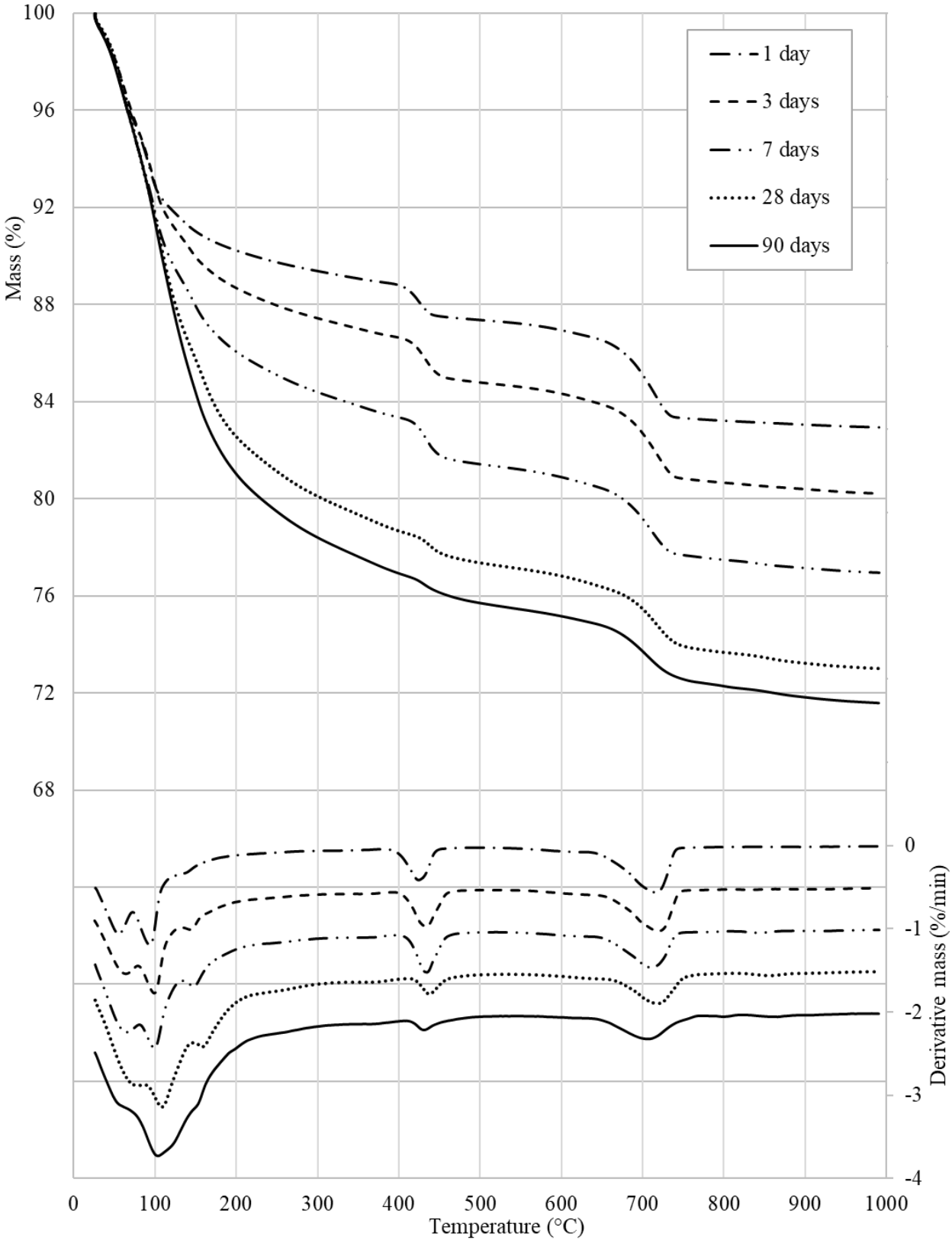

Figure 5.29: TGA and DTG curves of the LC^3-55(H:35/10) paste up to 90 days

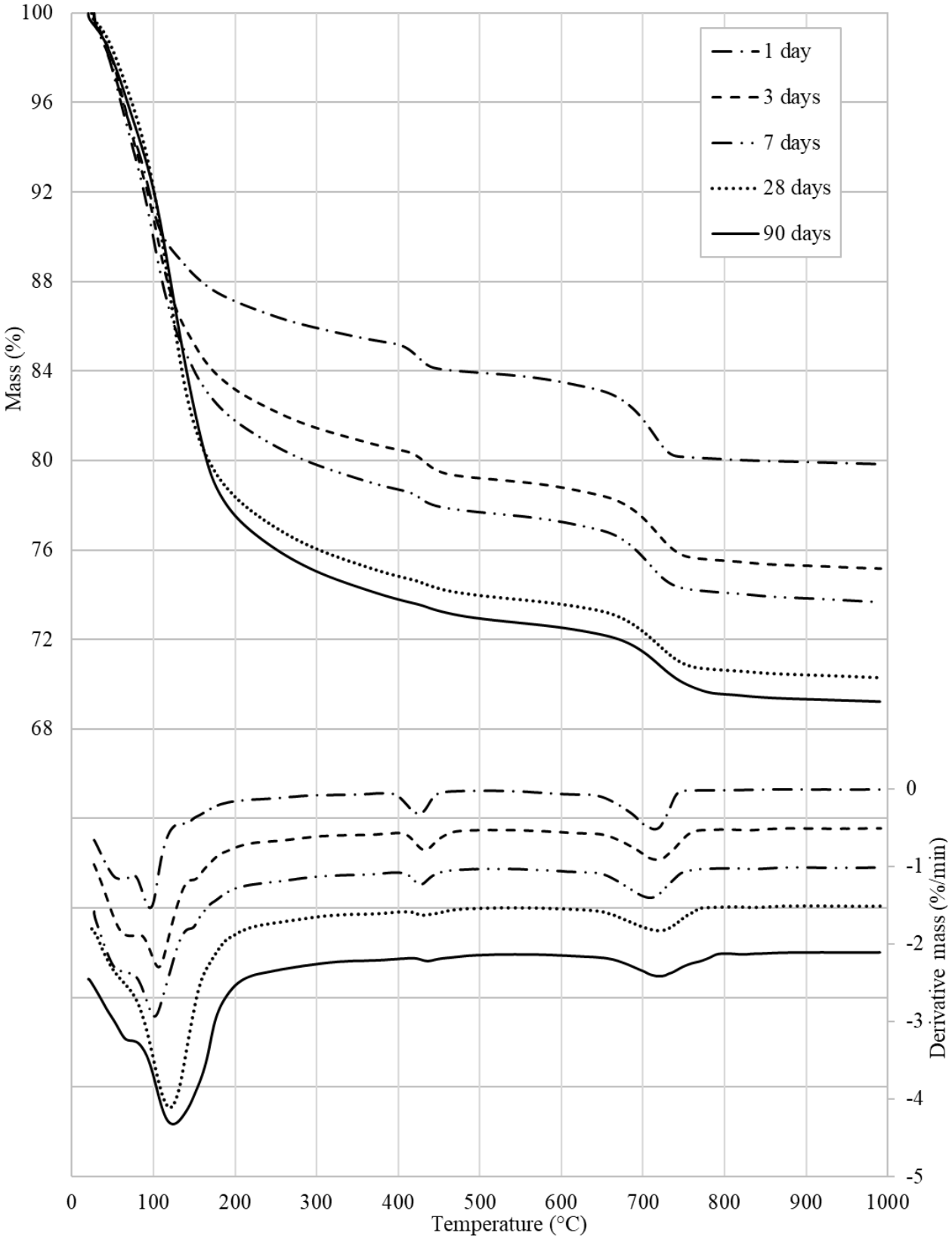

Figure 5.30: TGA and DTG curves of LC^3-55(PH:35/10) pastes up to 90 days

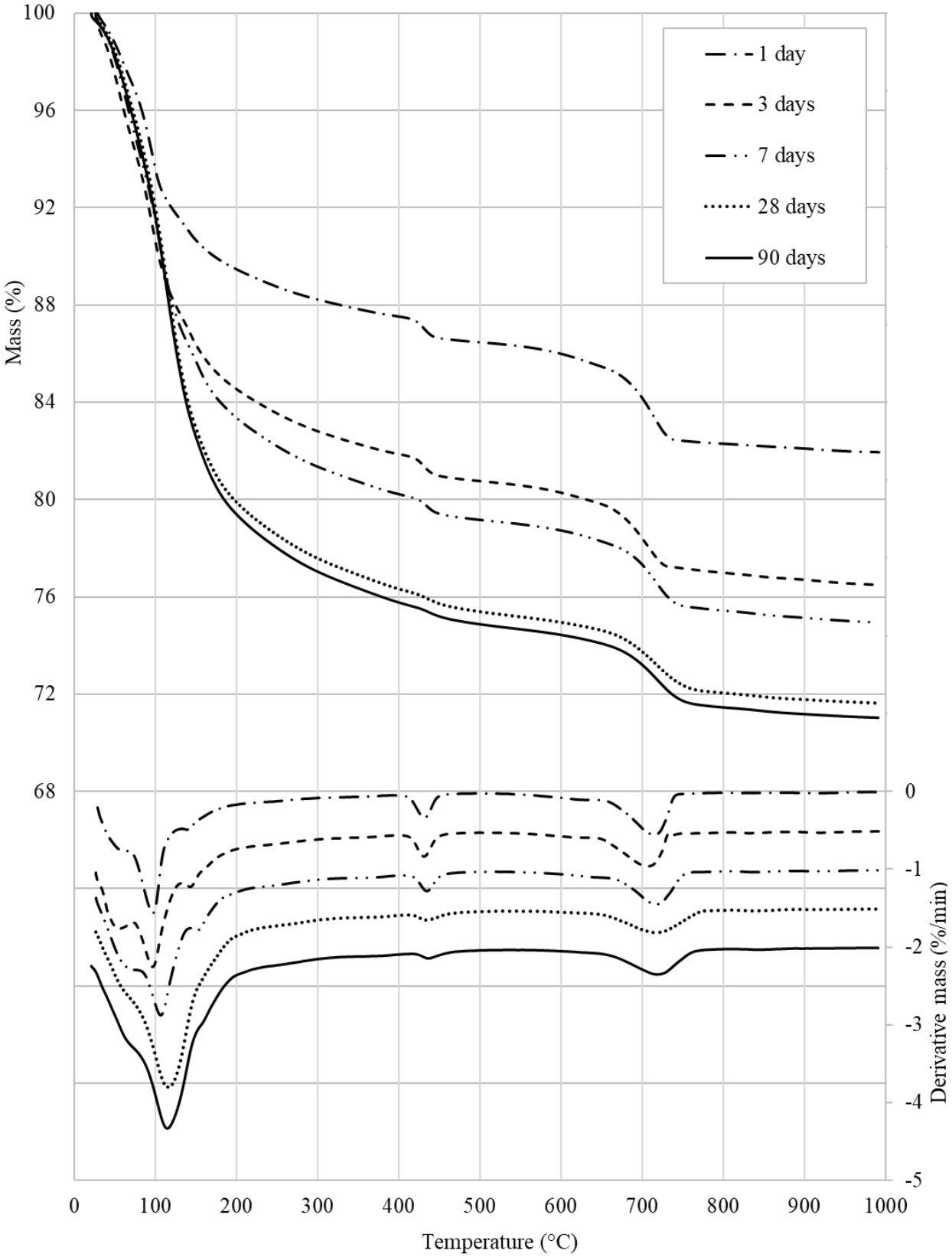

Figure 5.31: TGA and DTG curves of LC^3-55(HC:35/10) pastes up to 90 days

5.5 Summary and general discussion

This chapter began with an overview of the approach used in reducing the clinker factor in cementitious mixes. It presents results and discussion about the optimal proportions of binders for best performance.

The compressive strength of mortar was used as the performance parameter for optimization of the LC^3 binder composition. Results indicate that for optimum performance, regardless of the compressive strength values obtained for each of the LC^3 mixes with different CC, the lowest clinker factor is 0.55 at which the calcined clay factor is 0.35 and the limestone factor is 0.1. In the literature, the majority of researchers reported the performance of the LC^3-50 system (i.e., LC^3 mix with 50% clinker and CC/LS ratio of 2:1 by mass) using either mortar or concrete. This system was first reported in 2012 after a research work done on mortars with clinker content fixed at 50% (Antoni et al., 2012). However, it is important to note that the reactivity of both CC and LS depends on the availability of CH in the system (Krishnan, Dhoopadahalli and Bishnoi, 2020). In this case, it is obvious that the optimal LC^3 proportion would also depend on the reactivity/composition of the clinker (Krishnan and Bishnoi, 2020). Moreover, factors such as purity and fineness of the CC and LS may affect the performance of the system, even though literature suggests that only about 40% kaolinite content in the clay is sufficient for good performance (Alujas et al., 2015; Avet et al., 2016; Avet, 2017; Maraghechi et al., 2018) and that the purity of LS has minimal effect on the performance of the system (Krishnan, Emmanuel, et al., 2018; Krishnan, Kanaujia, et al., 2018). Furthermore, the revision of the European standard (BS EN 197-5, 2021) limits the clinker factor to greater than 0.5 and LS purity greater than 75%, but not the CC/LS ratio. The American standard (ASTM C595/C595M, 2021) limits LS purity to greater than 70% and the amount of LS and pozzolan at no more than 15% and 40%, respectively, but not the CC/LS ratio. In view of this and based on the understanding that high compressive strength is not necessarily a proxy for high durability, two other proportions of binder were considered to increase the understanding of the performance of LC^3-55(35/10) relative to the other mixes. The compositions included i) 65% clinker, 25% CC and 10% LS (LC^3-65(25/10)), and ii) 45% clinker, 40% CC and 15% LS (LC^3-45(40/15)).

Regarding fineness, it has been reported that the fineness of both clinker and CC significantly influences the compressive strength performance of the system, whereas the fineness of LS only influences the performance of the system at the early age, mainly through the formation of carboluminates (Anders et al., 2015). In this research, samples of clay were ground (before calcination) to have particle sizes with d_{90} < 30 µm and d_{50} < 10 µm based on the PSD analysis. After calcination, a slight increase of particle sizes (due to agglomeration of particles) was consistently noted for all the selected clays. However, the BET surface areas obtained by the nitrogen adsorption/desorption method indicated that HC-Clay has the highest ISA compared to other clays, and that H-Clay has the lowest ISA. This means that although these clays have similar PSD, the effective surface areas (i.e., external plus ISA) are not the same. In this case, it was expected that a mix with HC-Clay will demand more SP to get similar workability. On the other hand, improved hydration characteristics due to a higher surface area available for reaction are expected. However, after several trials, it was decided to exclude HC-Clay for the optimisation work as the required SP dosage for most of the LC^3 mortars with HC-Clay was above the limit (2%). The CEM II had particle sizes with d_{90} < 33.5 µm and d_{50} < 11.9 µm and LS with d_{90} < 16.4 µm and d_{50} < 8.2 µm as presented in Table 3.2 and Table 4.5.

The chapter also presented the HoH curves of all the selected mixes with different clays versus the reference mixes (R1 and R2, 100% CEM II/A-L 52.5 N, and 50% CEM II replaced by GGBS, respectively). The intensities and positions of the second, third and fourth hydration peaks of the LC^3 mixes are discussed, compared, and put into perspective to those of the reference mixes. In all cases, the results confirm the appearance of the aluminate peaks well after the second hydration (or silicate) peaks and between 13 and 18 hours, as expected. This indicates that the SO_3 adjustment was done successfully. The total heat curves are also presented and discussed. In general, the intensities and positions of the peaks of the LC^3 mixes as well as the cumulative total heat can be related to amount of CK in the clay and the ISAs of the clays. The results indicate that the ISA of the clays affects the performance of the system in two possible scenarios; one is by reducing the effective water to cement (w/c) ratio which in turn increases the cumulative total heat, and the second is the high surface area (including the ISA) which increases the rate of chemical reaction,

consequently increasing the cumulative total heat. So, in this case, it can be concluded that apart from the kaolinite content and other minerals present in the clay, the filler effect, the pozzolanic reaction, and the ISA of the clay also influence the performance of the system.

In addition, the hydration products at different ages (1, 3, 7, 28 and 90 days) of LC^3-55 mixes with different clays were characterised using XRD and TGA. XRD was used to identify phases appearing at each age and TGA was specifically used to quantify CH, $C\overline{C}$ and bound water at each age of the specimens. In summary, all mixes (including reference R1) show the presence of ettringite, CH and calcite (or $C\overline{C}$) at 1 day and no formation of monosulfoaluminate at all ages. The intensities of both CH and $C\overline{C}$ phases are observed to decrease with age, which indicates progress of both pozzolanic reaction and formation of carboaluminate phases. The estimated amounts of CH, $C\overline{C}$ and bound water in the LC^3 mixes were also related to the ISAs of the clays. In general, the following can be noted from the results:

i) The remaining amount of CH at any age depends on the available amount of CH produced initially, the amount consumed by the pozzolanic reaction, and the formation of carboaluminate and ettringite phases. The low amount of clinker in the LC^3 mixes implies a low CH in the system, which is also consumed by the pozzolanic reaction, causing the available CH to be low, compared to the 100% CEM II system.
ii) At 90 days, the remaining amount of $C\overline{C}$ ranges between 70% for the LC^3-55(New H) and 86% for the LC^3-55(HC), compared to the amounts available at 1 day, which agrees well with the intensities of the calcite phase appearing on the XRD scans at different ages (Figure 5.23). This support the fact that only a small amount of LS reacts in the LC^3 system and therefore the purity of LS has minimal influence on the performance of the LC^3 system, as noted by Antoni et al. (2012), Krishnan, Emmanuel, et al. (2018), and Krishnan, Kanaujia, et al. (2018). In general, the remaining amount at any age depends on the available amount of CH and CK to react with $C\overline{C}$ to produce carboaluminate and ettringite phases.
iii) In general, the progressive development in the amount of bound water shows good agreement with the results of compressive strength. The trend can also be related to the

ISA of the respective clay and the available amount of CK to react with the available CH. It is clear from the results that the amount of bound water is highest for the LC^3-55(PH:35/10) mainly because the PH-Clay has a higher ISA compared to B-Clay and H-Clay, but with more kaolinite content than HC-Clay. The LC^3-55(H:35/10) has the lowest amount, mainly because the H-Clay has the lowest ISA and low kaolinite content compared to all other clays.

Chapter 6 The performance of the selected concrete mixes

6.1 Introduction

One of the aims of this research was to develop LC^3 concretes with clinker content between 40% and 70%, relevant to the southern and east African contexts. The suitability of six samples of clay from selected deposits in South Africa and Tanzania was assessed based on results obtained by XRF, TGA and XRD discussed in Section 4.2. All selected clays composed mainly of quartz, illite and kaolinite. Only four samples of clays were selected for producing concrete mixes. The selection was mainly based on the kaolinite contents in the clays. Based on the literature, a suitable clay for clinker replacement is one with a kaolinite content of at least 40% (Alujas et al., 2015; Avet et al., 2016; Avet, 2017; Maraghechi et al., 2018). In this case, only B-Clay and H-Clay from South Africa and PH-Clay and HC-Clay from Tanzania were selected. As summarised in Table 6.1, B-Clay contains about 65% kaolinite, PH-Clay about 50% and H-Clay and HC-Clay about 40%.

The next task was to get the optimal proportions of binders with low clinker content. As described in Section 3.6, the compressive strength of mortar with a w/b ratio of 0.4 was used as the performance parameter for optimization. Two reference mixes were considered, one with 100% CEM II/A-L 52.5 N (R1), and a recommended mix for South African marine environments with 50% cement replaced by GGBS (R2). LC^3 mixes with clinker levels between 40% and 70% were selected using the so-called mixture design 3-factors approach. In general, the results obtained suggest that for optimal performance, regardless of the difference of the compressive strength values obtained for each of the LC^3 mixes with different CC, the lowest practical clinker factor is 0.55 at which the CC factor is 0.35 and the LS factor is 0.1. However, on the understanding that high compressive strength does not necessarily relate to excellent durability, two other proportions of binder were also considered for the design of concrete mixes: one with 65% clinker, 25% CC and 10% LS, and the other with 45% clinker, 40% CC and 15% LS.

The HoH curves of all the selected proportions (described above) with different clays and the reference mixes were also presented and discussed in Section 5.3. The intensities and positions of the hydration peaks of the LC^3 mixes were discussed and compared between

each other and with the reference mixes. In general, the results indicate that apart from kaolinite content and other minerals present in the clay, the filler effect, and pozzolanic reaction, the ISA of the clay also influences the performance of the system. In addition, the hydration products at different ages (1, 3, 7, 28 and 90 days) of LC^3-55(35/10) mixes with different clays were characterised using XRD and TGA (Section 5.4). XRD was used to identify phases appearing at each age and TGA was specifically used to quantify CH, $C\overline{C}$ and bound water at each age. In summary, all mixes (including reference R1) show the presence of ettringite, CH and or $C\overline{C}$ at 1 day and no formation of monosulfoaluminate and Stratlingite at all ages. The intensities of both CH and $C\overline{C}$ phases were observed to decrease as mixes get aged which indicate progress of both pozzolanic reaction and formation of carboaluminate phases.

Using the selected replacement levels and proportions obtained from the optimisation of proportion of binders as described previously, concrete mixes were optimised and prepared to determine their fresh and hardened properties (more details in Section 3.8). Tests that were carried out included workability, compressive strength, elastic modulus, free shrinkage, restrained shrinkage cracking, durability indexes, resistivity, bulk diffusion, and accelerated carbonation. This chapter presents results and discussion of the findings. The aim here was to understand the performance of the LC^3 mixes with different types of clays, compare the results between the mixes and with the reference mixes R1 and R2. The selected clays have different ISA and amount of kaolinite content but similar PSD before calcination as summarised in Table 6.1.

6.2 PSD of the selected materials for concrete work

The PSD curves of the selected CC samples, cement, GGBS, and LS for the concrete work are shown in Figure 6.1. The characteristics of the selected materials for concrete are summarised in Table 6.1 for the clays and Table 6.2 for the cement, limestone, GGBS, and aggregates.

Cement, GGBS, LS and aggregates were used as received from the suppliers. The aggregates were dried in an oven to constant weight. For the clays, the target was to obtain $d_{90} < 30$ µm and $d_{50} < 10$ µm before calcination. However, after calcination the particles

slightly increased in size largely because of agglomeration during calcination. This was also supported by the SEM images in Figure 4.5 to Figure 4.8 and the reduction in the BET surface areas presented in Table 4.5. The relative difference in the change of particle sizes between the clays before and after calcination is largely related to the difference in the amount of minerals present in the clays as different minerals may have different degrees of agglomeration during calcination.

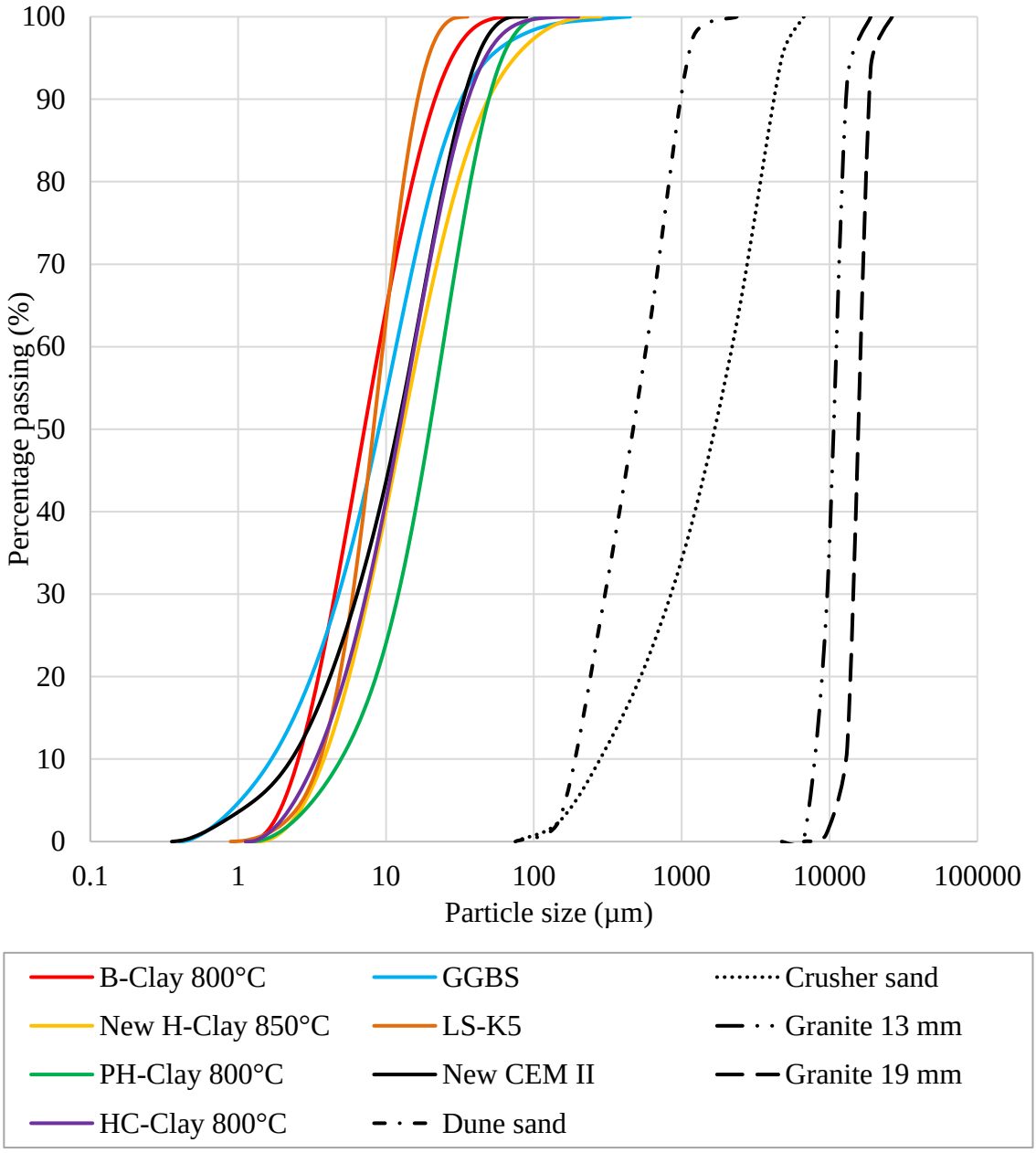

Figure 6.1: PSD curves of all the selected materials for the concrete work

Table 6.1: Characteristics of the selected clays for the concrete work (summary)

Material name	Before calcination									After calcination at 800°C						
	RD	Kaolinite (%)		Quartz (%)	Illite (%)	d_{10}	d_{50}	d_{90}	BET (m^2/g)	Due to agglomeration					Na_2O_{eq} (%)	SO_3 (%)
										RD	d_{10}	d_{50}	d_{90}	BET (m^2/g)		
		TGA	XRD			(µm)					(µm)					
B-Clay	2.61	65	72	18	8	2.3	5.9	16.5	12.6	2.60	2.6	7.1	21.4	11.1	0.48	<0.01
New H-Clay[1]	2.67	38	46	44	7	3.5	9.6	26.0	5.4	2.59	3.8	12.9	49.2	4.6	2.88	
PH-Clay	2.66	52	49	48	3	<1.0	5.9	29.2	14.4	2.64	5.0	19.7	49.5	14.5	0.32	
HC-Clay	2.73	39	46	42	9	2.4	8.5	27.7	45.8	2.70	3.4	12.3	35.9	37.0	0.60	
[1]Received already flash calcined by the supplier at 850°C																

Table 6.2: Characteristics of the cement, limestone, slag, and aggregates used for the concrete work (summary)

Material name	RD	d_{10}	d_{50}	d_{90}	Na_2O_{eq} (%)	SO_3 (%)	FM	CBD (kg/m^3)
		(µm)						
LS-K5	2.70	3.6	8.2	16.4	< 0.01	0.02	-	-
GGBS	2.90	1.7	9.0	32.3	0.68	1.93	-	-
New-CEM II	2.96	2.3	11.9	33.5	0.27	2.00	-	-
Dune sand	2.64	-	-	-	-	-	2.1	-
Crushed sand (granite)	2.65	-	-	-	-	-	3.7	-
Granite 13 mm	2.65	-	-	-	-	-	7.8	1540
Granite 19 mm	2.65	-	-	-	-	-	8.9	1560

6.3 Equivalent alkali in the selected mixes

As indicated in Section 3.6.1, apart from SO_3 optimisation, the LC^3 mixes also required adjustment of alkali content to increase early-age strength. Based on the literature, the recommended Na_2O_{eq} for optimum performance is between 0.6 and 0.8% (Antoni, 2013). In this work, 0.7% was selected and adjustment was done by adding NaOH. However, it was not possible to adjust the Na_2O_{eq} for the LC^3(H) as the alkalis in this clay were already high. Table 6.3 shows the equivalent alkali in each of the selected mixes. It can be seen that all the LC^3(H) have values already beyond the recommended maximum limit (0.8%). As noted in the literature, high alkali levels in the mix reduce the strength of the C-S-H gel (Beltzung and Wittmann, 2005; Sant et al., 2012; Li, Afshinnia and Rangaraju, 2016) and make the microstructure more porous (Sant et al., 2012), as a result impairing the mechanical and durability performance of the concrete.

Table 6.3: Equivalent alkali in the selected LC^3 mixes

Mix	Na_2O_{eq} [1] (%)						**Na_2O Added From NaOH [2] (%)**	Na_2O_{eq} ∑ (%)
	Calcined clay				LS-K5	New-CEM II		
	B	New-H	PH	HC				
LC^3-65(B:25/10)	0.48	-	-	-	0.01	0.27	0.40	0.70 [3]
LC^3-55(B:35/10)	0.48	-	-	-			0.38	0.70
LC^3-45(B:40/15)	0.48	-	-	-			0.38	0.70
LC^3-65(H:25/10)	-	2.88	-	-			-	0.90
LC^3-55(H:35/10)	-	2.88	-	-			-	1.16
LC^3-45(H:40/15)	-	2.88	-	-			-	1.28
LC^3-55(PH:35/10)	-	-	0.32	-			0.44	0.70
LC^3-55(HC:35/10)	-	-	-	0.60			0.34	0.70

Notes

[1]Data from Table 5.1; [2]Percentage by total mass of binder

New CEM II had 4% LS and 96% Clinker

[3]∑= 25%(0.48) + [10%-(65%/(1-4%)) + 65%)](0.01) + [(65%)/(1-4%)](0.27) + 0.4 = 0.70

6.4 Optimisation of the concrete mixes

In general, it is not easy or almost impossible to optimise certain concrete properties without affecting other properties. In this work, optimisation of concrete materials aimed

at further reducing the amount of binder in the system, and hence involved reduction of water content while maintaining the required proportions of binders and w/b ratios to an extent that fresh concrete properties were not adversely affected.

As indicated in Section 5.2.2.5, for B-Clay and H-Clay, three proportions of binders were considered for further studies. One was with 45% clinker, 40% CC and 15% LS (or LC^3-45(40/15)), the second one with 55% Clinker, 35% CC and 10% LS (or LC^3-55(35/10)), and the last with 65% clinker, 25% CC and 10% LS (or LC^3-65(25/10)). Due to limited amount of samples from Tanzania, the PH-Clay was considered only for the LC^3-55 mix with w/b ratio of 0.4, and HC-Clay for LC^3-55 mix with 0.55 w/b ratio.

Initially, the CCSA method coupled with MAAM (using the EMMA software) was used as a starting step in obtaining the concrete mix proportions. With the EMMA software, all mixes (including the reference mixes) were optimized by adjusting the quantity of the materials to better fit the modified Andreassen curve with PSD modulus (q) = 0.3 (Kumar and Santhanam, 2003). In this case, the quantity of the materials was adjusted while maintaining the selected proportions of binders and the w/b ratio. Other inputs were the particle density, quantity, PSD of each material and maximum and minimum particle size in the mixture. A typical example is given in Appendix V.

The obtained proportions were then adjusted by carrying out trial concrete mixes, and the target was to get a comparable workability with a slump of 100 ± 20 mm and a SP (Chryso@ Optima 175) dosage limit of 1.5%. To reduce powder content, the target was also to have a mix with water content as low as possible. In this case, mix trials were made with different amounts of water (at an interval of 5 kg/m^3 starting from 125 kg/m^3) while maintaining the selected proportions of binders and the w/b ratios. After several trials, it was decided to maintain the amount of water at 160 kg/m^3 and amount of stone at 1000 kg/m^3 for all the concrete mixes. However, with the HC-Clay, it was only possible to achieve a slump of 45 mm at a SP dosage of 2% in the case of the 0.55 w/b ratio mix. Table 6.4 present details on the final proportions decided on for the concrete materials, and SP dosage, and the slump values obtained for all the selected concrete mixes.

Table 6.4: Concrete mix proportions, SP dosage and slump obtained

w/b	Mix	Binder	Fine aggregate		Coarse Aggregate	Water	SP dosage (%wt. of binder)	Slump (mm)
			Dune (50%)	Crusher (50%)				
		kg/m^3						
0.4	R1	400	432	434	1000	160	0.60	80
	R2		431	432			0.55	120
	LC^3-65(B:25/10))		425	427			1.15	110
	LC^3-55(B:35/10)		422	424			1.20	100
	LC^3-45(B:40/15)		420	422			1.25	95
	LC^3-65(H:25/10)		425	427			1.10	120
	LC^3-55(H:35/10)		422	424			1.20	105
	LC^3-45(H:40/15)		420	422			1.25	110
	LC^3-55(PH:35/10)		424	425			1.50	90
0.55	R1	291	481	483			0.80	115
	LC^3-55(B:35/10)		474	476			1.20	90
	LC^3-55(H:35/10)		474	475			1.15	95
	LC^3-55(HC:35/10)		476	478			2.00	45

The results for the tests in comparison with the results of the reference mixes are discussed in the following sections. The results are also tabulated in Appendix VII.

6.5 Compressive strength results

6.5.1 Strength development

Figure 6.2 and Figure 6.6 presents the compressive strength results of the concrete specimens as the average of the three cubes of 100 mm size, tested for 0.4 w/b ratio and 0.55 w/b ratio, respectively. For clearness, Figure 6.3 to Figure 6.5 are plotted to show the compressive strength results based on the type of clay for the 0.4 w/b ratio mixes. The error bars are not included for figures clarity. The cubes were tested at 1, 3, 7, 28 and 90 days. The results are discussed in the next sections.

6.5.1.1 Mixes with a w/b of 0.4

In general, the results indicate that the performance of the LC^3 systems depends largely on the amount of clinker and the amount of calcined kaolinite (CK) in the system. However, to some extent the performance is also affected by the ISA of the clay and the amount of alkalis in the system. In this case, the PH-Clay has higher BET surface area than B-Clay and H-Clay, and the H-Clay has the lowest BET surface area and highest amount of alkalis.

Results indicate that at 1 day the reference mix R1 with 100% CEM II has the highest strength followed by LC^3-65(B:25/10) then LC^3-55(PH:35/10) and LC^3-55(B:35/10), and the reference mix R2 which has 50% CEM II has the lowest strength. On the other hand, although all the LC^3-45(40/15) mixes have lower clinker content compared to reference mix R2, their strengths are slightly higher than R2. However, in general, the performance of the mixes at 1 day depends largely on the amount of clinker in the mix.

Between 3 days and 7 days, although PH-Clay has a lower kaolinite content compared to B-Clay, the LC^3-55(PH:35/10) has the highest strength followed by LC^3-55(B:35/10) and LC^3-65(B:25/10) and then reference mix R1. Based on literature (Alujas et al., 2015; Avet et al., 2016; Avet, 2017; Maraghechi et al., 2018), only about 40% kaolinite content in the clay is enough to make an LC^3 system perform similar to a reference system. In this case, the PH-Clay has about 50% kaolinite content and B-Clay has about 65% kaolinite content. In view of this, it is not surprising that although PH-Clay has a lower kaolinite content than B-Clay, the LC^3-55(PH:35/10) performs slightly higher than LC^3-55(B:35/10). A marginal higher strength of the LC^3-55(PH:35/10) compared to LC^3-55(B:35/10), especially up to 7 days, is largely related to a slightly higher ISA of PH-Clay compared to B-Clay. In this case, the PH-Clay absorbs more some of the available water and hence reduces the effective w/b ratio. In addition, it is likely that the PH-Clay with a slightly higher BET surface area (14.5 m^2/g) than B-Clay (11.1 m^2/g) increased the rate of chemical reaction of the LC^3-55(PH:35/10) system compared to B-Clay.

At 28 days, the LC^3-65(B:25/10) has the highest compressive strength. Most likely this is because of the clinker factor and kaolinite content in the B-Clay; the strength of LC^3-55(B:35/10) and LC^3-55(PH:35/10) mixes are slightly lower than the reference mix R1 and slightly higher than the reference mix R2. The strength of the LC^3-55(H:35/10) is lower by about 11% compared to the LC^3-55 mixes with B-Clay and PH-Clay.

At 90 days, the compressive strength of the LC^3-65(B:25/10), LC^3-55(B:35/10) and LC^3-55(PH:35/10) are slightly lower or similar to the values of the reference mixes R1and R2. The compressive strength of the LC^3-65(H:25/10) is also slightly lower than that of the reference mix R2. The strength of the LC^3-55(H:35/10) is low by about 9% relative to the LC^3-55 mixes with B-Clay and PH-Clay.

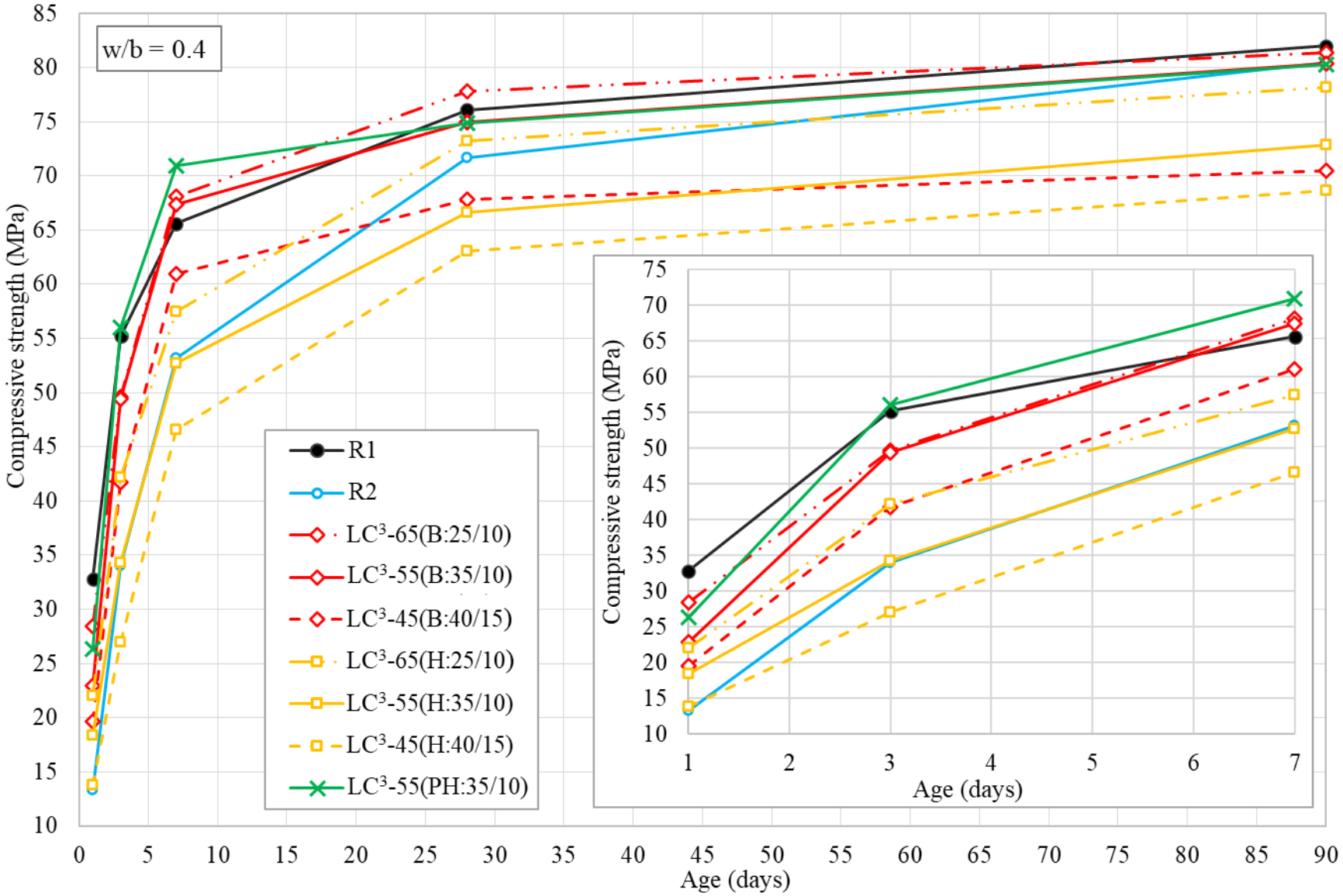

Figure 6.2: Compressive strength development of the concrete mixes to 90 days (w/b = 0.4)

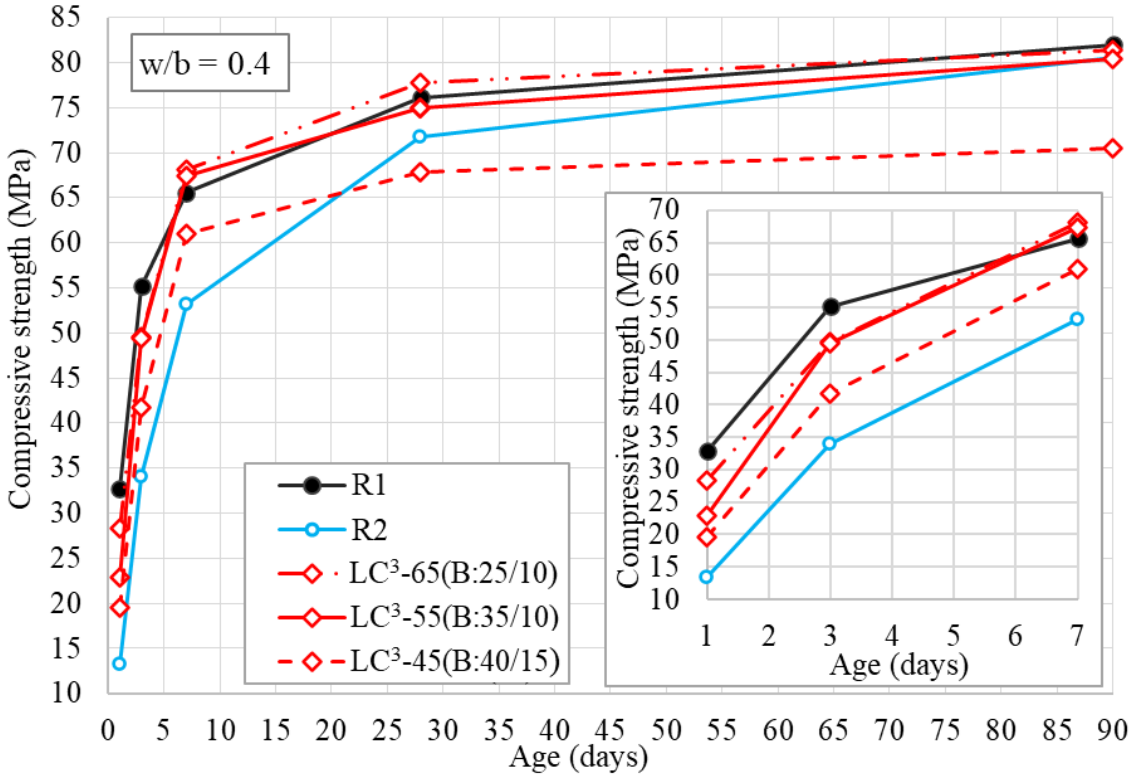

Figure 6.3: Compressive strength of the LC^3(B) and reference mixes (w/b = 0.4)

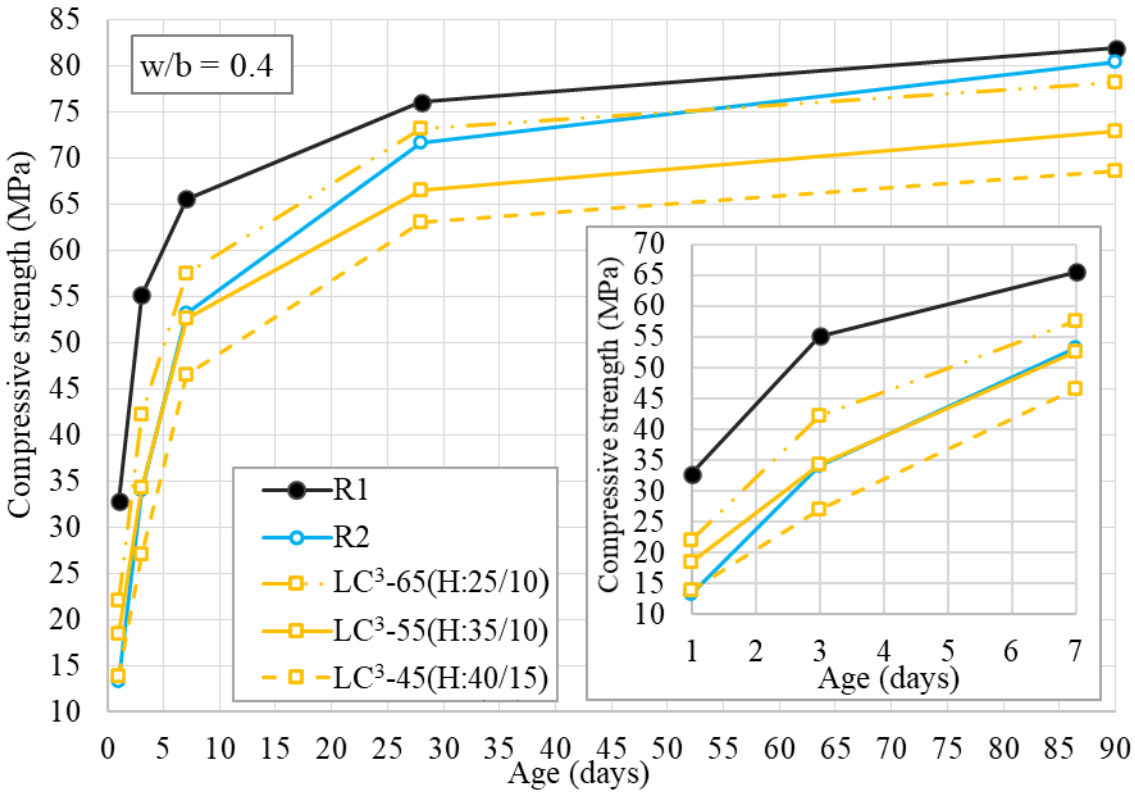

Figure 6.4: Compressive strength of the LC^3(H) and the reference mixes (w/b = 0.4)

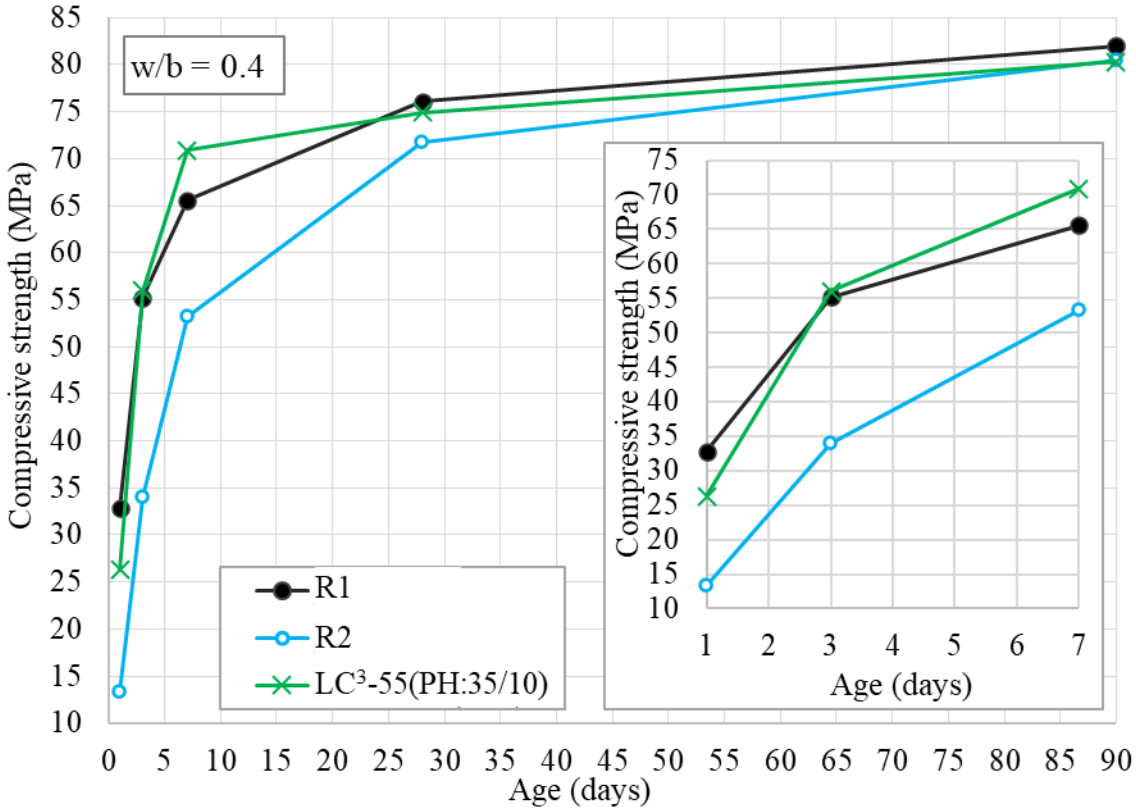

Figure 6.5: Compressive strength of the LC^3(PH) and reference mixes (w/b = 0.4)

6.5.1.2 Mixes with a w/b ratio of 0.55

In case of the mixes with a w/b ratio of 0.55, a trend very similar to the 0.4 w/b ratio mixes was observed. In general, the results (Figure 6.6) indicate that the performance of the LC^3 systems depend largely on the amount of clinker, the amount of CK in the system, the amount of alkalis in the system, and the ISA of the clay.

Up to 3 days, the reference mix R1 has the highest strength followed by LC^3-55(HC:35/10) then LC^3-55(B:35/10) and LC^3-55(H:35/10) has the lowest strength. Although the HC-Clay has lower kaolinite content than B-Clay, the strength of the LC^3-55(HC:35/10) is higher compared to LC^3-55(B:35/10). From the results, it is clear that, up to 3 days, the performance of the mixes depends largely on the amount of clinker in the system and the surface area of the clay.

HC-Clay has low kaolinite content similar to H-Clay, but the 7-day strength of LC^3-55(HC:35/10) is marginally lower than the strength of LC^3-55(B:35/10) and the reference mix. This again is because HC-Clay has more ISA than H-Clay and most likely absorbs

much of the available water during mixing and therefore reduce the effective water: cement ratio. However, the rate of strength gain of LC^3-55(HC:35/10) is observed to be very slow after 7 days.

At 28 and 90 days, the strength of LC^3-55(B:35/10) is slightly lower than that of R1. The LC^3-55(H:35/10) again has the lowest strength at all ages, and this is most likely because of high amount of alkalis coming from the H-Clay as pointed out in Section 6.5.1.1.

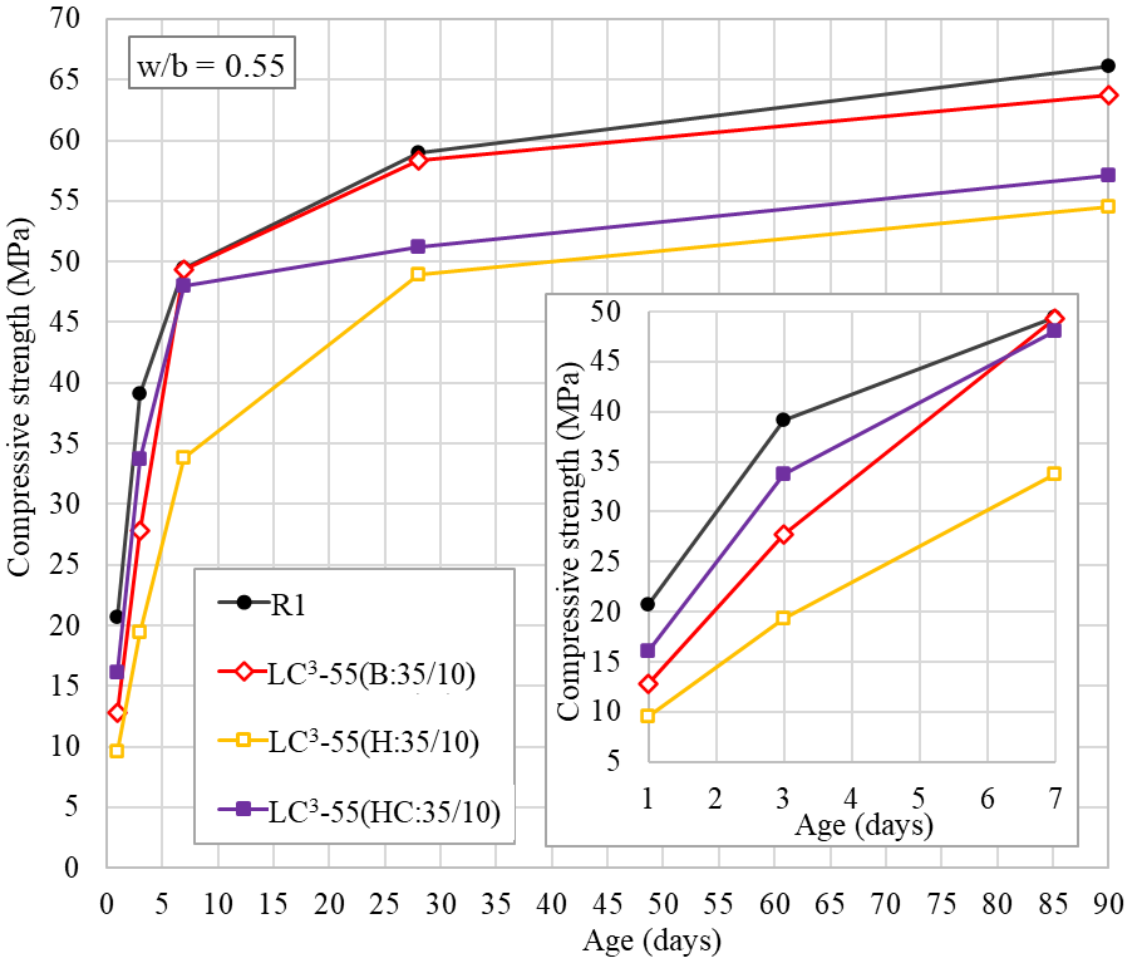

Figure 6.6: Compressive strength development of the concrete up to 90 days (w/b = 0.55)

6.5.2 Strength results normalized for clinker content

Figure 6.7 presents the compressive strength of the concrete mixes normalised for the clinker content in percentage. From these results, all LC^3 mixes perform better than the reference mix R1 and only LC^3-45(B), LC^3-45(H), LC^3-55(B), and LC^3-55(PH) perform better than the reference mix R2, especially up to about 7 days. This supports the literature,

confirming that LC^3 binders react more rapidly up to 7 days compared to most binary mixes, where the main problem is the slow gain of strength at the early ages (Bijen, 1996; Nehdi, 2001; Bentz, 2010; Antoni et al., 2012; Dhandapani et al., 2018). At 28 days, the LC^3-45(B) and the LC^3-55 mixes with B-Clay and PH-Clay outperform the reference mix R2. At 90 days, the performance of LC^3-45 mixes is close to the reference mix R2. In general, the performance also depends on the amount of clinker in the mix.

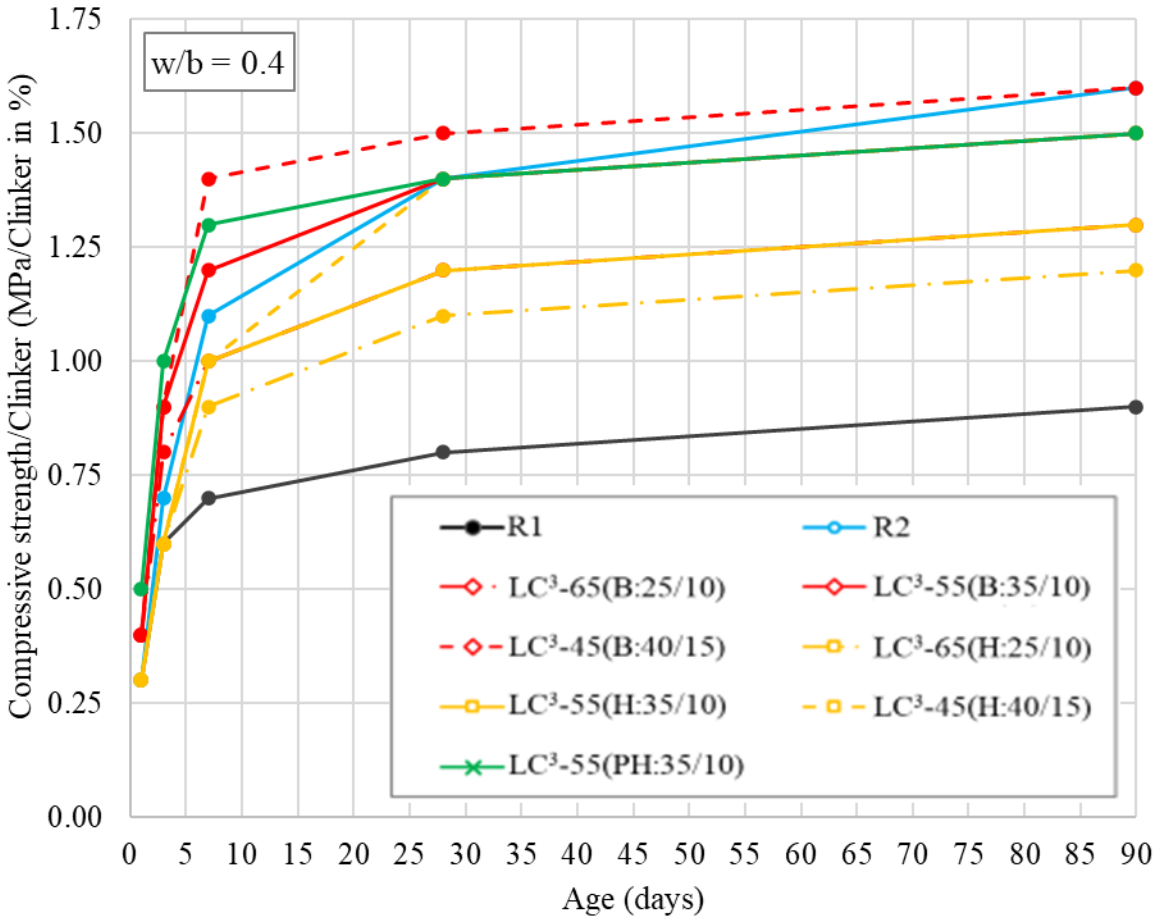

Figure 6.7: Compressive strength development of the concrete mixes normalised for clinker content (w/b = 0.4)

6.5.3 Binder intensity

Binder intensity reflects the amount of binder (regarded here as the 'active' binders, i.e. clinker and CC) per unit volume of concrete, necessary to achieve a unit compressive strength, expressed in $kg/m^3/MPa$ (Damineli et al., 2010). The intensity can be used to evaluate efficiency of the reactive binder in the concrete. Figure 6.8 presents the binder intensity of the concrete mixes as a function of 28-day compressive strength. Results show

that all mixes have binder intensity between 4.5 and 5.5 kg/m^3/MPa with compressive strength values between 45 and 60 MPa for mixes with a w/b ratio of 0.55 and between 60 and 80 MPa for mixes with a w/b ratio of 0.4.

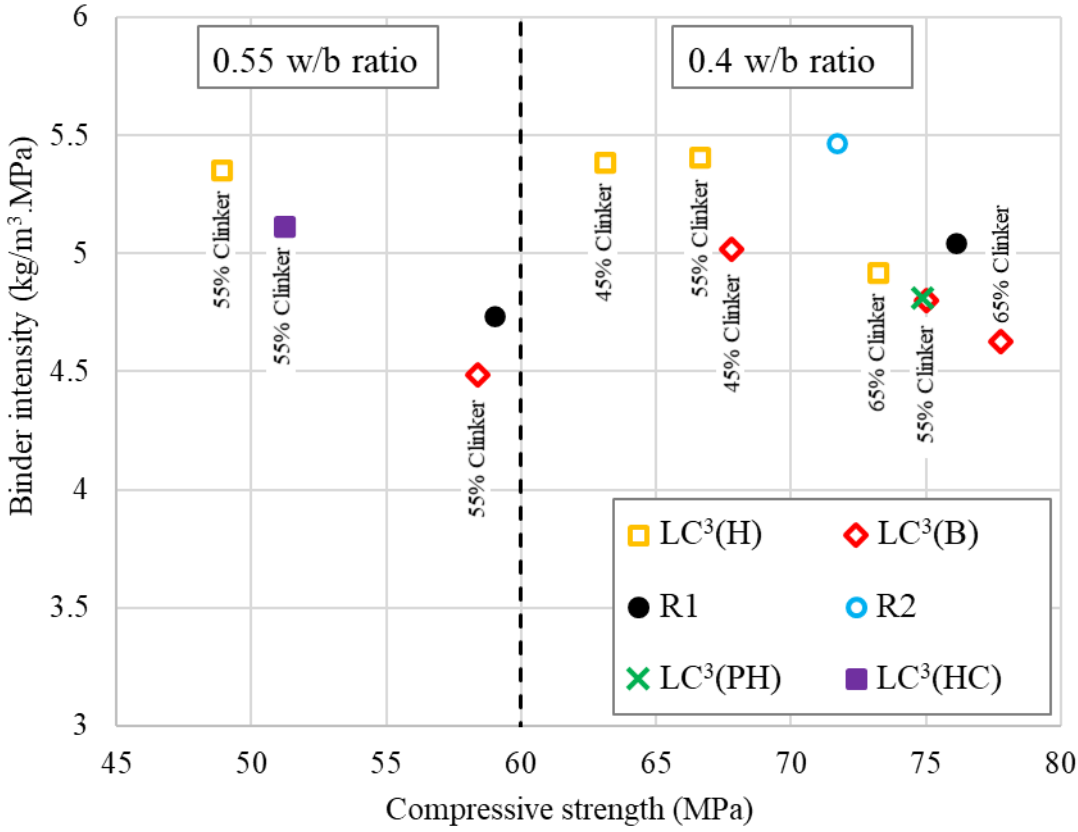

Figure 6.8: Binder intensity as a function of 28-day compressive strength

In the case of 0.4 w/b ratio, the reference mixes, LC^3-45(H:40/15), and LC^3-55(H:35/10) have values within the range of 5 – 6 kg/m^3/MPa, as proposed by Damineli, Pileggi and John (2013) for the efficient use of binders. For the LC^3-45(B:40/15), the binder intensity is slightly higher than 5 kg/m^3/MPa. Likewise, in the case of the 0.55 w/b ratio mixes, LC^3-45(H:55/10), and LC^3-55(HC:35/10) have values between 5 – 6 kg/m^3/MPa. The rest of the mixes have values below 5 kg/m^3/MPa, indicating very reactive blended systems, and that overall, good packing of aggregate was achieved in these mixes (Damineli et al., 2010). The reactivity of the LC^3 systems was, therefore, comparable to the refence mix R1, and superior to the reference mix R2.

Results presented in Table 5.9 and XRD curves in Figure 5.23 indicate that approximately 50% of the $C\overline{C}$ reacted in the system at 90 days, which implies that LS is also a reactive

component and not just a filler. Unlike Figure 6.8 which shows binder intensity without accounting for LS, Figure 6.9 presents binder intensity with inclusion of LS. In this case, only LC^3-45(H:40/15) has binder intensity above 6 kg/m^3/MPa. The intensity of LC^3-55(H:35/10) is exactly 6 kg/m^3/MPa whereas the rest of the mixes, both 0.4 and 0.55 w/b ratio, have intensities below 6 kg/m^3/MPa. In general, the intensities are slightly higher compared to those without accounting for LS as a reactive binder (Figure 6.8).

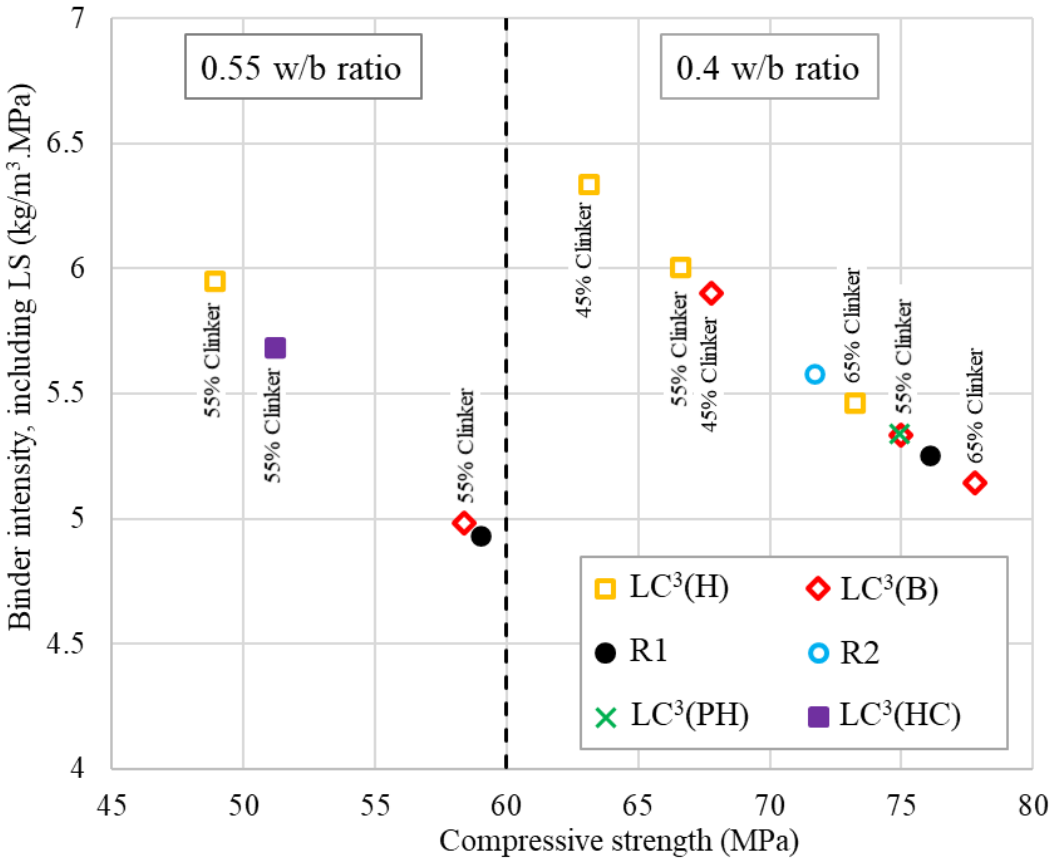

Figure 6.9: Binder intensity (including LS) as a function of 28-day compressive strength

6.5.4 The strength performance of the LC^3 mixes as a function of clinker content

Figure 6.10 shows the relationship between the compressive strength of the LC^3 mixes with B-Clay and H-Clay versus clinker content versus age. It also shows the compressive strength of the reference mixes at all ages. It is clear from the results that from 3 days onwards the LC^3 mixes with B-Clay have little or almost no gain of strength moving from 55% clinker content to 65% clinker content. This means that in this system the amount of clinker above 55% is not really needed unlike LC^3 mixes with H-Clay where the gain of strength also depends on the clinker factor, at least up to 65%.

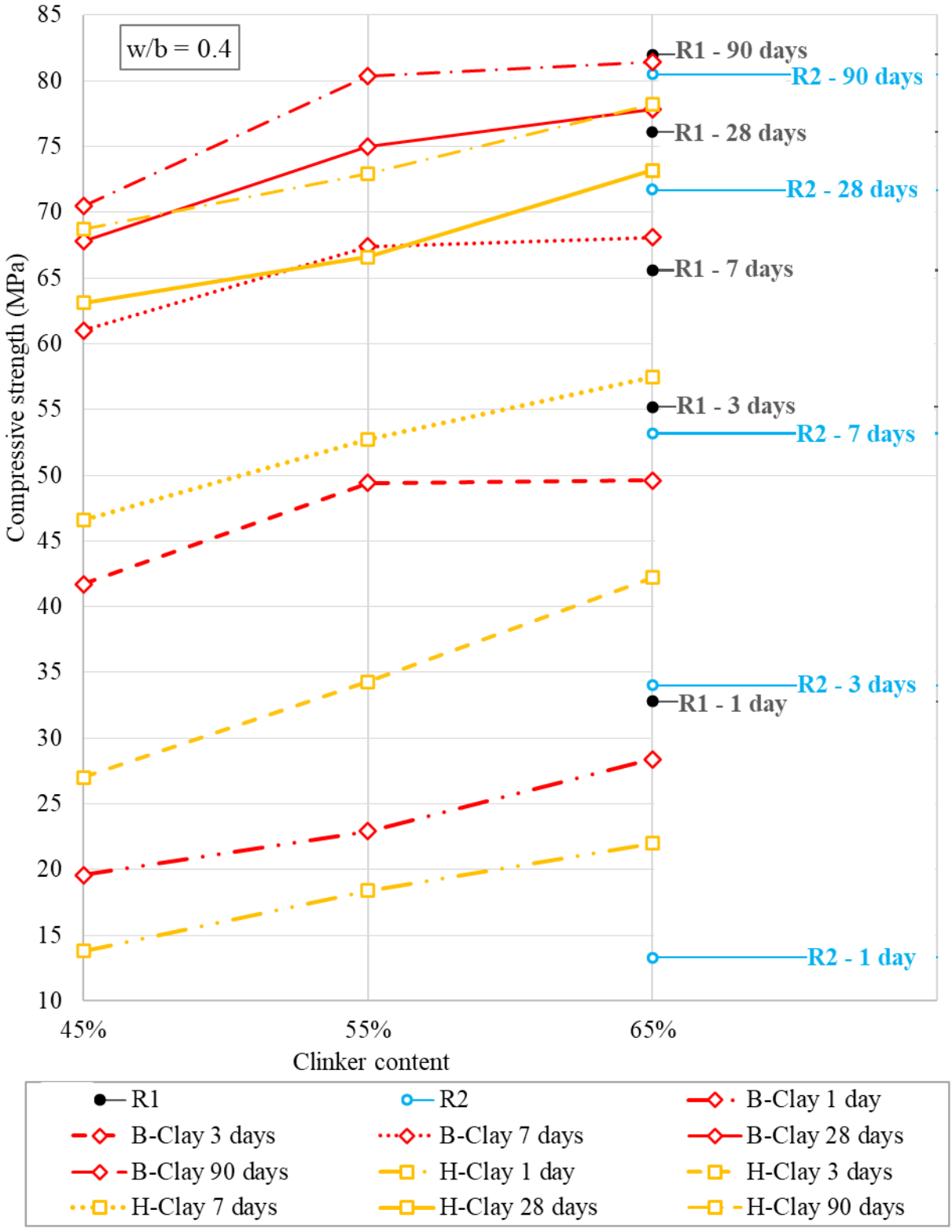

Figure 6.10: Compressive strength the LC^3 concrete mixes with B-Clay and H-Clay versus clinker factor versus age (w/b = 0.4)

6.5.5 Summary and discussion

From the results, the following can be noted:

i) Although LC^3-55(B:35/10) has a lower clinker content than LC^3-65(B:25/10), the strengths of the two mixes are quite similar, especially at 3, 7 and 90 days. In general, the performance of the LC^3 mixes depends on the available amount of CH from cement hydration, the amount of CK from the CC, and the amount of $C\overline{C}$ from LS for pozzolanic reaction and formation of carboaluminate phases. The high performance of LC^3-65(B:25/10) is mainly related to the clinker content. However, with the LC^3-55(B:35/10) mix there appears to be a good balance or good synergy of all these factors, which makes this mix perform almost similar to LC^3-65(B:25/10). This also agrees well with the results of the optimisation discussed earlier. In this case, it is most likely that with the LC^3-55(B:35/10) mix, there is always sufficient CH available to react with the available CK and $C\overline{C}$.

ii) The reference mix R2 has lower strength compared to most of the LC^3 mixes, especially up to 28 days. However, after 28 days, the rate of strength development is higher compared to all other mixes. On the other hand, the LC^3-55(35/10), especially with B-Clay and PH-Clay, and the LC^3-65(B:25/10) gain strength similar or better than the reference mix R1. This supports the fact that LC^3 systems react strongly during the first few days compared to most binary mixes where the main problem is the slow gain of strength at the early ages (Bijen, 1996; Nehdi, 2001; Bentz, 2010; Antoni et al., 2012; Dhandapani et al., 2018), which habitually restricts the effective application of most binary systems in construction, especially when early strength is a project requirement.

iii) After 28 days, the rate of strength gain for all the LC^3 mixes is similar or slightly lower than the reference mix R1 but lower than the reference mix R2. This suggests that with the LC^3 system extended curing is not really required to attain higher long-term strength as also observed by Dhandapani et al. (2018).

iv) In general, the LC^3(H) mixes have lower strength compared to other LC^3 mixes with the same proportions. This low performance is most likely because of the high alkali content coming from the H-Clay resulting in a porous microstructure and low strength of C-S-H gel developed in high alkali condition (Smaoui et al., 2005; Sant et al., 2012;

Li, Afshinnia and Rangaraju, 2016), also low kaolinite content and H-Clay has low ISA compared to B-Clay and PH-Clay.

6.6 Elastic modulus

Figure 6.11 presents the elastic modulus of the concrete mixes at different ages with a w/b ratio of 0.4. The same concrete specimens were tested at 7, 28 and 90 days.

At 7 days, all mixes have elastic modulus values just below or just above 40 GPa, and the difference is small between the highest value of 41.6 GPa from the reference mix R1 and lowest value of 36.8 GPa from the reference mix R2.

At 28 days, all mixes have values clustering around 42 GPa with the minimum value of 41.9 GPa from LC^3-45(H) and a maximum of 45 GPa from LC^3-65(B) (an increase of between 2 to 4 GPa from 7 days values).

At 90 days, all mixes have values clustering around 45 GPa with the minimum of 43.5 GPa from LC^3-45(B) and a maximum of 48.4 GPa from the reference mix R1 (an increase of between 2 to 4 GPa from 28 days values).

Similar trend is also observed in the case of the 0.55 w/b ratio mixes (Figure 6.12) with similar elastic modulus values as in the case of the 0.4 w/b ratio mixes with the same binder proportions. In general, all these mixes have similar E-Mod performance. Dhandapani et al. (2018), Avet, Sofia and Scrivener (2019), and Akindahunsi, Avet and Scrivener (2020) in their work also obtained similar elastic modulus values between the LC^3-50 systems and a system with only PC, a binary system with 30% cement replaced by fly ash, and a system with 50% cement replaced by GGBS.

In general, results indicate that the elastic modulus of concrete depends littler from factors such as concrete strength or cement paste but largely on the amount and the stiffness of the aggregates as discussed in Alexander (2021). However, the values at a later ages are quite significantly higher indicating slower densification of the ITZ compared to a system with condensed SF as suggested by Alexander and Milne (1995).

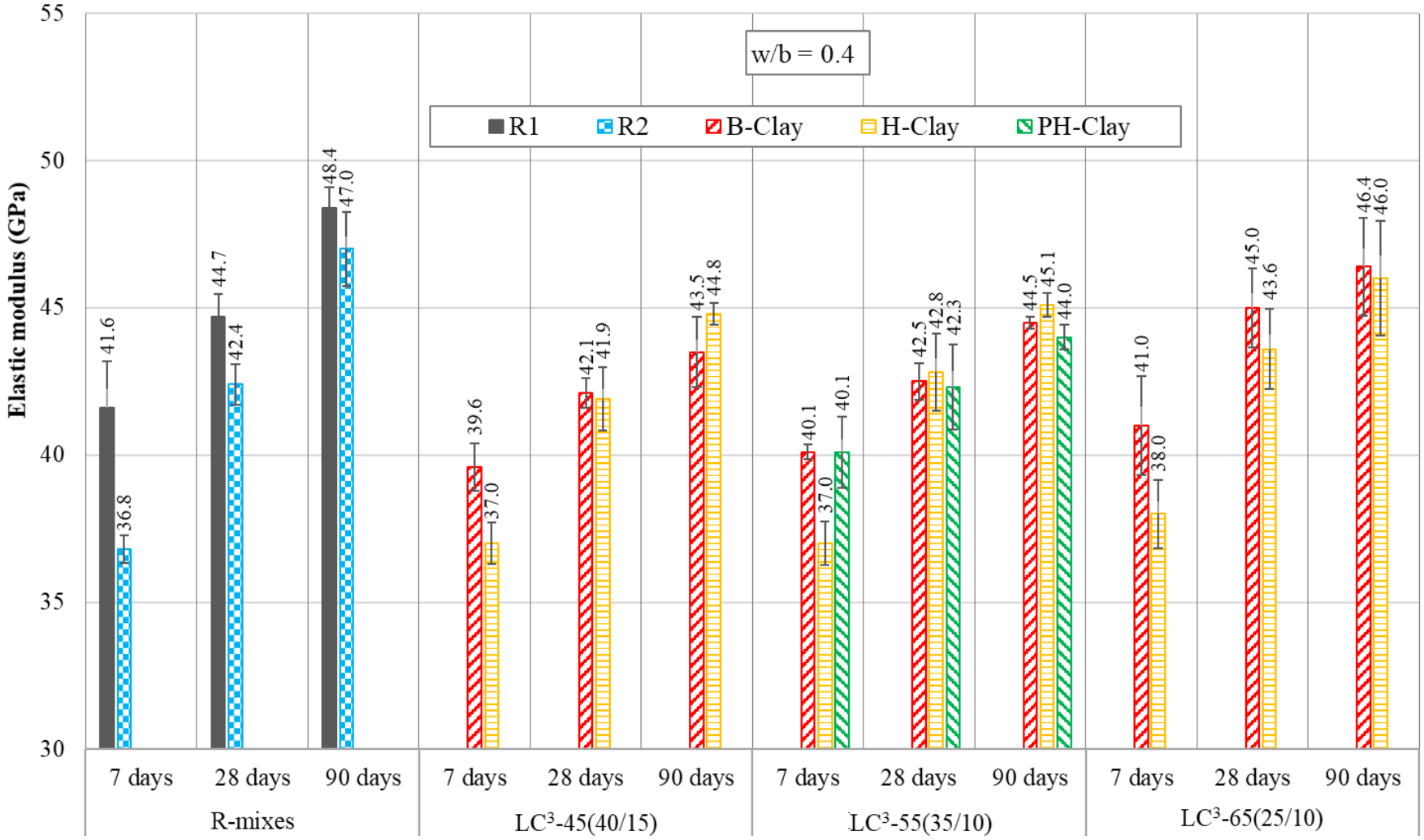

Figure 6.11: Elastic modulus development of LC^3 mixes and reference concrete mixes (w/b = 0.4)

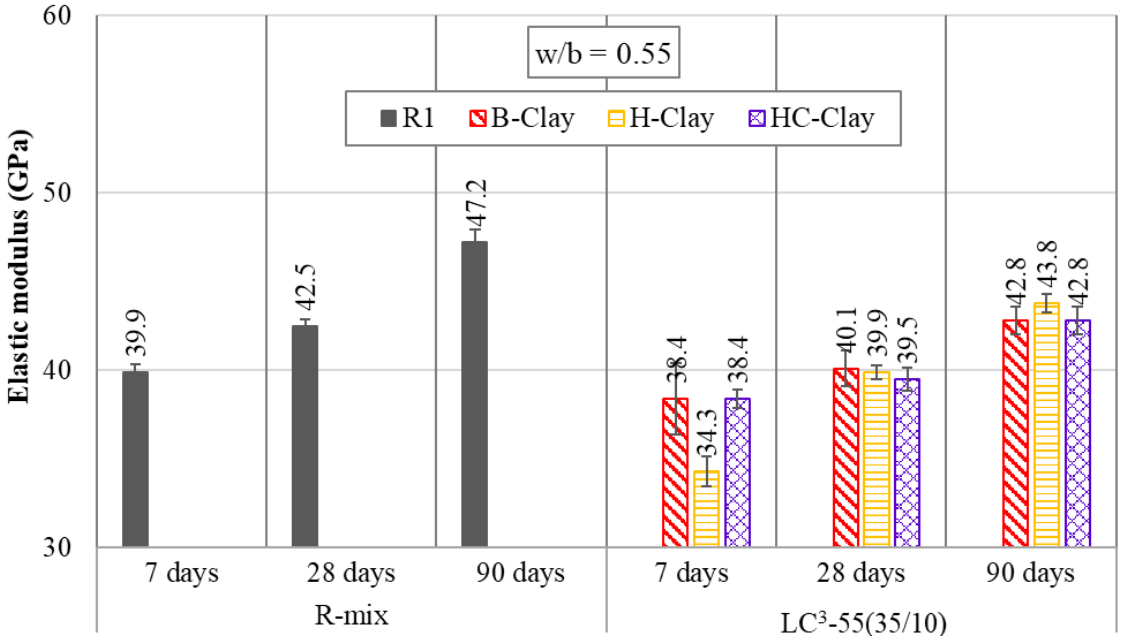

Figure 6.12: Elastic modulus development of LC^3 and reference concrete mixes (w/b = 0.55)

6.7 Drying shrinkage

6.7.1 Mixes with a w/b ratio of 0.40

Figure 6.13 presents the development of shrinkage strain in the concrete specimens. The error bars are not included for figure clarity. For each specimen, the first reading was taken after 28 days of curing. Further readings were taken up to 224 days. Based on the results, it can be noted that the LC^3 mixes with B-Clay and PH-Clay generally have lower shrinkage strain than the reference mixes. The LC^3 mixes with H-Clay (regardless of the clinker content) show higher shrinkage strain compared to the reference mixes, especially up to about 80 days.

Dhandapani et al. (2018) in their work noted that it is mainly the w/b ratio (not the binder system) that controls shrinkage development in the concrete. However, especially in the case of clays, it is hypothesised that the available water to react in the system initially is affected by the ISA of the clay. This means that a clay that has high ISA most likely will absorb more of the available water in the system which in turn reduce the rate of loss of moisture in the paste. This explains the low shrinkage strain in the LC^3 mixes with B-Clay and PH-Clay, compared to the reference mixes.

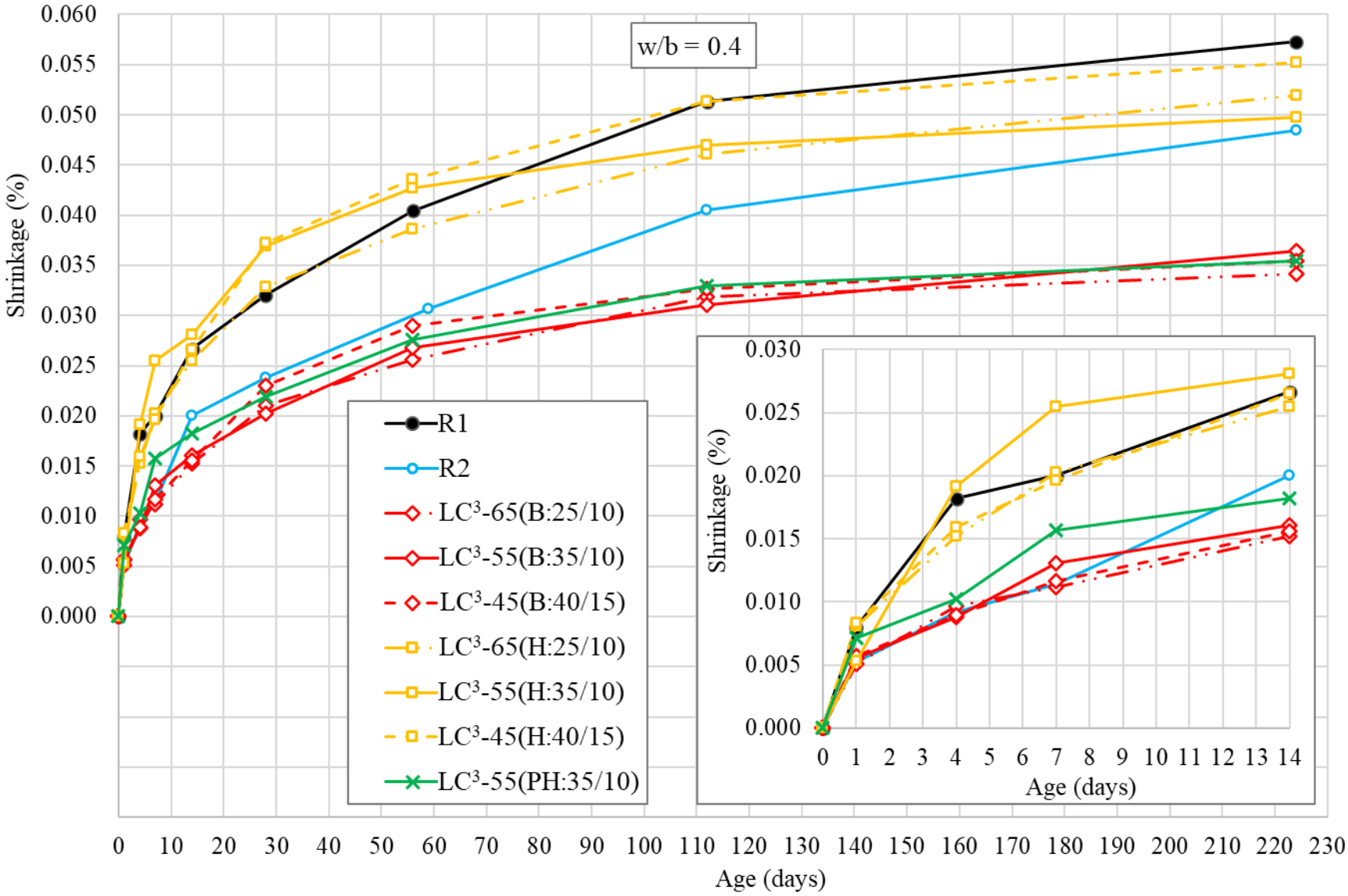

Figure 6.13: Shrinkage strains to 224 days (w/b = 0.4)

Comparing LC^3-55(35/10) mixes with PH-Clay and B-Clay, PH-Clay has a slightly higher ISA (14.5 m^2/g) than B-Clay (11.1 m^2/g) and therefore it would be expected that the LC^3-55(PH:35/10) has lower shrinkage strain than the LC^3-55(B:35/10), as explained in the previous paragraph. However, in this case the LC^3-55(PH:35/10) appear to have shrinkage strain marginally higher than LC^3-55(B:35/10); this might be attributed to a slightly higher SP dosage in LC^3-55(PH:35/10) (1.5% compared to 1.2% in LC^3-55(B:35/10)) (Ma, Wang, Liang, et al., 2007; Tam, Tam and Ng, 2012; Qian et al., 2020). High SP dosage might increase porosity in the binder matrix (Alsadey et al., 2016; Qian et al., 2020), consequently increasing the rate of moisture loss and shrinkage.

In the case of LC^3(H), apart from H-Clay having the lowest ISA compared to the other clays, the high shrinkage strain in these mixes relative to the other mixes is considered to be related to high amount of alkalis coming from the H-Clay (Beltzung and Wittmann, 2005; Sant et al., 2012; Li, Afshinnia and Rangaraju, 2016), which makes the microstructure more porous (Sant et al., 2012).

6.7.2 Mixes with a w/b ratio of 0.55

A similar trend is also observed in the case of concrete mixes with 0.55 w/b ratio (Figure 6.14). In this case the HC-Clay has higher ISA than the B-Clay, but the LC^3-55(HC:35/10) appears to have higher shrinkage strain compared to LC^3-55(B:35/10) which might be attributed to the higher dosage of SP (2%) in this mix compared to 1.2% in the LC^3-55(B:35/10) (Ma, Wang, Li, et al., 2007; Li, Yu and Brouwers, 2017; Qian et al., 2020).

6.7.3 General discussion

The factors affecting drying shrinkage in concrete are well explained in Alexander (2021). In this case, it is important to note that in all these mixes, the amount of water, amount of stone and the total amount of binder were fixed at 160 kg/m^3, 1000 kg/m^3 and 400 kg/m^3, respectively. Therefore, it is only the w/b ratio, type of binder and/or the proportion of binders that controlled drying shrinkage of the specimens.

In general, the LC^3 mixes, especially LC^3(B) and LC^3(PH), have lower shrinkage strain, almost 50% lower compared to reference mix R1. Presumably, with higher ISA there is more ‘absorbed water’ initially that can be slowly released back into the matrix with time

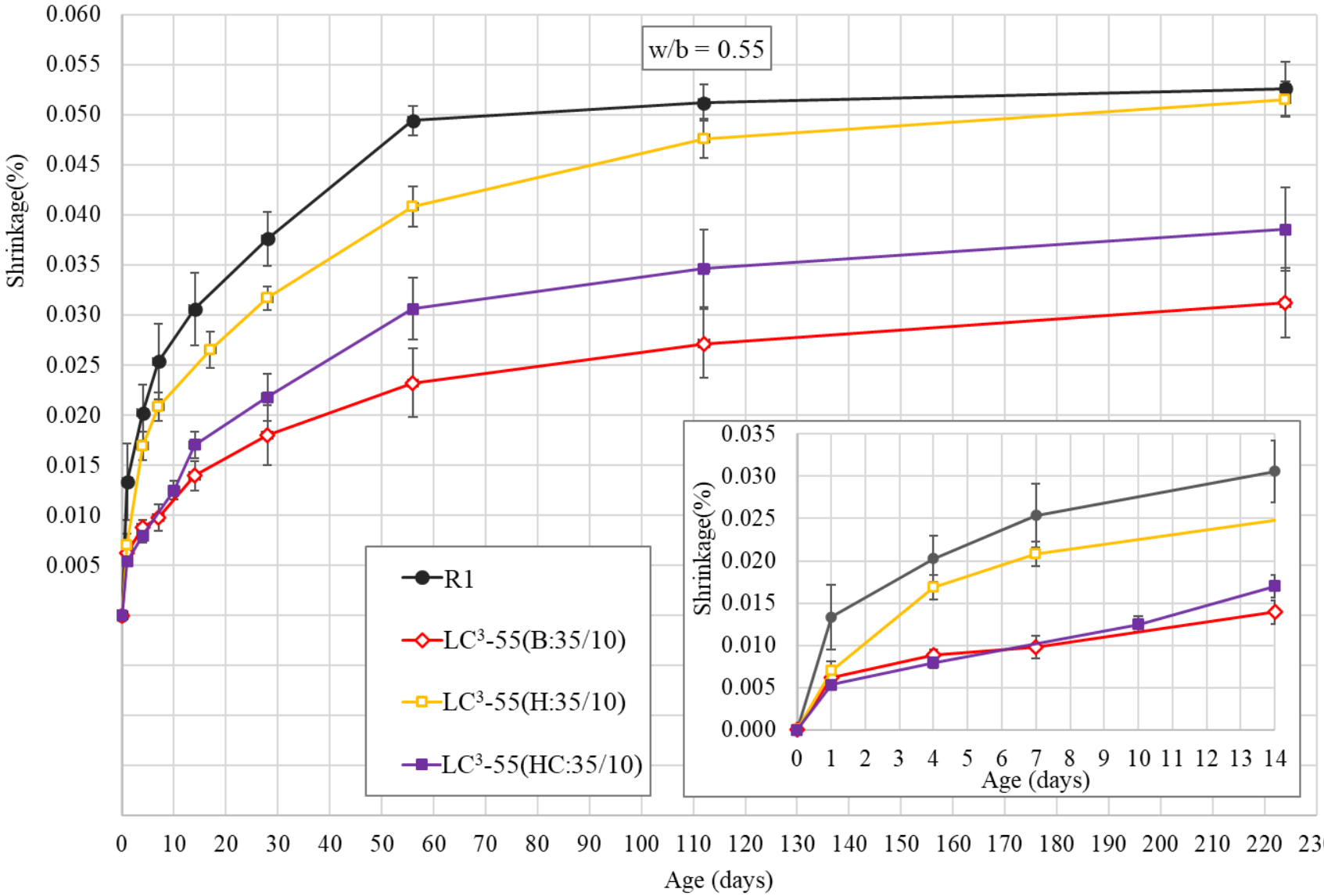

Figure 6.14: Shrinkage readings up to 224 days (w/b = 0.55)

as in the case of lightweight aggregates tested and discussed in Zhang, Li and Paramasivam (2005), Browning et al. (2011), Fenyvesi (2011) and Ahmed, Khalil and Jumaa (2018).

Comparing the results of the two cases, 0.4 w/b ratio (Figure 6.13) and 0.55 w/b ratio (Figure 6.14), the shrinkage strain for the reference mix R1 increases moving from a w/b ratio of 0.4 to a w/b ratio of 0.55. For example, at 28 days the shrinkage strain for reference mix R1 with a w/b ratio of 0.4 is 0.032% and 0.038% for the same reference mix but with a w/b ratio of 0.55. This was expected, since increasing the w/b ratio leads to increasing the amount of evaporable water, and thus an increase in shrinkage strains. Surprisingly, it is different in the case of LC^3-55(B) and LC^3-55(H) where the shrinkage strain appears to reduce going from a w/b ratio of 0.4 to a w/b ratio of 0.55. For the LC^3-55(B), the shrinkage strain at 28 days is 0.020% for 0.4 w/b ratio and 0.0180% for 0.55 w/b ratio likewise for the LC^3-55(H), it is 0.037% for 0.4 w/b ratio and 0.0317% for 0.55 w/b ratio. The reason for this is not yet clear, but most likely can be related to the high ISA of the clays and therefore how much water was available initially to react in the system, something that need further research.

6.8 Restrained ring shrinkage test results

Although free shrinkage is useful in comparing different concretes and different mix proportions, it does not provide sufficient information to compare how different concrete mixes will crack in service. In view of this, a restrained shrinkage ring test was adopted. The aim was to assess and compare the potential of early age cracking of the selected LC^3 concrete mixes versus the reference mixes under restrained conditions. In this case, the age at which the first crack appears on the surface of the ring gives an indication of the concrete's potential to resist cracking under restrained conditions.

Due to the limited amount of clay sample from Tanzania, only LC^3-55(B:35/10) and LC^3-55(H:35/10) were compared with the reference mixes. All specimens showed the appearance of the first cracks with a crack width of approximately 0.1 mm throughout the height of the specimens (155 mm). Figure 6.15 shows a typical crack on the surface of the specimens. The second cracks were observed to appear on the opposite side of the ring to the first crack as shown by the arrow on Figure 6.15. However, some of the specimens did

not show the appearance of the second crack even after 90 days, but the widths of the first crack on these specimens increased from 0.1 mm to 0.2 mm.

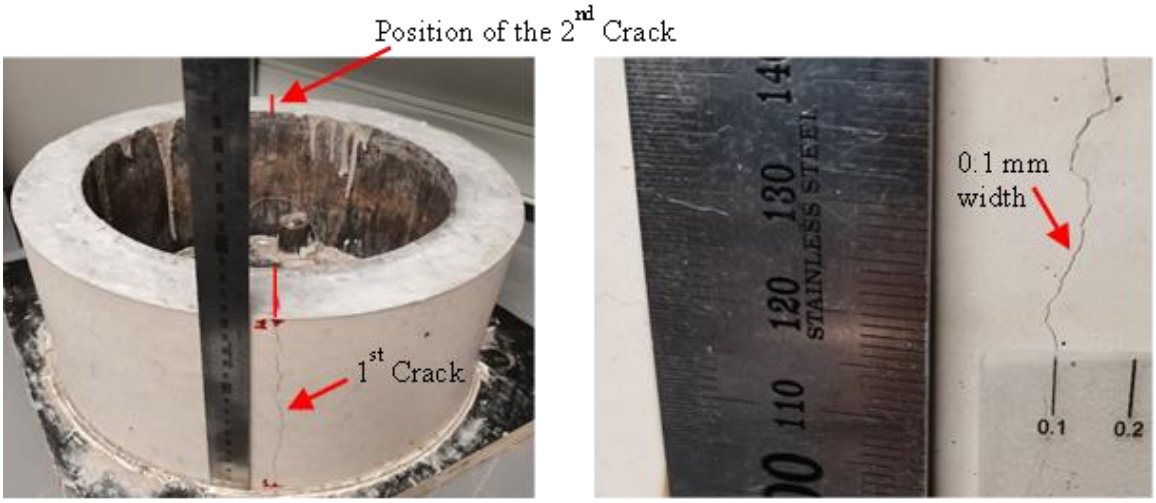

Figure 6.15: Typical cracks on the concrete ring specimens

Figure 6.16 shows the time of occurrence of the first crack as an average of three specimens and Table 6.5 provides a summary of other observations. It is clear from the results that the LC^3-55(B:35/10) mix outperform the reference mix R2 but have a performance similar to the reference mix R1. However, in general, partial replacement of PC by SCMs results in reducing the cracking age of concrete as reported by Khan et al. (2020).

The appearance of the first crack and the results of the free shrinkage tests up to 28 days are summarised in Table 6.6. In general, the results indicate that, for all the selected mixes, the first crack occurs when the equivalent free shrinkage strain is between 0.016% and 0.03%. The low cracking potential of the LC^3-55(B:35/10) compared to the reference mix R2 is largely related low rate of shrinkage development in this system. On the contrary, the highest cracking potential of the LC^3-55(H:35/10) compared to all other mixes is largely related to the high amount of alkalis coming from the H-Clay (He and Li, 2005) and therefore high rate of shrinkage development in this system.

As shown in Figure 6.11, the elastic modulus of concrete is generally less affected by the type or proportions of binders and therefore provides less influence on the early age cracking of concrete. For instance, at 7 days, the elastic modulus values of the LC^3 concrete mixes are in the range of 88% and 99% of the reference mix R1 and in the range of 100%

and 112% of the reference mix R2. At 28 days, the elastic modulus values are in the range of 93% and 100% of the reference mix R1 and in the range of 99% and 106% of the reference mix R2.

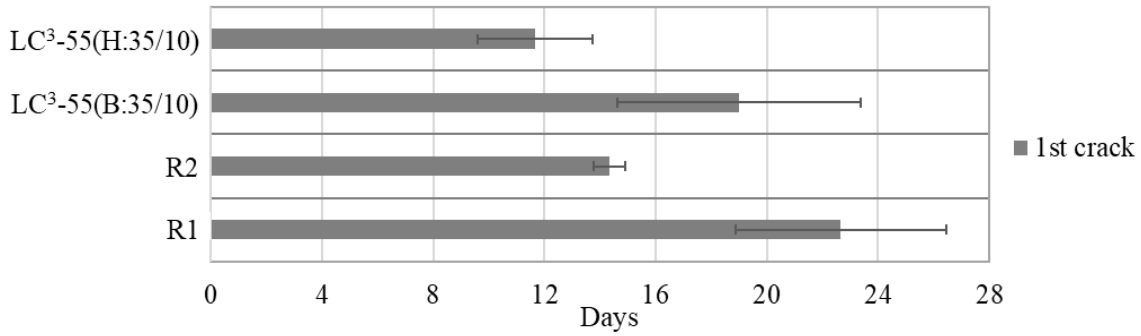

Figure 6.16: Age at first crack

Table 6.5: Appearance of first and second cracks on the concrete ring specimens

Mix	Specimen #	1st crack				2nd crack		1st Crack + 2nd Crack (mm) at 90 days
		Appearance	Crack increase			Appearance		
		Age (days)	Width (mm)	Age (days)	Width (mm)	Age (days)	Width (mm)	
R1	1	20	0.1	31	0.2	-	-	0.2
	2	21	0.1	-	-	34	0.1	0.2
	3	27	0.1	-	-	36	0.1	0.2
R2	1	14	0.1	34	0.2	-	-	0.2
	2	14	0.1	-	-	21	0.1	0.2
	3	15	0.1	-	-	23	0.1	0.2
LC3-55 (B:35/10)	1	16	0.1	-	-	30	0.1	0.2
	2	17	0.1	37	0.2	-	-	0.2
	3	24	0.1	-	-	-	-	0.2
LC3-55 (H:35/10)	1	10	0.1	29	0.2	-	-	0.2
	2	11	0.1	-	-	-	-	0.2
	3	14	0.1	-	-	20	0.1	0.2

Table 6.6: Shrinkage strain of the mixes selected for the ring test and their age at first crack

Mix	Shrinkage (%)			Age at first crack (Days)				
	7 days	14 days	28 days	Specimen			Average	SD
				#1	#2	#3		
R1	0.020	0.027	0.032	20	21	27	23	4
R2	0.011	0.020	0.024	14	14	15	14	1
LC3-55(B:35/10)	0.013	0.016	0.020	16	17	24	19	4
LC3-55(H:35/10)	0.025	0.028	0.037	10	11	14	12	2

6.9 Electrical resistivity measurements

As described in Section 3.8.8, for this test, cylindrical concrete specimens with 100 mm diameter and 200 mm height as recommended by AASHTO T 358 (2015) were tested using Resipod 4-point Wenner probe resistivity meter with fixed probes equally spaced 50 mm apart. The factors influencing electrical resistivity of concrete are well discussed by Azarsa and Gupta (2017) and Cheytani and Chan (2021). The edge effect was considered minimal and/or the same for all the specimens and therefore not further considered (Millard, 1991; Gowers and Millard, 1999; Robles, Yee and Kee, 2021).

The results show that, in both cases, 0.4 w/b ratio (Figure 6.17) and 0.55 w/b ratio (Figure 6.18), the LC^3 mixes especially mixes with B-Clay and PH-Clay have very high resistivity values at all the ages, compared to the reference mixes which show small increase in the resistivity between the ages. On the contrary, the LC^3 mixes with H-Clay have lower values compared to the mixes with B-Clay and PH-Clay but generally higher than the reference mixes R1 and R2. Therefore, in general, in both cases, it appears that all the LC^3 mixes with B-Clay, PH-Clay and HC-Clay are less penetrable (in terms of transfer of ions such as chloride ions or sulphate ions), compared to the reference mixes. In the case of 0.4 w/b ratio mixes, the LC^3-55(H:35/10) and LC^3-65(H:25/10) show similar performance compared to the reference mix R2.

Based on the chloride penetrability classification given by AASHTO TP 95 in kΩcm, all LC^3 mixes with B-Clay and PH-Clay have resistivity values above 254 kΩcm, suggesting that these mixes have negligible risk of chloride ingress. On the other hand, the LC^3 mixes with H-Clay and HC-Clay, and reference mix R2 have values between 37 and 254 kΩcm indicating that these mixes have very low risk of chloride ingress. The resistivity value of the reference mix R1 is between 12 and 21 kΩcm meaning this mix has moderate risk of chloride ingress. In general, as per classification given by AASHTO TP 95, the risk of chloride ingress in these mixes depends largely on the amount of CK in the system.

Comparing LC^3 mixes with different clinker content (Figure 6.17), especially mixes with B-Clay and H-Clay, it is clear that the resistivity values increase as the amount of calcined clay increases in the mix. This trend suggests that the performance of the LC^3 system, with

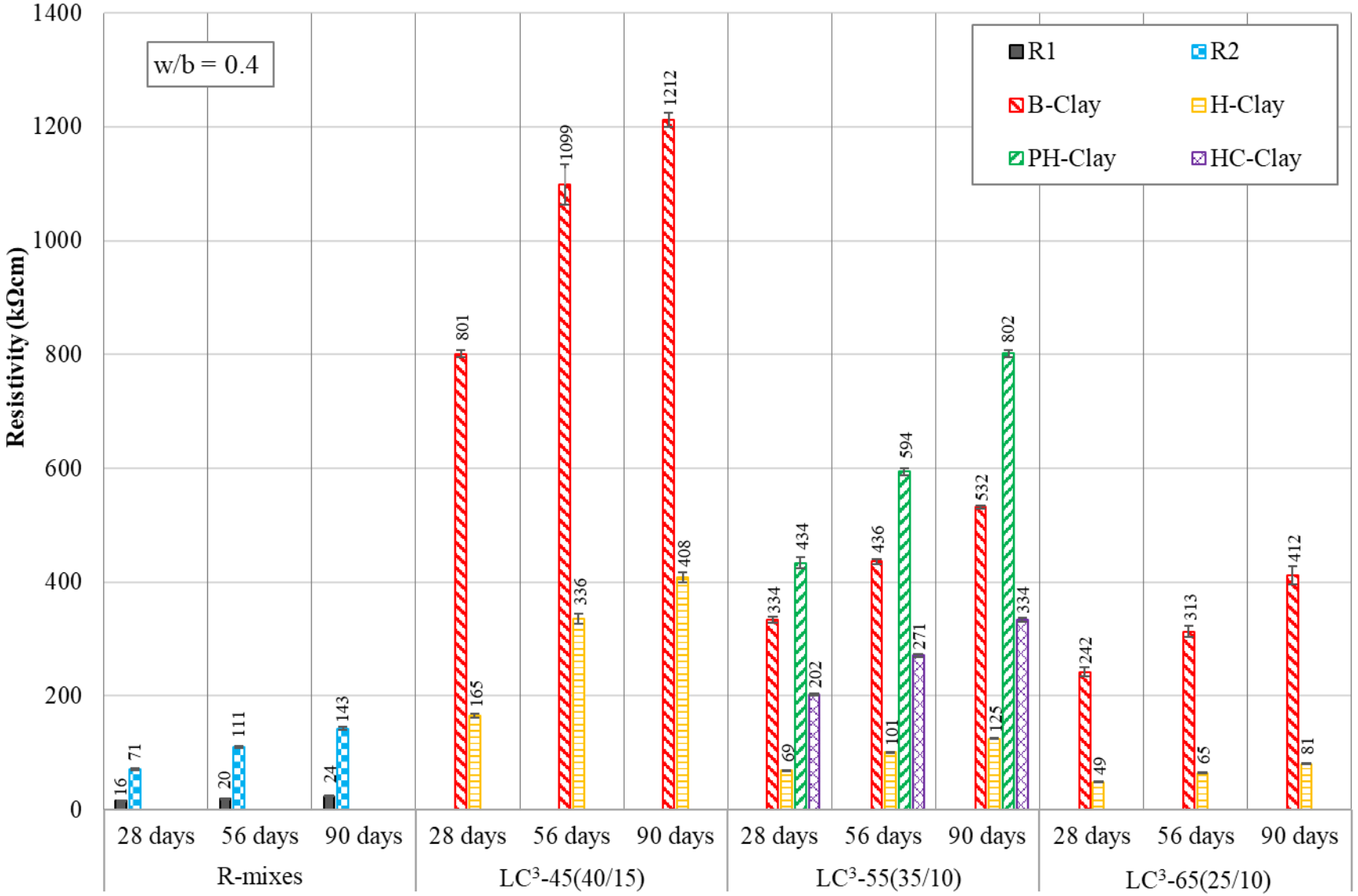

Figure 6.17: Resistivity results of the concrete mixes at 28, 56 and 90 days (w/b = 0.4)

regards to chloride ingress resistance, is strongly influenced by the amount of calcined clay in the mix. However, further research is required to fully understand the mechanisms in the system.

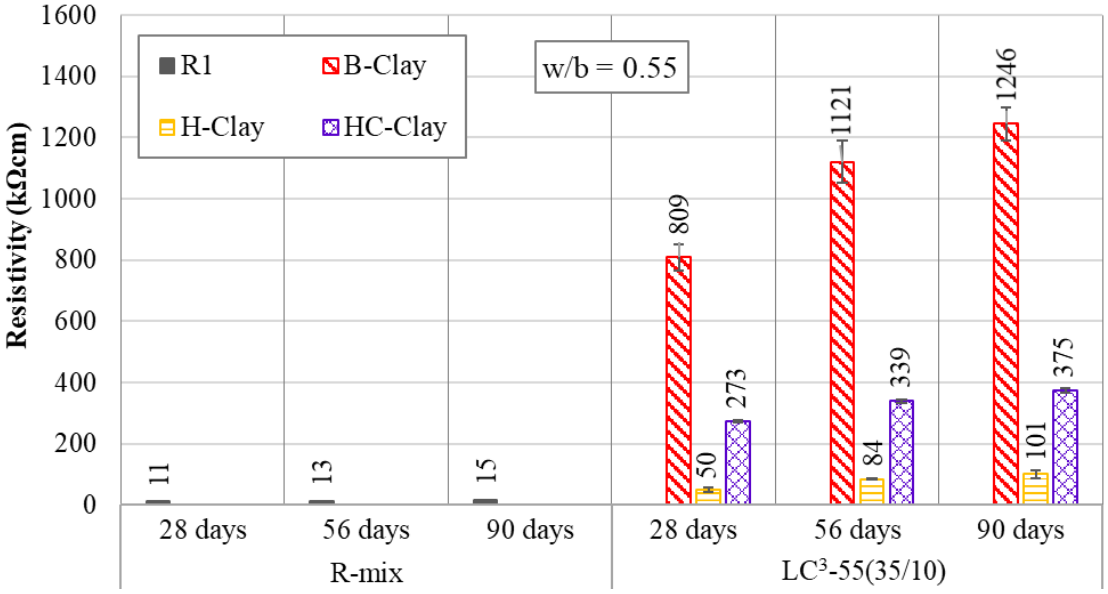

Figure 6.18: Resistivity results of the concretes mixes at 28, 56 and 90 days (w/b = 0.55)

Considering the resistivity values of all the LC^3 mixes only, especially in the case of LC^3-55 mixes (Figure 6.17), although the B-Clay has higher amount of CK (i.e., metakaolin), than PH-Clay, the resistivity values of the LC^3-55(PH:35/10) at all ages are higher compared to the resistivity values of the LC^3-55(B:35/10). Also, despite H-Clay (both 0.4 and 0.55 w/b ratio) and HC-Clay having similar amount of CK, the resistivity values of the LC^3-55(HC:35/10) at all ages are higher compared to the resistivity values of the LC^3-55(H:35/10). This trend is thought to be largely related to the amount of alkalis in the system, the higher the amount of alkalis in the system the lower the resistivity value. In this case, the LC^3-55(H:35/10) has the lowest resistivity values because of the high alkalis coming from the H-Clay (See Table 4.5), which increase porosity in the microstructure (Beltzung and Wittmann, 2005; Sant et al., 2012; Li, Afshinnia and Rangaraju, 2016).

Comparing the results of the two cases, 0.4 w/b ratio (Figure 6.17) and 0.55 w/b ratio (Figure 6.18), especially the LC^3-55 mixes and the reference mix R1, the resistivity values of the LC^3-55(H:35/10) and the reference mix R1 decrease going from 0.4 to 0.55 w/b ratio. For example, at 28 days the resistivity value for the reference mix R1

with a w/b ratio of 0.4 is 16 kΩcm and 11 kΩcm for the same reference mix but with 0.55 w/b ratio. This was expected, since increasing the w/b ratio results to more voids in the system and thus a low resistivity value or more permeable concrete. Surprisingly, it is different in the case of LC^3-55 mixes with B-Clay and HC-Clay where the resistivity values appear to increase going from 0.4 to 0.55 w/b ratio. For example, for LC^3-55(B:35/10), the resistivity value at 28 days is 334 kΩcm for 0.4 w/b ratio and 809 kΩcm for 0.55 w/b ratio likewise for LC^3-55(HC:35/10), it is 202 kΩcm for 0.4 w/b ratio and 273 kΩcm for 0.55 w/b ratio. Rupnow (2011) observed a similar behaviour moving from 0.35 to 0.65 w/b ratio for a system with 50% cement replaced by slag. The reason for this is not yet clear, but most likely can be related to the availability of CH in the system, how much is being consumed by the pozzolanic reaction, and formation of hydrated phases and therefore how pores are interconnected inside the concrete, something that needs further research.

6.10 Durability index test results

The three DI tests i.e., OPI, WSI and CCI, and a porosity test were carried out to assess the resistance of LC^3 specimens to penetration of gases, liquid, and ions in comparison with the reference mixes R1 and R2. In general, the indices can be used to characterise the quality of concrete with different types of binder and binder proportions. Table 6.7 (Alexander, Mackechnie and Ballim, 1999) and Table 6.8 (Moore, Bakera and Alexander, 2021) provides suggested ranges for durability index classification.

Table 6.7: Suggested ranges for durability classification using OPI and CCI values (Alexander, Mackechnie and Ballim, 1999)

Durability class	OPI (log scale)	Conductivity (mS/cm)
Excellent	>10	<0.75
Good	9.5-10	0.75-1.50
Poor	9.0-9.5	1.50-2.50
Very poor	<9.0	>2.50

Table 6.8: Suggested durability classification table for sorptivity and porosity values (Moore, Bakera and Alexander, 2021)

Sorptivity (mm/√h)	Porosity (%)	**Durability classification**
<6	<10	Excellent
6 – 10	<10 >10, <12	Excellent to Good Good to Poor
10 – 15	<12 >12, <15	Good to Poor Poor to Very poor
>15	-	Very poor

6.10.1 OPI, WSI and porosity results

6.10.1.1 Mixes with a w/b ratio of 0.4

Figure 6.19 presents the coefficient of permeability (k) of the LC^3 mixes in comparison with the reference mixes, for the 0.4 w/b ratio mixes. The corresponding OPI values are presented in Figure 6.20. From the results, all mixes have k-values less than 10^{-11} m/s (or OPI values > 10) indicating a very dense concrete, low permeability, and thus high resistance to penetration of deleterious gases such CO_2. However, by examining the k-values and/or OPI values, it is clear that the LC^3 mixes outperform the reference mixes. A similar finding was also noted by Dhandapani et al. (2018). In general, results also indicate that the LC^3 mixes, regardless of the clinker content and type of clay, have k-values between 1.9 x 10^{-12} and 4.5 x 10^{-12} m/s or OPI values between 11.4 and 11.7 (log scale) with overlapping error bars indicating similar performance. However, this does not mean that the test is less sensitive to binder proportions but rather less sensitive when the concrete is very dense with OPI values above 11 (log scale).

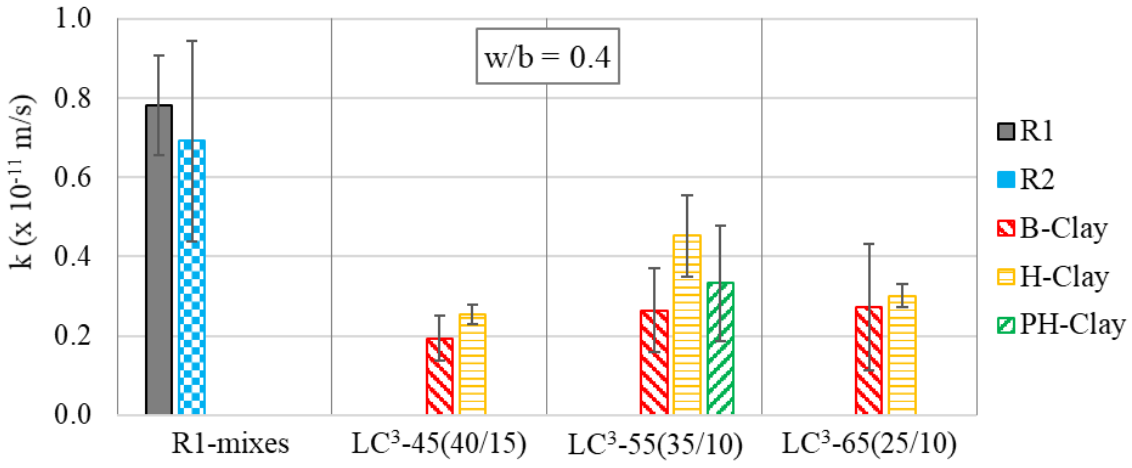

Figure 6.19: k-values of LC^3 and reference concrete specimens (w/b = 0.4)

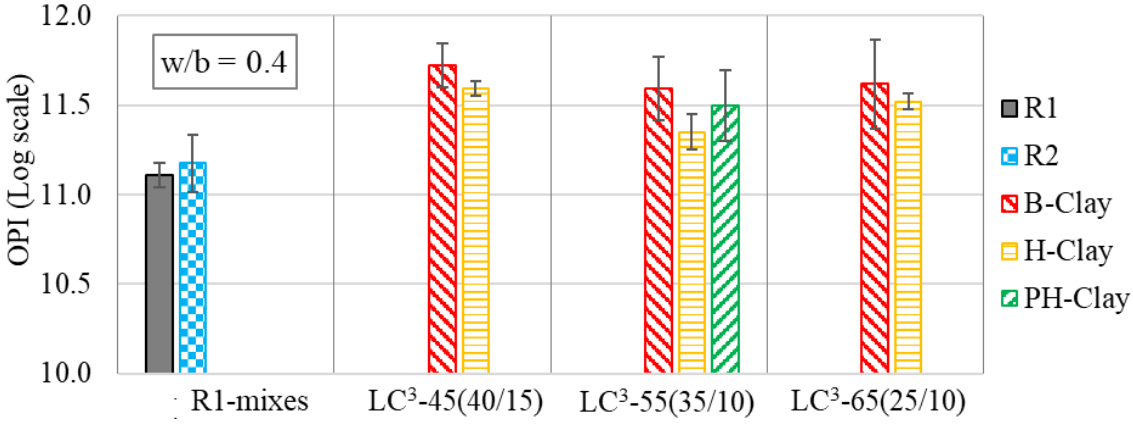

Figure 6.20: OPI results of LC^3 and reference concrete specimens (w/b = 0.4)

In the case of WSI (Figure 6.21), all mixes perform almost similar with values ranging between 6 and 10 mm/hr$^{0.5}$ indicating excellent to good quality concrete as per Table 6.8 and in the case of porosity (Figure 6.22), all mixes have values less than 10% indicating excellent quality concrete as proposed in Table 6.8. In general, all mixes had low porosity and low sorptivity values implying a dense and relatively impenetrable binder matrix. However, based on the values obtained, it is clear that the LC^3 mixes outperform reference mix R1 but similar to reference mix R2 except the LC^3 mixes with H-Clay when it comes to porosity. The higher porosity in the LC^3(H) compared to other LC^3 mixes is considered to be related to the high amount of alkalis coming from the H-Clay (Beltzung and Wittmann, 2005; Sant et al., 2012; Li, Afshinnia and Rangaraju, 2016) which make the microstructure more porous (Sant et al., 2012), and also H-Clay has lower CK compared to other clays.

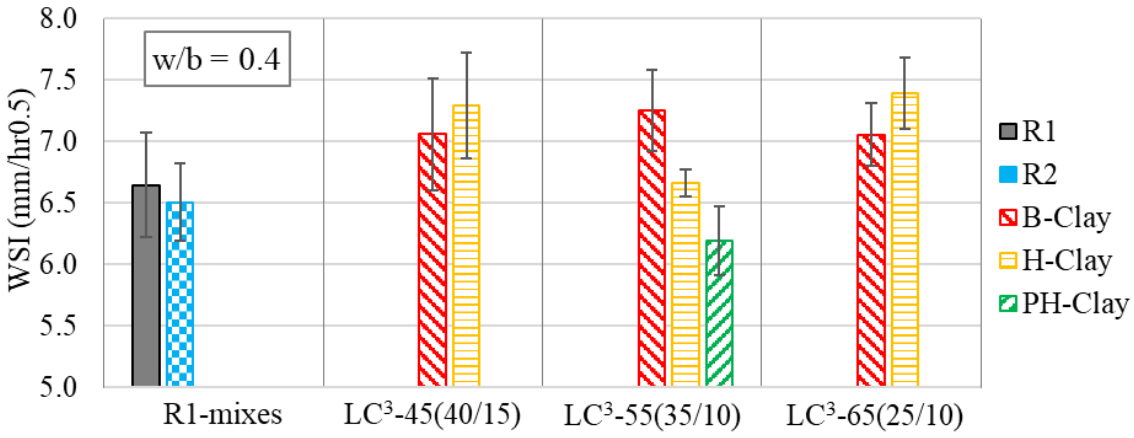

Figure 6.21: WSI results of LC^3 and reference concrete specimens (w/b = 0.4)

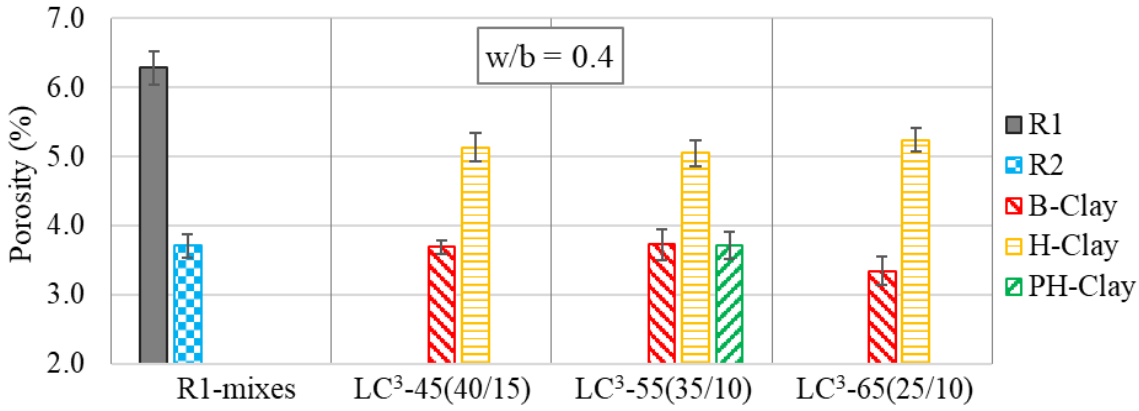

Figure 6.22: Porosity (using CH Solution) of the concrete specimens (w/b = 0.4)

In general, the performance of the LC^3 mixes is largely related to the combination of the filler effect, pozzolanic reaction, formation of carboaluminate phases, and stabilization of ettringite which help to reduce porosity. In this case, it can be concluded that the LC^3 mixes have a finer pore network with less connectivity compared to the reference mixes.

6.10.1.2 Mixes with a w/b ratio of 0.55

In this case, the trend is similar as in the case of 0.4 w/b ratio. All mixes have k-values below 10^{-11} (Figure 6.23) or corresponding OPI values above 10 (Figure 6.24) and sorptivity (Figure 6.25) and porosity (Figure 6.26) values less than 10% indicating that all specimens are very dense and have very low permeability. Results also show that the LC^3 mixes have k-values lower than the reference mix or OPI values higher than the reference mix which suggest that the LC^3 mixes are better than the reference mix when it comes to resistance to penetration of deleterious gases.

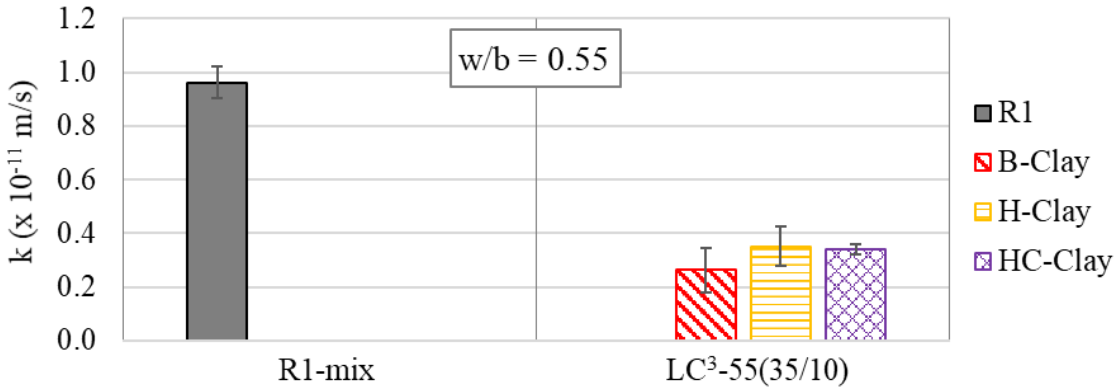

Figure 6.23: Coefficients of permeability of LC^3 and reference concrete specimens (w/b = 0.55)

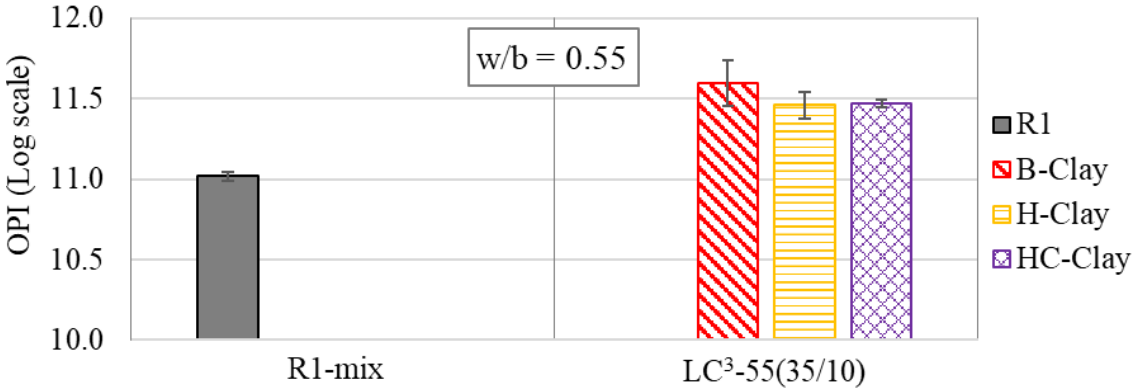

Figure 6.24: OPI results of LC^3 and reference concrete specimens (w/b = 0.55)

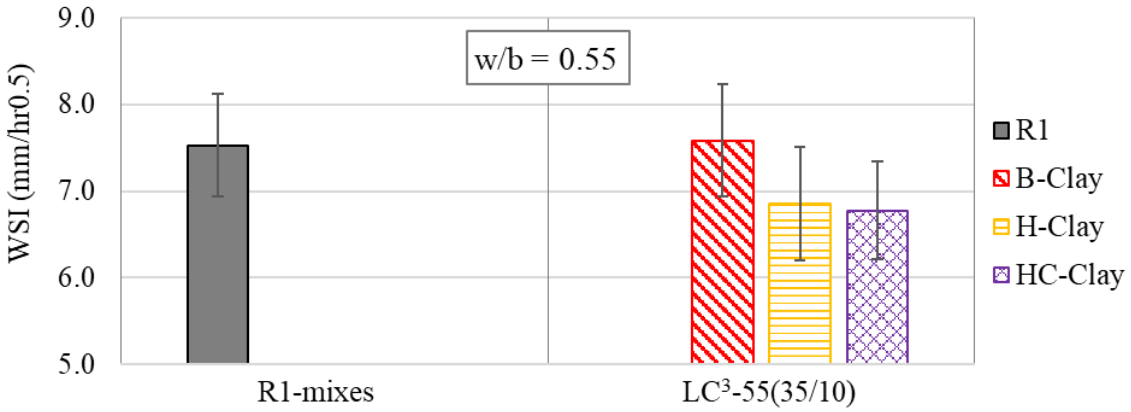

Figure 6.25: WSI results of LC^3 and reference concrete specimens (w/b = 0.55)

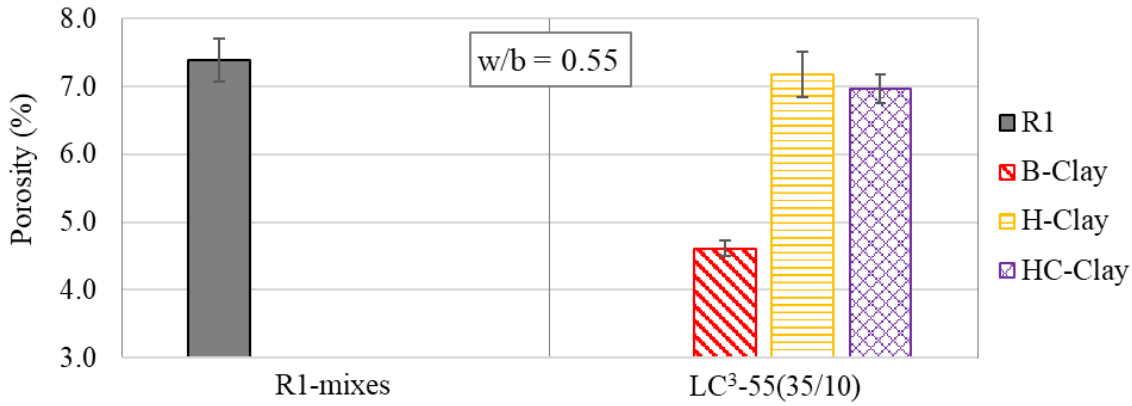

Figure 6.26: Porosity (using CH Solution) results of the concrete specimens (w/b = 0.55)

In general, there is little difference between the results of the mixes with 0.4 and 0.55 w/b ratio which is mainly related to the influence of curing. It is important to note that with full curing, the differences diminish and the concretes approach similar values as these indexes were mainly derived to characterise the influence of curing (Alexander, Mackechnie and Ballim, 1999; Alexander, 2021). With limited curing, the results would be very different (Gouws, Alexander and Maritz, 2001; Du Preez and Alexander, 2004; Surana, Pillai and Santhanam, 2017).

6.10.2 CCI results

6.10.2.1 Mixes with a w/b ratio of 0.4

Figure 6.27 presents the results of the CCI test, for the 0.4 w/b ratio mixes. From the results, all mixes have values less than 0.75 mS/cm, indicating that they all have excellent resistance to chloride ingress as per Table 6.7. It is clear that the LC^3 mixes outperform the reference mix R1 but are similar to reference mix R2. It needs to be

noted here that reference mix R2 is expected to have excellent chloride resistance, due to the high amount of cement replacement with GGBS. At the scale of the test results, i.e., with very low CCI values at around 0.15, it can be seen that the LC^3 mixes have equivalent high expected durability, compared to the GGBS mixes accepted in industry.

The corresponding porosity results are presented in Figure 6.28; the trend agrees well with the porosity results presented in Figure 6.22. Results also indicate that the LC^3 mixes, regardless of the clinker content and type of clay, have CCI values less than 2 mS/cm implying little difference in the performance of these mixes. In general, apart from the filler effect and pozzolanic reaction, the performance of the LC^3 mixes is also related to the formation of carboaluminate phases and stabilization of ettringite which reduces porosity and interconnectivity of pores within the LC^3 matrix.

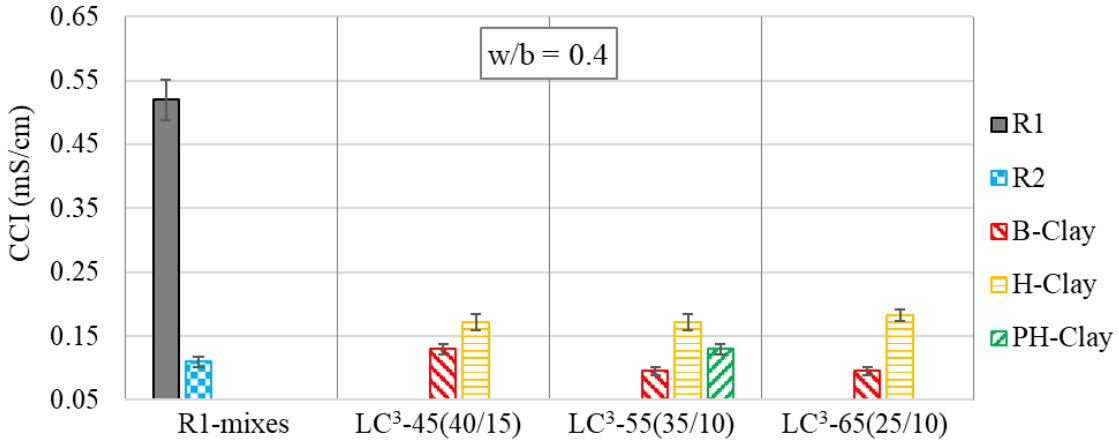

Figure 6.27: CCI results of the concrete specimens (w/b = 0.4)

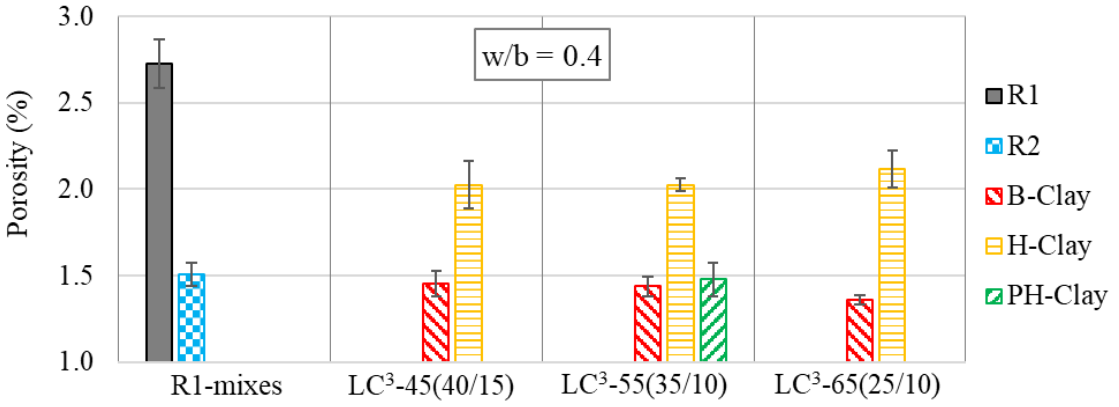

Figure 6.28: Porosity (using NaCl solution) results of the concrete specimens (w/b = 0.4)

6.10.2.2 Mixes with a w/b ratio of 0.55

Figure 6.29 shows the results of CCI test, a case of 0.55 w/b ratio. From the results, all LC^3 mixes have values less than 0.75 mS/cm while the value for the reference mix is between 0.75 and 1 mS/cm. In general, as in the case of 0.4 w/b ratio, it means that the LC^3 mixes are better than the reference mix in terms of resistance to chloride ingress. The corresponding porosity results presented in Figure 6.30 show similar trend compared to the porosity results presented in Figure 6.26.

Comparing the results of the two cases, 0.4 w/b ratio (Figure 6.27) and 0.55 w/b ratio (Figure 6.29), the CCI value of the reference mix R1 increased from 0.52 to 0.96 mS/cm going from 0.4 to 0.55 w/b ratio. Similarly, for the LC^3-55 mixes, the CCI values increased from 0.1 to 0.16 mS/cm for the LC^3-55(B) and from 0.17 to 0.3 mS/cm for the LC^3-55(H). This was expected, since increasing the w/b ratio leads to greater porosity in the system and thus high CCI value or less resistance to ingress of ions. However, it is clear that for the LC^3 mixes the increase is very small (0.06 mS/cm for the LC^3-55(B) and 0.13 for the LC^3-55(H)) compared to the reference mix R1 (0.44 mS/cm) which indicate little change in the performance of the LC^3 mixes moving from 0.4 to 0.55 w/b ratio. Further, as pointed out in Section 6.10.1.2, the small difference between the results of the mixes with 0.4 and 0.55 w/b ratio is mainly related to the influence of curing. With continuous curing, the differences diminish and the concretes approach similar values (Alexander, Mackechnie and Ballim, 1999; Alexander, 2021). With limited curing, the change in the performance would be very different (Gouws, Alexander and Maritz, 2001; Du Preez and Alexander, 2004).

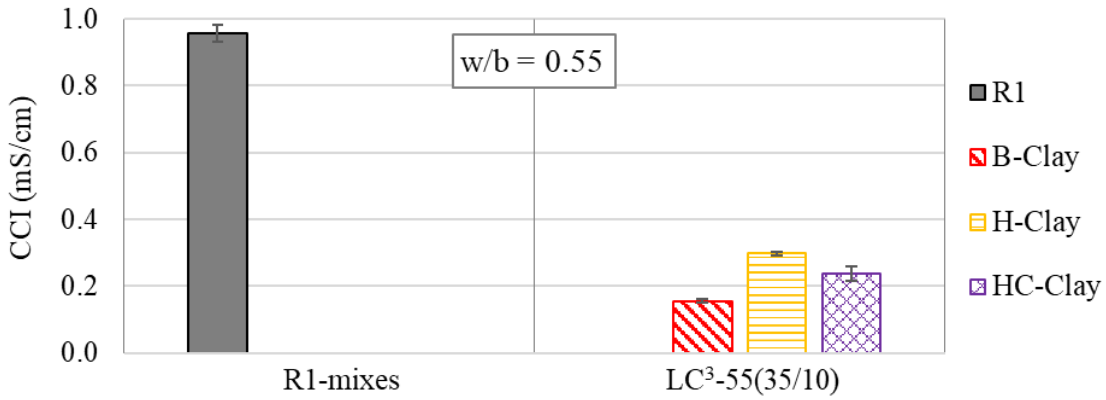

Figure 6.29: CCI results of the concrete specimens (w/b = 0.55)

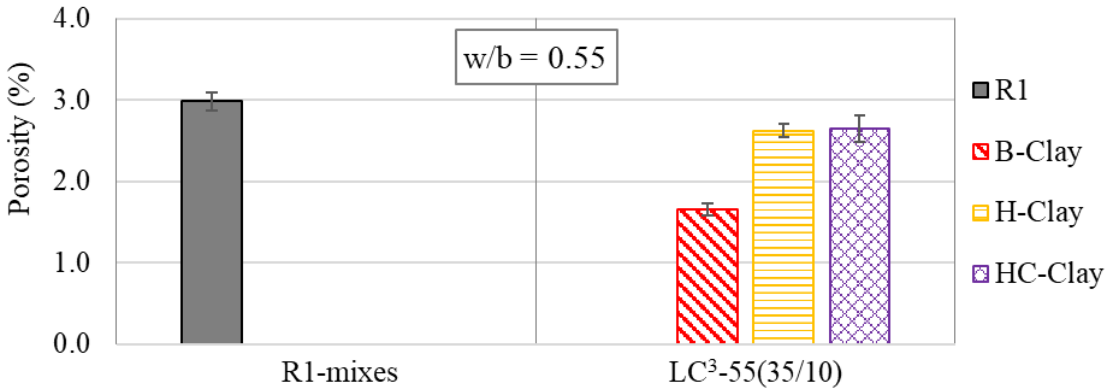

Figure 6.30: Porosity (using NaCl solution) results of the concrete specimens (w/b = 0.55)

6.10.3 Summary and conclusion

From the results, all mixes irrespective of the w/b ratio and amount of clinker have k-values less than 10^{-11} m/s or OPI values greater than 10 (log scale). This implies that, overall, all specimens fall into the "excellent" durability class as per Table 6.7, which gives proposed ranges for durability index classification. Therefore, all specimens have very low oxygen permeability, which represents concrete with a very dense matrix, and which implies high resistance to penetration of gases such as CO_2.

In the case of the WSI and porosity results, for both 0.4 and 0.55 w/b ratio, all specimens have values less than 10 ($mm/hr^{0.5}$ or %) implying that all concrete specimens fall into "excellent to good" class as per Table 6.8. Results also show that the CCI values of all tested specimens (regardless of the w/b ratio) are less than 0.75 mS/cm except the reference mix R1 (case of 0.55 w/b ratio) which has a value between 0.75 and 1 mS/cm. From Table 6.7, these results represent concrete of excellent resistance to chloride ingress.

The results further indicate that there is little change in the OPI, CCI and WSI values of the LC^3-55 mixes compared to the reference mix R1, moving from a w/b ratio of 0.4 to a w/b ratio of 0.55, which is largely related to the influence of curing. However, in general, based on the DI values, it can be concluded that the LC^3 mixes, regardless of the clinker factor and type of clay, are very dense and have fine pore networks with lower connectivity compared to the reference mix R1 and that they have a similar performance to reference mix R2.

6.11 Accelerated carbonation results

Figure 6.31 and Figure 6.32 present the accelerated carbonation test results of concrete mixes with 0.4 and 0.55 w/b ratio, respectively. The carbonation depths were measured at 12 weeks and 24 weeks after exposure to a CO_2 level of 2%. A good review of the carbonation of concrete with different SCMs is given in the literature (von Greve-Dierfeld et al., 2020). In general, results show that the LC^3 mixes have lower carbonation resistance compared to reference mix R1, which contains 100% CEM II. For the LC^3 mixes, the carbonation depth increases with a decrease in clinker content, as expected. For example, the carbonation depth is higher in the LC^3-45 mixes, compared to the LC^3-65 mixes. Khan, M.S.H., Nguyen, Q.D. and Castel (2018) observed a similar trend. Also, in the case of LC^3-55 mixes, it is clear that the depth of carbonation increases with an increasing w/b ratio. This indicates that the depth of carbonation depends largely on the amount of clinker and/or CaO present in the mix, as well as the density of the pore structure, which in turn is related to the w/b ratio.

The observed trend was expected in the case of LC^3 mixes due to the lower amount of CH in the system, which is also partially consumed by the pozzolanic reaction. However, a certain amount of CH still remains in the system as shown by the XRD scans (Figure 5.23) and quantification of CH from TGA results (Figure 5.24). On the other hand, the OPI results (Figure 6.20 and Figure 6.24) indicate that the LC^3 mixes are dense and have high resistance to penetration of deleterious gases compared to the reference mixes R1 and R2. In this case, while the lower amount of CH in the LC^3 mixes favours higher carbonation rates, the slower penetration of moisture and CO_2 through the concrete may partially reduce the carbonation rate, especially when a good concrete cover is provided. In addition, E. Díaz et al. (2018) on their ongoing work, made preliminary conclusions that LC^3 concrete may perform similarly or better than a reference PC in some environments. On the other hand, a study done by Shah and Bishnoi (2018b) on carbonation resistance of concretes containing different SCMs exposed to different accelerated conditions (i.e., different CO_2 concentrations, RH and temperature), versus samples exposed to natural environments, concluded that the rate of carbonation is largely controlled by the amount of clinker, RH, and w/c ratio. Furthermore, a review done by Angst et al. (2020) on about 1000 documented cases of RC structures with carbonation front at the level of reinforcement noted that, in general,

carbonation did not automatically lead to corrosion and that the main factor controlling the corrosion rate is the degree of moisture at the steel-concrete interface. This means that carbonation of concrete may not be the primary problem for corrosion of reinforcement and associated damage in concrete. In view of this, further work is required to fully understand corrosion of steel in carbonated concrete.

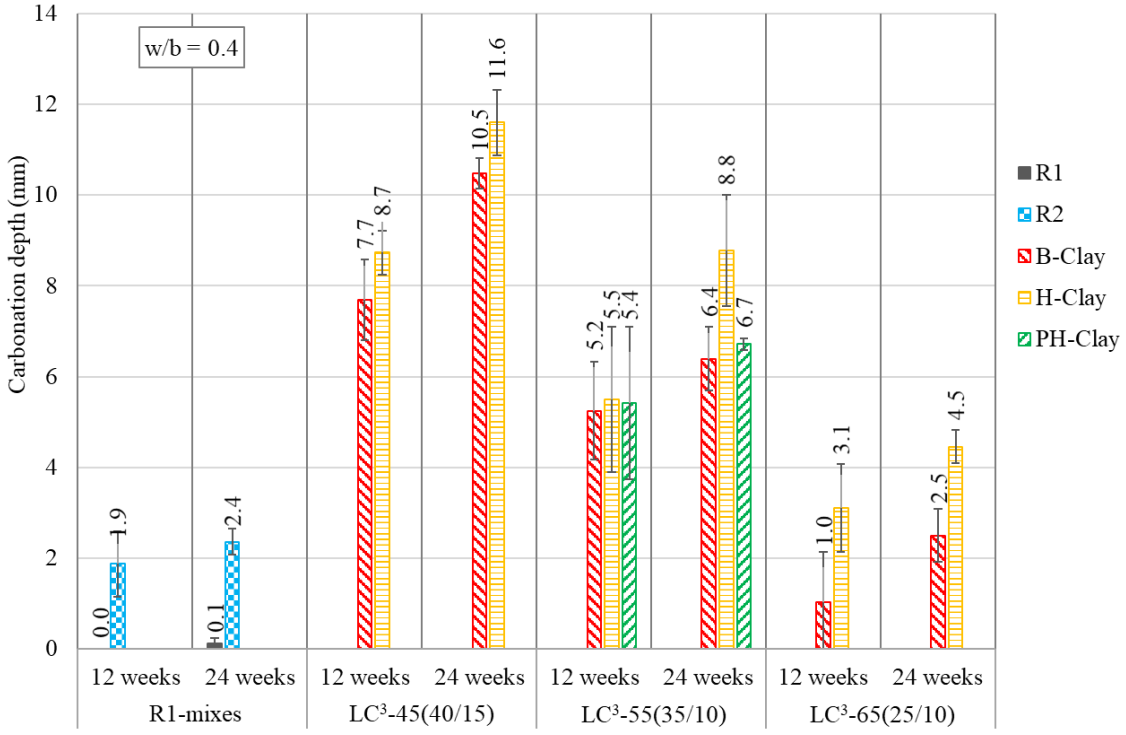

Figure 6.31: Carbonation depth measured after 12 and 24 weeks (w/b = 0.4)

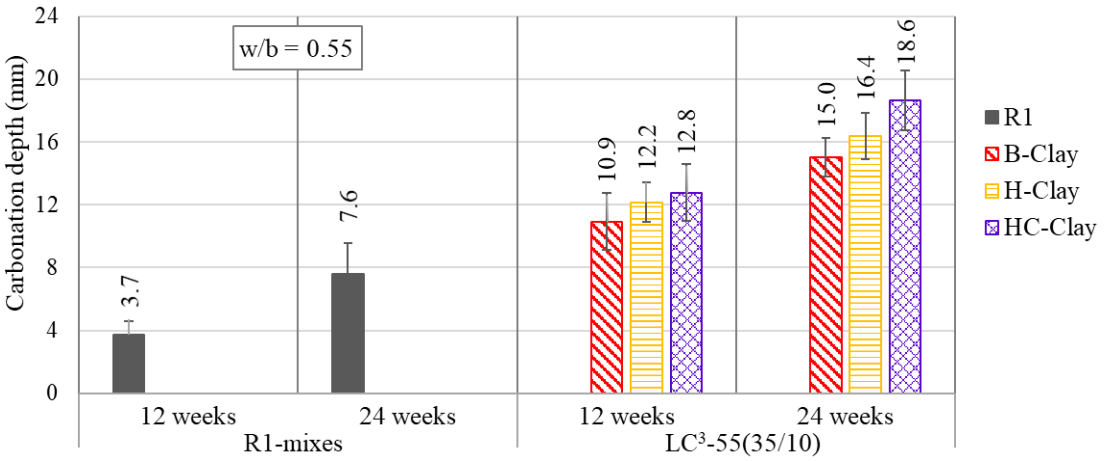

Figure 6.32: Carbonation depth measured after 12 and 24 weeks (w/b = 0.55)

Comparing the LC^3 mixes, results show that although the H-Clay has very high alkali content compared the other clays, the LC^3(H) mixes have low carbonation resistance compared to LC^3 mixes with the other clays. This low performance might be because of the high alkali content in the system which makes the microstructure more porous (Smaoui et al., 2005; Sant et al., 2012; Li, Afshinnia and Rangaraju, 2016) consequently less resistance to ingress of CO_2. In general, it important to note that although consumption of CH during the pozzolanic reaction decreases the quantity of carbonatable matter within the binder matrix, the reaction also reduces the capillary porosity and hence the ingress of CO_2 into the matrix.

6.12 Bulk diffusion test results

The test was carried out as per ASTM C 1556. The specimens were coated with epoxy so that only one face was exposed to a 2.8 M NaCl solution at 23°C and RH of 50% for 180 days. The estimation of chloride was done as per ASTM C1152 (2020) and presented as the percentage by total mass of binder. Figure 6.33 and Figure 6.34 show the chloride profiles of the concrete specimens with 0.4 w/b ratio, curve fitted, and experimental points joined by a straight line, respectively. Figure 6.35 and Figure 6.36 show profiles of specimens with 0.55 w/b ratio, curve fitted, and experimental points joined by a straight line, respectively. For clarity, the results of each individual mix are presented in Appendix VII.

It is important to note that with the approach of using slices and 180 days of exposure in the NaCl solution, it was not possible to curve-fit results of some of the mixes and obtain both surface chloride concentration (C_s) and diffusion coefficient (D_a) using Ficks's second law of diffusion, especially the LC^3 mixes with B-Clay and PH-Clay and reference mix R2, most likely because the mixes have very high resistance to chloride penetrability. In view of this, the C_s for these mixes was estimated by extending a straight line joining the first two "chloride content" points. With this point (0, C_s) and the rest of the "chloride content" points (making a total of seven points), it was possible to curve-fit the results of these mixes using Ficks's second law of diffusion. The estimated C_s and D_a-values for mixes with a w/b ratio of 0.4 are presented in Figure 6.37 and Figure 6.38, respectively. For mixes with a w/b ratio of 0.55, the C_s and D_a-values are presented in Figure 6.39 and Figure 6.40, respectively.

In general, in both cases, 0.4 (Figure 6.37) and 0.55 w/b ratios (Figure 6.39), results show that the LC^3 mixes, regardless of clinker content and type of clay, have lower C_s-values compared to those of the reference mixes. For example, in the case of 0.4 w/b ratio, the C_s-values of the LC^3 mixes are in range of 59% to 95% compared to that of the reference mix R1 and between 55% and 86% compared to that of the reference mix R2. In the case of 0.55 w/b ratio, the C_s-values of the LC^3 mixes are in the range of 57% and 77% compared to that of reference mix R1. In general, there is no clear relationship between the C_s-values (Figure 6.37 and Figure 6.39) and the WSI or OPI results presented in Section 6.10.1. However, results indicate that the C_s is the main driving force of chloride ions into the concrete, the higher the C_s, the faster the rate of chloride ion transport into the concrete (depending also on the diffusion coefficient). The trend is different in the case of reference mix R2 which could be because of high interaction between GGBS and water that needed more time for hydration (Song and Jennings, 1999; Richardson, 2000).

Similar to the results of CCI and electrical resistivity, in both cases, 0.4 (Figure 6.38) and 0.55 w/b ratio (Figure 6.40) results show that the LC^3 mixes, especially mixes with B-Clay (regardless of clinker content), PH-Clay, and HC-Clay, have lower D_a-values compared to those of the reference mixes. In the case of 0.4 w/b ratio, the D_a-values of the LC^3 mixes (except mixes with H-Clay) are in range of 19% to 26% compared to that of the reference mix R1 and between 68% and 89% compared to that of the reference mix R2. In the case of 0.55 w/b ratio, the D_a-values of the LC^3 mixes (including H-Clay) are in the range of 16% and 35% compared to that of the reference mix R1. In general, results indicate that the LC^3 mixes, regardless of clinker content and type of clay, have higher resistance to chloride diffusion compared to the reference mixes. Nguyen, Afroz and Castel (2020) and Sahamitmongkol, Khuon and Thitikavanont (2020) observed a similar performance of the LC^3 mix compared to a reference system with 100% PC. The increased penetration resistance is mainly related to a refinement in the pore structure due to pozzolanic reaction and formation of carboaluminate phases as well as the chloride-binding capacity of the LC^3 hydrates, especially C-A-S-H and AFM phases (Dhandapani and Santhanam, 2017; Avet and Scrivener, 2018; Dhandapani et al., 2018; Sui et al., 2019). The binding of chloride ions

in the LC^3 hydrates, especially carboaluminate phases and C-A-S-H, slows down the permeation of chloride ions in the concrete (Maraghechi et al., 2018).

Comparing the LC^3 mixes, results (Figure 6.38 and Figure 6.40) show that the LC^3(H), regardless of the clinker content, have higher D_a-values and therefore lower resistance to chloride penetration compared to the LC^3 mixes with other clays. This lower resistance might be because of the high alkali content coming from the H-Clay which makes the microstructure more porous (Smaoui et al., 2005; Sant et al., 2012; Li, Afshinnia and Rangaraju, 2016) consequently less resistant to ingress of chloride. This lower performance of the LC^3(H) mixes compared to the LC^3 mixes with other clays agrees well with the observation made from the results of all other tests discussed previously, especially CCI and electrical resistivity results. However, in the case of 0.55 w/b ratio, unlike in the case of 0.4 w/b ratio, although B-Clay has high amount of kaolinite compared to H-Clay and HC-Clay, the chloride content in the LC^3-55(B) from about 9 mm and 16 mm depth appears to be higher than in LC^3-55(HC) and LC^3-55(H), respectively. This was not expected and could be because of anomalies resulting from laboratory testing, especially LC^3-55(B).

Comparing LC^3 mixes with different clinker contents (Figure 6.33 or Figure 6.34), especially mixes with B-Clay and H-Clay, results suggest that the penetration resistance to chloride increases as the amount of clay increases in the mix, although there is little difference in the case of LC^3(B) and between LC^3-45(H) and LC^3-55(H). This trend suggests that the performance of the LC^3 system is strongly influenced by the amount of calcined clay in the mix.

Comparing the results of the two cases, 0.4 w/b ratio (Figure 6.34) and 0.55 w/b ratio (Figure 6.36), especially the LC^3-55 mixes with B-Clay and H-Clay and the reference mix R1, it is clear that the penetration resistance of chloride decreased with an increasing w/b ratio, as expected. For example, in the case of LC^3-55(B:35/10) and LC^3-55(H:35/10), the D_a-value increased from 0.48 x 10^{-12} m^2/s to 1.22 x 10^{-12} m^2/s (about 154% increase) and from 1.29 x 10^{-12} m^2/s to 2.41 x 10^{-12} m^2/s (about 86% increase) respectively, and for the reference mix R1, the increase is from 2.44 x 10^{-12} m^2/s to 7.06 x 10^{-12} m^2/s (about 189%). In general, results indicate that the performance of the LC^3 mixes is less affected by increasing w/b ratio compared to a reference mix with 100% cement.

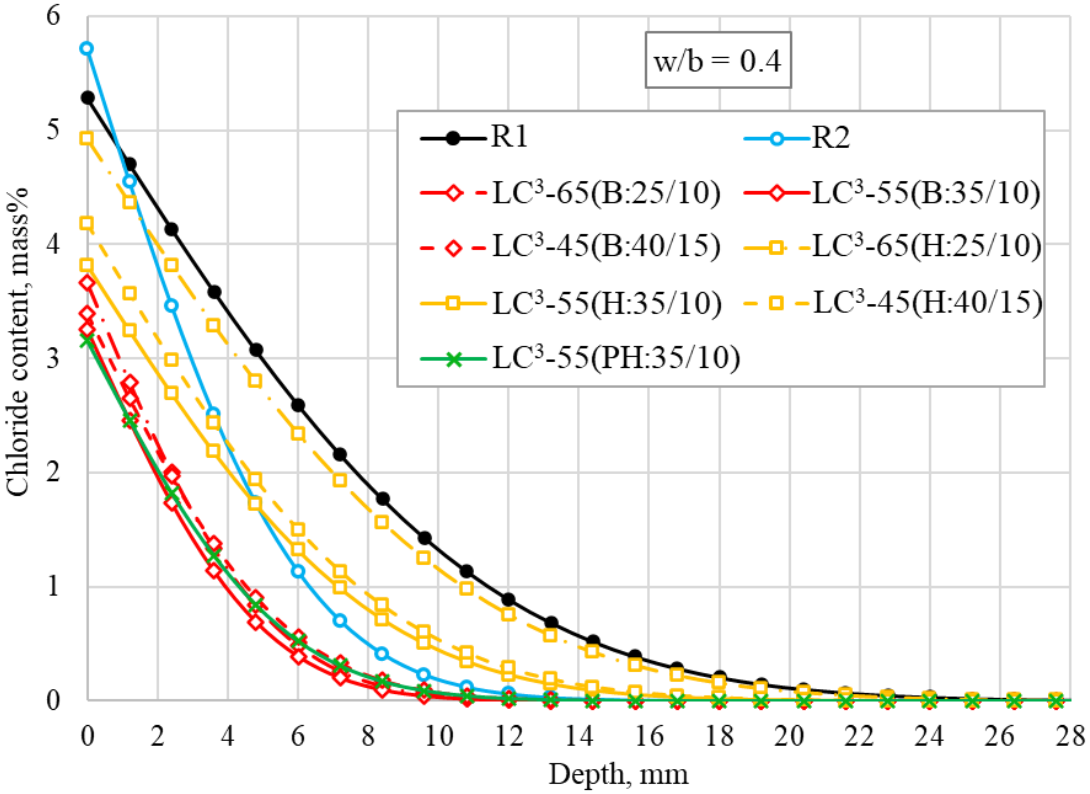

Figure 6.33: Chloride profile of the LC^3 mixes and reference mixes (w/b = 0.4) (Curve fitted, Fick's 2nd law)

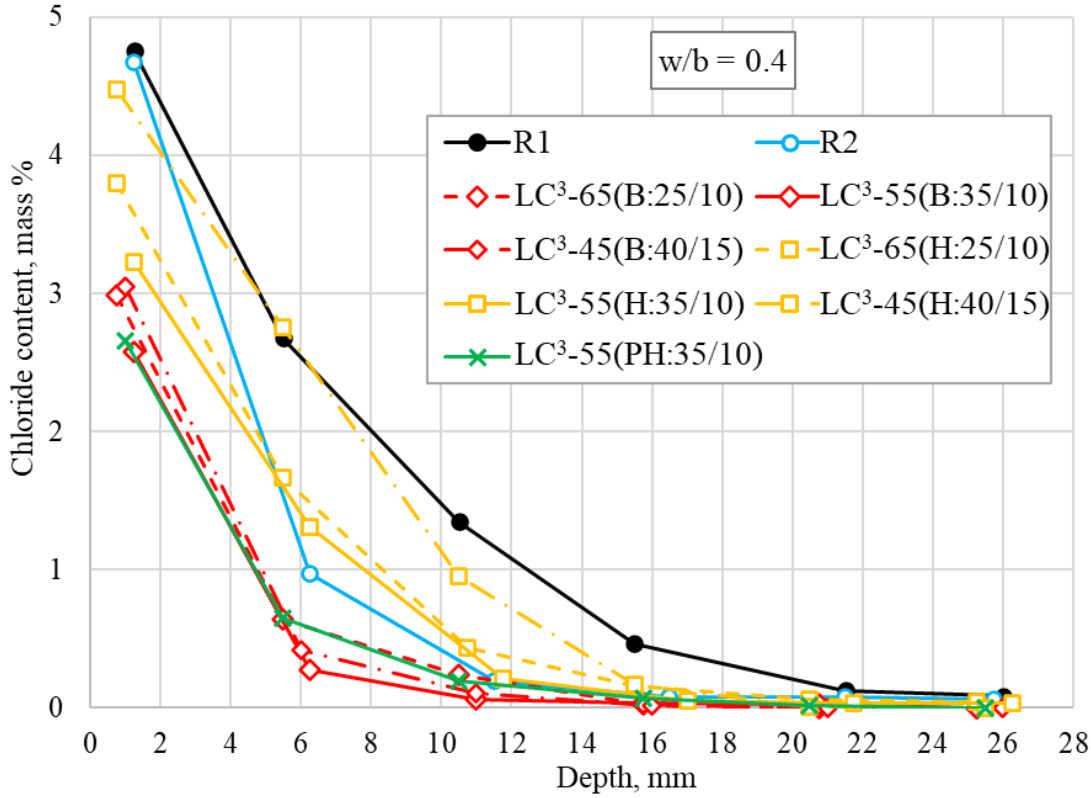

Figure 6.34: Chloride profile of the LC^3 mixes and reference mixes (w/b = 0.4) (Points joined by straight lines)

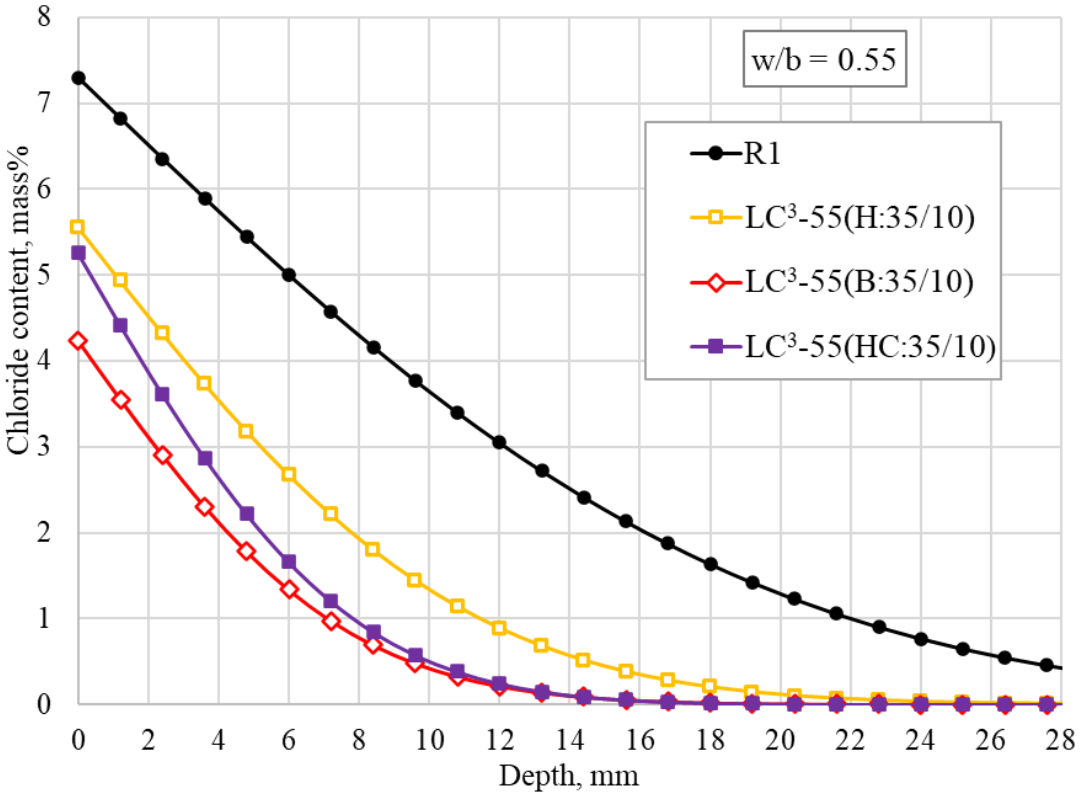

Figure 6.35: Chloride profile of the LC^3 mixes and reference mix R1 (w/b = 0.55) (Curve fitted, Fick's 2nd law)

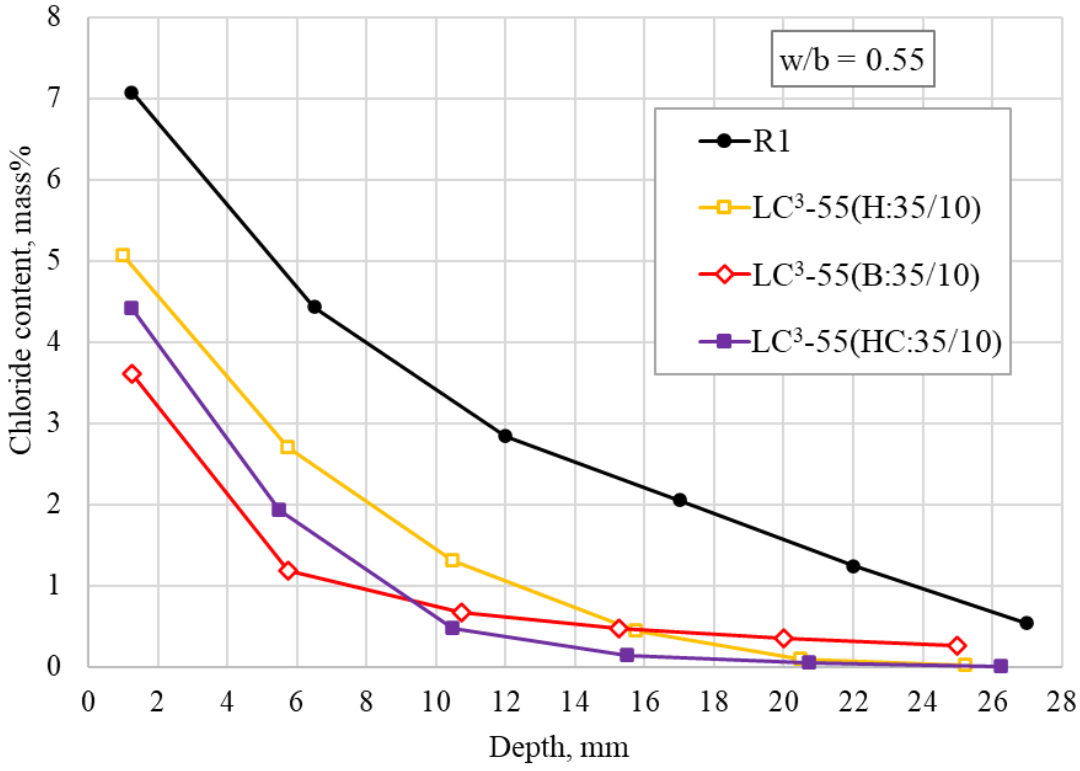

Figure 6.36: Chloride profile of the LC^3 mixes and reference mix R1 (w/b = 0.55) (Points joined by straight lines)

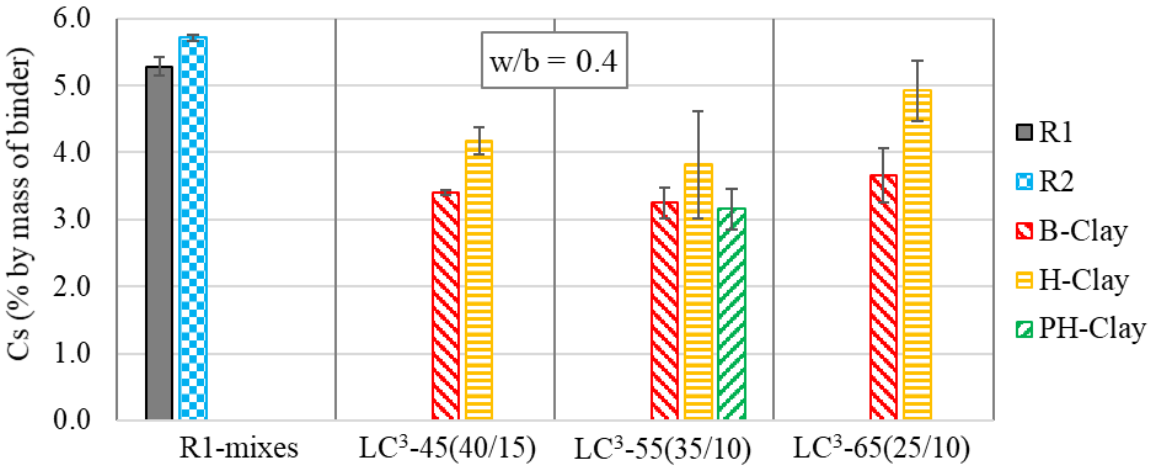

Figure 6.37: Estimated C_s-values for the LC^3 and reference mixes (w/b = 0.4)

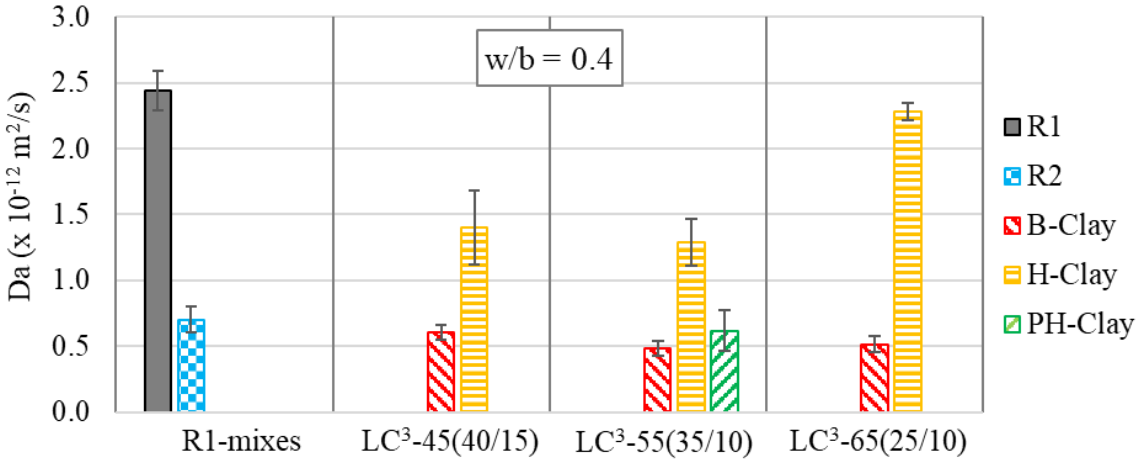

Figure 6.38: Estimated D_a-values for the LC^3 and reference mixes (w/b = 0.4)

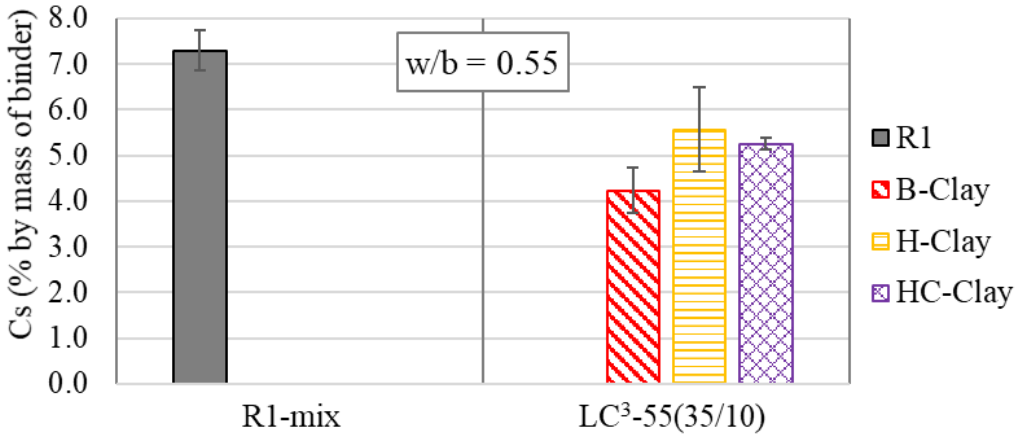

Figure 6.39: Estimated C_s-values for the LC^3 and reference mixes (w/b = 0.55)

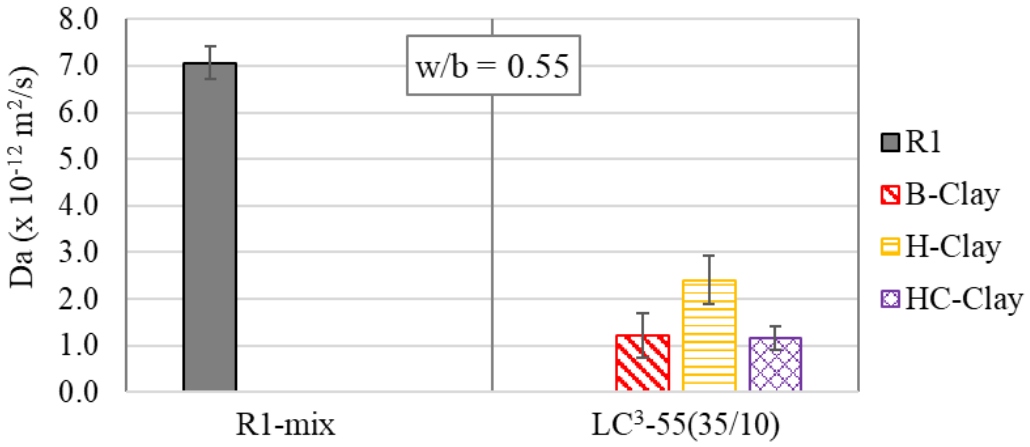

Figure 6.40: Estimated D_a-values for the LC^3 and reference mixes (w/b = 0.55)

6.13 Summary and general discussion

The chapter present results and discussion following testing for fresh and hardened properties of the selected LC^3 concrete mixes and reference mixes. Tests that were carried out included workability, free shrinkage, restrained shrinkage cracking, compressive strength development up to 90 days, durability index tests, resistivity measurements, bulk diffusion, and accelerated carbonation test.

Only four samples of clay were selected for the concrete work. Two samples from South Africa (abbreviated as B-Clay and H-Clay) and two samples from Tanzania (abbreviated as PH-Clay and HC-Clay). For B-Clay and H-Clay, three proportions of binder were considered, one is with 45% clinker, 40% CC and 15% LS, the second one is with 55% Clinker, 35% CC and 10% LS and the last one with 65% clinker, 25% CC and 10% LS. Due to limited amount of samples from Tanzania, the PH-Clay was considered only for LC^3-55 mix with w/b ratio of 0.4 and HC-Clay for LC^3-55 mix with 0.55 w/b ratio. Initially, the CCSA method coupled with the EMMA software were used to optimise proportions of all the concrete materials. The obtained proportions were then adjusted by carrying out trial mixes, and the target was to get a comparable workability with a slump of 100 ± 20 mm and a superplasticizer (Chryso@ Optima 175) dosage limit of 1.5%. However, with the HC-Clay, it was only possible to achieve a slump of 45 mm at a SP dosage of 2%. After several trials, the decision was to maintain the amount of water at 160 kg/m^3 and amount of stone at 1000 kg/m^3 for all the concrete mixes.

From the results, the following have been noted:

i) Results show that the early age gain of strength of the LC^3 mixes with 0.55 and 0.65 clinker factor, especially LC^3 mixes with B-Clay, PH-Clay, and HC-Clay, is similar or better than that of the reference mixes. This indicates that despite the higher clinker substitution rate of the LC^3 system, the binders react strongly during the first few days, thus overcoming the main problem of most binary mixes which is the slow gain of strength at early ages. As explained in Section 6.5.5, the slow strength gain of the LC^3(H) mixes (compared to LC^3 mixes with the other clays and the reference mix R1) is mainly because of high alkali content coming from the H-Clay, however, as can be seen from the results, the performance is similar or better than the reference mix R2.

ii) For LC^3(B), results show that from 3 days onwards there is almost no gain of strength moving from 0.55 to 0.65 clinker factor unlike LC^3(H) where the gain of strength also depends on the clinker factor. The main difference between the two clays is kaolinite and Na_2O_{eq} in the clays. B-Clay has about 70% kaolinite content and 0.48% Na_2O_{eq} whereas the New H-Clay has about 40% kaolinite content and 2.41% Na_2O_{eq}. This indicates that in this system the required minimum amount of clinker for best performance depends on the amount of CK in the clay. In other words, it can be said that there must be a certain amount of CK in this system where the amount of clinker above 55% is not really required for best performance.

iii) For elastic modulus, results show that the performance of the LC^3 mixes is similar to that of the reference mixes. Dhandapani et al. (2018), Avet, Sofia and Scrivener (2019), and Akindahunsi, Avet and Scrivener (2020) in their work also obtained similar elastic modulus values between the LC^3-50 system and concrete with different binder systems. This indicates that the LC^3 systems like other conventional systems, do not affect the elastic modulus of concrete.

iv) Results from the free shrinkage test show that all the LC^3 mixes with B-Clay, PH-Clay and HC-Clay perform better than the reference mixes R1 and R2. The poor performance of the LC^3(H) compared to all other mixes, especially at the early ages, is primarily because of high alkali content in the mix coming from the H-Clay. In general, it can be said that the LC^3 mixes produce lower shrinkage strain than a mix with 100% cement or a mix with 50% cement replaced by slag provided that the equivalent alkali in the system is 0.7%. The performance is mainly related

to the high ISA of the clays which absorb some of the available water in the system as a result the rate of loss of moisture in the paste is reduced.

v) The restrained ring test was carried out to assess and compare the potential of early age cracking of the selected LC^3 concrete mixes versus the reference mixes under restrained conditions. Results indicate that the LC^3 mixes perform better than a mix with 50% cement replaced by GGBS and generally similar to the reference mix with 100% cement provided that the equivalent alkali in the system is 0.7%.

vi) The resistivity test is done by measuring the resistance of concrete against the flow of current. In general, the test reflects how pores are interconnected in the concrete. Results show that the LC^3 specimens have very high resistivity values at all ages compared to the reference mixes. So, in this case it means that the LC^3 specimens have smaller pore network with less connectivity compared to the reference mixes which makes them less permeable (in terms of transfer of ions such as chloride ions or sulfite ions) than the reference mixes. Results also suggest that the performance of the LC^3 system is strongly influenced by the amount of calcined clay in the mix.

vii) The three DI tests i.e., OPI, WSI and CCI, and a porosity test were conducted to evaluate the resistance of LC^3 specimens to ingress of gases, liquid, and ions in contrast with the reference mixes with 100% cement and 50% cement replaced by GGBS. In general, results indicate that the LC^3 specimens, regardless of the clinker content, type of clay, and w/b ratio, are very dense, have high resistance to penetration of deleterious gases such as CO_2 and have excellent resistance to chloride ingress compared to the reference mixes. In general, a combination of the filler effect, pozzolanic reaction, formation of carboaluminate phases and stabilization of ettringite help in reducing porosity, pores connectivity and hence less penetration of gases, liquid, and chloride ions within the LC^3 matrix. The little difference between the results of the mixes with 0.4 and 0.55 w/b ratio is mainly related to the influence of curing. With limited curing, the results would be very much different (Gouws, Alexander and Maritz, 2001; Du Preez and Alexander, 2004; Surana, Pillai and Santhanam, 2017).

viii) The carbonation depths of the specimens were measured after 12 weeks and 24 weeks of exposure to 2% concentration of CO_2 in a chamber controlled at 20°C and 50% RH. In general, results indicate that the depth of carbonation depends largely on the amount of clinker present in the mix and the w/b ratio. The high

carbonation depths of the LC^3 specimens are due to low amount of CH in the system after being consumed by the pozzolanic reaction. However, this does not necessarily mean that the LC^3 specimens have poor carbonation resistance compared to the reference mixes especially when it comes to real environment. In addition, the OPI results indicate that the LC^3 specimens are dense and have high resistance to penetration of deleterious gases compared to the reference mixes. In this case, it important to note that although the pozzolanic reaction reduces the amount of CH within the binder matrix, the reaction also reduces the capillary porosity, pores connectivity and hence the ingress of CO_2 into the matrix.

ix) For chloride diffusivity, the results of both cases, 0.4 and 0.55 w/b ratio, indicate that the LC^3 mixes, regardless of clinker content and type of clay, have higher resistance to chloride diffusion compared to the reference mixes. The increased penetration resistance is mainly related to a refinement in the pore structure due to pozzolanic reaction and formation of carboaluminate phases as well as chloride-binding capacity of the LC^3 system (Dhandapani and Santhanam, 2017; Avet and Scrivener, 2018; Dhandapani et al., 2018; Sui et al., 2019). The binding of chloride ions in the LC^3 hydrates, especially carboaluminate phases and C-A-S-H, slows down the permeation of chloride ions in the concrete (Maraghechi et al., 2018). Comparing LC^3 mixes with different clinker content (Figure 6.34), especially mixes with B-Clay and H-Clay, results suggest that the penetration resistance of chloride increases as the amount of clay increases in the mix though there is little difference in the case of LC^3(B) and between LC^3-45(H) and LC^3-55(H). This trend suggests that the performance of the LC^3 system is strongly influenced by the amount of calcined clay in the mix. As expected, results also show that the penetration resistance of chloride in the concrete specimens decreases going from a w/b ratio of 0.4 to a w/b ratio of 0.55. However, comparing LC^3 and reference mix R1, results indicate that the performance of the LC^3 mixes is less affected by the increasing w/b ratio compared to a mix with 100% CEM II.

In general, there is good agreement between all the results obtained from all the tests carried out in this research work to assess the performance of the concrete mixes. Overall, it can be said that the LC^3 mixes perform similar or better than the reference mixes with 100% cement and with 50% cement replaced by GGBS. The results of the

LC^3 mixes indicate that apart from the filler effect and pozzolanic reaction, there is a strong synergistic chemical effect happening between the constituent materials. Both CK (from calcined clay) and $C\overline{C}$ (from LS) also react chemically during hydration and enhance the formation of carboaluminate phases which increase compressive strength and reduce porosity. On the other hand, as suggested in Section 5.5, the ISA of the clays also affects the performance of the system in two possible scenarios, one is by reducing the effective w/c ratio which in turn increase the compressive strength of the concrete and second is the high surface area (including the ISA) which increases the rate of chemical reaction, consequently porosity is reduced, and compressive strength is enhanced.

Chapter 7 General discussion, conclusions and recommendations

7.1 Introduction

The main objective of this research was to use a performance-based approach in the development of low-clinker LC^3 concrete relevant to the southern and east African contexts while reasonably maintaining the required properties of workability, compressive strength, and durability for structural and non-structural applications. Hence, the aim was to develop locally applicable knowledge for the practical implementation of LC^3 systems in the construction industry with a target of minimising cost and environmental impact of cement/concrete associated with the development of infrastructure which is anticipated to occur in Africa in the near future.

The first specific objective (i.e., summarise existing knowledge about the materials and performance of LC^3 systems) was achieved through a literature review and summarised in Chapter 2. Focus was given to previous studies done on kaolinite clays, performance of LC^3 systems, and why this system is of interest for the reduction of the CO_2 emissions, at the same time achieving concrete with good mechanical and durability properties.

To achieve the second specific objective (i.e., characterise the selected materials for chemical and mineralogical composition), the first task was to identify potential kaolinite clay deposits in South Africa and Tanzania and obtain samples of clays from the deposits. Based on the amount of clay at the deposit, the potential sources in South Africa are Bronkhorstspruit, Grahamstown, and Hopefield deposits. In Tanzania, the potentials are Pugu, Matamba, and Malangali deposits. However, for Tanzania, it was only possible to obtain samples from the Pugu deposit and from HeidelbelgCement plant area in Dar es Salaam. The next task was to check the suitability of these clays and their optimal calcination temperature. This involved XRF, TGA, XRD analysis and reactivity test.

To achieve the third specific objective (i.e., optimising system chemistry and mineralogy to achieve synergistic effects with all constituents, for the selected sources of clays from the two countries), the so-called mixture design 3-factors approach described in Section 3.6 was used. Mixes with clinker content between 40% and 70%

were selected. The target was to obtain the optimum proportions of LC^3 binder with low clinker content. The compressive strength of mortar with a w/b ratio of 0.4 was used as the performance parameter for optimisation. Two reference mixes were considered, one with 100% CEM II/A-L 52.5 N, and a recommended mix for South African marine environments with 50% cement replaced by GGBS. Further, the HoH curves of the optimum LC^3 proportion and two other selected proportions with different CC, their intensities and positions of the hydration peaks were studied and compared between themselves and with the reference mixes.

To achieve the fourth specific objective (i.e., optimising proportions of concrete materials to further reduce powder content in the concrete), the CCSA method coupled with MAAM (using the EMMA software) were used as a starting step in obtaining proportions of concrete materials. In this case, the quantity of the materials was adjusted while maintaining the selected proportions of binders and w/b ratio. To reduce powder content, the target was to have a mix with water content as low as possible. In this case, mix trials were made with different amount of water (at an interval of 5 kg/m^3 starting from 125 kg/m^3) while maintaining the selected proportions of binders and w/b ratio. The targeted slump and SP (Chryso@ Optima 175) dosage limits were 100 ± 20 mm and 1.5%, respectively. After several trials, it was decided to maintain the amount of water at 160 kg/m^3 and amount of stone at 1000 kg/m^3 for all the concrete mixes. However, with the HC-Clay, it was only possible to achieve a slump of 45 mm at a SP dosage of 2%.

To achieve the fifth specific objective (i.e., assessing the performance of the selected low-clinker LC^3 mixes, including but not exclusively, in comparison with the recommended concrete mixes for marine concrete structures in South Africa), the performance of the LC^3 mixes with different clays was compared between the LC^3 mixes themselves and with the reference mixes. In this case, using the optimum LC^3 proportion obtained from the optimisation work, and the two selected proportions, concrete mixes were optimised and prepared to determine their fresh and hardened properties. Tests that were carried out included workability, compressive strength, elastic modulus, free shrinkage, restrained ring shrinkage, durability indexes, resistivity, bulk diffusion, and accelerated carbonation.

Based on the results obtained, the following sections provide the general discussion, conclusions, and recommendations.

7.2 General discussion

The most promising current strategy for lowering costs and environmental impact of cement entails the partial substitution of PC clinker by the combined addition of CC and LS. In general, the increase of compressive strength and resistance to ingress of aggressive substances of this LC^3 system are linked to the porosity refinement produced by the pozzolanic reaction, formation of carboaluminate phases, and stabilization of ettringite. However, improper use of the constituent materials may result in concrete with inferior strength and durability properties compared with a conventional concrete. Therefore, it is important to understand the way in which these materials can be blended to achieve the required strength and durability performance. In this research, the performance of LC^3 mixes with kaolinite clays from selected deposits in east and southern Africa was optimised based on the compressive strength of mortars. LC^3 mixes with clinker levels in the range of 40% to 70% were selected using the mixture design 3-factors approach.

The selection of the clays was generally based on the amount of kaolinite, estimated using TGA and XRD. Literature suggests a clay with at least 40% kaolinite content is needed for producing LC^3 binders (Alujas et al., 2015; Avet et al., 2016; Avet, 2017; Maraghechi et al., 2018). However, apart from the kaolinite content, the selected clays also have different amount of other minerals, specifically illite and quartz, different ISAs, and different Na_2O_{eq}, which also influence the performance of the clay. In addition, a slight increase of particle sizes was consistently noted for all the clays, based on the results of the PSD analysis, before and after calcination. The increase of particle sizes was mainly due to the agglomeration of particles, supported by the SEM images and BET surface areas of the clays (except PH-Clay). However, results indicate that the clays have different degree of agglomeration. Moreover, although PSD results indicate a large change in the PSD values of the PH-Clay compared to other clays, the BET surface area of this clay remained the same after calcination. In general, the results indicate that these clays are not generally the same and kaolinite content might not be the only factor to consider when assessing the suitability level of these clays for

producing LC^3 binders for different applications. For example, although HC-Clay has about 40% kaolinite content, its ISA is very high as reflected by its BET surface area (37 m^2/g), as a result of which the LC^3 mix with HC-Clay demanded higher amounts of water or high dosage of SP which is not practical for most structural applications where satisfactory workability and setting time is usually required to produce high quality concrete. However, the mix can be used in situations where a low workability mix is required, and compaction can be done by mechanical means, such as in precast and factory applications. Or possible roller-compacted concrete.

The aim of the optimisation work was to obtain the optimum LC^3 proportion with the lowest clinker content. In general, the results obtained suggest that, for optimum performance, regardless of the compressive strength values obtained for each of the LC^3 mix with different CC, the lowest practical clinker content is 55% at which the CC content is 35% and the LS content is 10% abbreviated as LC^3-55(35/10). In the literature, the majority of researchers report the compressive strength performance of an LC^3-50 (i.e., LC^3 mix with 50% clinker and CC/LS ratio of 2:1 by mass) which was first reported in 2012 after a study done on mortars with clinker content fixed at 50% and with CC and LS purity greater than 95% (Antoni et al., 2012). However, the CC-LS-Clinker ternary plots presented in Figure 5.14 to Figure 5.17 show that, up to about 24 hours, the performance of the LC^3 system is mainly contributed by the hydration of clinker phases, whereas from about 3 days the system needs more CC than LS which suggests that the main contribution comes from the pozzolanic reaction. Regarding LS, results presented in Table 5.9 and XRD curves in Figure 5.23 indicate that approximately 50% of the $C\overline{C}$ remains unreacted in the system at 90 days, which implies that the purity of LS may not be the dominant factor in the performance of the LC^3 system. However, with quarry-grade LS, only part of LS is reactive as pure LS, which bring doubt if the $C\overline{C}$ component will react to form carboaluminate phases in the same way as in the case of pure LS. Further, in a study by Avet and Scrivener (2018) on the LC^3-50 pastes with different amount of CK in the CC show that the amount of carboaluminate phases increases with increasing amount of CK only up to 65%. Above 65%, the excess alumina coming from the CC forms C-A-S-H, which suggest that the relative amount of C-A-S-H and carboaluminate phases in the LC^3 system depends on the purity of LS and CC. On the other hand, the reactivity of both CC and LS depends

on the availability of CH in the system (Krishnan, Dhoopadahalli and Bishnoi, 2020). Further, some studies (Avet et al., 2016; Krishnan, Dhoopadahalli and Bishnoi, 2020; Cardinaud et al., 2021; Dixit, Du and Pang, 2021) show that the hydration of clinker phases, particularly C_2S, is reduced when CC with high CK is used. This means that the optimum proportion of any LC^3 system also depends on the reactivity/composition of the clinker (Krishnan and Bishnoi, 2020). In view of all this, it means that, apart from the ISA of the clay and proper adjustment of SO_3 and Na_2O_{eq} in the system, the optimum performance of any LC^3 system will depend on the clinker composition and/or available amount of CH from hydration of cement, amount of $C\overline{C}$ from LS, and amount of CK from CC for pozzolanic reaction and formation of carboaluminate phases. A balance of all these factors is what will make one system better than the other. In this case, with the LC^3-55(35/10) system, it is most likely that at any time the system has sufficient CH to react with the available CK and $C\overline{C}$. However, from an economic point of view, a system with low amount of clinker and more amount of LS would be preferred, but it will also depend on the required performance of the mix.

On the knowledge that high compressive strength does not necessarily mean durable concrete (Alexander, 2021), two other mixes were also selected together with LC^3-55 (35/10) for the concrete work: LC^3-45(40/15) and LC^3-65(25/10). In general, all results indicate that LC^3 mixes, especially all the LC^3-65 and LC^3-55 with B-Clay and PH-Clay, perform similarly or better than the reference mixes. Although the compressive strength performance of the LC^3-55(H:35/10) and all the LC^3-45(40/15) mixes is lower compared to the reference mixes (largely due low amount of clinker in the system), their durability performance is similar or better than the reference mixes. In general, the performance of the LC^3 mixes is enhanced by the filler effect of the SCMs (i.e., CC and LS) and the strong synergistic chemical effect (i.e., pozzolanic reaction, formation of carboaluminate phases, and stabilisation of ettringite) occurring between the constituent materials which reduce porosity and interconnectivity of pores. On the other hand, as indicated previously, the ISA of the clay also influences the performance of the system in two possible ways: one by reducing the effective w/c ratio which in turn enhances the performance of the concrete, and the other the high surface area (including the ISA) which increases the rate of chemical reaction; consequently, porosity is reduced, and performance is enhanced. The relatively poorer performance of the LC^3 mixes with H-

Clay and HC-Clay compared to the reference mixes and LC^3 mixes with B-Clay and PH-Clay is related to the low amount of kaolinite, which is about 40% compared to about 50% and 65% for the PH-Clay and B-Clay, respectively. Nevertheless, the low performance of the LC^3 mixes with H-Clay is further linked to the low ISA of the H-Clay and the high alkali content associated with this clay, resulting in a porous microstructure and low strength of C-S-H gel developing in high alkali condition.

7.3 Conclusions

Based on the results obtained, the following sections provide the conclusions, both specific and general.

7.3.1 Suitability of the selected clays for producing LC^3 binders

The suitability of the six samples of clay from the selected deposits in South Africa and Tanzania were assessed based on results obtained by XRF, TGA and XRD. All selected clays were composed mainly of quartz, illite and kaolinite. The scope of this research was limited to two sources from each country. The selection was mainly based on the amount of kaolinite in the clays. Based on the literature, a suitable clay for producing LC^3 binders is the one with at least 40% kaolinite content (Alujas et al., 2015; Avet et al., 2016; Avet, 2017; Maraghechi et al., 2018).

In general, there is good agreement between XRF, XRD and TGA results. As summarised in Table 4.3, B-Clay has about 65% kaolinite, PH-Clay about 50% kaolinite and H-Clay, PS-Clay, and HC-Clay about 40% kaolinite. Based on these results, only B-Clay and H-Clay from South Africa and PH-Clay and HC-Clay from Tanzania were selected for the concrete work.

The selected clays have different ISAs and Na_2O_{eq}. As summarised in Table 3.3, the BET surface area of the B-Clay, H-Clay, PH-Clay, and HC-Clay before calcination were 12.6, 5.4, 14.4 and 45 m^2/g, respectively. The Na_2O_{eq} of the H-Clay is very high (2.88%) whereas this parameter is 0.48%, 0.32%, and 0.6% for B-Clay, PH-Clay, and HC-Clay, respectively.

The optimum calcination temperature of each clay was also investigated using the R^3 bound water method. Results indicate that all samples of clays have high amount of

bound water when calcined at 800°C. In view of this, it can be concluded that all the selected clays are more reactive when calcined at 800°C.

7.3.2 Optimisation of LC^3 binders

As described previously, the so-called mixture design 3-factors approach was used to get the optimum proportion of LC^3 binders. The target was to obtain an optimum proportion with the lowest practical clinker content. The three lowest boundaries for the different constituents were 40% clinker content, 20% CC, and 10% LS, and the upper boundaries were 70% clinker, 50% CC, and 40% LS. The compressive strength of mortar with a w/b ratio of 0.4 was used as the performance parameter for optimization.

Two reference mixes were considered, one with 100% CEM II/A-L 52.5 N, and a recommended mix for South African marine environment with 50% cement replaced by GGBS. Based on the results obtained (presented in Section 5.2), it can be concluded that for optimum performance, regardless of the difference in the compressive strength values obtained for each of the LC^3 mortars with different CC, the lowest practical clinker content with these materials was 55% at which the CC content is 35% and the LS content is 10%. However, if the mix performance requirements were adjusted, then it would be possible to use even lower clinker factors in practical mixes.

On the knowledge that high compressive strength does not necessarily mean concrete of high durability, two other LC^3 proportions were also considered for the concrete work by increasing and reducing clinker content by 10%: one with 65% clinker, 25% CC and 10% LS, and the other with 45% clinker, 40% CC and 15% LS.

7.3.3 Hydration products of the selected LC^3 mixes (done on cement paste)

The hydration products at different ages (1, 3, 7, 28 and 90 days) of the LC^3-55(35/10) mixes with different CC were characterised using XRD and TGA. XRD was used to identify phases appearing at each age and TGA was specifically used to quantify unreacted CH, $C\overline{C}$, and bound water at each age.

In general, all mixes (including the reference mix with 100% CEM II) show the presence of CH, and $C\overline{C}$, and no formation of stratlingite and monosulfoaluminate; instead ettringite is stabilised at all ages.

The amount of both CH and $C\overline{C}$ phases were observed to decrease with age indicating progress of both the pozzolanic reaction and formation of carboaluminate phases. In general, the hemicarboaluminate phase appeared from 3 days and monocarboaluminate phases from 7 days. The formation of these phases in the system helps to reduce porosity and pore connectivity, thus enhancing compressive strength and durability performance.

Results also indicate that a large portion (> 50%) of the $C\overline{C}$ remains unreacted in the system even at 90 days. In general, based on the results obtained, it can be inferred that a LS with about 50% purity should be sufficient to give full performance of the LC^3 system with 55% clinker, 35% CC and 10% LS.

7.3.4 Mechanical performance of the selected LC^3 concrete mixes

The mechanical properties of selected LC^3 concretes assessed in this research were compressive strength, elastic modulus, free shrinkage, and restrained shrinkage.

The compressive strength results indicate that the performance of the LC^3 mixes with B-Clay and PH-Clay, specifically LC^3-55(B:35/10), LC^3-55(PH:35/10), and LC^3-65(B:25/10), is similar to the reference mix R1 but better than the reference mix R2, especially when considering the early age strength gain. The performance of the LC^3-65(H:25/10) is slightly lower than the reference mix R1 but similar or better compared to reference mix R2. In general, it can be concluded that the performance of the LC^3-55 with B-Clay and PH-Clay and the LC^3-65, regardless of the type of clay, perform similarly or better than the reference mixes. The performance of the LC^3-55(H:35/10), LC^3-45, regardless of the type of clay, is lower than the reference mixes.

For the elastic modulus, results indicate that the LC^3 mixes have values very similar to the reference mixes. This indicates that the LC^3 systems, like other conventional systems, minimally affect the elastic modulus of concrete. In general, it can be concluded that the elastic modulus performance of the LC^3 concrete, regardless of the clinker content and type of clay, is similar to that of the reference mixes.

Based on the results of the free shrinkage test, it can be concluded that the LC^3 mixes with B-Clay, PH-Clay, and HC-Clay have lower shrinkage strain than the reference mixes, in a long-term test. The LC^3 mixes with H-Clay (regardless of the clinker

content) have higher shrinkage strain compared to the LC^3 mixes with other clays (an increase of > 50% from 7 days), similar or slightly lower/higher compared to the reference mix R1, and generally higher compared to the reference mix R2.

The earlier appearance of the first crack on the concrete ring specimens agrees well with the results of free shrinkage. In general, based on the results of the restrained ring shrinkage test, it can be concluded that the potential of early age cracking of the LC^3-55(B:35/10) is marginally higher than the reference mix R1 but lower than the reference mix R2 whereas for the LC^3-55(H:35/10), the potential is higher than the two reference mixes.

7.3.5 Durability performance of the selected LC^3 concrete mixes

The durability performance of the selected LC^3 concrete was assessed by carrying out electrical resistivity, durability index, accelerated carbonation, and bulk diffusion tests. In general, all the LC^3 mixes, regardless of the clinker content and type of clay, perform similarly or better than the reference mixes.

The resistivity test results showed that the LC^3 mixes, especially mixes with B-Clay, PH-Clay, and HC-Clay, have very higher resistivity values at all ages compared to the reference mixes. The LC^3 mixes with H-Clay have lower values compared to the mixes with other clays, but higher than the reference mix R1 and similar to the reference mix R2, especially LC^3-55(H:35/10) and LC^3-65(H:25/10). In general, it can be concluded that all the LC^3 mixes with B-Clay, PH-Clay and HC-Clay are less penetrable (in terms of transfer of ions such as chloride ions or sulphate ions) than the reference mixes. The LC^3-55(H:35/10) and LC^3-65(H:25/10) show similar performance compared to the reference mix R2.

The results of the DI tests (i.e., OPI, WSI and CCI) and a porosity test showed that the LC^3 mixes, regardless of the clinker content and type of clay, have OP1 values greater than 10 (log scale), similar or higher than the reference mixes, WSI values less than 10 mm/√h, similar to the reference mixes, porosity less than 10%, similar or less than the references mixes, and CCI values less than 0.75 mS/cm, less or similar than the reference mixes. In general, it can be concluded that the LC^3 specimens, regardless of the clinker content, type of clay, and w/b ratio, are very dense, have high resistance to

penetration of deleterious gases such as CO_2, and have excellent resistance to chloride ingress compared to the reference mixes.

For chloride diffusivity, results show that the samples of the LC^3 mixes with B-Clay, PH-Clay, and HC-Clay obtained at different depth of the concrete specimens have low chloride content (% by mass of binder) compared to samples of the reference mixes obtained from the same depths. The samples obtained from LC^3-45 and LC^3-55 with H-Clay have chloride contents similar to the reference mix R2 but lower than the reference mix R1 at the same depth. The LC^3-65(H:25/10) samples have chloride content slightly lower than the reference mix R1 at the same depth. In general, it can be concluded that the LC^3 mixes with B-Clay (regardless of clinker content), PH-Clay and HC-Clay have higher resistance to chloride diffusion compared to the reference mixes. The LC^3-45(H:40/15) and LC^3-55(H:35/10) outperform the reference mix R1 but similar to reference mix R2. The LC^3-65(H:25/10) performs marginally better than the reference mix R1.

The carbonation resistance of the concrete specimens was assessed using the accelerated carbonation test. Results show that the LC^3 mixes have higher carbonation depth compared to the reference mixes at the tested ages. In general, it can be concluded that the LC^3 mixes have significantly lower carbonation resistance than the reference mixes. The lower the amount of clinker in the concrete, the less the carbonation resistance.

7.3.6 General conclusions

All clays selected have kaolinite content of 40% and above but with different ISAs and Na_2O_{eq}. In general, based on the results and observations made in this research it can be concluded that apart from kaolinite content, other minerals present in the clay, the filler effect, pozzolanic reaction, formation of carboaluminate phases, and stabilisation of ettringite phase, the ISA of the clay and the amount of alkalis present in the clay also influence the performance of the system.

The LC^3 system requires adjustment of sulphate and alkali contents. Based on the literature (Zunino and Scrivener, 2019, 2020a), SO_3 content is adjusted due to the filler effect of the SCMs. In this research, adjustment was done by ensuring that the aluminate

reaction peak occurred shortly after the silicate reaction peak, at between 13 and 18 hours. As indicated in Section 5.2.1.2, the LC^3(HC) and LC^3(PH) demanded 2.0% SO_3, and the LC^3(B) and LC^3(H) demanded 1.8% SO_3 and 1.2% SO_3, respectively. Alkali content was adjusted so as to eliminate this variable as much as possible, and also to increase early age strength. Literature suggests Na_2O_{eq} between 0.6 and 0.8% (Antoni, 2013), thus 0.7% was selected. However, it was not possible to adjust the Na_2O_{eq} for the LC^3(H) mixes as the alkalis in the H-Clay were already high (2.88% Na_2O_{eq}). As shown in Table 6.3, the LC^3-65(H:25/10), LC^3-55(H:35/10), and LC^3-45(H:40/15) contained already 0.9%, 1.16%, and 1.28% Na_2O_{eq}, respectively, without adding NaOH. In this case, it is important to note that, apart from the kaolinite content, the main difference between the selected clays is the ISA and the Na_2O_{eq}. Comparing LC^3 mixes with HC-Clay, PH-Clay, and B-Clay, although the clays have difference ISAs, the SO_3 demand is almost similar. In view of this, it can be concluded that the demand of SO_3 in the system is less influenced by the ISA of the clay but is rather sensitive to the amount of Na_2O_{eq} in the system.

In this research, to ensure comparable workability, SP (Chryso® optima 175) was added in all the concrete mixes to achieve a target slump of 100 ± 20 mm. The dosage limit was 1.5% of the total mass of binder. However, with the LC^3-55(HC:35/10), it was only possible to achieve a slump of 45 mm at SP dosage of 2%. As shown in Table 6.3, for the LC^3-55(PH:35/10), the slump obtained was 90 mm at SP dosage of 1.5%, for the LC^3-55(B:35/10), the slump was 100 mm at a SP dosage of 1.2%, and for the LC^3-55(H:35/110), the slump was 105 mm at a SP dosage of 1.2%. In this case, the LC^3-55(HC:35/10) with HC-Clay, which has the highest ISA (37 m^2/g), demanded a high dosage of SP, followed by the LC^3 mix with PH-Clay (14.5 m^2/g) and B-Clay (11.1 m^2/g), then the LC^3 mix with H-Clay which has the lowest ISA (4.6 m^2/g). In general, it can be concluded that, for the LC^3 mixes, the demand of SP dosage also depends on the ISA of the clay.

Globally, the trend is to reduce the clinker factor to 0.6 or less without adversely affecting the performance of the system (Scrivener, John and Gartner, 2018; WBCSD and IEA, 2018). In this research, optimisation results indicated that for optimum performance of concrete made with the tested African raw materials, regardless of the

type of CC, the lowest practical clinker content was 55% at which the CC content is 35% and the LS content is 10%. However, since high compressive strength does not necessarily relate to excellent durability, two other LC^3 proportions were also considered for the concrete work: one with a slightly higher clinker content (i.e., 65% clinker, 25% CC and 10% LS), and the other with a slightly lower clinker content (i.e., 45% clinker, 40% CC and 15% LS). In general, there is good agreement between all the results obtained from all the tests carried out in this research work to assess the mechanical and durability performance of the LC^3 mixes. Overall, it can be concluded that the LC^3 mixes perform similarly or better than the reference mixes with 100% CEM II/A-L 52.5 N and with 50% cement replaced by GGBS. In addition, it can be concluded that the LC^3 system is the promising option for lowering costs and environmental impact of cement, especially in Africa where the availability of the well-known SCMs such as fly ash and GGBS is limited or non-available.

The results of compressive strength also show that the early-age gain of strength of the LC^3-55(35/10), especially with B-Clay and PH-Clay, and the LC^3-65(B:25/10) is similar or better than the reference mix R1, and generally better than the reference mix R2. In this case, it can be concluded that the LC^3 systems react strongly during the first few days compared to most binary mixes where the main problem is the slow gain of strength at the early ages which usually restricts the effective application of these systems in construction.

The lower performance of the LC^3 mixes with H-Clay and HC-Clay compared to the reference mixes and LC^3 mixes with B-Clay and PH-Clay is related to the lower amount of kaolinite, which was about 40% compared to about 50% and 65% for the PH-Clay and B-Clay, respectively. However, H-Clay has also the lowest ISA (4.6 m^2/g) compared to 11.1 m^2/g for B-Clay, 14.5 m^2/g for PH-Clay, and 37 m^2/g for HC-Clay after calcination and the highest Na_2O_{eq} (2.88%) compared to 0.48% for B-Clay, 0.32% for PH-Clay, and 0.6% for HC-Clay. In this case, it can be concluded that the general low performance of the LC^3 mixes with H-Clay compared to all other mixes is due to the low ISA of the H-Clay and high alkali content coming from the H-Clay.

7.4 Recommendations for further research

7.4.1 The BET surface area of the PH-Clay

Grinding of cementitious materials increases the specific surface area and thus reactivity. In this research grinding was done before calcination with a target of achieving $d_{50} < 10$ μm and $d_{90} < 30$ μm. However, after calcination, a slight increase of particle sizes (due to agglomeration of particles) was consistently noted for all the clays. The results also agree well with the BET surface areas of the clays, except PH-Clay. With the PH-Clay, although PSD results indicate a large change in the PSD values compared to other clays, the BET surface area of this clay remained the same after calcination. In view of this, further work for a deeper understanding on the behaviour of this clay is recommended.

7.4.2 Test for assessing the reactivity of SCMs

Recently, the so called ''R^3 method" has been developed for assessing pozzolanic reactivity of SCMs (Avet et al., 2016). This test, in comparison with other tests, has been observed to have a very good correlation to a reference 28-day relative strength of standard mortar (Li et al., 2018; Parashar and Bishnoi, 2020). In view of this, this test was used to evaluate the reactivity of the selected clays calcined at different temperatures. The aim was to find the optimum calcination temperature of the clays. However, the test needs 7 days to obtain results as the test is accelerated by continuously heating the R^3 paste at 40°C either in isothermal calorimetry (for measuring cumulative heat release at 7 days) or in the oven (for determination of bound water at 7 days). Considering the fact that most of the research or industry work is carried out within a limited time, the 7 days is considered a long period. In view of this, further work, or improvement of this method on how to quickly evaluate the reactivity of the SCMs is recommended.

7.4.3 Kaolinite clays are not the same, each source should be examined

All the selected clays in this research were composed mainly of kaolinite, quartz, and illite. However, literature suggest that a suitable clay for the LC^3 system is the one with kaolinite content of at least 40%, and that secondary minerals have less influence on the reactivity of the clay (Alujas et al., 2015; Avet et al., 2016; Avet, 2017; Maraghechi et al., 2018). In general, based on the results and observations made in this research, it can be concluded that apart from kaolinite content, the ISA of the clay also influences

the performance of the clay. In view of this, it is clear that these clays are not the same universally, and it is recommended that the suitability of each source of kaolinite clay and the influence of the secondary minerals on the performance of the clay be examined.

7.4.4 Reduction of powder content in concrete

It is also important to note that in this research the CCSA method coupled with MAAM (using the EMMA software) were used as a starting step in obtaining proportions of concrete materials. With the EMMA software, it was only possible to adjust the quantity of the materials (while maintaining the selected proportions of binders and w/b ratio) to better fit the modified Andreassen curve. The PSD of each material, maximum and minimum particle size remained fixed in the mixture as the materials were used as received from the suppliers/after grinding. In view of this, more work in attempting to further reduce powder content in practical systems is recommended.

7.4.5 Mechanism behind the ISA of the clay and the strength gain of the system

In general, the results obtained, and observations made from all the tests carried out in this research (especially compressive strength, shrinkage, HoH, and results from XRD and TGA analysis) are also linked to the ISAs of the clays. For example, the XRD scans (Figure 5.23) show that the LC^3-55(PH:35/10) and LC^3-55(HC:35/10) have noticeable hemicarboaluminate peaks from 1 day whereas the reference R1, LC^3-55(B:35/10), and (LC^3-55(H:35/10) show visible hemicarboaluminate peaks from 3 days. In addition, a study by Antoni et al. (2012) showed formation of hemicarboaluminate from 1 day whereas another study conducted by Avet and Scrivener (2018) showed no formation of hemicarboaluminate at 1 day. As shown in Equations 2.7 and 2.9, the formation of hemicarboaluminate also depends on the availability of water and CH in the system. In view of this, it has been suggested that since HC-Clay and PH-Clay have high ISAs compared to B-Clay and H-Clay, the performance of the system is affected in two possible ways: one is reducing the effective water to cement (w/c) ratio which in turn affects the availability of water and/or CH in the system to react with $C\overline{C}$ and aluminates, consequently enhancing the early age strength gain of the system; and the second is the high surface area (including the ISA) which increases the rate of chemical

reaction, consequently increasing the strength gain of the system. However, further research is recommended to fully understand the mechanisms.

7.4.6 The ISA of the clay and shrinkage performance of the system

The results of the free shrinkage test indicate that the LC^3 mixes (regardless of the clinker content), especially mixes with B-Clay, PH-Clay, and HC-Clay, have low shrinkage values compared to the reference mixes. For example, at 224 days in the case of 0.4 w/b ratio, the shrinkage strain of the LC^3 mixes with B-Clay and PH-Clay is almost half that of the reference mix R1. This performance was generally linked to the ISAs of the clays. The reason is that since the clays have high ISA, most likely they absorb more of the available water in the system, which can be slowly released back into the matrix with time and in turn reduces the rate of loss of moisture in the paste. However, further work is recommended to confirm this suggestion. In addition, comparing the results of the two cases, 0.4 w/b ratio (Figure 6.13) and 0.55 w/b ratio (Figure 6.14), the shrinkage strain for the reference mix R1 increases moving from 0.4 to 0.55 w/b ratio as expected. Surprisingly, it is different in the case of LC^3-55(B) and LC^3-55(H) where the shrinkage strain appears to reduce going from 0.4 to 0.55 w/b ratio. The reason for this is not yet clear, but most likely can also be related to the high ISA of the clays and therefore how much water was available initially to react in the system. Further research is recommended to get a deeper understanding of what is happening in the system.

7.4.7 Electrical resistivity of LC^3 concrete

Comparing the results of the two cases, 0.4 w/b ratio (Figure 6.17) and 0.55 w/b ratio (Figure 6.18), especially the LC^3-55 mixes and the reference mix R1, the resistivity values of the LC^3-55(H:35/10) and the reference mix R1 decreased going from 0.4 to 0.55 w/b ratio as expected. Surprisingly, it is different in the case of LC^3-55 mixes with B-Clay and HC-Clay where the resistivity values appeared to increase going from 0.4 to 0.55 w/b ratio. The reason for this is not yet clear, but most likely can be related to the availability of CH in the system, how much is being consumed by the pozzolanic reaction, and formation of hydrated phases and therefore how pores are interconnected inside the concrete, something that needs further research. In addition, comparing LC^3 mixes with different clinker content (Figure 6.17), especially mixes with B-Clay and H-Clay, results show that the resistivity values increase as the amount of clay increases

in the mix. This trend suggests that the performance of the LC^3 system is strongly influenced by the amount of calcined clay and not clinker content. However, further research is recommended to fully understand what is happening in the system.

7.4.8 Carbonation resistance of LC^3 concrete

In this research, the selected concrete mixes were tested for carbonation resistance using the accelerated carbonation test. In general, results showed that the LC^3 mixes have somewhat lower carbonation resistance compared to reference mixes, and the depth of carbonation depends largely on the amount of clinker and/or CaO present in the mix. However, it is not clear whether this observation reflects what will happen in the 'real' environment. In addition, the OPI results (Figure 6.20 and Figure 6.24) indicate that the LC^3 mixes are dense and have high resistance to penetration of deleterious gases compared to the reference mixes. Furthermore, Angst et al. (2020), after reviewing several documented cases of RC structures with carbonation front at the level of reinforcement, concluded that carbonation is not necessarily the primary problem for corrosion of reinforcement in concrete and that the main factor controlling the corrosion rate is the level of moisture at the steel-concrete interface. In view of this, further work is recommended to get a deeper understanding of the performance of the LC^3 mixes under carbonation and/or corrosion of steel in carbonated LC^3 concrete.

7.4.9 Other considerations

The results of the optimisation work presented in Section 5.2 suggest that for optimum performance, regardless of the difference in the compressive strength values obtained for each of the LC^3 mortars with different CC, the lowest clinker content is around 55% at which the CC content is 35% and the LS content is 10%. Based on this finding, further work is recommended to get a deeper understanding as to why these clays with different characteristics gave similar optimum LC^3 proportion with less clinker content. It is important to note that in this research, only CEM II/A-L 52.5 N from AfriSam and LS with 97% $C\overline{C}$ purity from Idwala Carbonates (SA) were used for all the mixes with different CC and the lowest boundary for the amount of LS was set at 10%. In view of this, further work is recommended particularly to see what would happen in the system if a low-grade or quarry-grade LS and/or a different source of cement is used.

In general, because of the high surface area of the clays, high dosage of SP is usually required for the LC^3 system compared to conventional systems (Ferreiro, Herfort and Damtoft, 2017; Dhandapani et al., 2018; Muzenda et al., 2020; Nair et al., 2020). In this research, the selected LC^3 mixes, especially with B-Clay, PH-Clay, and HC-Clay, were observed to demand SP dosage almost two-times higher compared to the reference mixes to get a similar workability (i.e., a slump of 100 ± 20 mm). With the HC-Clay, it was only possible to achieve a slump of 45 mm at SP dosage of 2%. It is important to note that high dosage of SP also affect the performance of the system (Ma, Wang, Li, et al., 2007; Li, Yu and Brouwers, 2017; Qian et al., 2020). In addition, the LC^3 mixes were observed to set quicker than the reference mixes which might restrict the application of these systems in certain situations. In view of all these, the following are recommended: research on the new types of SP for use with the LC^3 mixes; research on how grinding and blending can be optimised to reduce SP/water demand; research on how to balance workability, setting time and strength gain of the system.

The tests that were caried out to study the mechanical performance of selected LC^3 mixes were limited to compressive strength, elastic modulus, free shrinkage, and restrained shrinkage. In this case, further work on the flexural and tensile strength performance of these LC^3 mixes is recommended, as well as creep.

Regarding the durability performance of the selected LC^3 mixes, only resistivity, durability index, accelerated carbonation, and bulk diffusion tests were carried out. In this case, additional work on the performance of these LC^3 mixes to other deterioration mechanisms, such as alkali-silica reaction and sulphate attack is recommended. In addition, all the LC^3 mixes, regardless of the clinker content and type of clay, were observed to perform similarly or better than the reference mixes. However, all the results, observations and conclusions made in this research are only based on laboratory investigations. In view of this, field exposure of these mixes is highly recommended to get a better understanding on the performance of these mixes in real environments.

References

AASHTO T 358 (2015) 'Standard Method of Test for Surface Resistivity Indication of Concrete's Ability to Resist Chloride Ion Penetration', *American Association of State Highway and Transportation Officials* [Preprint].

ACI Committee 209 (2005) *Report on factors affecting shrinkage and creep of hardened concrete, American Concrete Institute.*

Ahmed, H., Khalil, W. and Jumaa, N.H. (2018) 'Shrinkage of high performance lightweight concrete exposed to hot-dry weather conditions', *MATEC Web of Conferences*, 162, pp. 4–11. doi:10.1051/matecconf/201816202004.

Aïtcin, P.C. (2000) 'Cements of yesterday and today - concrete of tomorrow', *Cement and Concrete Research*, 30(9), pp. 1349–1359. doi:10.1016/S0008-8846(00)00365-3.

Akindahunsi, A.A., Avet, F. and Scrivener, K. (2020) 'The Influence of some calcined clays from Nigeria as clinker substitute in cementitious systems', *Case Studies in Construction Materials*, 13. doi:10.1016/j.cscm.2020.e00443.

Akkaya, Y., Ouyang, C. and Shah, S.P. (2007) 'Effect of supplementary cementitious materials on shrinkage and crack development in concrete', *Cement and Concrete Composites*, 29(2), pp. 117–123. doi:10.1016/j.cemconcomp.2006.10.003.

Akwilapo, L.D. and Wiik, K. (2004) 'Ceramic properties of Pugu kaolin clays. Part I: Porosity and modulus of rupture', *Bulletin of the Chemical Society of Ethiopia*, 17(2), pp. 147–154. doi:10.4314/bcse.v17i2.61661.

Alderete, N.M. *et al.* (2016) 'Particle size distribution and specific surface area of SCMs compared through experimental techniques', in *International RILEM Conference on Materials, Systems and Structures in Civil Engineering*, pp. 61–72.

Alexander, M. and Mindess, S. (2005) *Aggregates in Concrete*. Taylor & Francis.

Alexander, M.G. (2016) *Marine concrete structures: Design, Durability and Performance, Woodhead Publishing*.

Alexander, M.G. (ed.) (2021) *Fulton's Concrete Technology*. Johannesburg, South Africa: Cement & Concrete SA.

Alexander, M.G., Ballim, Y. and Mackechnie, J.R. (2009) *Durability Index Testing Procedure Manual, University of Cape Town, CoMSIRU.*

Alexander, M.G., Mackechnie, J.R. and Ballim, Y. (1999) 'Guide to the use of durability indexes for achieving durability in concrete structures', p. 35.

Alexander, M.G. and Milne, T.I. (1995) 'Influence of cement blend and aggregate type on the stress-strain behavior and elastic modulus of concrete', *Materials Journal*, 92(3), pp. 227–235.

Almenares, R.S. *et al.* (2017) 'Industrial calcination of kaolinitic clays to make reactive pozzolans', *Case Studies in Construction Materials*, 6(January), pp. 225–232. doi:10.1016/j.cscm.2017.03.005.

Alsadey, S. *et al.* (2016) 'Influence of Superplasticizer Compatibility on the Setting Time, Strength and Stiffening Characteristics of Concrete', *Advances in Applied Sciences*, 1(2), pp. 30–36. doi:10.11648/j.aas.20160102.12.

Alujas, A. *et al.* (2015) 'Pozzolanic reactivity of low grade kaolinitic clays: Influence of calcination temperature and impact of calcination products on OPC hydration', *Applied Clay Science*, 108, pp. 94–101. doi:10.1016/j.clay.2015.01.028.

Ambroise, J., Murat, M. and Péra, J. (1985) 'Hydration reaction and hardening of calcined clays and related minerals V. Extension of the research and general

conclusions', *Cement and Concrete Research*, 15(2), pp. 261–268. doi:10.1016/0008-8846(85)90037-7.
Anders, L. *et al.* (2015) 'Effect of fineness in clinker-calcined clays-limestone cement', *Advances in Cement Research*, 27(9), pp. 546–556.
Andrew, R.M. (2018) 'Global CO2 emissions from cement production', *Earth System Science Data*, 10, pp. 195–217. doi:http://dx.doi.org.kuleuven.ezproxy.kuleuven.be/10.5194/essd-10-195-2018.
Angst, U. *et al.* (2020) 'Corrosion of steel in carbonated concrete: Mechanisms, practical experience, and research priorities – A critical review by RILEM TC 281-CCC', *RILEM Technical Letters*, 5, pp. 85–100. doi:10.21809/rilemtechlett.2020.127.
Anil, A., Mohan Misra, N. and Misra, S.N. (2018) 'Characterization of Some Red Clays from Morbi-Wankaner Region (Gujarat, India)', *Transactions of the Indian Ceramic Society*, 77(2), pp. 73–83. doi:10.1080/0371750X.2018.1463870.
Antoni, M. *et al.* (2012) 'Cement substitution by a combination of metakaolin and limestone', *Cement and Concrete Research*, 42(12), pp. 1579–1589. doi:10.1016/j.cemconres.2012.09.006.
Antoni, M. (2013) *Investigation of cement substitution by combined addition of calcined clays and limestone, PhD Thesis, ÉCOLE POLYTECHNIQUE FÉDÉRALE DE LAUSANNE*.
Aras, A. *et al.* (2007) 'Evaluation of selected kaolins as raw materials for the Turkish cement and concrete industry', *Clay Minerals*, 42(2), pp. 233–244. doi:10.1180/claymin.2007.042.2.08.
Arvaniti, E.C. *et al.* (2015) 'Determination of particle size, surface area, and shape of supplementary cementitious materials by different techniques', *Materials and Structures*, 48(11), pp. 3687–3701. doi:10.1617/s11527-014-0431-3.
Ashraf, W. (2016) 'Carbonation of cement-based materials: Challenges and opportunities', *Construction and Building Materials*, 120(September 2016), pp. 558–570. doi:10.1016/j.conbuildmat.2016.05.080.
ASTM C 1581-18a (2009) *Standard Test Method for Determining Age at Cracking and Induced Tensile Stress Characteristics of Mortar and Concrete under Restrained Shrinkage, ASTM International*. doi:10.1520/C1581.
ASTM C109/C109M-20b (2020) 'Standard test method for compressive strength of hydraulic cement mortars (Using 2-in . or [50-mm] cube specimens)', pp. 1–9. doi:10.1520/C0109.
ASTM C1152 (2020) 'Standard Test Method for Acid-Soluble Chloride in Mortar and Concrete'.
ASTM C1556 (2016) 'Standard Test Method for Determining the Apparent Chloride Diffusion Coefficient of Cementitious Mixtures by Bulk Diffusion1'.
ASTM C595/C595M (2021) 'Standard Specification for Blended Hydraulic Cements', p. 10. doi:10.1520/C0595.
Avet, F. *et al.* (2016) 'Development of a new rapid, relevant and reliable (R3) test method to evaluate the pozzolanic reactivity of calcined kaolinitic clays', *Cement and Concrete Research*, 85, pp. 1–11. doi:10.1016/j.cemconres.2016.02.015.
Avet, F. (2017) *Investigation of the grade of calcined clays used as clinker substitute in Limestone Calcined Clay Cement (LC3) - Ph.D Thesis. EPFL*.
Avet, F. and Scrivener, K. (2018) 'Investigation of the calcined kaolinite content on the hydration of Limestone Calcined Clay Cement (LC3)', *Cement and Concrete Research*, 107(January), pp. 124–135. doi:10.1016/j.cemconres.2018.02.016.

Avet, F., Sofia, L. and Scrivener, K. (2019) 'Concrete performance of limestone calcined clay cement (LC3) compared with conventional cements', *Advances in Civil Engineering Materials*, 8(3), pp. 275–286. doi:10.1520/ACEM20190052.

Azarsa, P.. and Gupta, R. (2017) 'Resistivity of Concrete for Electrical Durability Evaluation: A Review', *Advances in Materials Science and Engineering*, 2017, pp. 1–30.

Beltzung, F. and Wittmann, F.H. (2005) 'Role of disjoining pressure in cement based materials', *Cement and Concrete Research*, 35(12), pp. 2364–2370. doi:10.1016/j.cemconres.2005.04.004.

Bentur, A. and Mitchell, D. (2008) 'Material performance lessons', *Cement and Concrete Research*, 38(2), pp. 259–272. doi:10.1016/j.cemconres.2007.09.009.

Bentz, D.P. (2010) 'Powder Additions to Mitigate Retardation in High-Volume Fly Ash Mixtures', *ACI Materials Journal*, (107), pp. 508–514.

Bernal, S.A. *et al.* (2017) 'Characterization of supplementary cementitious materials by thermal analysis', *Materials and Structures/Materiaux et Constructions*, 50(1), pp. 1–13. doi:10.1617/s11527-016-0909-2.

Berriel, S.S. *et al.* (2016) 'Assessing the environmental and economic potential of Limestone Calcined Clay Cement in Cuba', *Journal of Cleaner Production*, 124, pp. 361–369. doi:10.1016/j.jclepro.2016.02.125.

Beushausen, H. (2014) 'Principles of the Performance-Based Approach for Concrete Durability', in, pp. 341–349.

Beushausen, H. *et al.* (2021) 'Developments in defining exposure classes for durability design and specification', *Structural Concrete*, (December 2020), pp. 1–17. doi:10.1002/suco.202000792.

Beushausen, H., Torrent, R. and Alexander, M.G. (2019) 'Performance-based approaches for concrete durability: State of the art and future research needs', *Cement and Concrete Research*, 119(January), pp. 11–20. doi:10.1016/j.cemconres.2019.01.003.

Bijen, J. (1996) 'Benefits of slag and fly ash', *Construction and Building Materials*, 10(5), pp. 309–314. doi:10.1016/0950-0618(95)00014-3.

Bishnoi, S. *et al.* (2014) 'Pilot scale manufacture of limestone calcined clay cement : The Indian experience', *Indian Concrete Journal*, 88(7), pp. 22–28.

Bissonnette, B., Pierre, P. and Pigeon, M. (1999) 'Influence of key parameters on drying shrinkage of cementitious materials', *Cement and Concrete Research*, 29(10), pp. 1655–1662. doi:10.1016/S0008-8846(99)00156-8.

Black, L. *et al.* (2006) 'In situ Raman analysis of hydrating C3A and C4AF pastes in presence and absence of sulphate', *Advances in Applied Ceramics*, 105(4), pp. 209–216. doi:10.1179/174367606X120179.

Bonavetti, V.L., Rahhal, V.F. and Irassar, E.F. (2001) 'Studies on the carboaluminate formation in limestone filler-blended cements', *Cement and Concrete Research*, 31(6), pp. 853–859. doi:10.1016/S0008-8846(01)00491-4.

Briki, Y. *et al.* (2021) 'Impact of limestone fineness on cement hydration at early age', *Cement and Concrete Research*, 147(July 2020), p. 106515. doi:10.1016/j.cemconres.2021.106515.

Broomfield, J.P. (2007) *Corrosion of steel in concrete: understanding, investigation and repair 2nd Edition*, *CRC Press*.

Brouwers, H.J.H. and Radix, H.J. (2005) 'Self-compacting concrete: Theoretical and experimental study', *Cement and Concrete Research*, 35(11), pp. 2116–2136. doi:10.1016/j.cemconres.2005.06.002.

Brown, I.W.M. *et al.* (1985) 'Outstanding Problems in the Kaolinite-Mullite ReactionSequence Investigated by 29Si and 27Al Solid-state Nuclear Magnetic Resonance: 11, High-Temperature Transformations of Metakaolinite', *Journal of the American Ceramic Society*, 68(6), pp. 298–301.

Browning, J.A. *et al.* (2011) 'Lightweight aggregate as internal curing agent to limit concrete shrinkage', *ACI Materials Journal*, 108(6), pp. 638–644. doi:10.14359/51683467.

BS 1881 (1983) 'Testing concrete Part 121. Method for determination of static modulus of elasticity in compression', p. 7.

BS EN 197-5 (2021) 'Portland-composite cement CEM II/C-M and Composite cement CEM VI', p. 14.

Cancio Díaz, Y. *et al.* (2017) 'Limestone calcined clay cement as a low-carbon solution to meet expanding cement demand in emerging economies', *Development Engineering*, 2(May 2016), pp. 82–91. doi:10.1016/j.deveng.2017.06.001.

Cardinaud, G. *et al.* (2021) 'Calcined clay – Limestone cements: Hydration processes with high and low-grade kaolinite clays', *Construction and Building Materials*, 277, p. 122271. doi:10.1016/j.conbuildmat.2021.122271.

Castillo, R. *et al.* (2010) 'Activación de arcillas de bajo grado a altas temperaturas', *Revista Ingeniería de Construcción*, 25(3), pp. 329–352. doi:10.4067/S0718-50732010000300001.

Chandrasekhar, S. and Ramaswamy, S. (2002) 'Influence of mineral impurities on the properties of kaolin and its thermally treated products', *Applied Clay Science*, 21(3–4), pp. 133–142. doi:10.1016/S0169-1317(01)00083-7.

Chandrasekhar, S. and Ramaswamy, S. (2006) 'Iron minerals and their influence on the optical properties of two Indian kaolins', *Applied Clay Science*, 33(3–4), pp. 269–277. doi:10.1016/j.clay.2006.06.008.

Cheytani, M. and Chan, S.L.I. (2021) 'The applicability of the Wenner method for resistivity measurement of concrete in atmospheric conditions', *Case Studies in Construction Materials*, 15(February), p. e00663. doi:10.1016/j.cscm.2021.e00663.

Chotoli, F.F. *et al.* (2015) 'Clay activation and color modification in reducing calcination process: development in lab and industrial scale', in *Calcined Clays for Sustainable Concrete*, pp. 479–486. doi:10.1007/978-94-017-9939-3.

Cole, D.I., Ngcofe, L. and Halenyane, K. (2014) *Mineral commodities in the Western Cape province, South Africa, Council for Geoscience, Western Cape Regional Office, Report 12*.

Collepardi, M. (1998) 'Admixtures used to enhance placing characteristics of concrete', *Cement and Concrete Composites*, 20, pp. 103–112. doi:10.1016/S0958-9465(98)00071-7.

Cornell, J.A. (2002) *Experiments With Mixtures Design, Models and Analysis of Mixture Data, John Wiley & Sons, New York.* . doi:10.1198/004017002320256620.

Damineli, B.L. *et al.* (2010) 'Measuring the eco-efficiency of cement use', *Cement and Concrete Composites*, 32(8), pp. 555–562. doi:10.1016/j.cemconcomp.2010.07.009.

Damineli, B.L., Pileggi, R.G. and John, V.M. (2013) 'Lower binder intensity eco-efficient concretes', *Eco-Efficient Concrete*, pp. 26–44. doi:10.1533/9780857098993.1.26.

Damineli, B.L., Pillegi, R.G. and John, V.M. (2017) 'Influence of packing and

dispersion of particles on the cement content of concretes', *Revista IBRACON de Estruturas e Materiais*, 10(5), pp. 998–1024. doi:10.1590/s1983-41952017000500004.

Dhandapani, Y. *et al.* (2018) 'Mechanical properties and durability performance of concretes with Limestone Calcined Clay Cement (LC3)', *Cement and Concrete Research*, 107(November 2017), pp. 136–151. doi:10.1016/j.cemconres.2018.02.005.

Dhandapani, Y. *et al.* (2020) 'Perspectives on blended cementitious systems with calcined clay-limestone combination for sustainable low carbon cement transition', *Indian Concrete Journal*, 94(2), pp. 31–45.

Dhandapani, Y. *et al.* (2021) 'Towards ternary binders involving limestone additions — A review', *Cement and Concrete Research*, 143(February), p. 106396. doi:10.1016/j.cemconres.2021.106396.

Dhandapani, Y. and Santhanam, M. (2017) 'Assessment of pore structure evolution in the limestone calcined clay cementitious system and its implications for performance', *Cement and Concrete Composites*, 84, pp. 36–47. doi:10.1016/j.cemconcomp.2017.08.012.

Díaz, A.A. *et al.* (2018) 'Proposal of a methodology for the preliminary assessment of kaolinitic clay deposits as a source of SCMs', in *Calcined Clays for Sustainable Concrete*, pp. 29–34.

Díaz, E. *et al.* (2018) 'Carbonation of concrete with low carbon cement LC3 exposed to different environmental conditions', in *Calcined Clays for Sustainable Concrete*. Springer, Dordrecht., pp. 141–146.

Dilnesa, B.Z. *et al.* (2011) 'Fe-Containing Hydrates in Cementitious System', *13th International Congress on the Chemistry of Cement.*, pp. 1–7.

Dittmer, T. and Beushausen, H. (2014) 'The effect of coarse aggregate content and size on the age at cracking of bonded concrete overlays subjected to restrained deformation', *Construction and Building Materials*, 69, pp. 73–82. doi:10.1016/j.conbuildmat.2014.06.056.

Dixit, A., Du, H. and Pang, S.D. (2021) 'Performance of mortar incorporating calcined marine clays with varying kaolinite content', *Journal of Cleaner Production*, 282(xxxx), p. 124513. doi:10.1016/j.jclepro.2020.124513.

Dondi, M. *et al.* (2001) 'Chemical, mineralogical and ceramic properties of kaolinitic materials from the Tresnuraghes mining district (Western Sardinia, Italy)', *Applied Clay Science*, 18(3–4), pp. 145–155. doi:10.1016/S0169-1317(00)00042-9.

Ekosse, G.E. (2010) 'Kaolin deposits and occurrences in Africa : Geology , mineralogy and utilization', *Applied Clay Science*, 50(2), pp. 212–236. doi:10.1016/j.clay.2010.08.003.

Emmanuel, A.C. *et al.* (2016) 'Second pilot production of limestone calcined clay cement in India: The experience', *Indian Concrete Journal*, 90(5), pp. 57–63.

EN 206-1 (2000) *Concrete - Part 1: Specification, performance, production and conformity*.

EN 206 (2013) 'BSI Standards Publication Concrete — Specification , performance , production and conformity', *British Standard* [Preprint], (May).

Escobar, K.D., Díaz, A.A.G. and Pérez, L.A. (2020) 'Pozzolanic Reactivity of the Calcination Products Obtained from Yaguajay Clay Deposit', in *Proceedings of the International Conference of Sustainable Production and Use of Cement and Concrete*. Springer, Cham, pp. 47–58.

Ez-zaki, H. *et al.* (2021) 'A fresh view on limestone calcined clay cement (LC3) pastes', *Materials*, 14(11). doi:10.3390/ma14113037.
Fabbri, B., Gualtieri, S. and Leonardi, C. (2013) 'Modifications induced by the thermal treatment of kaolin and determination of reactivity of metakaolin', *Applied Clay Science*, 73(1), pp. 2–10. doi:10.1016/j.clay.2012.09.019.
Fennis, S.A.A.M. and Walraven, J.C. (2011) 'Ecological concrete and workability: A marriage with the future', in *36th Conference on our World in Concrete & Structures*. Singapore: CI - Premier PTE LTD, p. 11.
Fennis, S.A.A.M. (2010) *Design of Ecological Concrete by Particle Packing Optimization*. Edited by S.A.A.M. Fennis. Available at: http://repository.tudelft.nl/view/ir/uuid:5a1e445b-36a7-4f27-a89a-d48372d2a45c/.
Fennis, S.A.A.M., Walraven, J.C. and Den Uijl, J.A. (2013) 'Compaction-interaction packing mode: Regarding the effect of fillers in concrete mixture design', *Materials and Structures/Materiaux et Constructions*, 46(3), pp. 463–478. doi:10.1617/s11527-012-9910-6.
Fenyvesi, O. (2011) 'Affect of lightweight aggregate to early age cracking in concrete', *Periodica Polytechnica Civil Engineering*, 55(1), pp. 63–71. doi:10.3311/pp.ci.2011-1.08.
Fernandez, R., Martirena, F. and Scrivener, K.L. (2011) 'The origin of the pozzolanic activity of calcined clay minerals: A comparison between kaolinite, illite and montmorillonite', *Cement and Concrete Research*, 41(1), pp. 113–122. doi:10.1016/j.cemconres.2010.09.013.
Fernandez, R. and Scrivener, K. (2009) *Calcined clayey soils as a potential replacement for cement in developing countries. Ph.D Thesis, Ecole Polytechnique Fédérale de Lausanne*.
Ferreiro, S. *et al.* (2019) 'Influence of fineness of raw clay and calcination temperature on the performance of calcined clay-limestone blended cements', *Applied Clay Science*, 169(December 2018), pp. 81–90. doi:10.1016/j.clay.2018.12.021.
Ferreiro, S., Herfort, D. and Damtoft, J.S. (2017) 'Effect of raw clay type, fineness, water-to-cement ratio and fly ash addition on workability and strength performance of calcined clay – Limestone Portland cements', *Cement and Concrete Research*, 101(March), pp. 1–12. doi:10.1016/j.cemconres.2017.08.003.
Flatt, R.J. (2004) 'Dispersion forces in cement suspensions', *Cement and Concrete Research*, 34(3), pp. 399–408. doi:10.1016/j.cemconres.2003.08.019.
Flatt, R.J. and Houst, Y.F. (2001) 'A simplified view on chemical effects perturbing the action of superplasticizers', *Cement and Concrete Research*, 31(8), pp. 1169–1176. doi:10.1016/S0008-8846(01)00534-8.
Funk, J.E. and Dinger, D.R. (1994) *Predictive process control of crowded particulate suspensions: Applied to Ceramic Manufacturing*, *Springer Science+Business Media New York*. doi:10.1007/978-1-4615-3118-0.
Gámiz, E. *et al.* (2005) 'Relationships between chemico-mineralogical composition and color properties in selected natural and calcined Spanish kaolins', *Applied Clay Science*, 28(1-4 SPEC. ISS.), pp. 269–282. doi:10.1016/j.clay.2004.02.004.
Garcia-Valles, M. *et al.* (2020) 'Mineralogical and Thermal Characterization of Kaolinitic Clays from Terra Alta (Catalonia, Spain)', *Minerals*, 10(2), p. 142.
Gartner, E. (2004) 'Industrially interesting approaches to "low-CO2" cements', *Cement and Concrete Research*, 34(9), pp. 1489–1498.

doi:10.1016/j.cemconres.2004.01.021.
Gartner, E. and Sui, T. (2016) 'Alternative cement clinkers', *Cement and Concrete Research*, p. 13. doi:10.1016/j.cemconres.2017.02.002.
Gettu, R. *et al.* (2018) 'Service Life and Life-Cycle Assessment of Reinforced Concrete with Fly ash and Limestone Calcined Clay Cement', *Sixth International Conference on the Durability of Concrete Structures* [Preprint], (July).
Ghosh, P. and Tran, Q. (2015) 'Influence of parameters on surface resistivity of concrete', *Cement and Concrete Composites*, 62, pp. 134–145. . doi:10.1016/j.cemconcomp.2015.06.003.
Goltermann, P., Johansen, V. and Palbøl, L. (1997) 'Packing of aggregates: An alternative tool to determine the optimal aggregate mix', *ACI Materials Journal*, 94(5), pp. 435–443.
Gouws, S.M., Alexander, M.G. and Maritz, G. (2001) 'Use of Durability Index Tests for the Assessment and Control of Concrete Quality on Site', *Concrete Beton*, 98(April), pp. 5–16. Available at: www.concretesociety.co.za.
Gowers, K. and Millard, S. (1999) 'Measurement of Concrete Resistivity for Assessment of Corrosion', *ACI Materials Journal*, 96(5), pp. 536–541.
von Greve-Dierfeld, S. *et al.* (2020) 'Understanding the carbonation of concrete with supplementary cementitious materials : a critical review by RILEM TC 281-CCC', *Materials and Structures*, 53(6), pp. 1–34. doi:10.1617/s11527-020-01558-w.
Gudissa, W. and Dinku, A. (2010) 'The use of limestone powder as an alternative cement replacement material: an experimental study', *Journal of EEA*, 27.
Habert, G. *et al.* (2010) 'Cement production technology improvement compared to factor 4 objectives', *Cement and Concrete Research*, 40(5), pp. 820–826. doi:10.1016/j.cemconres.2009.09.031.
Hanssen, T. (2012) 'Elkem Materials-Mixture Analyser (EMMA)'.
He, C., Osbaeck, B. and Makovicky, E. (1995) 'Pozzolanic reactions of six principal clay minerals: Activation, reactivity assessments and technological effects', *Cement and Concrete Research*, 25(8), pp. 1691–1702. doi:10.1016/0008-8846(95)00165-4.
He, Z. and Li, Z. (2005) 'Influence of alkali on restrained shrinkage behavior of cement-based materials', *Cement and Concrete Research*, 35(3), pp. 457–463. doi:10.1016/j.cemconres.2004.06.026.
Heckroodt, R.O. (1991) 'Clay and clay materials in South Africa*', 91(10), pp. 343–363.
Van Den Heede, P. and De Belie, N. (2012) 'Environmental impact and life cycle assessment (LCA) of traditional and "green" concretes: Literature review and theoretical calculations', *Cement and Concrete Composites*, 34(4), pp. 431–442. doi:10.1016/j.cemconcomp.2012.01.004.
Heller-Kallai, L. (2006) 'Chapter 7.2 Thermally Modified Clay Minerals', *Developments in Clay Science*, pp. 289–308. doi:10.1016/S1572-4352(05)01009-3.
Holmes, M. (2018) *Powder packing optimisation for clinker reduction in concrete. MSc Thesis, UCT.*
Hosterman, J.W., Patterson, S.H. and Good, E.E. (1978) *World nonbauxite aluminum resources; alunite (No. 1076-A).* doi:10.15713/ins.mmj.3.
Huang, Z. *et al.* (2020) 'Development of limestone calcined clay cement concrete in South China and its bond behavior with steel reinforcement', *Zhejiang*

University-SCIENCE A, 21(11), pp. 892–907.
Hüsken, G. and Brouwers, H.J.H. (2008) 'A new mix design concept for earth-moist concrete: A theoretical and experimental study', *Cement and Concrete Research*, 38(10), pp. 1246–1259. doi:10.1016/j.cemconres.2008.04.002.
Instruments, M. (2000) *Mastersizer 2000 user manuel*. Worcestershire, United Kingdom.: Malvern Instruments Ltd.
Instruments, M. (2007) *Sample dispersion and refractive index guide*, *MAN0396 1.0*. United Kingdom: Malvern Instruments Ltd.
Ipavec, A. *et al.* (2011) 'Carboaluminate phases formation during the hydration of calcite-containing Portland cement', *Journal of the American Ceramic Society*, 94(4), pp. 1238–1242. doi:10.1111/j.1551-2916.2010.04201.x.
Jewell, R. and Rathbone, R. (2009) 'Optical Properties of Coal Combustion Byproducts for Particle-Size Analysis by Laser Diffraction', *Coal Combustion and Gasification Products*, 1(1), pp. 1–6. doi:10.4177/ccgp-d-09-00001.
Ji, G.M., Kanstad, T. and Bjøntegaard (2018) 'Numerical modelling of field test for crack risk assessment of early age concrete containing fly ash', *Advances in Materials Science and Engineering*, 2018. doi:10.1155/2018/1058170.
Johansen, V. and Andersen, P.J. (1991) 'Particle packing and concrete properties', in Mindess, J.S. and S. (ed.) *Material science of concrete II*. The American Ceramic Society Inc., pp. 111–147.
Jones, R., Zheng, L. and Newlands, M. (2002) 'Comparison of particle packing models for proportioning concrete constituents for minimum voids ratio', *Materials and Structures*, 35, pp. 301–309. doi:10.1007/BF02482136.
Justnes, H. and De Weerdt, K. (2007) *Separate Grinding versus Intergrinding*. SINTEF Report SBF BK A, 7022. doi:10.1017/CBO9781107415324.004.
Kevin, D. and Kenneth, E. (1991) 'A review of limestone additions to Portland cement and concrete', *Cement and Concrete Composites*, 13, pp. 165–170.
Khan, M.S.H., Nguyen, Q.D. and Castel, A. (2018) 'Carbonation of limestone calcined clay cement concrete', in *Calcined Clays for Sustainable Concrete*. Springer, Dordrecht., pp. 238–243.
Khan, I. *et al.* (2020) 'Effect of Various Supplementary Cementitious Materials on Early-Age Concrete Cracking', *Journal of Materials in Civil Engineering*, 32(4), pp. 1–9. doi:10.1061/(ASCE)MT.1943-5533.0003120.
Khayat, K. and Libre, N. (2014) *Roller Compacted Concrete : Field Evaluation and Mixture Optimization, A National University Transportation Center at Missouri University of Science and Technology*. doi:10.13140/2.1.1647.2962.
Khayat, K. and Mehdipour, I. (2015) *Design and Performance of Crack-Free Environmentally Friendly Concrete Design and Performance of Crack-Free Environmentally Friendly Concrete " Crack-Free Eco-Crete "*. doi:10.13140/2.1.1397.4409.
Klee, H. *et al.* (2011) *Getting the numbers right: a database of energy performance and carbon dioxide emissions for the cement industry, Greenhouse Gas Measurement & Management, 1(2)*. doi:978-3-940388-48-3.
Klemm, W.A. and Adams, L.D. (1990) 'An investigation of the formation of carboaluminates', *ASTM Special Technical Publication*, (1064), pp. 60–72. doi:10.1520/stp23472s.
Knop, Y. and Peled, A. (2016) 'Packing density modeling of blended cement with limestone having different particle sizes', 102, pp. 44–50. doi:10.1016/j.conbuildmat.2015.09.063.

Krishnan, S., Emmanuel, A.C., *et al.* (2018) 'Hydration and mechanical properties of limestone calcined clay cement produced with marble dust', in *Calcined Clays for Sustainable Concrete*. Springer, Dordrecht., pp. 249–253.

Krishnan, S., Kanaujia, S.K., *et al.* (2018) 'Hydration kinetics and mechanisms of carbonates from stone wastes in ternary blends with calcined clay', *Construction and Building Materials*, 164, pp. 265–274. doi:10.1016/j.conbuildmat.2017.12.240.

Krishnan, S. and Bishnoi, S. (2018) 'Understanding the hydration of dolomite in cementitious systems with reactive aluminosilicates such as calcined clay', *Cement and Concrete Research*, 108(March), pp. 116–128. doi:10.1016/j.cemconres.2018.03.010.

Krishnan, S. and Bishnoi, S. (2020) 'A numerical approach for designing composite cements with calcined clay and limestone', *Cement and Concrete Research*, 138(August), p. 106232. doi:10.1016/j.cemconres.2020.106232.

Krishnan, S., Dhoopadahalli, G.R. and Bishnoi, S. (2020) 'Why Low-Grade Calcined Clays Are the Ideal for the Production of Limestone Calcined Clay Cement (LC3)', in *Calcined Clays for Sustainable Concrete*. Springer, Singapore., pp. 125–130.

Krishnan, S., Emmanuel, A.C. and Bishnoi, S. (2019) 'Hydration and phase assemblage of ternary cements with calcined clay and limestone', *Construction and Building Materials*, 222, pp. 64–72. doi:10.1016/j.conbuildmat.2019.06.123.

Krishnan, S., Singh, A. and Bishnoi, S. (2021) 'Impact of Alkali Salts on the Hydration of Ordinary Portland Cement and Limestone–Calcined Clay Cement', *Journal of Materials in Civil Engineering*, 33(9), p. 04021223. doi:10.1061/(asce)mt.1943-5533.0003861.

Kumar, S. and Santhanam, M. (2003) 'Particle packing theories and applications in concrete mixture proportioning: A review', *Indian Concrete Journal*, 77(9), pp. 1324–1331.

Kumar, S. V. and Santhanam, M. (2003) 'Particle packing theories and their application in concrete mixture proportioning: A review', *Indian Concrete Journal*, 77(9), pp. 1324–1331.

L'Hôpital, E. *et al.* (2015) 'Incorporation of aluminium in calcium-silicate-hydrates', *Cement and Concrete Research*, 75(December 2016), pp. 91–103. doi:10.1016/j.cemconres.2015.04.007.

De La Torre, A.G., Bruque, S. and Aranda, M.A.G. (2001) 'Rietveld quantitative amorphous content analysis', *Journal of Applied Crystallography*, 34(2), pp. 196–202.

Lambert, J.., Millman, W.. and Fripiat, J.. (1989) 'Revisiting kaolinite dehydroxylation: A silicon-29 and aluminum-27 MAS NMR study', *Journal of the American Chemical Society*, 111, pp. 3517–3522. doi:10.1021/ja00192a005.

De Larrard, F. (1999) *Concrete mixture proportioning: A scientific approach*. CRC Press.

Lawson, J. and Willden, C. (2016) 'Mixture Experiments in *R* Using **mixexp**', *Journal of Statistical Software*, 72(Code Snippet 2). doi:10.18637/jss.v072.c02.

Lecomte, A., Mechling, J.M. and Diliberto, C. (2009) 'Compaction index of cement paste of normal consistency', *Construction and Building Materials*, 23(10), pp. 3279–3286. doi:10.1016/j.conbuildmat.2009.05.005.

Lema, E.A. and Lweikiza, S.J. (2014) 'Use of Local Pozzolan for Stabilization of Subbase and Basecourse for Road Construction in Tanzania: Case Study of

TANZAM Highway (Chalinze-Melela Section)', in *Annual Road Convention, Dar es Salaam, Tanzania, 27-28 November 2014*, p. 31. doi:10.13140/2.1.5058.3367.
Li, P.P., Yu, Q.L. and Brouwers, H.J.H. (2017) 'Effect of PCE-type superplasticizer on early-age behaviour of ultra-high performance concrete (UHPC)', *Construction and Building Materials*, 153, pp. 740–750. doi:10.1016/j.conbuildmat.2017.07.145.
Li, X. *et al.* (2018) 'Reactivity tests for supplementary cementitious materials: RILEM TC 267-TRM phase 1', *Materials and Structures/Materiaux et Constructions*, 51(6). doi:10.1617/s11527-018-1269-x.
Li, Z., Afshinnia, K. and Rangaraju, P.R. (2016) 'Effect of alkali content of cement on properties of high performance cementitious mortar', *Construction and Building Materials*, 102, pp. 631–639. doi:10.1016/j.conbuildmat.2015.10.110.
Lim, T.Y.D. *et al.* (2016) 'Durability of Very-High-Strength Concrete with Supplementary Cementitious Materials for Marine Environments', *ACI Materials Journal*, 113(1).
Lin, R.S. *et al.* (2019) 'Hydration and microstructure of cement pastes with calcined Hwangtoh Clay', *Materials*, 12(3). doi:10.3390/ma12030458.
Lobo, C., Lemay, L. and Obla, K. (2005) 'Performance-based specifications for concrete', *Indian Concrete Journal*, 79(12), pp. 13–17. doi:10.1061/40798(190)45.
Lothenbach, B. *et al.* (2008) 'Influence of limestone on the hydration of Portland cements', *Cement and Concrete Research*, 38(6), pp. 848–860. doi:10.1016/j.cemconres.2008.01.002.
Lothenbach, B., Scrivener, K. and Hooton, R.D. (2011) 'Supplementary cementitious materials', *Cement and Concrete Research*, 41(12), pp. 1244–1256. doi:10.1016/j.cemconres.2010.12.001.
Ma, B., Wang, X., Li, X., *et al.* (2007) 'Influence of superplasticizers on strength and shrinkage cracking of cement mortar under drying conditions', *Journal Wuhan University of Technology, Materials Science Edition*, 22(2), pp. 358–361. doi:10.1007/s11595-005-2358-6.
Ma, B., Wang, X., Liang, W., *et al.* (2007) 'Study on early-age cracking of cement-based materials with superplasticizers', *Construction and Building Materials*, 21(11), pp. 2017–2022. doi:10.1016/j.conbuildmat.2006.04.012.
Mackechnie, J.R. (2001) *Predictions of reinforced concrete durability in the marine environment, RESEARCH MONOGRAPH NO. 1*.
Mackechnie, J.R. and Alexander, M.G. (2002) 'Durability Predictions Using Early-Age Durability Index Testing', *Proceedings, 9th Durability and Building Materials Conference, Australian Corrosion Association, Brisbane*, (1993), p. 11.
Maraghechi, H. *et al.* (2018) 'Performance of Limestone Calcined Clay Cement (LC3) with various kaolinite contents with respect to chloride transport', *Materials and Structures/Materiaux et Constructions*, 51(5), pp. 1–17. doi:10.1617/s11527-018-1255-3.
Martirena, F. *et al.* (2020) 'Color control in industrial clay calcination', *RILEM Technical Letters*, 5, pp. 1–7. doi:10.21809/RILEMTECHLETT.2020.107.
Matschei, T., Lothenbach, B. and Glasser, F.P. (2007) 'The role of calcium carbonate in cement hydration', *Cement and Concrete Research*, 37(4), pp. 551–558. doi:10.1016/j.cemconres.2006.10.013.
Megat Johari, M.A. *et al.* (2011) 'Influence of supplementary cementitious materials

on engineering properties of high strength concrete', *Construction and Building Materials*, 25(5), pp. 2639–2648. doi:10.1016/j.conbuildmat.2010.12.013.
Mehdipour, I. and Khayat, K.H. (2018) 'Understanding the role of particle packing characteristics in rheo-physical properties of cementitious suspensions: A literature review', *Construction and Building Materials*, 161, pp. 340–353. doi:10.1016/j.conbuildmat.2017.11.147.
Mehta, P.K. (2001) 'Reducing the environmental impact of concrete', *Concrete International*, 23(10), pp. 61–66. doi:10.1016/S1351-4210(05)70693-4.
Millard, S.G. (1991) 'Reinforced concrete resistivity measurement techniques', *Proceedings - Institution of Civil Engineers. Part 2. Research and theory*, 91(pt 2), pp. 71–88. doi:10.1680/iicep.1991.13583.
Ministry of energy and minerals (2008) *Industrial minerals in Tanzania - An Investor's guide*.
Mohammed, S. (2017) 'Processing, effect and reactivity assessment of artificial pozzolans obtained from clays and clay wastes: A review', *Construction and Building Materials*, 140, pp. 10–19. doi:10.1016/j.conbuildmat.2017.02.078.
Moore, A.J., Bakera, A.T. and Alexander, M.G. (2021) 'A critical review of the Water Sorptivity Index (WSI) parameter for potential durability assessment : Can WSI be considered in isolation of porosity?', *Journal of the South African Institution of Civil Engineering*, 63(2), pp. 27–34.
Moutassem, F. (2016) 'Assessment of Packing Density Models and Optimizing Concrete Mixtures', *International Journal of Civil, Mechanical and Energy Science (IJCMES)*, 2(4), pp. 2455–5304. Available at: www.ijcmes.com.
Mueller, F. V., Wallevik, O.H. and Khayat, K.H. (2014) 'Linking solid particle packing of Eco-SCC to material performance', *Cement and Concrete Composites*, 54, pp. 117–125. doi:10.1016/j.cemconcomp.2014.04.001.
Müller, N. and Harnisch, J. (2008) *A Blueprint for a Climate-Friendly Cement Industry: How to Turn Around the Trend of Cement Related Emissions in the Developing World, Gland, Switzerland: World Wide Fund for Nature*. Available at: http://d2ouvy59p0dg6k.cloudfront.net/downloads/english_report_lr_pdf.pdf%0Ahttp://scholar.google.com/scholar?hl=en&btnG=Search&q=intitle:A+blueprint+for+a+climate+friendly+cement+industry#0.
Murra, H.H. and Lyons, S.C. (1960) 'Further Correlations of Kaolinite Crystallinity With Chemical and Physical Properties', *Clays and Clay Minerals*, pp. 11–17. doi:10.1016/b978-0-08-009351-2.50008-8.
Muzenda, T.R. *et al.* (2020) 'The role of limestone and calcined clay on the rheological properties of LC3', *Cement and Concrete Composites*, 107(January), p. 103516. doi:10.1016/j.cemconcomp.2020.103516.
Nair, N. *et al.* (2020) 'A study on fresh properties of limestone calcined clay blended cementitious systems', *Construction and Building Materials*, 254, p. 119326. doi:10.1016/j.conbuildmat.2020.119326.
Nehdi, M. (2001) 'Ternary and Quaternary Cements for Sustainable Development', *Concrete International*, 23(4), pp. 35–42.
Neville, A. (2001) 'Consideration of durability of concrete structures : Past , present , and future', *Materials and Structures*, 34(March), pp. 114–118.
Nguyen, Q.D. *et al.* (2019) 'Mitigating the risk of early age cracking in fly ash blended cement-based concrete using ferronickel slag sand', *Journal of Advanced Concrete Technology*, 17(6), pp. 295–308. doi:10.3151/jact.17.295.
Nguyen, Q.D., Afroz, S. and Castel, A. (2020) 'Influence of Calcined Clay Reactivity

on the Mechanical Properties and Chloride Di ff usion Resistance of Limestone Calcined Clay Cement (LC3) Concrete', *Journal of Marine Science and Engineering*, 8(Figure 1), pp. 1–14.

Nguyen, Q.D., Khan, M.S.H. and Castel, A. (2018) 'Engineering properties of limestone calcined clay concrete', *Journal of Advanced Concrete Technology*, 16(8), pp. 343–357. doi:10.3151/jact.16.343.

Obla, K.H. *et al.* (2003) 'Properties of concrete containing ultra-fine fly ash', *ACI Materials Journal*, 100(5), pp. 426–433.

Okoronkwo, M.U. and Glasser, F.P. (2016) 'Stability of strätlingite in the CASH system', *Materials and Structures/Materiaux et Constructions*, 49(10), pp. 4305–4318. doi:10.1617/s11527-015-0789-x.

Olivier, J.G.J., Schure, K.M. and Peters, J.A.H.W. (2017) *Trends in global CO2 and total greenhouse gas emissions*, *PBL Netherlands Environmental Assessment Agency*. Available at: http://edgar.jrc.ec.europa.eu/news_docs/jrc-2016-trends-in-global-co2-emissions-2016-report-103425.pdf.

Papadakis, V.G. (2000) 'Effect of supplementary cementing materials on concrete resistance against carbonation and chloride ingress', *Cement and Concrete Research*, 30(2), pp. 291–299. doi:10.1016/S0008-8846(99)00249-5.

Papadakis, V.G., Fardis, M.N. and Vayenas, C.G. (1992) 'Hydration and carbonation of pozzolanic cements', *ACI Materials Journal*, 89(2), pp. 119–130. doi:10.14359/2185.

Parashar, A. and Bishnoi, S. (2020) 'A comparison of test methods to assess the strength potential of plain and blended supplementary cementitious materials', *Construction and Building Materials*, 256, p. 119292. doi:10.1016/j.conbuildmat.2020.119292.

Pardal, X., Pochard, I. and Nonat, A. (2009) 'Experimental study of Si–Al substitution in calcium-silicate-hydrate (C-S-H) prepared under equilibrium conditions', *Cement and Concrete Research*, 39(8), pp. 637–643. doi:10.1016/J.CEMCONRES.2009.05.001.

Park, S.S., Kwon, S.J. and Jung, S.H. (2012) 'Analysis technique for chloride penetration in cracked concrete using equivalent diffusion and permeation', *Construction and Building Materials*, 29, pp. 183–192. doi:10.1016/j.conbuildmat.2011.09.019.

Payá, J. *et al.* (2003) 'Determination of the pozzolanic activity of fluid catalytic cracking residue. Thermogravimetric analysis studies on FC3R-lime pastes', *Cement and Concrete Research*, 33(7), pp. 1085–1091. doi:10.1016/S0008-8846(03)00014-0.

Pérez, A. *et al.* (2015) 'Influence of the manufacturing process on the performance of low-clinker, calcined clay - limestone portland cement', in *In Calcined Clays for Sustainable Concrete. Springer, Dordrecht.*, pp. 283–289. doi:10.1007/978-94-017-9939-3.

Pérez, A. *et al.* (2018) 'Influence grinding procedure, limestone content and PSD of components on properties of clinker-calcined clay-limestone cements produced by intergrinding', in *In Calcined Clays for Sustainable Concrete. Springer, Dordrecht.*, pp. 358–365.

Pillai, R.G. *et al.* (2019) 'Service life and life cycle assessment of reinforced concrete systems with limestone calcined clay cement (LC3)', *Cement and Concrete Research*, 118(March 2018), pp. 111–119. doi:10.1016/j.cemconres.2018.11.019.

Pillai, R.G., Gettu, R. and Santhanam, M. (2020) 'Use of supplementary cementitious materials (SCMs) in reinforced concrete systems – Benefits and limitations', *Revista ALCONPAT*, 10(2), pp. 147–164. doi:10.21041/ra.v10i2.477.

Du Preez, A.A. and Alexander, M.G. (2004) 'A site study of durability indexes for concrete in marine conditions', *Materials and Structures/Materiaux et Constructions*, 37(267), pp. 146–154. doi:10.1617/13998.

Pretorius, I. *et al.* (2015) 'A perspective on South African coal fired power station emissions', *Journal of Energy in Southern Africa*, 26(3), pp. 27–40. Available at: http://www.scielo.org.za/scielo.php?script=sci_arttext&pid=S1021-447X2015000300004&nrm=iso.

Proske, T. *et al.* (2013) 'Eco-friendly concretes with reduced water and cement contents - Mix design principles and laboratory tests', *Cement and Concrete Research*, 51, pp. 38–46. doi:10.1016/j.cemconres.2013.04.011.

Proske, T. *et al.* (2014) 'Eco-friendly concretes with reduced water and cement content--Mix design principles and application in practice', *Construction and Building Materials*, 67(September), pp. 413–421. doi:10.1016/j.conbuildmat.2013.12.066.

Van Der Putten, J. *et al.* (2017) 'Determination of packing profiles for the verification of the compressible packing model in case of UHPC pastes', *Materials and Structures/Materiaux et Constructions*, 50(2), pp. 1–14. doi:10.1617/s11527-016-0986-2.

Qian, X. *et al.* (2020) 'Influence of Superplasticizer Type and Dosage on Early-age Drying Shrinkage of Cement Paste with Consideration of Pore Size Distribution and Water Loss', *Journal Wuhan University of Technology, Materials Science Edition*, 35(4), pp. 758–767. doi:10.1007/s11595-020-2318-1.

Quennoz, A. and Scrivener, K.L. (2013) 'Interactions between alite and C3A-gypsum hydrations in model cements', *Cement and Concrete Research*, 44, pp. 46–54. doi:10.1016/j.cemconres.2012.10.018.

Radwan, M.M. and El Hemaly, S.A.S. (2011) 'Hydration characteristics of tetracalcium alumino-ferrite phase in the presence calcium carbonate', *Ceramics - Silikaty*, 55(4), pp. 337–342.

Rajendran Nair, P.B. and Paramasivam, R. (1999) 'Effect of grinding aids on the time-flow characteristics of the ground product from a batch ball mill', *Powder Technology*, 101(1), pp. 31–42. doi:10.1016/S0032-5910(98)00121-1.

Ramezanianpour, A.A. and Bahrami Jovein, H. (2012) 'Influence of metakaolin as supplementary cementing material on strength and durability of concretes', *Construction and Building Materials*, 30, pp. 470–479. doi:10.1016/j.conbuildmat.2011.12.050.

Republic of South Africa (2019) 'Carbon Tax Act 15', *Government Gazette*, pp. 1–65.

Richardson, I.G. (2000) 'Nature of the hydration products in hardened cement pastes', *Cement and Concrete Composites*, 22(2), pp. 97–113. . doi:10.1016/S0958-9465(99)00036-0.

Richardson, I.G. and Groves, G.W. (1993) 'The incorporation of minor and trace elements into calcium silicate hydrate (C□S□H) gel in hardened cement pastes', *Cement and Concrete Research*, 23(1), pp. 131–138. doi:10.1016/0008-8846(93)90143-W.

RILEM, T. (1994) 'CPC-18 measurement of hardened concrete carbonation depth, 1988', *RILEM Recommendations for the Testing and Use of Constructions Materials*, pp. 56–58.

Robles, K.P. V., Yee, J.J. and Kee, S.H. (2021) 'Effect of the Geometrical Constraints

to the Wenner Four-Point Electrical Resistivity Test of Reinforced Concrete Slabs', *Sensors (Basel, Switzerland)*, 21(13), pp. 1–16. doi:10.3390/s21134622.
Rodriguez, C. and Tobon, J.I. (2020) 'Influence of calcined clay/limestone, sulfate and clinker proportions on cement performance', *Construction and Building Materials*, 251, p. 119050. doi:10.1016/j.conbuildmat.2020.119050.
Roussel, N. (2012) *Understanding the rheology of concrete*. Woodhead Publishing Limited.
Rupnow, T.A.P.I. (2011) *Evaluation of surface resistivity measurements as an alternative to the rapid chloride permeability test for quality assurance and acceptance (No. FHWA/LA. 11/479), Louisiana Transportation Research Center*.
Safiuddin, M. *et al.* (2018) 'Early-age cracking in concrete: Causes, consequences, remedialmeasures, and recommendations', *Applied Sciences (Switzerland)*, 8(10). doi:10.3390/app8101730.
Sahamitmongkol, R., Khuon, N. and Thitikavanont, Y. (2020) 'Chloride Resistance of Cementitious Materials Containing Calcined Clay and Limestone Powder', in *Calcined Clays for Sustainable Concrete*, pp. 601–612.
Salvador, S. (1995) 'Pozzolanic properties of flash-calcined kaolinite: A comparative study with soak-calcined products', *Cement and Concrete Research*, 25(1), pp. 102–112. doi:10.1016/0008-8846(94)00118-I.
Salvoldi, B.G., Beushausen, H. and Alexander, M.G. (2015) 'Oxygen permeability of concrete and its relation to carbonation', *Construction and Building Materials*, 85, pp. 30–37. doi:10.1016/j.conbuildmat.2015.02.019.
SANS 3001-CO3-1:2015 (no date) 'Civil engineering test methods Part CO3-1: Concrete durability index testing — Preparation of test specimens', *SOUTH AFRICAN NATIONAL STANDARD* [Preprint].
SANS 3001-CO3-2:2015 (no date) 'Civil engineering test methods Part CO3-2: Concrete durability index testing — Oxygen permeability test', *SOUTH AFRICAN NATIONAL STANDARD* [Preprint].
SANS 5862-2 (2006) 'Concrete tests — Consistence of freshly mixed concrete — Flow test'.
Sant, G. *et al.* (2012) 'The influence of sodium and potassium hydroxide on volume changes in cementitious materials', *Cement and Concrete Research*, 42(11), pp. 1447–1455. doi:10.1016/j.cemconres.2012.08.012.
Schneider, M. *et al.* (2011) 'Sustainable cement production-present and future', *Cement and Concrete Research*, 41(7), pp. 642–650. doi:10.1016/j.cemconres.2011.03.019.
Schreiner, W.H. and Wypych, F. (2002) '2002 Structural and Morphological Characterization of the PP-0559 Kaolinite from the - Cópia.pdf', 13(2), pp. 270–275.
Schulze, D.G. (2005) 'Clay minerals', *Encyclopedia of Soils in the Environment*. Volume 1. Academic Press; 1 edition (November 8, 2004).
Scrivener, K. *et al.* (2019) ' Impacting factors and properties of limestone calcined clay cements (LC 3) ', *Green Materials*, 7(1), pp. 3–14. doi:10.1680/jgrma.18.00029.
Scrivener, K., Snellings, R. and Lothenbach, B. (2018) *A Practical Guide to Microstructural Analysis of Cementitious Materials, A Practical Guide to Microstructural Analysis of Cementitious Materials*. doi:10.1201/b19074.
Scrivener, K.L. (2014) 'Options for the future of cement', *The Indian Concrete Journal*, 88(7), pp. 11–21. Available at: http://www.lc3.ch/wp-content/uploads/2014/09/0851_ICJ_Article.pdf.

Scrivener, K.L., John, V.M. and Gartner, E.M. (2016) *Eco-efficient cements: Potential economically viable solutions for a low-CO2 cement-based materials industry*.
Scrivener, K.L., John, V.M. and Gartner, E.M. (2018) 'Eco-efficient cements: Potential economically viable solutions for a low-CO2 cement-based materials industry', *Cement and Concrete Research*, 114(February), pp. 2–26. doi:10.1016/j.cemconres.2018.03.015.
Scrivener, K.L. and Nonat, A. (2011) 'Hydration of cementitious materials, present and future', *Cement and Concrete Research*, 41(7), pp. 651–665. doi:10.1016/j.cemconres.2011.03.026.
Sengul, O. (2014) 'Use of electrical resistivity as an indicator for durability', *Construction and Building Materials*, 73, pp. 434–441. doi:10.1016/j.conbuildmat.2014.09.077.
Shah, V. *et al.* (2020) 'Influence of cement replacement by limestone calcined clay pozzolan on the engineering properties of mortar and concrete', *Advances in Cement Research*, 32(3), pp. 101–111. doi:10.1680/jadcr.18.00073.
Shah, V. and Bishnoi, S. (2018a) 'Analysis of Pore Structure Characteristics of Carbonated Low-Clinker Cements', *Transport in Porous Media*, 124(3), pp. 861–881. doi:10.1007/s11242-018-1101-7.
Shah, V. and Bishnoi, S. (2018b) 'Carbonation resistance of cements containing supplementary cementitious materials and its relation to various parameters of concrete', *Construction and Building Materials*, 178, pp. 219–232. doi:10.1016/j.conbuildmat.2018.05.162.
Sharma, M. *et al.* (2021) 'Limestone calcined clay cement and concrete: A state-of-the-art review', *Cement and Concrete Research*, 149(July), p. 106564. doi:10.1016/j.cemconres.2021.106564.
Shvarzman, A. *et al.* (2003) 'The effect of dehydroxylation/amorphization degree on pozzolanic activity of kaolinite', *Cement and Concrete Research*, 33(3), pp. 405–416. doi:10.1016/S0008-8846(02)00975-4.
Sirajuddin, M. and Gettu, R. (2018) 'Plastic shrinkage cracking of concrete incorporating mineral admixtures and its mitigation', *Materials and Structures/Materiaux et Constructions*, 51(2). doi:10.1617/s11527-018-1173-4.
Smaoui, N. *et al.* (2005) 'Effects of alkali addition on the mechanical properties and durability of concrete', *Cement and Concrete Research*, 35(2), pp. 203–212. doi:10.1016/j.cemconres.2004.05.007.
Snehal, K. and Das, B.B. (2020) 'Application of Andreassen and Modified Andreassen Model on Cementitious Mixture Design: A Review', in *Recent Developments in Sustainable Infrastructure*, pp. 729–750.
Snellings, R. (2016) 'Assessing, Understanding and Unlocking Supplementary Cementitious Materials', *RILEM Technical Letters*, 1, pp. 50–55. doi:10.21809/rilemtechlett.2016.12.
Snellings, R. *et al.* (2018) 'RILEM TC-238 SCM recommendation on hydration stoppage by solvent exchange for the study of hydrate assemblages', *Materials and Structures/Materiaux et Constructions*, 51(6). doi:10.1617/s11527-018-1298-5.
Snellings, R., Mertens, G. and Elsen, J. (2012) 'Supplementary Cementitious Materials', *Reviews in Mineralogy & Geochemistry*, 74, pp. 211–278. doi:10.2138/rmg.2012.74.6.
Snellings, R. and Scrivener, K.L. (2016) 'Rapid screening tests for supplementary cementitious materials: past and future', *Materials and Structures/Materiaux et*

Constructions, 49(8), pp. 3265–3279. doi:10.1617/s11527-015-0718-z.
Song, H.W. *et al.* (2006) 'Predicting carbonation in early-aged cracked concrete', *Cement and Concrete Research*, 36(5), pp. 979–989. doi:10.1016/j.cemconres.2005.12.019.
Song, S. and Jennings, H.M. (1999) 'Pore solution chemistry of alkali-activated ground granulated blast-furnace slag', *Cement and Concrete Research*, 29(2), pp. 159–170. doi:10.1016/S0008-8846(98)00212-9.
Souri, A. *et al.* (2015) 'Pozzolanic activity of mechanochemically and thermally activated kaolins in cement', *Cement and Concrete Research*, 77, pp. 47–59. doi:10.1016/j.cemconres.2015.04.017.
Stovall, T., De Larrard, F. and Buil, M. (1986) 'Linear packing density model of grain mixtures', *Powder Technology*, 48(1), pp. 1–12. doi:10.1016/0032-5910(86)80058-4.
Sui, S. *et al.* (2019) 'Towards a generic approach to durability: Factors affecting chloride transport in binary and ternary cementitious materials', *Cement and Concrete Research*, 124(July), p. 105783. doi:10.1016/j.cemconres.2019.105783.
Surana, S., Pillai, R.G. and Santhanam, M. (2017) 'Performance evaluation of field curing methods using durability index tests', *Indian Concrete Journal*, 91(7), pp. 37–50.
Tam, C.M., Tam, V.W.Y. and Ng, K.M. (2012) 'Assessing drying shrinkage and water permeability of reactive powder concrete produced in Hong Kong', *Construction and Building Materials*, 26(1), pp. 79–89. doi:10.1016/j.conbuildmat.2011.05.006.
Tanesi, J. and Ardani, A. (2012) 'Surface Resistivity Test Evaluation as an Indicator of the Chloride Permeability of Concrete (No. FHWA-HRT-13-024)', *United States. Federal Highway Administration.*, pp. 1–6.
Taylor, H.F.W. (1997) *Cement Chemistry*. 2nd edn. UK: Thomas Telford.
Thomas, M. (2013) *Supplementary Cementing Materials in Concrete*. Boca Raton: CRC Press. doi:10.1007/978-3-642-17866-5.
Tironi, A. *et al.* (2012) 'Kaolinitic calcined clays: Factors affecting its performance as pozzolans', *Construction and Building Materials*, 28(1), pp. 276–281. doi:10.1016/j.conbuildmat.2011.08.064.
Tironi, A. *et al.* (2013) 'Assessment of pozzolanic activity of different calcined clays', *Cement and Concrete Composites*, 37, pp. 319–327. doi:10.1016/j.cemconcomp.2013.01.002.
Tironi, A. *et al.* (2015) 'Blended Cements Elaborated with Kaolinitic Calcined Clays', *Procedia Materials Science*, 8, pp. 211–217. doi:10.1016/j.mspro.2015.04.066.
U.S. Geological Survey (2021) *Mineral Commodity Summaries*. Reston, Virginia.
UN (2014) *World urbanization prospects: The 2014 revision, highlights., United Nations, Department of economic and social affairs, Population Division*. New York. doi:10.4054/DemRes.2005.12.9.
UN (2016) *The Demographic Profile of African Countries, United Nations, Economic Commission for Africa, Addis Ababa*. Available at: https://www.uneca.org/sites/default/files/PublicationFiles/demographic_profile_rev_april_25.pdf.
UN (2019) *World Population Prospects, Department of Economic and Social Affairs, Population Division*. New York. Available at: http://www.ncbi.nlm.nih.gov/pubmed/12283219.

United States Department of Agriculture (2005) *Global Soil Regions Map, Natural Resources Conservations Service*. Available at: https://www.nrcs.usda.gov/wps/portal/nrcs/detail/soils/use/?cid=nrcs142p2_054013.

Vargas, J.F.G. *et al.* (2020) 'Use of Grinding Aids for Grinding Ternary Blends Portland Cement-Calcined Clay-Limestone', in *In Proceedings of the International Conference of Sustainable Production and Use of Cement and Concrete (pp. 11-21). Springer, Cham*. Springer International Publishing, p. 438. doi:10.1007/978-3-030-22034-1.

Vizcaíno-Andrés, L.M. *et al.* (2015) 'Industrial trial to produce a low clinker, low carbon cement', *Materiales de Construcción*, 65(317). doi:10.3989/mc.2015.00614.

Walenta, G. and Füllmann, T. (2004) 'Advances in quantitative XRD analysis for clinker, cements, and cementitious additions', *Powder Diffraction*, 19(1), pp. 40–44.

Wassermann, R., Katz, A. and Bentur, A. (2009) 'Minimum cement content requirements: A must or a myth?', *Materials and Structures/Materiaux et Constructions*, 42(7), pp. 973–982. doi:10.1617/s11527-008-9436-0.

WBCSD and IEA (2009) *Cement Technology Roadmap 2009: Carbon emissions reductions up to 2050*. doi:978-3-940388-47-6.

WBCSD and IEA (2018) *Technology Roadmap: Low-Carbon Transition in the Cement Industry*.

World Steel Association (2020) *World Steel in Figures*. Brussels, Belgium: World Steel Association.

World Steel Association (2021) *Press release - World steel in figures*. Brussels, Belgium: World Steel Association.

Yu, J. *et al.* (2021) 'Compressive strength and environmental impact of sustainable blended cement with high-dosage Limestone and Calcined Clay (LC2)', *Journal of Cleaner Production*, 278, p. 123616. doi:10.1016/j.jclepro.2020.123616.

Yu, Q.L., Spiesz, P. and Brouwers, H.J.H. (2013) 'Development of cement-based lightweight composites - Part 1: Mix design methodology and hardened properties', *Cement and Concrete Composites*, 44, pp. 17–29. doi:10.1016/j.cemconcomp.2013.03.030.

Yu, R., Spiesz, P. and Brouwers, H.J.H. (2014) 'Mix design and properties assessment of Ultra-High Performance Fibre Reinforced Concrete (UHPFRC)', *Cement and Concrete Research*, 56, pp. 29–39. doi:10.1016/j.cemconres.2013.11.002.

Yu, R., Spiesz, P. and Brouwers, H.J.H. (2015) 'Development of an eco-friendly Ultra-High Performance Concrete (UHPC) with efficient cement and mineral admixtures uses', *Cement and Concrete Composites*, 55, pp. 383–394. doi:10.1016/j.cemconcomp.2014.09.024.

Zajac, M. *et al.* (2014) 'Influence of limestone and anhydrite on the hydration of Portland cements', *Cement and Concrete Composites*, 46, pp. 99–108. doi:10.1016/j.cemconcomp.2013.11.007.

Zhang, M.H., Li, L. and Paramasivam, P. (2005) 'Shrinkage of high-strength lightweight aggregate concrete exposed to dry environment', *ACI Materials Journal*, 102(2), pp. 86–92. doi:10.14359/14301.

Zingg, A., Winnefeld, F., *et al.* (2008) 'Adsorption of polyelectrolytes and its influence on the rheology, zeta potential, and microstructure of various cement and hydrate phases', *Journal of Colloid and Interface Science*, 323(2), pp. 301–312.

doi:10.1016/j.jcis.2008.04.052.
Zingg, A., Holzer, L., *et al.* (2008) 'The microstructure of dispersed and non-dispersed fresh cement pastes - New insight by cryo-microscopy', *Cement and Concrete Research*, 38(4), pp. 522–529. doi:10.1016/j.cemconres.2007.11.007.
Zunino, F., Boehm-Courjault, E. and Scrivener, K. (2020) 'The impact of calcite impurities in clays containing kaolinite on their reactivity in cement after calcination', *Materials and Structures/Materiaux et Constructions*, 53(2). doi:10.1617/s11527-020-01478-9.
Zunino, F. and Scrivener, K. (2019) 'The influence of the filler effect on the sulfate requirement of blended cements', *Cement and Concrete Research*, 126(August), p. 105918. doi:10.1016/j.cemconres.2019.105918.
Zunino, F. and Scrivener, K. (2020a) 'Factors influencing the sulfate balance in pure phase C3S/C3A systems', *Cement and Concrete Research*, 133(January), p. 106085. doi:10.1016/j.cemconres.2020.106085.
Zunino, F. and Scrivener, K. (2020b) 'Increasing the kaolinite content of raw clays using particle classification techniques for use as supplementary cementitious materials', *Construction and Building Materials*, 244, p. 118335. doi:10.1016/j.conbuildmat.2020.118335.
Zunino, F. and Scrivener, K. (2021a) 'Assessing the effect of alkanolamine grinding aids in limestone calcined clay cements hydration', *Construction and Building Materials*, 266, p. 121293. doi:10.1016/j.conbuildmat.2020.121293.
Zunino, F. and Scrivener, K. (2021b) 'The reaction between metakaolin and limestone and its effect in porosity refinement and mechanical properties', *Cement and Concrete Research*, 140(August 2020), p. 106307. doi:10.1016/j.cemconres.2020.106307.

APPENDICES

Appendix I CEM II/A-L 52.5 N Received at UCT (Old vs New CEM II)

Background

A batch of CEM II A-L 52.5N ("Old" CEM II) was received in May 2019 from AfriSam Ulco factory for the LC^3 work at UCT. However, due to the limiting factors beyond our control it was not possible to utilize this cement within a reasonable period and so there was a doubt that its quality might have deteriorated. The factors included delays in receiving, grinding, and calcination of kaolinite clay samples and the prominent lockdown due to the outbreak of Covid-19. in view of this, we requested new bags of CEM II A-L 52.5N ("New" CEM II) and received in October 2020 from the same factory. This report compares salient test results of the two cements.

Particle size distribution

The particle size distribution (PSD) was determined by laser diffraction analysis using Malvern Mastersizer 2000. Since Mastersizer uses Mie theory to calculate particle size, the test involves defining optical properties of the material i.e., refractive index and absorption index. A refractive index chosen for the cement was 1.68 and absorption value chosen was 0.1 (Instruments, 2000, 2007). Ethanol was used as a dispersing liquid. The sample was added to the dispersion tank until the obscuration level is within the recommended range (10 – 20%). A good fit between the measure data and calculated data was indicated by a residual value that is below 1%. The PSD curves are shown in Figure I.1. The PSD values (d_{10}, d_{50} and d_{90}) of the two cements are presented in Table I.1.

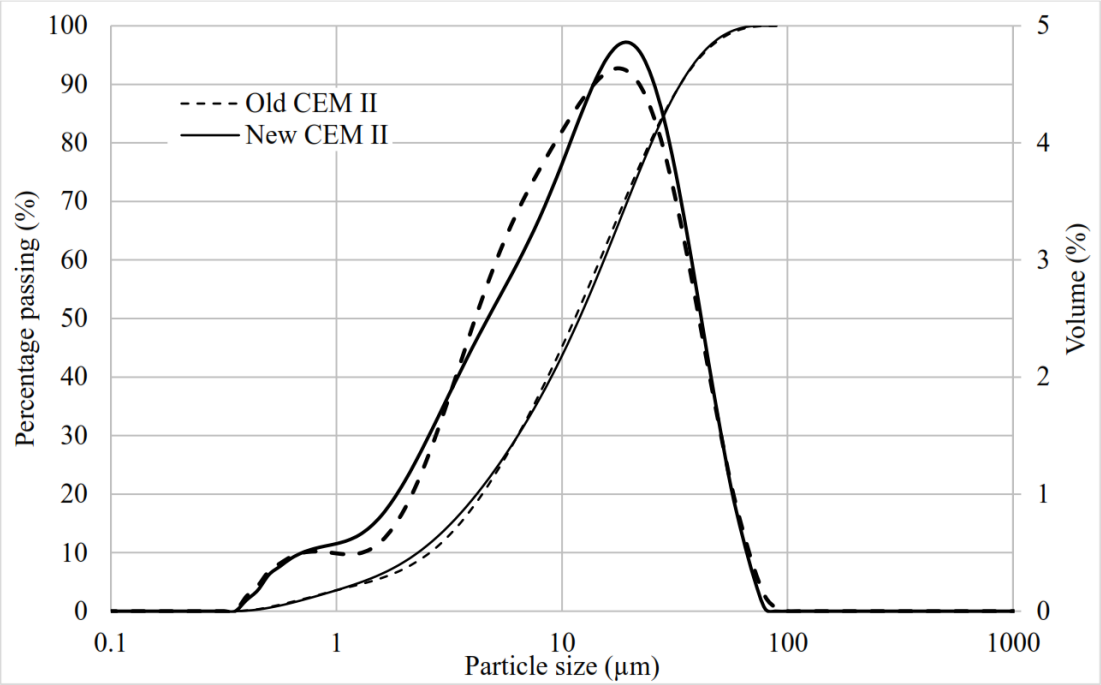

Figure I.1: PSD curves of Old and New CEM

Table I.1: PSD Values of Old and New CEM II

Material name	d_{10} (µm)	d_{50} (µm)	d_{90} (µm)
Old CEM II	2.6	11.4	33.5
New CEM II	2.3	11.9	33.5

Chemical composition

The chemical composition of each cement was obtained using Panalytical Axios wavelength dispersive XRF spectrometer. Major oxides (except H_2O- and LOI) were measured on fused disks prepared from ignited powders. H_2O- represents mass loss upon heating the sample at 110°C for 12 hours. The Loss on ignition (LOI) was determined by heating samples to 800°C for 4 hours. The XRF results are presented in Table 2.

Table I.2. Chemical composition of Old and New CEM II

Sample	**SiO_2**	**TiO_2**	**Al_2O_3**	**Fe_2O_3**	**MnO**	**MgO**	**CaO**	**Na_2O**
	wt.%	**wt.%**	**wt.%**	**wt.%**	**wt.%**	**wt.%**	**wt.%**	**wt.%**
Old CEM II	20.55	0.22	4.22	2.06	1.55	2.90	65.38	b.d.
New CEM II	20.49	0.24	4.21	2.21	1.09	1.99	63.69	b.d.

Na_2O	**K_2O**	**P_2O_5**	**SO_3**	**Cr_2O_3**	**NiO**	**H_2O-**	**LOI**	**Total**
wt.%	**wt.%**	**wt.%**	**wt.%**	**wt.%**	**wt.%**	**wt.%**	**wt.%**	**wt.%**
b.d.	0.48	0.06	2.17	b.d.	0.01	0.10	4.43	99.53
b.d.	0.42	0.05	2.00	0.01	0.01	0.10	3.07	99.44

"b.d." is an abbreviation of "below detection" meaning that the concentration of the element was too low to quantify (generally <0.01 wt.% for major elements)

Compressive strength

To reduce amount of materials for the research, mortar cubes of 50 mm size are used for optimisation purposes. 50 mm cube mortars with binder and sand in the ratio of 1:3 and w/b ratio of 0.4 were prepared. In all mixes, superplasticiser (Chryso® optima 175) was added to maintain a flow of 150 ± 5 mm (SANS 5862-2, 2006). After casting, all specimens were cured in a water tank until tested at 1, 3, 7, 28 and 90 days. The cubes were tested following guidelines given in ASTM C109/C109M-20b (2020) using an INSTRON 1000RD-E4-H2 hydraulic dynamic testing machine. Specimens were loaded without shock until failure at a uniform rate of 0.36 MPa/s. The results of the compressive strength of the mortars at 1, 3, and 7 are presented in Table 3.

Table I.3: compressive strength of cement mortar

	1 day	3 days	7 days	28 days	90 days
New CEM II (MPa)	30.0	64.2	73.5	94.1	103.7
Old CEM II (MPa)	32.3	67.3	79.8	89.7	104.8

Heat of hydration

This test was done using I-Cal 2000 HPC Isothermal calorimeter (2-channels) at 20°C. Pastes were cast using water binder ratio of 0.4. The pastes were mixed using an electric hand motor mixer for 2 minutes. 20 g of pastes were then poured in vials, sealed, and put in the calorimeter. The test was then allowed to run for 24 hours. Results for heat of hydration (HoH) and total heat are presented in Figure 2.

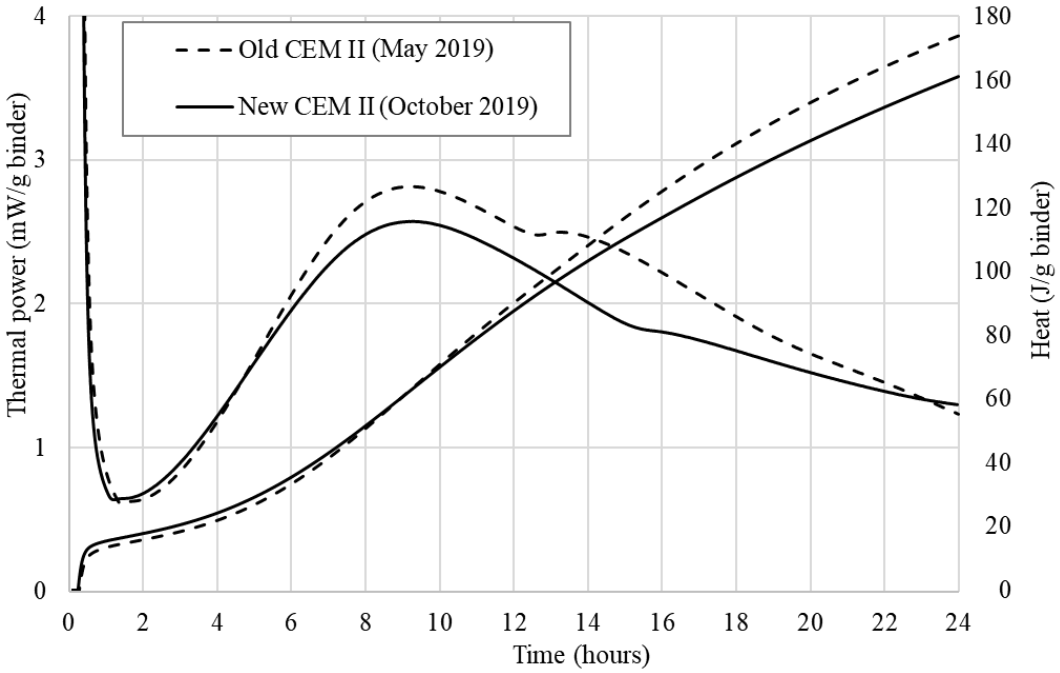

Figure I.2: HoH and total heat curves of CEM II pastes (new cement vs old cement)

Amount of limestone in the cement

Thermogravimetric analysis (TGA) was used to estimate the amount of limestone (LS) in the cement. Measurements were taken from room temperature to 1000ºC, at a heating rate of 10 ºC/min, using alumina crucibles with no lids under a 30 ml/min flow of nitrogen gas. The mass change over the calcium carbonate decomposition interval (about 600°C to 800°C) was used to estimate the amount of LS in the cement. The results are presented in Figure 4.

For the old CEM II, the mass change between 600°C and 800°C was 3.1% and for the new CEM II, the mass change was 1.7%. Using the molar masses of $C\overline{C}$ (100.09 g/mol) and CO_2 (44.01 g/mol), the amount of LS in the Old CEM II was estimated at approximate 7.0% and for the new CEM II, the amount was estimated at 4.0%.

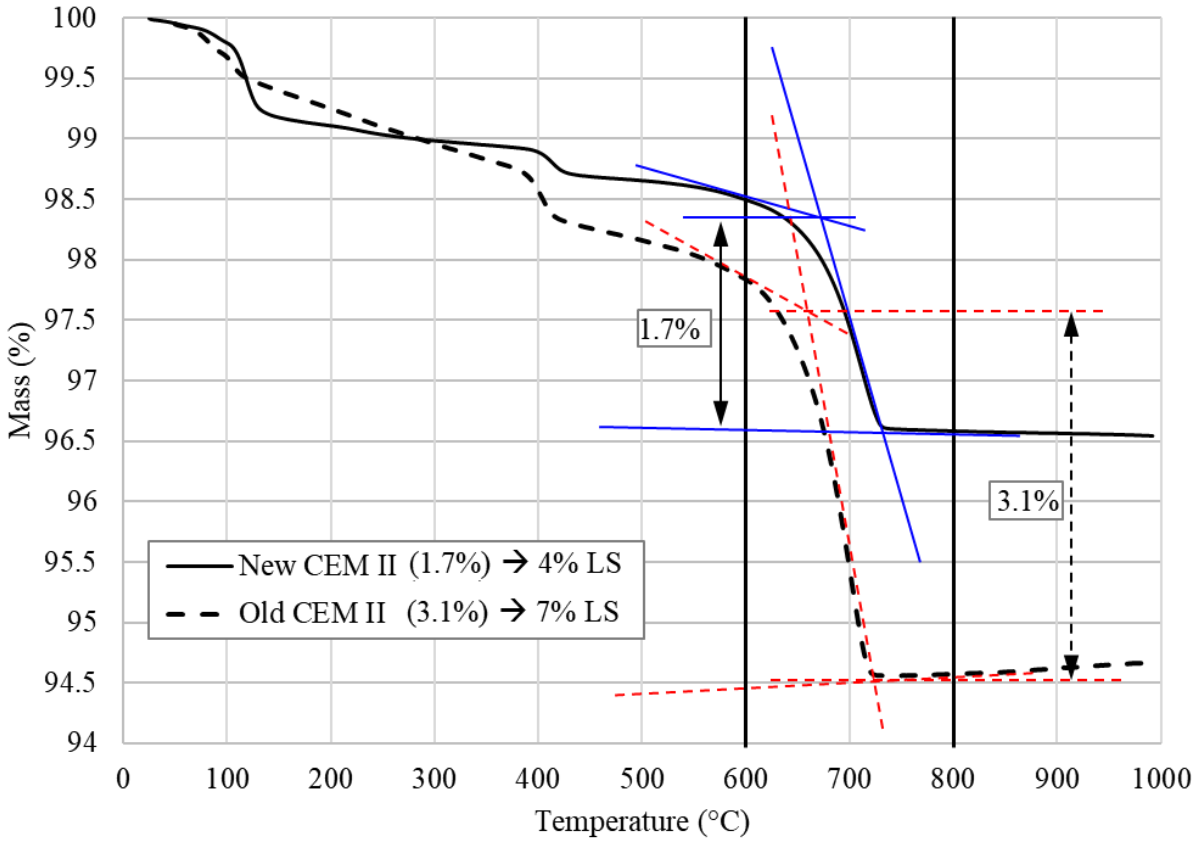

Figure I.4: TGA curves of CEM II (old versus new cement)

Conclusions

- Both old and new CEM II had similar PSD.
- XRF data also looks similar, however, the LOI for the new CEM II is lower by more than 30%.
- Both cements had maximum heat flow at about 9 hours with values approximate 2.8 mW/g for the old CEM II and 2.6 mW/g for the new CEM II. The total heat at 24 hours was about 175 J/g for the old CEM II and about 160 J/g for the new CEM II. **Note**: The maximum heat flow of the old CEM II (2nd bag opened on 1st September 2020) was 2.6 mW/g at 10.5 hours. The total heat at 24 hours was about 170 J/g.
- As expected, the compressive strength values of new CEM II mortars were lower than the values of the old CEM II mortars.
- From the TGA results, the amount of LS was estimated at 7.0% in the old CEM II and 4.0% in the new CEM II.

Appendix II Estimation of kaolinite content from TGA curve

Typical example (a case of PH-Clay)

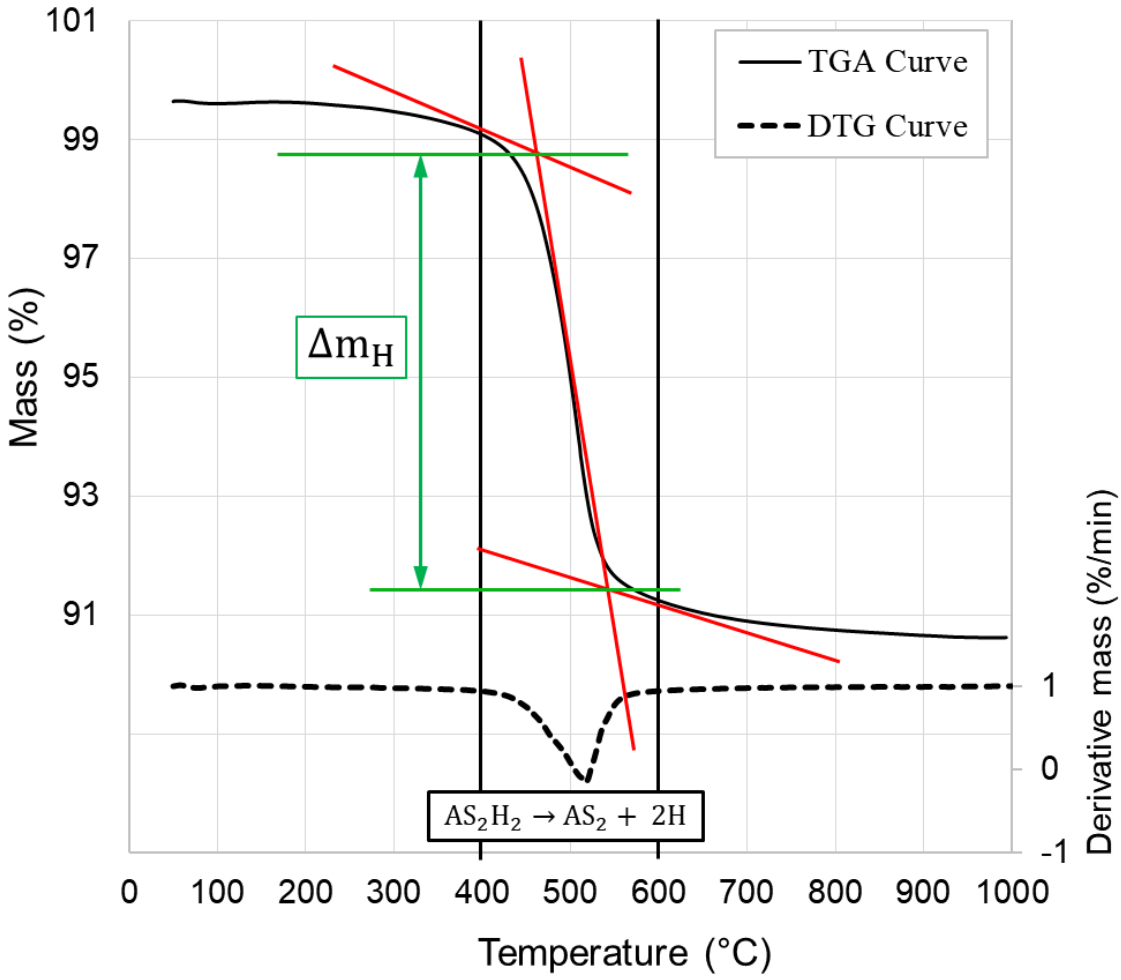

Figure II.1: TGA and DTG curves of PH-Clay

$$\text{Kaolinite K\%} = \Delta m_H \cdot \frac{M_{AS_2H_2}}{2M_H} =$$

Where; Δm_H = change of mass due to the dehydroxylation of kaolinite

$M_{AS_2H_2}$ = Molar mass of kaolinite

M_H = Molar mass of water

$$\therefore \quad \text{Kaolinite K\%} = 7.2 \cdot \frac{258.07}{2 \cdot 18.012} = 51.6\%$$

Appendix III

R^3 reactivity test results

B-Clay 850°C

	Porcelain Crucible g	Crucible + Paste (40°C) g	Crucible +Paste (105°C) g	Crucible + Paste (350°C) g	Bound water (%)			
						Average	SD	COV
1	120.63	130.63	125.65	125.24	8.17			
2	93.03	103.03	98.03	97.61	8.40	8.32	0.13	1.56
3	53.29	63.29	58.3	57.88	8.38			

B-Clay 800°C

	Porcelain Crucible g	Crucible + Paste (40°C) g	Crucible + Paste (105°C) g	Crucible + Paste (350°C) g	Bound water (%)			
						Average	SD	COV
1	91.18	101.18	96.24	95.80	8.70			
2	94.41	104.41	99.45	99.02	8.53	**8.65**	0.10	1.16
3	85.70	95.7	90.75	90.31	8.71			

B-Clay 750°C

	Porcelain Crucible g	Crucible + Paste (40°C) g	Crucible + Paste (105°C) g	Crucible + Paste (350°C) g	Bound water (%)			
						Average	SD	COV
1	98.46	108.46	103.51	103.09	8.32			
2	110.68	120.68	115.74	115.31	8.50	8.43	0.10	1.19
3	112.21	122.21	117.28	116.85	8.48			

Old H-Clay 850°C (Received already flash calcined)

	Porcelain Crucible g	Crucible + Paste (40°C) g	Crucible + Paste (105°C) g	Crucible + Paste (350°C) g	Bound water (%)			
						Average	SD	COV
1	88.96	98.96	94.00	93.69	6.15			
2	86.86	96.86	91.92	91.61	6.13	6.08	0.10	1.64
3	87.65	97.65	92.68	92.38	5.96			

Old H-Clay 850°C

	Porcelain Crucible g	Crucible + Paste (40°C) g	Crucible + Paste (105°C) g	Crucible + Paste (350°C) g	Bound water (%)			
						Average	SD	COV
1	86.85	96.85	91.91	91.63	5.53			
2	87.64	97.64	92.70	92.43	5.34	5.46	0.1	1.83
3	88.96	98.96	94.05	93.77	5.50			

Old H-Clay 800°C

	Porcelain Crucible g	Crucible + Paste (40°C) g	Crucible + Paste (105°C) g	Crucible + Paste (350°C) g	Bound water (%)			
						Average	SD	COV
1	98.95	108.95	104.00	103.69	6.14			
2	85.69	95.69	90.77	90.46	6.10	**6.13**	0.02	0.33
3	53.28	63.28	58.33	58.02	6.14			

Old H-Clay 750°C

	Porcelain Crucible g	Crucible + Paste (40°C) g	Crucible + Paste (105°C) g	Crucible + Paste (350°C) g	Bound water (%)			
						Average	SD	COV
1	90.30	100.30	95.35	95.04	6.14			
2	96.02	106.02	101.10	100.79	6.10	6.05	0.12	1.98
3	55.83	65.83	60.90	60.60	5.92			

New H-Clay (Received already flash calcined at 850°C)

	Porcelain Crucible g	Crucible + Paste (40°C) g	Crucible + Paste (105°C) g	Crucible + Paste (350°C) g	Bound water (%)			
						Average	SD	COV
1	98.98	108.98	103.88	103.63	5.10			
2	94.40	104.4	99.33	99.08	5.07	5.09	0.02	0.39
3	55.82	65.82	60.72	60.47	5.10			

G-Clay 850°C

	Porcelain Crucible g	Crucible + Paste (40°C) g	Crucible + Paste (105°C) g	Crucible + Paste (350°C) g	Bound water (%)			
						Average	SD	COV
1	120.63	130.63	125.97	125.77	3.75			
2	110.68	120.68	116.36	116.14	3.87	3.80	0.06	1.58
3	112.21	122.21	117.52	117.32	3.77			

G-Clay 800°C

	Porcelain Crucible g	Crucible + Paste (40°C) g	Crucible + Paste (105°C) g	Crucible + Paste (350°C) g	Bound water (%)			
						Average	SD	COV
1	102.46	112.46	107.78	107.57	3.95			
2	109.21	119.21	114.54	114.33	3.94	4.02	0.12	2.99
3	53.28	63.28	58.57	58.35	4.16			

G-Clay 750°C

	Porcelain Crucible g	Crucible + Paste (40°C) g	Crucible + Paste (105°C) g	Crucible + Paste (350°C) g	Bound water (%)			
						Average	SD	COV
1	98.45	108.45	103.87	103.64	4.24			
2	93.04	103.04	98.49	98.27	4.04	**4.19**	0.13	3.1
3	55.83	65.83	61.19	60.96	4.29			

PH-Clay 850°C

	Porcelain Crucible g	Crucible + Paste (40°C) g	Crucible + Paste (105°C) g	Crucible + Paste (350°C) g	Bound water (%)			
						Average	SD	COV
1	90.30	100.30	94.72	94.54	4.07			
2	85.69	95.69	90.60	90.40	4.07	4.08	0.01	0.25
3	98.96	108.96	103.85	103.65	4.09			

PH-Clay 800°C

	Porcelain Crucible g	Crucible + Paste (40°C) g	Crucible + Paste (105°C) g	Crucible + Paste (350°C) g	Bound water (%)			
						Average	SD	COV
1	98.95	108.95	103.99	103.73	5.16			
2	88.96	98.96	94.00	93.74	5.16	**5.17**	0.02	0.39
3	53.27	63.27	58.27	58.01	5.20			

PH-Clay 750°C

	Porcelain Crucible g	Crucible + Paste (40°C) g	Crucible + Paste (105°C) g	Crucible + Paste (350°C) g	Bound water (%)			
						Average	SD	COV
1	88.96	98.96	93.89	93.66	4.67			
2	98.96	108.96	103.94	103.71	4.62	4.65	0.03	0.65
3	55.82	65.82	60.77	60.54	4.65			

PS-Clay 850°C

	Porcelain Crucible g	Crucible + Paste (40°C) g	Crucible + Paste (105°C) g	Crucible + Paste (350°C) g	Bound water (%)			
						Average	SD	COV
1	53.27	63.27	58.20	57.98	4.46			
2	88.97	98.97	93.90	93.67	4.67	4.59	0.11	2.40
3	96.04	106.04	101.01	100.78	4.63			

PS-Clay 800°C

	Porcelain Crucible g	Crucible + Paste (40°C) g	Crucible + Paste (105°C) g	Crucible + Paste (350°C) g	Bound water (%)			
						Average	SD	COV
1	85.69	95.69	90.68	90.43	5.01			
2	90.30	100.30	95.33	95.07	5.17	**5.04**	0.12	2.38
3	55.82	65.82	60.88	60.63	4.94			

PS-Clay 750°C

	Porcelain Crucible g	Crucible + Paste (40°C) g	Crucible + Paste (105°C) g	Crucible + Paste (350°C) g	Bound water (%)			
						Average	SD	COV
1	85.68	95.68	90.67	90.44	4.61			
2	90.31	100.31	95.27	95.04	4.64	4.60	0.05	1.09
3	53.27	63.27	58.34	58.11	4.54			

HC-Clay 850°C

	Porcelain Crucible g	Crucible + Paste (40°C) g	Crucible + Paste (105°C) g	Crucible + Paste (350°C) g	Bound water (%)			
						Average	SD	COV
1	86.87	96.87	91.77	91.52	5.10			
2	98.96	108.96	103.85	103.60	5.11	5.05	0.09	1.78
3	87.71	97.71	92.76	92.51	4.95			

HC-Clay 800°C

	Porcelain Crucible g	Crucible + Paste (40°C) g	Crucible + Paste (105°C) g	Crucible + Paste (350°C) g	Bound water (%)			
						Average	SD	COV
1	90.31	100.31	95.37	95.06	6.13			
2	96.04	106.04	101.04	100.73	6.20	**6.15**	0.05	0.81
3	55.82	65.82	60.89	60.58	6.11			

HC-Clay 750°C

	Porcelain Crucible g	Crucible + Paste (40°C) g	Crucible + Paste (105°C) g	Crucible + Paste (350°C) g	Bound water (%)			
						Average	SD	COV
1	85.69	95.69	90.66	90.36	6.04			
2	88.96	98.96	93.96	93.66	6.00	6.00	0.04	0.67
3	53.27	63.27	58.30	58.00	5.96			

Appendix IV

Sulphate adjustment

Table 1: Addition of sulphate to achieve the required amount in the system

Mix	SO_3 [1] (%)						**SO_3 added from Gypsum [2] (%)**	SO_3 [3] ∑ (%) (Required)
	Calcined clay				LS-K5	New-CEM II		
	B	New-H	PH	HC				
LC[3]-65(B:25/10)	0.04	-	-	-	0.02	2.0	0.44	1.80 [3]
LC[3]-55(B:35/10)	0.04	-	-	-			0.64	1.800
LC[3]-45(B:40/15)	0.04	-	-	-			0.84	1.80
LC[3]-65(H:25/10)	-	0.01	-	-			0.00	1.34(>1.20)
LC[3]-55(H:35/10)	-	0.01	-	-			0.05	1.20
LC[3]-45(H:40/15)	-	0.01	-	-			0.26	1.20
LC[3]-55(PH:35/10)	-	-	< 0.01	-			0.85	2.00
LC[3]-55(HC:35/10)	-	-	-	< 0.01			0.85	2.00

Notes

[1]Data from Table 5.1 (Chapter 5)

[2]Percentage by total mass of binder

New CEM II has 4% LS and 96% Clinker

[3]∑=+ 25%(0.04) + [10%-65%/(1-4%) + 65%)](0.02) + [(65%)/(1-4%)](2)) + 0.44 = 1.8

Appendix V Concrete mix design (CCSA and MAAM)

Example [Case of LC^3-55(B:35/10)]

The CCSA method was used as a starting step

Table V.1: Characteristics of materials

Material name	RD	d_{10} (µm)	d_{50} (µm)	d_{90} (µm)	FM	CBD (kg/m^3)
B-Clay 800°C	2.61	2.3	5.9	16.5	-	-
LK-K5	2.70	3.6	8.2	16.4	-	-
New-CEM II	2.96	2.3	11.9	33.5	-	-
Dune sand	2.64	-	-	-	2.09	-
Crushed sand (granite)	2.65	-	-	-	3.67	-
Granite 19 mm	2.65	-	-	-	8.93	1560

Note: As shown in Appendix II, New CEM II/A-L 52.5 N has already 4% LS

$To\ have\ 55\%\ clinker\ in\ LC^3-55(B{:}35/10), 55\%/(1-4\%) = 57.3\%\ CEM\ II\ is\ required$

$To\ have\ 10\%\ LS\ in\ LC^3-55(B{:}35/10), 10\%-(57.3-55)\% = 7.7\%\ LS\ more\ is\ required$

$$RD_{binder} = \frac{100}{\left(\frac{57.3}{2.96}\right)+\left(\frac{35}{2.61}\right)+\left(\frac{7.7}{2.70}\right)} = 2.81$$

$$RD_{sand} = \frac{100}{\left(\frac{50}{2.64}\right)+\left(\frac{50}{2.65}\right)} = 2.645\ (Try\ 50\%\ Dune\ sand\ and\ 50\%\ crusher\ sand)$$

Table V.2: Fineness modulus

	Dune sand			Crusher sand			50% Dune + 50% Crusher		
Sieve size	Particles retained		Cumulative	Particles retained		Cumulative	Particles retained		Cumulative
	Mass (g)	%	%	Mass (g)	%	%	Mass (g)	%	%
9500	0.00	0.00	0.00	0.00	0.00	0.00	0.00	0.00	0.00
6700	0.00	0.00	0.00	0.00	0.00	0.00	0.00	0.00	0.00
4750	0.00	0.00	0.00	20.31	5.00	5.00	20.31	2.22	2.22
2360	0.00	0.00	0.00	130.56	32.11	37.11	130.56	14.27	16.49
1180	14.14	2.78	2.78	98.06	24.12	61.23	112.20	12.27	28.76
600	179.28	35.28	38.07	66.24	16.29	77.52	245.52	26.84	55.60
300	164.66	32.41	70.47	46.87	11.53	89.05	211.53	23.13	78.73
150	135.89	26.74	97.22	34.40	8.46	97.51	170.29	18.62	97.34
75	14.15	2.78	100.00	10.14	2.49	100.00	24.29	2.66	100.00
	508.12			406.58			914.70		
			FM = 2.09			FM = 3.67			FM = 2.79

w/b ratio = 0.4

To reduce powder content, the target was to have a mix with water content as low as possible. In this case, trials were made with different amount of water (at an interval of 5 kg/m^3 starting from 125 kg/m^3) while maintaining the selected proportions of binders and w/b ratio.

$$M_{binder} = \frac{water\ content}{w/b} = \frac{125}{0.4} \approx 312\ kg/m^3$$

K = 1 (Fulton 2021, Table 7.6)

$$M_{stone} = CBD(K - 0.1FM = 1560(1 - 0.1 \cdot 2.79) \approx 1125\ kg/m^3$$

$$M_{sand} = 2.645\ \cdot 1000\left[1 - \left(\frac{312}{2.81 \cdot 1000} + \frac{1125}{2.65 \cdot 1000} + \frac{125}{1000}\right)\right] \approx 898\ kg/m^3$$

Therefore, the quantities are

$M_{binder} = 310\ kg/m^3$

$$M_{clinker} = 55\% \cdot 312\ \approx 172\ kg/m^3\ \textbf{or}\ M_{CEM\ II}$$
$$= 57.3\% \cdot 312\ \approx 179\ kg/m^3$$
$$M_{CC} = 35\% \cdot 312\ \approx 109\ kg/m^3$$
$$M_{LS\ (total)} = 10\% \cdot 312\ \approx 31\ kg/m^3\ \textbf{or}\ M_{LS\ (add)}$$
$$= 7.7\% \cdot 312\ \approx 24\ kg/m^3$$

$M_{sand} = 860\ kg/m^3$

$$M_{Dune} = 50\% \cdot 898\left(\frac{2.64}{2.65}\right) \approx 447\ kg/m^3$$
$$M_{Crusher} = 50\% \cdot 898\left(\frac{2.65}{2.64}\right) \approx 451\ kg/m^3$$

$M_{stone} = 1125\ kg/m^3$

As a second step, MAAM (using EMMA software available for free on Elkem website) was used to optimize packing of the materials. In this case, PSD modulus (q) and water to binder ratio (w/b) were fixed at 0.3 and 0.4, respectively. Other inputs were the particle density, quantity, and PSD of each material and maximum and minimum particle size in the mixture. All mixes were optimized by adjusting the quantity of the materials to better fit the modified Andreassen curve with q = 0.3. The quantity of each material was adjusted while maintaining the required proportions of CC, LS, and clinker. Table 3 present quantity

of the materials with water content fixed at 125 kg/m^3. Table 4 present quantity of the materials with water content at 140 and 160 kg/m^3. Figure 1 to Figure 4 shows how closely the grading of the optimised mixtures (blue curve) matches the ideal curve (red curve).

The obtained proportions were then adjusted by carrying out trial mixes, and the target was to get a workability with a slump of 100 ± 20 mm and a SP (Chryso@ Optima 175) dosage limit of 1.5%. After several trials, it was decided to maintain the amount of water at 160 kg/m^3 and amount of stone at 1000 kg/m^3 for all the concrete mixes (**Case C**). However, with the HC-Clay, it was only possible to achieve a slump of 45 mm at a SP dosage of 2% in the case of 0.55 w/b ratio.

Table V.3: Quantity of materials with water content fixed at 125 kg/m^3

Material name	Quantity (kg/m^3)		
	Case A (Figure 1)	**Case B** (Figure 2)	Notes
Water	**125**	**125**	Fixed proportions [LC^3-55(B:35/10)]
B-Clay 800°C	109	109	Fixed PSD,
LK-K5	24	24	Fixed minimum size
New-CEM II	179	179	Can only be adjusted by adjusting w/b ratio
Dune sand	447	**510**	Fixed PSD
Crushed sand (granite)	451	**512**	Fixed maximum size
Granite 19 mm	1125	**1000**	Quantities can be adjusted

Table V.4: Quantity of materials with water content at 140 and 160 kg/m^3

Material name	Quantity (kg/m^3)	
	Case C (Figure 3)	**Case D (**Figure 4)
Water	**140**	**160**
B-Clay 800°C	123	140
LK-K5	27	31
New-CEM II	201	229
Dune sand	472	422
Crushed sand (granite)	474	424
Granite 19 mm	**1000**	**1000**

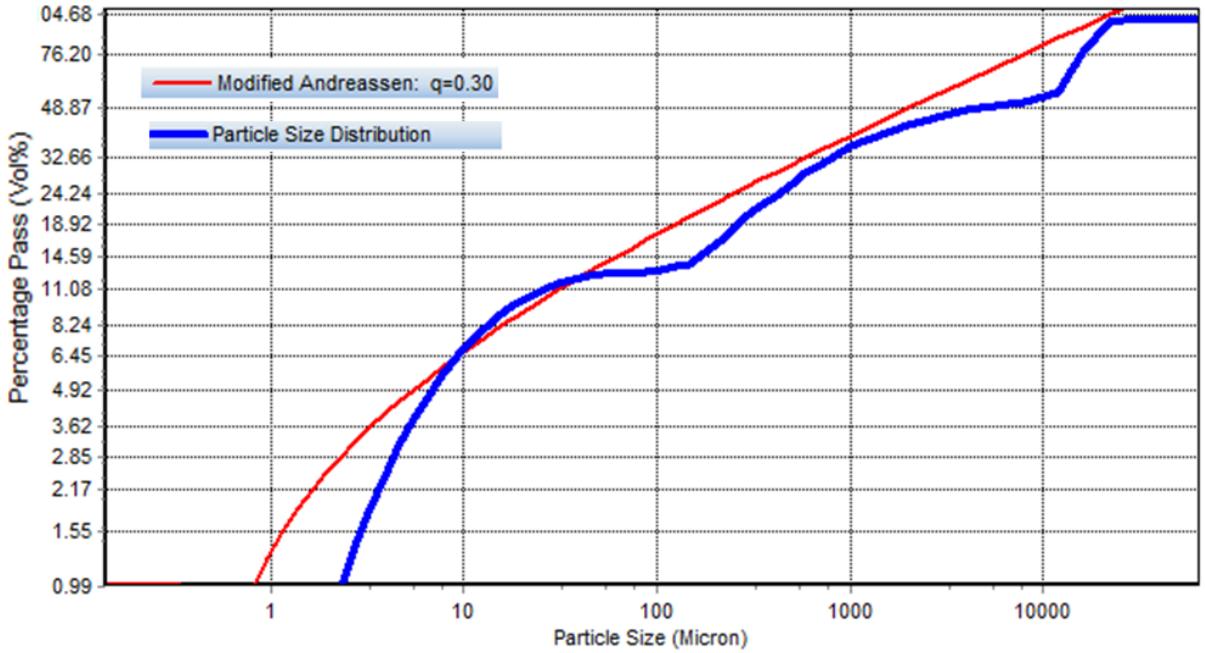

Figure V.1: Case A (Table 2)

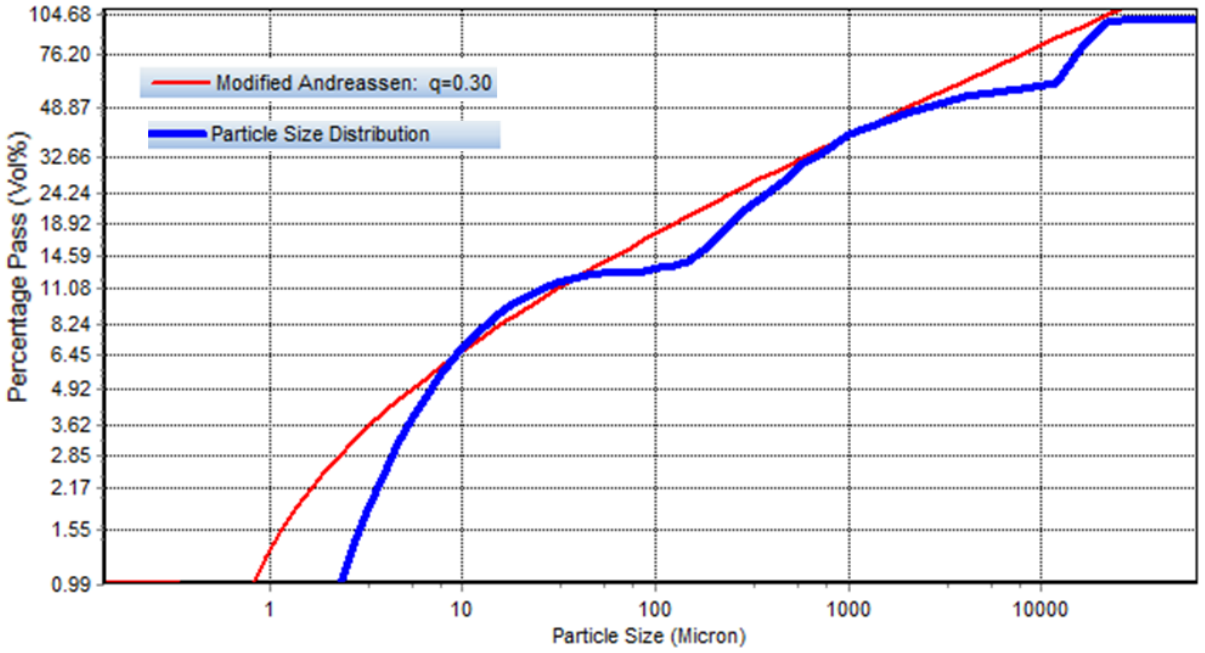

Figure V.2: Case B (Table 2) after reducing amount of stone to 1000 kg/m^3

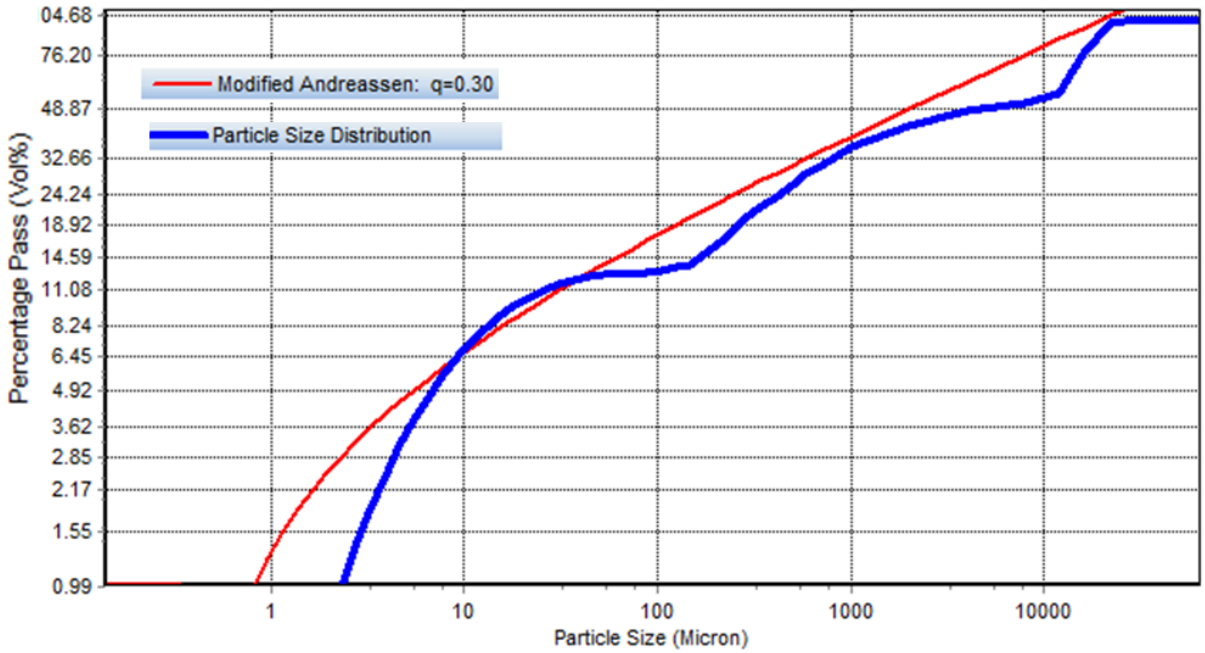

Figure V.3: Case C (Table 4) after increasing amount of water to 140 kg/m^3

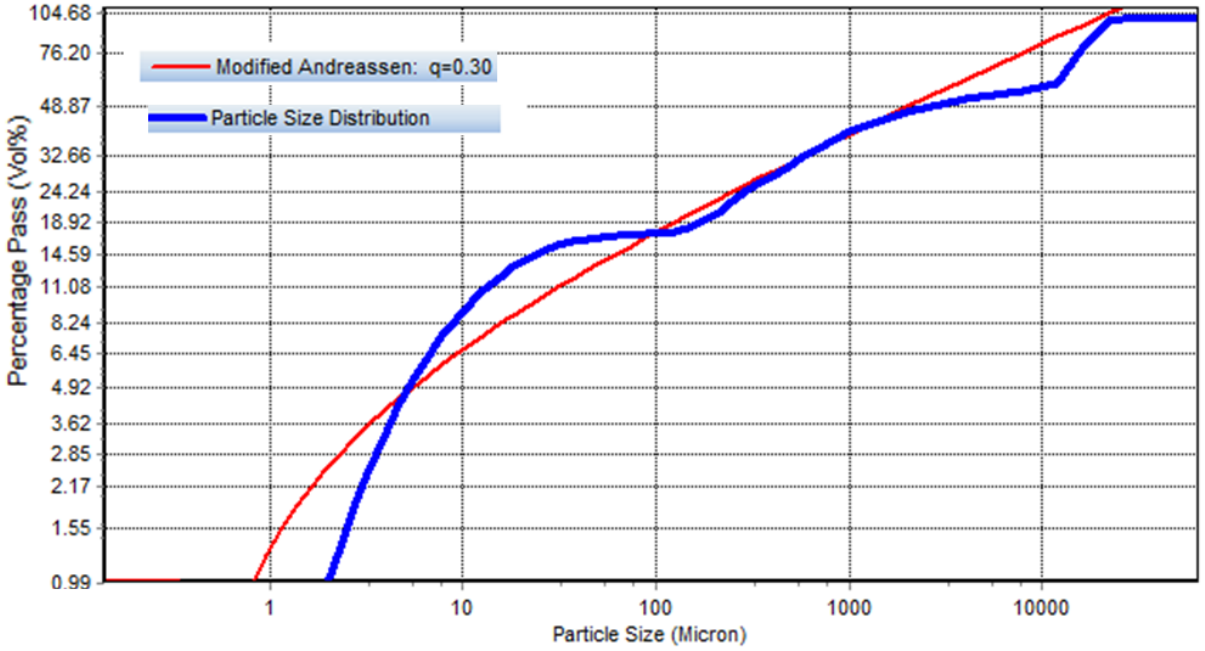

Figure V.4: Case D (Table 4) after increasing amount of water to 160 kg/m^3

Appendix VI Mapping pseudo proportion to real proportion

Example (**Case of point A**)

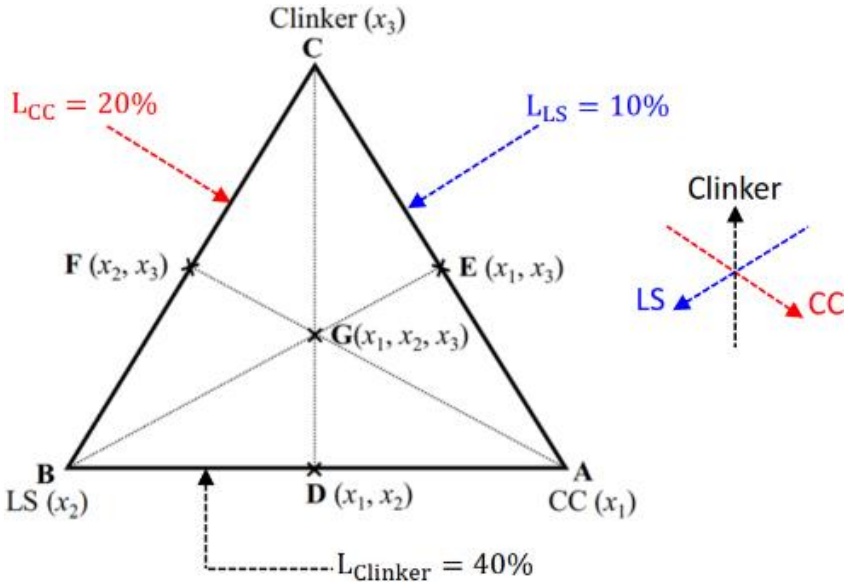

Figure VI.1: Mixture design region

Table VI.1: Required proportions of calcined clay, limestone, and clinker for optimisation

Point	Pseudo proportions (x_i^P)			Σ	Real proportions (x_i^R)			Σ
	CC	LS	Clinker		CC	LS	Clinker	
A	**1**	**0**	**0**	**1**	**0.50**	**0.10**	**0.40**	**1**

$$x_i^R = x_i^p\left(1 - \sum_{i=1}^{3} L_i\right) + L_i \quad ; \qquad L_i = \text{Lower boundary for factor i}$$

$$x_{CC}^R = x_{CC}^p\left(1 - \sum_{i=1}^{3} L_i\right) + L_{CC} = 1 \cdot (1 - (0.2 + 0.1 + 0.4) + 0.2 = \mathbf{0.5}$$

$$x_{LS}^R = x_{LS}^p\left(1 - \sum_{i=1}^{3} L_i\right) + L_{LS} = 0 \cdot (1 - (0.2 + 0.1 + 0.4) + 0.1 = \mathbf{0.1}$$

$$x_{Clinker}^R = x_{Clinker}^p\left(1 - \sum_{i=1}^{3} L_i\right) + L_{Clinker} = 0 \cdot (1 - (0.2 + 0.1 + 0.4) + 0.4 = \mathbf{0.4}$$

Appendix VII Concrete test results

Table VII.1: Compressive strength results (0.4 w/b ratio)

Mix	Days	Compressive strength (MPa)					Mass (g)			Unit Weight (kN/m^3)
		1	2	3	Average	SD	1	2	3	
R1	1	32.93	32.90	32.52	32.80	0.23	2480	2445	2450	24.58
	3	55.40	54.69	55.58	55.20	0.47	2420	2465	2420	24.35
	7	64.31	67.42	65.07	65.60	1.62	2490	2490	2420	24.67
	28	76.20	75.70	76.41	76.10	0.36	2485	2475	2460	24.73
	90	80.80	83.37	81.68	82.00	1.31	2460	2460	2470	24.63
R2	**1**	13.12	13.44	13.35	13.30	0.17	2460	2470	2415	24.48
	3	33.95	32.70	35.27	34.00	1.29	2460	2405	2415	24.27
	7	53.79	52.33	53.37	53.20	0.75	2475	2455	2450	24.60
	28	71.60	71.50	72.02	71.70	0.28	2485	2490	2470	24.82
	90	80.30	81.83	79.22	80.50	1.31	2445	2440	2420	24.35
LC^3-55 (B:35/10)	**1**	23.28	22.79	22.55	22.90	0.37	2415	2400	2415	24.10
	3	50.15	49.30	48.67	49.40	0.74	2420	2410	2400	24.10
	7	69.29	66.26	66.77	67.40	1.62	2415	2435	2475	24.42
	28	76.08	75.58	73.19	75.00	1.54	2445	2415	2455	24.38
	90	78.43	82.32	80.53	80.40	1.95	2430	2480	2460	24.57
LC^3-55 (H:35/10)	**1**	18.73	18.40	18.12	18.40	0.31	2410	2415	2410	24.12
	3	34.07	33.93	34.93	34.30	0.54	2435	2425	2460	24.40
	7	52.94	52.90	52.16	52.70	0.44	2415	2430	2425	24.23
	28	67.24	66.22	66.23	66.60	0.59	2450	2435	2415	24.33
	90	73.07	73.46	72.08	72.90	0.71	2420	2440	2445	24.35
LC^3-55 (PH:35/10)	**1**	26.28	26.40		26.30	0.08	2410	2440		24.25
	3	55.81	57.26	54.81	56.00	1.23	2420	2450	2420	24.30
	7	68.12	72.94	71.61	70.90	2.49	2435	2425	2470	24.43
	28	74.10	75.37	75.35	74.90	0.73	2415	2455	2435	24.35
	90	81.61	80.09	79.09	80.30	1.27	2455	2435	2460	24.50
LC^3-65 (B:25/10)	**1**	27.82	28.90		28.40	0.76	2465	2445		24.55
	3	49.77	47.37	51.76	49.60	2.20	2430	2415	2455	24.33
	7	66.23	67.56	70.65	68.10	2.27	2430	2445	2445	24.40
	28	76.07	78.34	79.06	77.80	1.56	2435	2475	2440	24.50
	90	80.49	82.37	81.22	81.40	0.95	2445	2415	2450	24.37

LC^3-65 (H:25/10)	**1**	22.41	22.05	21.60	22.00	0.41	2475	2410	2400	24.28
	3	42.47	42.38	41.62	42.20	0.47	2425	2460	2465	24.50
	7	55.58	59.15	57.81	57.50	1.80	2465	2475	2485	24.75
	28	74.84	73.49	71.41	73.20	1.73	2465	2460	2445	24.57
	90	76.71	78.59	79.37	78.20	1.37	2455	2490	2470	24.72
LC^3-45 (H:40/15)	**1**	13.95	13.62		13.80	0.23	2420	2430		24.25
	3	27.14	27.06	26.71	27.00	0.23	2435	2460	2405	24.33
	7	46.06	48.22	45.37	46.60	1.49	2495	2435	2440	24.57
	28	62.06	62.18	65.05	63.10	1.69	2405	2435	2450	24.30
	90	67.95	69.53	68.58	68.70	0.80	2425	2440	2445	24.37
LC^3-45 (B:40/15)	**1**	19.63	19.49		19.60	0.10	2410	2425		24.18
	3	40.68	41.76	42.72	41.70	1.02	2395	2405	2455	24.18
	7	60.35	62.71	59.95	61.00	1.49	2420	2415	2395	24.10
	28	68.30	66.80	68.28	67.80	0.86	2425	2400	2415	24.13
	90	69.78	69.71	72.14	70.50	1.38	2440	2440	2410	24.30

Table VII.2: Compressive strength results (0.55 w/b ratio)

Mix	Days	Compressive strength (MPa)					Mass (g)			Unit Weight (kN/m^3))
		1	2	3	Average	SD	1	2	3	
R1	1	21.59	19.88		20.70	1.21	2470	2440		24.55
	3	38.52	39.64	39.00	39.10	0.56	2440	2505	2450	24.65
	7	47.42	50.65	50.23	49.40	1.76	2470	2485	2465	24.73
	28	58.65	60.87	57.53	59.00	1.70	2445	2470	2435	24.50
	90	65.64	67.23	65.36	66.10	1.01	2470	2460	2460	24.63
LC^3-55 (B:35/10)	**1**	13.20	12.34		12.80	0.61	2430	2390		24.10
	3	27.83	27.09	28.61	27.80	0.76	2450	2400	2455	24.35
	7	48.75	49.88	49.13	49.30	0.58	2440	2395	2400	24.12
	28	59.83	57.87	57.39	58.40	1.29	2410	2400	2410	24.07
	90	64.55	63.15	63.38	63.70	0.75	2435	2420	2445	24.33
LC^3-55 (H:35/10)	**1**	9.30	9.86		9.60	0.40	2400	2410		24.05
	3	18.90	19.61	19.68	19.40	0.43	2395	2410	2425	24.10
	7	34.91	33.54	32.86	33.80	1.04	2450	2435	2430	24.38
	28	48.70	50.24	47.72	48.90	1.27	2410	2425	2410	24.15
	90	53.53	55.30	54.58	54.50	0.89	2425	2440	2445	24.37
LC^3-55 (HC:35/10)	**1**	16.14	16.13		16.10	0.01	2435	2450		24.43
	3	32.48	34.54	34.11	33.70	1.09	2395	2430	2405	24.10
	7	48.96	48.05	46.97	48.00	1.00	2445	2420	2410	24.25
	28	52.07	50.95	50.55	51.20	0.79	2410	2430	2410	24.17
	90	56.02	57.68	57.73	57.10	0.97	2435	2430	2450	24.38

Table VII.3: Elastic modulus test results (0.4 w/b ratio)

Mix	Days	Elastic modulus (GPa)					Mass (g)			Unit Weight (kN/m^3)
		1	2	3	Average	SD	1	2	3	
R1	7	40.3	41.2	43.4	41.6	1.6	3805	3765	3800	24.1
	28	44.0	44.5	45.5	44.7	0.8	3810	3770	3805	24.2
	90	47.7	48.6	49.0	48.4	0.7	3815	3780	3810	24.2
R2	**7**	37.0	37.2	36.3	36.8	0.5	3745	3755	3735	23.9
	28	42.6	43.0	41.7	42.4	0.7	3750	3760	3740	23.9
	90	45.6	48.1	47.3	47.0	1.3	3755	3760	3745	23.9
LC^3-55 (B:35/10)	**7**	39.8	40.1	40.3	40.1	0.3	3730	3725	3720	23.7
	28	42.1	43.2	42.2	42.5	0.6	3735	3730	3720	23.8
	90	44.5	44.7	44.3	44.5	0.2	3735	3730	3725	23.8
LC^3-55 (H:35/10)	**7**	37.0	37.7	36.3	37.0	0.7	3700	3720	3715	23.6
	28	42.0	44.3	42.0	42.8	1.3	3705	3725	3720	23.7
	56	45.0	45.5	44.8	45.1	0.4	3705	3725	3720	23.7
LC^3-55 (PH:35/10)	**7**	40.2	41.2	38.8	40.1	1.2	3705	3740	3720	23.7
	28	42.6	43.5	40.7	42.3	1.5	3705	3740	3720	23.7
	90	43.8	44.5	43.8	44.0	0.4	3710	3740	3725	23.7
LC^3-65 (B:25/10)	**7**	39.6	40.8	43.0	41.1	1.7	3750	3740	3735	23.8
	28	44.8	43.8	46.5	45.0	1.4	3755	3745	3740	23.9
	90	45.7	45.2	48.3	46.4	1.7	3750	3740	3735	23.8
LC^3-65 (H:25/10)	**7**	38.0	39.2	36.9	38.0	1.2	3770	3740	3735	23.9
	28	42.4	45.0	43.2	43.6	1.4	3775	3745	3745	23.9
	90	44.4	48.2	45.6	46.0	2.0	3780	3750	3750	24.0
LC^3-45 (H:40/15)	**7**	37.0	37.7	36.3	37.0	0.7	3690	3695	3700	23.5
	28	41.0	43.1	41.6	41.9	1.1	3690	3695	3705	23.6
	90	44.9	45.2	44.4	44.8	0.4	3690	3700	3705	23.6
LC^3-45 (B:40/15)	**7**	38.8	40.4	39.5	39.6	0.8	3690	3715	3705	23.6
	28	41.6	42.6	42.1	42.1	0.5	3690	3715	3710	23.6
	90	42.4	44.8	43.2	43.5	1.2	3690	3715	3710	23.6

Table VII.4: Elastic modulus test results (0.55 w/b ratio)

Mix	Days	Elastic modulus (GPa)					Mass (g)			Unit Weight (kN/m^3)
		1	2	3	Average	SD	1	2	3	
R1	**7**	41.7	39.9	38.3	39.9	1.7	3730	3735	3720	23.8
	28	42.9	42.4	42.2	42.5	0.4	3735	3740	3725	23.8
	90	47.4	47.7	46.5	47.2	0.6	3740	3745	3730	23.8
LC^3-55 (B:35/10)	**7**	36.4	40.4	38.3	38.4	2.0	3645	3610	3690	23.2
	28	39.0	41.0	40.3	40.1	1.0	3645	3615	3690	23.3
	90	41.9	43.1	43.3	42.8	0.8	3645	3615	3690	23.3
LC^3-55 (H:35/10)	**7**	34.2	35.1	33.4	34.3	0.8	3685	3660	3650	23.3
	28	40.2	40.1	39.4	39.9	0.4	3690	3665	3655	23.4
	90	44.1	44.1	43.2	43.8	0.5	3690	3670	3660	23.4
LC^3-55 (HC:35/10)	**7**	38.9	38.6	37.9	38.5	0.5	3675	3635	3665	23.3
	28	39.5	39.7	38.8	39.3	0.5	3675	3635	3665	23.3
	90	42.0	43.6	42.9	42.8	0.8	3675	3635	3665	23.3

Table VII.5: Free shrinkage test results (0.4 w/b ratio)

Mix	Days	Shrinkage readings (mm)			Shrinkage strain		Mass (g)			Unit Weight (kN/m^3)
		1	2	3	Average (%)	SD (%)	1	2	3	
R1	0	0.000	0.000	0.000	0.0000	0.0000	3885	3905	3845	24.62
	1	0.022	0.021	0.024	0.0080	0.0005	3870	3890	3830	24.53
	4	0.050	0.054	0.049	0.0182	0.0009	3860	3880	3820	24.47
	7	0.062	0.057	0.049	0.0200	0.0023	3855	3875	3820	24.44
	14	0.078	0.077	0.069	0.0267	0.0018	3855	3875	3815	24.43
	28	0.095	0.092	0.082	0.0320	0.0024	3850	3870	3810	24.40
	56	0.098	0.101	0.088	0.0404	0.0024	3840	3860	3805	24.35
	112	0.144	0.154	0.133	0.0513	0.0038	3830	3850	3795	24.29
	224	0.158	0.168	0.155	0.0573	0.0024	3825	3845	3785	24.24
R2	0	0.000	0.000	0.000	0.0000	0.0000	3840	3795	3805	24.21
	1	0.014	0.017	0.013	0.0052	0.0007	3830	3780	3795	24.14
	4	0.022	0.029	0.026	0.0092	0.0013	3825	3775	3790	24.11
	7	0.030	0.036	0.030	0.0114	0.0012	3825	3775	3790	24.11
	14	0.049	0.060	0.059	0.0200	0.0022	3820	3770	3785	24.07
	28	0.058	0.073	0.069	0.0238	0.0028	3815	3765	3780	24.04
	56	0.073	0.077	0.079	0.0307	0.0011	3810	3760	3775	24.01
	112	0.101	0.113	0.126	0.0405	0.0045	3800	3755	3765	23.96
	224	0.123	0.136	0.148	0.0485	0.0045	3795	3750	3760	23.93

LC^3-55(B:35/10)	0	0.000	0.000	0.000	0.0000	0.0000	3770	3830	3860	24.25
	1	0.015	0.009	0.023	0.0056	0.0025	3755	3820	3850	24.18
	4	0.023	0.021	0.030	0.0088	0.0017	3755	3815	3845	24.16
	7	0.033	0.038	0.039	0.0131	0.0011	3750	3815	3840	24.14
	14	0.041	0.045	0.049	0.0161	0.0014	3745	3810	3835	24.11
	28	0.051	0.055	0.064	0.0202	0.0024	3745	3805	3835	24.10
	56	0.053	0.057	0.066	0.0268	0.0024	3740	3800	3830	24.06
	112	0.087	0.085	0.089	0.0311	0.0007	3735	3795	3825	24.03
	224	0.108	0.106	0.092	0.0364	0.0031	3725	3790	3815	23.98
LC^3-55(H:35/10)	0	0.000	0.000	0.000	0.0000	0.0000	3850	3820	3830	24.34
	1	0.014	0.016	0.018	0.0054	0.0006	3835	3805	3815	24.24
	4	0.042	0.052	0.067	0.0192	0.0045	3825	3790	3810	24.18
	7	0.059	0.068	0.087	0.0255	0.0051	3815	3785	3805	24.14
	14	0.067	0.075	0.094	0.0281	0.0050	3810	3780	3795	24.10
	28	0.099	0.095	0.116	0.0369	0.0040	3805	3775	3790	24.06
	56	0.108	0.103	0.121	0.0427	0.0033	3795	3765	3785	24.01
	112	0.125	0.122	0.147	0.0469	0.0049	3785	3755	3770	23.94
	224	0.133	0.130	0.155	0.0498	0.0049	3775	3745	3765	23.88
LC^3-55(PH:35/10)	0	0.000	0.000	0.000	0.0000	0.0000	3895	3840	3890	24.60
	1	0.024	0.016	0.020	0.0071	0.0014	3885	3830	3880	24.54
	4	0.030	0.026	0.030	0.0102	0.0008	3880	3825	3875	24.51
	7	0.046	0.039	0.047	0.0157	0.0016	3875	3820	3870	24.48
	14	0.054	0.045	0.054	0.0182	0.0019	3875	3820	3870	24.48
	28	0.059	0.066	0.059	0.0219	0.0014	3870	3815	3865	24.44
	56	0.063	0.074	0.069	0.0276	0.0020	3865	3810	3865	24.42
	112	0.090	0.091	0.096	0.0330	0.0011	3860	3805	3855	24.38
	224	0.099	0.100	0.099	0.0355	0.0002	3850	3795	3845	24.32
LC^3-65(B:25/10)	0	0.000	0.000	0.000	0.0000	0.0000	3960	3890	3905	24.88
	1	0.014	0.012	0.017	0.0051	0.0009	3945	3880	3895	24.80
	4	0.028	0.024	0.029	0.0096	0.0009	3940	3875	3890	24.77
	7	0.032	0.028	0.034	0.0112	0.0011	3940	3875	3890	24.77
	14	0.044	0.041	0.043	0.0152	0.0005	3935	3870	3885	24.74
	28	0.058	0.056	0.063	0.0211	0.0013	3930	3865	3880	24.71
	56	0.070	0.068	0.077	0.0256	0.0017	3930	3860	3880	24.70
	112	0.089	0.086	0.093	0.0319	0.0013	3920	3855	3870	24.65
	224	0.097	0.094	0.096	0.0342	0.0005	3915	3850	3865	24.61

LC^3-65(H:25/10)	0	0.000	0.000	0.000	0.0000	0.0000	3875	3870	3855	24.55
	1	0.021	0.025	0.022	0.0081	0.0007	3865	3860	3845	24.49
	4	0.042	0.044	0.042	0.0152	0.0004	3860	3850	3835	24.43
	7	0.058	0.057	0.055	0.0202	0.0005	3855	3845	3830	24.40
	14	0.075	0.072	0.067	0.0255	0.0014	3850	3840	3825	24.37
	28	0.097	0.092	0.087	0.0329	0.0018	3840	3835	3820	24.33
	56	0.114	0.102	0.108	0.0386	0.0021	3835	3825	3810	24.28
	112	0.132	0.126	0.129	0.0461	0.0011	3820	3815	3795	24.19
	224	0.148	0.140	0.148	0.0519	0.0016	3815	3805	3790	24.15
LC^3-45(H:40/15)	0	0.000	0.000	0.000	0.0000	0.0000	3870	3835	3850	24.46
	1	0.025	0.025	0.020	0.0083	0.0010	3855	3820	3840	24.37
	4	0.048	0.047	0.039	0.0160	0.0018	3845	3810	3830	24.31
	7	0.058	0.057	0.050	0.0196	0.0016	3840	3805	3820	24.26
	14	0.077	0.077	0.069	0.0265	0.0016	3830	3800	3815	24.22
	28	0.097	0.113	0.103	0.0373	0.0029	3820	3790	3805	24.16
	56	0.113	0.132	0.121	0.0436	0.0034	3810	3775	3790	24.07
	112	0.136	0.153	0.142	0.0513	0.0031	3790	3760	3775	23.97
	224	0.147	0.165	0.152	0.0552	0.0033	3790	3760	3775	23.97
LC^3-45(B:40/15)	0	0.000	0.000	0.000	0.0000	0.0000	3830	3845	3810	24.31
	1	0.019	0.018	0.011	0.0057	0.0016	3820	3840	3800	24.25
	4	0.022	0.028	0.025	0.0089	0.0011	3815	3830	3795	24.21
	7	0.031	0.035	0.032	0.0117	0.0007	3810	3830	3790	24.19
	14	0.043	0.047	0.041	0.0156	0.0011	3810	3825	3785	24.17
	28	0.073	0.052	0.068	0.0230	0.0039	3805	3820	3780	24.14
	56	0.092	0.069	0.082	0.0289	0.0041	3795	3815	3775	24.10
	112	0.103	0.079	0.092	0.0326	0.0043	3780	3800	3760	24.00
	224	0.109	0.088	0.101	0.0355	0.0038	3780	3795	3760	23.99

Table VII.6: Free shrinkage test results (0.55 w/b ratio)

Mix	Days	Shrinkage readings (mm)			Shrinkage strain		Mass (g)			Unit Weight (kN/m^3)
		1	2	3	Average (%)	SD (%)	1	2	3	
R1	0	0.000	0.000	0.000	0.0000	0.0000	3840	3890	3890	24.59
	1	0.035	0.028	0.049	0.0133	0.0038	3825	3875	3875	24.50
	4	0.059	0.048	0.063	0.0202	0.0028	3810	3860	3860	24.40
	7	0.070	0.061	0.082	0.0254	0.0038	3795	3845	3845	24.31
	14	0.083	0.077	0.097	0.0306	0.0037	3785	3835	3835	24.24
	28	0.100	0.102	0.114	0.0376	0.0027	3770	3820	3820	24.15
	56	0.137	0.135	0.143	0.0494	0.0015	3760	3810	3810	24.08
	112	0.142	0.139	0.149	0.0512	0.0018	3755	3805	3805	24.05
	224	0.144	0.142	0.156	0.0526	0.0027	3755	3805	3805	24.05
LC^3-55(B:35/10)	0	0.000	0.000	0.000	0.0000	0.0000	3830	3850	3790	24.28
	1	0.018	0.014	0.020	0.0062	0.0011	3820	3840	3770	24.19
	4	0.024	0.023	0.027	0.0088	0.0007	3810	3830	3775	24.16
	7	0.023	0.030	0.029	0.0098	0.0014	3810	3830	3770	24.15
	14	0.035	0.043	0.039	0.0139	0.0014	3805	3820	3765	24.11
	28	0.045	0.060	0.046	0.0180	0.0030	3795	3815	3760	24.06
	56	0.056	0.075	0.064	0.0232	0.0034	3790	3805	3750	24.01
	112	0.067	0.086	0.075	0.0271	0.0034	3770	3790	3735	23.90
	224	0.079	0.098	0.085	0.0312	0.0035	3770	3790	3730	23.89
LC^3-55(H:35/10)	0	0.000	0.000	0.000	0.0000	0.0000	3850	3830	3835	24.37
	1	0.019	0.023	0.017	0.0070	0.0011	3835	3810	3815	24.25
	4	0.051	0.048	0.043	0.0169	0.0014	3820	3795	3800	24.16
	7	0.059	0.062	0.054	0.0208	0.0014	3810	3785	3790	24.10
	14	0.079	0.075	0.069	0.0265	0.0018	3795	3775	3780	24.02
	28	0.091	0.090	0.085	0.0317	0.0011	3780	3760	3765	23.93
	56	0.120	0.114	0.109	0.0408	0.0020	3770	3750	3755	23.86
	112	0.139	0.133	0.128	0.0476	0.0020	3750	3735	3735	23.75
	224	0.150	0.142	0.141	0.0515	0.0018	3750	3735	3735	23.75
LC^3-55(HC:35/10)	0	0.000	0.000	0.000	0.0000	0.0000	3795	3840	3830	24.26
	1	0.015	0.016	0.014	0.0054	0.0004	3780	3825	3815	24.17
	4	0.020	0.024	0.023	0.0080	0.0007	3770	3815	3805	24.11
	7	0.036	0.037	0.032	0.0125	0.0009	3760	3805	3795	24.04
	14	0.046	0.052	0.045	0.0170	0.0014	3755	3800	3790	24.01
	28	0.060	0.068	0.055	0.0218	0.0023	3745	3790	3780	23.95
	56	0.084	0.095	0.078	0.0306	0.0031	3735	3780	3770	23.88
	112	0.094	0.109	0.088	0.0346	0.0039	3725	3770	3760	23.82
	224	0.104	0.121	0.099	0.0386	0.0041	3715	3760	3750	23.76

Table VII.7: Resistivity test results (0.4 w/b ratio)

Mix	Days	Resistivity (kΩcm)										
		Specimen 1			Specimen 2			Specimen 3			Average	SD
		A	B	C	A	1	C	A	B	C		
R1	28	16	16	16	15	16	16	16	17	17	16	0.7
	56	20	22	22	19	21	21	20	20	20	20	1.0
	90	25	25	25	22	24	25	23	23	24	24	0.9
R2	28	70	73	73	72	72	73	70	71	69	71	1.3
	56	108	111	111	115	112	112	110	112	108	111	2.0
	90	143	143	145	143	145	145	139	141	137	142	3.1
LC^3-55(B:35/10)	28	316	336	334	328	350	342	336	334	334	334	9.3
	56	423	441	430	429	454	434	438	434	438	436	8.8
	90	523	542	534	524	536	526	534	530	538	532	6.6
LC^3-55(H:35/10)	28	74	67	66	75	68	67	66	69	71	69	3.4
	56	96	102	101	110	98	98	96	103	103	101	4.4
	90	120	124	127	135	121	123	121	127	129	125	4.7
LC^3-55(PH:35/10)	28	439	449	451	426	439	420	435	420	430	434	11.4
	56	582	594	602	586	594	587	604	595	602	594	7.8
	90	806	806	810	790	802	794	812	794	808	802	7.9
LC^3-65(B:25/10)	28	245	245	252	246	247	246	242	225	233	242	8.2
	56	320	314	326	313	321	320	311	297	298	313	10.1
	90	418	416	427	421	426	420	410	386	387	412	15.5

LC^3-65(H:25/10)	28	48	49	48	54	49	48	48	48	52	49	2.2
	56	63	65	63	69	63	64	64	66	68	65	2.2
	90	79	82	79	88	79	80	80	81	85	81	3.3
LC^3-45(H:40/15)	28	166	171	160	156	157	169	169	171	166	165	5.9
	56	282	287	261	253	260	283	282	289	275	275	13.3
	90	422	426	400	380	390	410	412	428	402	408	16.4
LC^3-45(B:40/15)	28	798	814	810	794	800	804	794	795	799	801	7.1
	56	1007	1037	1054	1111	1081	1081	1026	1021	1031	1050	34.4
	90	1185	1218	1222	1234	1226	1215	1182	1218	1206	1212	17.8
LC^3-55(HC:35/10)	28	201	202	205	196	205	200	202	204	200	202	2.9
	56	272	273	274	268	269	272	269	275	271	271	2.4
	90	335	335	340	326	330	336	332	341	335	334	4.7

Table VII.8: Resistivity test results (0.55 w/b ratio)

Mix	Days	Resistivity (kΩcm)									Average	SD
		Specimen 1			Specimen 2			Specimen 3				
		A	B	C	A	1	C	A	B	C		
R1	28	11	11	11	12	11	12	10	11	10	11	0.6
	56	13	13	13	14	13	14	12	13	12	13	0.7
	90	15	15	15	16	14	15	14	14	14	15	0.7
LC^3-55(B:35/10)	28	756	764	769	835	804	801	800	884	868	809	45.3
	56	1050	1037	1050	1153	1135	1125	1138	1240	1164	1121	65.8
	90	1150	1200	1210	1300	1230	1250	1245	1350	1280	1246	58.9
LC^3-55(H:35/10)	28	49	49	51	52	52	50	50	50	51	50	1.2
	56	76	76	78	80	82	77	77	78	79	78	2.1
	90	100	99	103	104	108	100	98	99	101	101	3.1
LC^3-55(HC:35/10)	28	268	278	275	270	265	272	268	274	284	273	5.9
	56	341	343	340	345	325	332	335	345	349	339	7.5
	90	368	381	390	370	368	368	368	376	390	375	9.4

Table VII.9: OPI results (0.4 w/b ratio)

Mix	OPI (Log scale)					
	Specimen #				Average	SD
	1	2	3	4		
R1	Leakage		11.06	11.16	11.11	0.07
R2			11.29	11.06	11.18	0.16
LC^3-55(B:35/10)			11.47	11.72	11.60	0.18
LC^3-55(H:35/10)			11.28	11.42	11.35	0.10
LC^3-55 (PH:35/10)			11.36	11.64	11.50	0.20
LC^3-65(B:25/10)	11.54	11.88	11.75	11.31	11.62	0.25
LC^3-65(H:25/10)	11.59	11.49	11.50	11.51	11.52	0.05
LC^3-45(H:40/15)	11.60	11.55	11.58	11.65	11.60	0.04
LC^3-45(B:40/15)	11.71	11.81	11.56	11.82	11.73	0.12

Table VII.10: OPI results (0.55 w/b ratio)

Mix	WSI ($mm/hr^{0.5}$)					
	Specimen #				Average	SD
	1	2	3	4		
R1	11.05	11.03	11.00	10.99	11.02	0.03
LC^3-55(B:35/10)	11.59	11.78	11.59	11.43	11.60	0.14
LC^3-55(H:35/10)	11.34	11.48	11.50	11.52	11.46	0.08
LC^3-55(HC:35/10)	11.46	11.45	11.51	11.46	11.47	0.03

Table VII.11: WSI results (0.4 w/b ratio)

Mix	WSI ($mm/hr^{0.5}$)					
	Specimen #				Average	SD
	1	2	3	4		
R1	6.83	6.97	6.02	6.77	6.65	0.43
R2	6.06	6.63	6.79	6.54	6.51	0.31
LC^3-55(B:35/10)	6.78	7.39	7.54	7.32	7.26	0.33
LC^3-55(H:35/10)	6.75	6.51	6.72	6.67	6.66	0.11
LC^3-55 (PH:35/10)	6.42	6.37	5.80	6.18	6.19	0.28
LC^3-65(B:25/10)	7.16	6.84	6.86	7.37	7.06	0.25
LC^3-65(H:25/10)	7.70	7.00	7.49	7.39	7.40	0.29
LC^3-45(H:40/15)	7.20	7.66	7.60	6.72	7.30	0.43
LC^3-45(B:40/15)	7.37	7.46	6.46	6.95	7.06	0.46

Table VII.12: WSI results (0.55 w/b ratio)

Mix	WSI ($mm/hr^{0.5}$)					
	Specimen #				Average	SD
	1	2	3	4		
R1	6.92	7.13	8.05	8.02	7.53	0.59
LC^3-55(B:35/10)	8.30	7.81	6.75	7.49	7.59	0.65
LC^3-55(H:35/10)	6.56	7.05	6.84	6.97	6.86	0.21
LC^3-55(HC:35/10)	6.31	7.57	6.45	6.77	6.78	0.56

Table VII.13: Porosity results (0.4 w/b ratio)

Mix	Porosity (%)					
	Specimen #				Average	SD
	1	2	3	4		
R1	6.41	6.19	6.00	6.55	6.29	0.24
R2	3.74	3.77	3.86	3.46	3.71	0.17
LC^3-55(B:35/10)	3.85	3.63	3.96	3.45	3.72	0.23
LC^3-55(H:35/10)	5.26	5.07	4.81	5.05	5.05	0.18
LC^3-55 (PH:35/10)	3.59	3.56	3.99	3.69	3.71	0.20
LC^3-65(B:25/10)	3.40	3.61	3.22	3.14	3.34	0.21
LC^3-65(H:25/10)	5.05	5.16	5.43	5.31	5.24	0.17
LC^3-45(H:40/15)	5.04	5.29	5.31	4.89	5.13	0.20
LC^3-45(B:40/15)	3.81	3.65	3.57	3.71	3.69	0.10

Table VII.14: Porosity results (0.55 w/b ratio)

Mix	Porosity (%)					
	Specimen #				Average	SD
	1	2	3	4		
R1	7.53	7.00	7.73	7.29	7.39	0.31
LC^3-55(B:35/10)	4.54	4.59	4.78	4.53	4.61	0.12
LC^3-55(H:35/10)	6.91	7.39	6.86	7.54	7.18	0.34
LC^3-55(HC:35/10)	6.80	6.81	7.25	7.01	6.97	0.21

Table VII.15: CCI results (0.4 w/b ratio)

Mix	CCI (mS/cm)					
	Specimen #				Average	SD
	1	2	3	4		
R1	0.49	0.5	0.56	0.53	0.52	0.03
R2	0.11	0.11	0.10	0.12	0.11	0.01
LC^3-55(B:35/10)	0.09	0.09	0.10	0.10	0.10	0.01
LC^3-55(H:35/10)	0.17	0.19	0.17	0.16	0.17	0.01
LC^3-55 (PH:35/10)	0.12	0.13	0.13	0.14	0.13	0.01
LC^3-65(B:25/10)	0.09	0.1	0.10	0.09	0.10	0.01
LC^3-65(H:25/10)	0.17	0.19	0.18	0.19	0.18	0.01
LC^3-45(H:40/15)	0.16	0.17	0.17	0.19	0.17	0.01
LC^3-45(B:40/15)	0.13	0.13	0.12	0.14	0.13	0.01

Table VII.16: CCI results (0.55 w/b ratio)

Mix	CCI (mS/cm)					
	Specimen #				Average	SD
	1	2	3	4		
R1	0.99	0.93	0.95	0.96	0.96	0.03
LC^3-55(B:35/10)	0.15	0.16	0.15	0.16	0.16	0.01
LC^3-55(H:35/10)	0.29	0.29	0.31	0.30	0.30	0.01
LC^3-55(HC:35/10)	0.23	0.21	0.26	0.25	0.24	0.02

Table VII.17: Accelerated carbonation test results (0.4 w/b ratio)

Mix	Weeks	Carbonation depth (mm)									
		Specimen 1				Specimen 2				Average	SD
		Side A		Side B		Side A		Side B			
		Min	Max	Min	Max	Min	Max	Min	Max		
R1	12	0.00	0.00	0.00	0.00	0.00	0.00	0.00	0.00	0.00	0.00
	24	0.00	0.24	0.00	0.26	0.00	0.21	0.00	0.20	0.13	0.11
R2	12	1.52	2.93	1.97	2.12	1.25	2.74	1.10	1.34	1.87	0.72
	24	1.60	3.22	1.26	3.72	1.35	3.12	1.51	3.11	2.36	0.29
LC^3-55(B:35/10)	12	3.78	6.11	4.57	7.85	3.89	6.22	4.29	5.27	5.25	1.08
	24	4.99	9.66	3.13	8.74	4.06	7.98	4.02	8.52	6.39	0.70
LC^3-55(H:35/10)	12	4.60	8.02	4.16	6.96	3.39	4.40	4.95	7.48	5.50	1.60
	24	7.90	8.95	6.81	10.80	6.34	11.94	6.84	10.64	8.78	1.23
LC^3-55(PH:35/10)	12	5.24	9.01	2.37	5.50	3.93	5.83	3.54	7.90	5.42	1.68
	24	6.77	8.49	4.34	8.33	4.16	8.54	4.45	8.65	6.72	0.13
LC^3-65(B:25/10)	12	0.00	0.00	0.37	1.75	0.31	1.90	1.31	2.58	1.03	1.10
	24	1.35	4.21	1.76	3.19	1.95	2.85	1.07	3.63	2.50	0.59
LC^3-65(H:25/10)	12	1.71	5.74	1.69	4.53	1.73	4.36	1.68	3.38	3.10	0.97
	24	2.72	6.15	3.09	5.53	3.07	5.74	2.98	6.33	4.45	0.37
LC^3-45(H:40/15)	12	7.39	11.10	7.10	10.20	6.16	10.89	6.86	10.13	8.73	0.49
	24	9.95	11.75	11.33	12.28	11.74	13.36	10.45	11.93	11.60	0.72
LC^3-45(B:40/15)	12	5.14	10.06	5.55	9.40	5.96	8.50	6.36	10.54	7.69	0.88
	24	9.48	10.93	10.20	11.57	9.20	11.58	9.82	11.05	10.48	0.34

Table VII.18: Accelerated carbonation test results (0.55 w/b ratio)

Mix	Weeks	Carbonation depth (mm)								Average	SD
		Specimen 1				Specimen 2					
		Side A		Side B		Side A		Side B			
		Min	Max	Min	Max	Min	Max	Min	Max		
R1	12	3.04	4.64	3.08	4.41	2.90	4.16	2.81	4.75	3.72	0.84
	24	6.16	8.57	4.43	9.10	7.12	9.53	5.93	9.87	7.59	1.97
LC^3-55(B:35/10)	12	9.78	13.64	8.83	12.13	9.56	12.10	9.22	12.24	10.94	1.79
	24	14.01	16.32	14.31	16.94	13.52	15.29	14.04	15.80	15.03	1.24
LC^3-55 (H:35/10)	12	11.11	12.89	10.12	13.73	11.59	13.04	11.40	13.35	12.15	1.27
	24	14.98	17.77	14.80	15.87	15.17	18.55	15.95	17.95	16.38	1.49
LC^3-55 (HC:35/10)	12	10.65	14.33	12.33	13.89	10.85	13.10	11.39	15.66	12.78	1.79
	24	16.49	20.60	16.37	20.03	16.33	19.42	19.32	20.63	18.65	1.92

Table VII.19: Bulk diffusion test - titration results (0.4 w/b ratio)

Core Label	#	Depth (mm)	Average depth (mm)	mass of sample (g)	Volume of titrant consumed (ml)	Chloride Content % (by mass of concrete)	Chloride Content % (by mass of cement)	Average (Overall)		
								#	Depth (mm)	CL content % (by mass of cement)
R1-1	1	0.0 - 5.5	1.25	2.286	5.294	0.8210	4.926	1	1.25	4.755
	2	5.5 - 11.0	6.75	2.226	2.041	0.3250	1.950	2	5.50	2.678
	3	11.0 - 16.5	12.25	2.250	1.457	0.2296	1.377	3	10.50	1.346
	4	16.5 - 21.5	17.50	2.252	0.244	0.0384	0.230	4	15.50	0.463
	5	21.5 - 26.5	22.50	2.255	0.072	0.0113	0.068	5	21.50	0.127
	6	26.5 - 31.5	27.50	2.288	0.231	0.0358	0.215(ignored)	6	26.00	0.085
R1-2	1	0.0 - 4.5	0.75	2.309	5.214	0.8005	4.803			
	2	4.5 - 9.5	5.50	2.307	2.960	0.4548	2.729			
	3	9.5 - 14.5	10.50	2.306	1.227	0.1886	1.132			
	4	14.5 - 19.5	15.50	2.306	0.281	0.0432	0.259			
	5	19.5 - 25.0	21.50	2.304	0.166	0.0255	0.153			
	6	25.0 - 30.0	26.00	2.300	0.161	0.0248	0.149			
R2-1	1	0.0 - 5.0	1.00	2.322	5.304	0.8098	4.859	1	1.25	4.669
	2	5.0 - 10.5	6.00	2.198	0.981	0.1582	0.949	2	6.25	0.974
	3	10.5 - 15.5	11.50	2.208	0.111	0.0178	0.107	3	11.50	0.192
	4	15.5 - 19.5	16.50	2.249	0.079	0.0125	0.075	4	16.50	0.083
	5	19.5 - 24.5	20.50	2.252	0.087	0.0137	0.082	5	21.50	0.076
	6	24.5 - 30.0	25.75	2.231	0.071	0.0113	0.068	6	25.75	0.060
R2-2	1	0.0 - 5.5	1.25	2.244	4.932	0.7791	4.675			
	2	5.5 - 10.0	6.25	2.263	1.103	0.1728	1.037			
	3	10.0 - 15.5	11.25	2.318	0.312	0.0477	0.286			
	4	15.5 - 20.5	16.50	2.273	0.097	0.0151	0.091			
	5	20.5 - 25.5	21.50	2.314	0.080	0.0123	0.074			
	6	25.5 - 30.0	26.25	2.261	0.054	0.0085	0.051			

Core Label	#	Depth (mm)	Average depth (mm)	mass of sample (g)	Volume of titrant consumed (ml)	Chloride Content % (by mass of concrete)	Chloride Content % (by mass of cement)	Average (Overall)		
								#	Depth (mm)	CL content % (by mass of cement)
LC^3-55(B:35/10) (1)	1	0.0 - 5.5	1.25	2.321	2.687	0.4104	2.462	1	1.25	2.574
	2	5.5 - 10.0	6.25	2.339	0.319	0.0483	0.290	2	6.25	0.279
	3	10.0 - 15.0	11.00	2.308	0.055	0.0084	0.051	3	11.00	0.061
	4	15.0 - 19.5	15.75	2.363	0.024	0.0036	0.022	4	15.75	0.030
	5	19.5 - 24.0	20.25	2.353	0.036	0.0054	0.033	5	20.75	0.026
	6	24.0 - 29.5	25.25	2.368	0.000	0.0000	0.000	6	25.25	0.002
LC^3-55(B:35/10) (2)	1	0.0 - 5.0	1.00	2.331	3.081	0.4686	2.811			
	2	5.0 - 10.0	6.00	2.342	0.306	0.0463	0.278			
	3	10.0 - 14.5	10.75	2.317	0.079	0.0121	0.073			
	4	14.5 - 19.5	15.25	2.340	0.044	0.0067	0.040			
	5	19.5 - 25.0	20.75	2.334	0.025	0.0038	0.023			
	6	25.0 - 30.0	26.00	2.339	0.000	0.0000	0.000			
LC^3-55(H:35/10) (1)	1	0.0 - 5.0	1.00	2.338	4.222	0.6402	3.841	1	1.25	3.227
	2	5.0 - 10.5	6.25	2.306	1.741	0.2676	1.606	2	6.25	1.309
	3	10.5 - 16.0	11.75	2.305	0.226	0.0348	0.209	3	11.75	0.209
	4	16.0 - 21.0	17.00	2.300	0.037	0.0057	0.034	4	17	0.052
	5	21.0 - 25.5	21.75	2.310	0.044	0.0068	0.041	5	21.75	0.038
	6	25.5 - 30.0	26.25	2.314	0.042	0.0064	0.039	6	26.25	0.035
LC^3-55(H:35/10) (2)	1	0.0 - 5.5	1.25	2.310	2.953	0.4532	2.719			
	2	5.5 - 11.0	6.75	2.308	0.913	0.1402	0.841			
	3	11.0 - 16.5	12.25	2.310	0.160	0.0246	0.147			
	4	16.5 - 21.5	17.50	2.319	0.066	0.0101	0.061			
	5	21.5 - 26.5	22.50	2.302	0.033	0.0051	0.030			
	6	26.5 - 31.0	27.25	2.315	0.034	0.0052	0.031			

Core Label	#	Depth (mm)	Average depth (mm)	mass of sample (g)	Volume of titrant consumed (ml)	Chloride Content % (by mass of concrete)	Chloride Content % (by mass of cement)	Average (Overall)		
								#	Depth (mm)	CL content % (by mass of cement)
LC^3-55(PH:35/10) (1)	1	0.0 - 4.5	0.75	2.306	3.186	0.4898	2.939	1	1.00	2.660
	2	4.5 - 9.5	5.50	2.309	0.558	0.0857	0.514	2	5.50	0.651
	3	9.5 - 14.5	10.50	2.307	0.203	0.0312	0.187	3	10.50	0.198
	4	14.5 - 19.5	15.50	2.302	0.043	0.0066	0.040	4	15.75	0.066
	5	19.5 - 24.5	20.50	2.300	0.036	0.0055	0.033	5	20.50	0.020
	6	24.5 - 29.5	25.50	2.306	0.000	0.0000	0.000	6	25.50	0.000
LC^3-55(PH:35/10) (2)	1	0.0 – 5.0	1.00	2.308	2.723	0.4182	2.509			
	2	5.0 - 10.5	6.25	2.306	0.543	0.0835	0.501			
	3	10.5 - 15.0	11.25	2.308	0.170	0.0261	0.157			
	4	15.0 - 19.5	15.75	2.303	0.101	0.0155	0.093			
	5	19.5 - 24.5	20.50	2.310	0.000	0.0000	0.000			
	6	24.5 - 29.5	25.50	2.309	0.000	0.0000	0.000			
LC^3-65(B:25/10) (1)	1	0.0 - 5.0	1.00	2.314	3.563	0.5458	3.275	1	1.00	3.053
	2	5.0 - 10.0	6.00	2.311	0.410	0.0629	0.377	2	6.00	0.415
	3	10.0 - 15.0	11.00	2.312	0.140	0.0215	0.129	3	11.00	0.106
	4	15.0 - 20.0	16.00	2.318	0.000	0.0000	0.000	4	16.00	0.014
	5	20.0 - 25.0	21.00	2.302	0.000	0.0000	0.000	5	21.00	0.000
	6	25.0 - 30.0	26.00	2.323	0.000	0.0000	0.000	6	26.00	0.000
LC^3-65(B:25/10) (2)	1	0.0 - 5.0	1.00	2.306	3.070	0.4719	2.832			
	2	5.0 - 10.0	6.00	2.304	0.490	0.0754	0.452			
	3	10.0 - 15.0	11.00	2.307	0.090	0.0138	0.083			
	4	15.0 - 20.0	16.00	2.311	0.031	0.0048	0.029			
	5	20.0 - 25.0	21.00	2.316	0.000	0.0000	0.000			
	6	25.0 - 30.0	26.00	2.309	0.000	0.0000	0.000			

Core Label	#	Depth (mm)	Average depth (mm)	mass of sample (g)	Volume of titrant consumed (ml)	Chloride Content % (by mass of concrete)	Chloride Content % (by mass of cement)	Average (Overall)		
								#	Depth (mm)	CL content % (by mass of cement)
LC^3-65(H:25/10) (1)	1	0.0 - 4.5	0.75	2.302	5.214	0.8029	4.818	1	0.75	4.477
	2	4.5 - 9.5	5.50	2.312	3.006	0.4609	2.765	2	5.50	2.757
	3	9.5 - 14.5	10.50	2.319	1.177	0.1799	1.080	3	10.50	0.955
	4	14.5 - 19.5	15.50	2.310	0.238	0.0365	0.219	4	15.50	0.166
	5	19.5 - 24.5	20.50	2.316	0.023	0.0035	0.021	5	20.50	0.011
	6	24.5 - 29.5	25.50	2.305	0.000	0.0000	0.000	6	25.50	0.000
LC^3-65(H:25/10) (2)	1	0.0 - 4.5	0.75	2.304	4.480	0.6893	4.136			
	2	4.5 - 9.5	5.50	2.311	2.986	0.4580	2.748			
	3	9.5 - 14.5	10.50	2.307	0.900	0.1383	0.830			
	4	14.5 - 19.5	15.50	2.318	0.124	0.0190	0.114			
	5	19.5 - 24.5	20.50	2.312	0.000	0.0000	0.000			
	6	24.5 - 29.5	25.50	2.306	0.000	0.0000	0.000			
LC^3-45(H:40/15) (1)	1	0.0 - 4.5	0.75	2.309	4.015	0.6164	3.699	1	0.75	3.801
	2	4.5 - 10.0	5.75	2.306	1.808	0.2779	1.668	2	5.50	1.670
	3	10.0 - 15.0	11.00	2.313	0.503	0.0771	0.463	3	10.75	0.435
	4	15.0 - 20.5	16.25	2.312	0.158	0.0242	0.145	4	15.50	0.156
	5	20.5 - 25.0	21.25	2.311	0.057	0.0087	0.052	5	20.50	0.058
	6	25.0 - 30.0	26.00	2.306	0.032	0.0049	0.030	6	25.25	0.041
LC^3-45(H:40/15) (2)	1	0.0 - 4.5	0.75	2.313	4.244	0.6505	3.903			
	2	4.5 - 9.5	5.50	2.302	1.701	0.2619	1.572			
	3	9.5 - 14.5	10.75	2.304	0.379	0.0583	0.350			
	4	14.5 - 19.5	15.50	2.315	0.131	0.0201	0.120			
	5	19.5 - 24.5	20.50	2.317	0.053	0.0081	0.049			
	6	24.5 - 29.0	25.25	2.313	0.054	0.0083	0.050			

Core Label	#	Depth (mm)	Average depth (mm)	mass of sample (g)	Volume of titrant consumed (ml)	Chloride Content % (by mass of concrete)	Chloride Content % (by mass of cement)		Average (Overall)		
									#	Depth (mm)	CL content % (by mass of cement)
LC^3-45(B:40/1) (1)	1	0.0 - 4.5	0.75	2.310	3.279	0.5032	3.019		1	0.75	2.985
	2	4.5 - 9.5	5.50	2.313	0.754	0.1156	0.693		2	5.50	0.639
	3	9.5 - 14.5	10.50	2.306	0.232	0.0357	0.214		3	10.50	0.235
	4	14.5 - 20.0	15.75	2.305	0.000	0.0000	0.000		4	15.75	0.026
	5	20.0 - 25.0	21.00	2.302	0.000	0.0000	0.000		5	20.75	0.000
	6	25.0 - 30.5	26.25	2.306	0.000	0.0000	0.000		6	25.25	0.000
LC^3-45(B:40/15) (2)	1	0.0 - 4.5	0.75	2.310	3.205	0.4918	2.951				
	2	4.5 - 9.5	5.50	2.307	0.634	0.0974	0.585				
	3	9.5 - 15.0	10.75	2.308	0.260	0.0399	0.240				
	4	15.0 - 20.0	16.00	2.305	0.047	0.0072	0.043				
	5	20.0 - 24.5	20.75	2.306	0.000	0.0000	0.000				
	6	24.5 - 29.0	25.25	2.310	0.000	0.0000	0.000				

Table VII.20: Bulk diffusion test - titration results (0.55 w/b ratio)

Core Label	#	Depth (mm)	Average depth (mm)	mass of sample (g)	Volume of titrant consumed (ml)	Chloride Content % (by mass of concrete)	Chloride Content % (by mass of cement)	Average (Overall)		
								#	Depth (mm)	CL content % (by mass of cement)
R1-1	1	0.0 - 5.5	1.25	2.311	5.478	0.8403	6.930	1	1.25	7.078
	2	5.5 - 11.0	6.5	2.309	3.231	0.4961	4.091	2	6.50	4.431
	3	11.0 - 16.5	12.25	2.309	2.054	0.3153	2.601	3	12.00	2.835
	4	16.5 - 22.0	17.75	2.305	1.638	0.2519	2.078	4	17.00	2.053
	5	22.0 - 27.0	23.0	2.305	0.897	0.1380	1.138	5	22.00	1.240
	6	27.0 - 32.0	28.0	2.303	0.378	0.0582	0.480	6	27.00	0.533
R1-2	1	0.0 - 5.5	1.25	2.313	5.716	0.8761	7.225			
	2	5.5 - 11.0	6.5	2.307	3.765	0.5785	4.771			
	3	11.0 - 16.0	12.0	2.305	2.369	0.3643	3.005			
	4	16.0 - 21.0	17.0	2.303	1.542	0.2374	1.958			
	5	21.0 - 26.0	22.0	2.306	0.918	0.1411	1.164			
	6	26.0 - 31.0	27.0	2.308	0.359	0.0551	0.455			
LC^3-55(B:35/10) (1)	1	0.0 - 5.5	1.25	2.310	2.711	0.4160	3.431	1	1.25	3.614
	2	5.5 - 10.0	6.25	2.307	0.864	0.1328	1.095	2	5.75	1.184
	3	10.0 - 14.5	10.75	2.305	0.537	0.0826	0.681	3	10.75	0.674
	4	14.5 - 19.0	15.25	2.304	0.373	0.0574	0.473	4	15.25	0.467
	5	19.0 - 24.0	20.0	2.301	0.250	0.0385	0.318	5	20.00	0.350
	6	24.0 - 29.0	25.0	2.302	0.180	0.0277	0.229	6	25.00	0.261
LC^3-55(B:35/10) (2)	1	0.0 - 4.5	0.75	2.310	3.241	0.4974	4.102			
	2	4.5 - 10.0	5.75	2.309	0.821	0.1260	1.040			
	3	10.0 - 15.0	11.0	2.306	0.511	0.0786	0.648			
	4	15.0 - 20.5	16.25	2.307	0.329	0.0506	0.417			
	5	20.5 - 25.5	21.5	2.301	0.289	0.0445	0.367			
	6	25.5 - 30.5	26.5	2.302	0.207	0.0319	0.263			

Core Label	#	Depth (mm)	Average depth (mm)	mass of sample (g)	Volume of titrant consumed (ml)	Chloride Content % (by mass of concrete)	Chloride Content % (by mass of cement)	Average (Overall)		
								#	Depth (mm)	CL content % (by mass of cement)
LC^3-55(H:35/10) (1)	1	0.0 - 4.5	0.75	2.309	4.574	0.7022	5.792	1	1.00	5.064
	2	4.5 - 10.0	5.75	2.304	2.185	0.3362	2.773	2	5.75	2.704
	3	10.0 - 15.0	10.5	2.307	0.973	0.1495	1.233	3	10.50	1.308
	4	15.0 - 19.5	15.75	2.303	0.326	0.0502	0.414	4	15.75	0.444
	5	19.5 - 24.5	20.50	2.306	0.054	0.0083	0.068	5	20.50	0.097
	6	24.5 - 29.0	25.25	2.306	0.000	0.0000	0.000	6	25.25	0.011
LC^3-55(H:35/10) (2)	1	0.0 – 5.0	1.0	2.308	3.543	0.5442	4.488			
	2	5.0 - 10.5	6.25	2.305	1.923	0.2957	2.439			
	3	10.5 - 16.0	11.75	2.307	0.846	0.1300	1.072			
	4	16.0 - 21.5	17.25	2.314	0.198	0.0303	0.250			
	5	21.5 - 26.5	22.5	2.311	0.038	0.0058	0.048			
	6	26.5 - 31.5	27.5	2.309	0.000	0.0000	0.000			
LC^3-55(HC:35/10) (1)	1	0.0 - 5.5	1.25	2.313	3.476	0.5327	4.394	1	1.25	4.418
	2	5.5 - 10.5	6.5	2.305	1.207	0.1856	1.531	2	5.50	1.926
	3	10.5 - 16.0	11.75	2.307	0.383	0.0589	0.485	3	10.50	0.475
	4	16.0 - 21.0	17.0	2.306	0.073	0.0112	0.093	4	15.50	0.132
	5	21.0 - 25.5	22.25	2.307	0.035	0.0054	0.044	5	20.75	0.049
	6	25.5 - 31.0	26.75	2.305	0.000	0.0000	0.000	6	26.25	0.000
LC^3-55(HC:35/10) (2)	1	0.0 - 4.5	0.75	2.311	3.760	0.5768	4.757			
	2	4.5 - 9.5	5.5	2.309	1.402	0.2153	1.775			
	3	9.5 - 14.5	10.5	2.308	0.170	0.0261	0.215			
	4	14.5 - 19.5	15.5	2.303	0.046	0.0071	0.058			
	5	19.5 - 25.0	20.75	2.304	0.032	0.0049	0.041			
	6	25.0 - 30.5	26.25	2.304	0.000	0.0000	0.000			

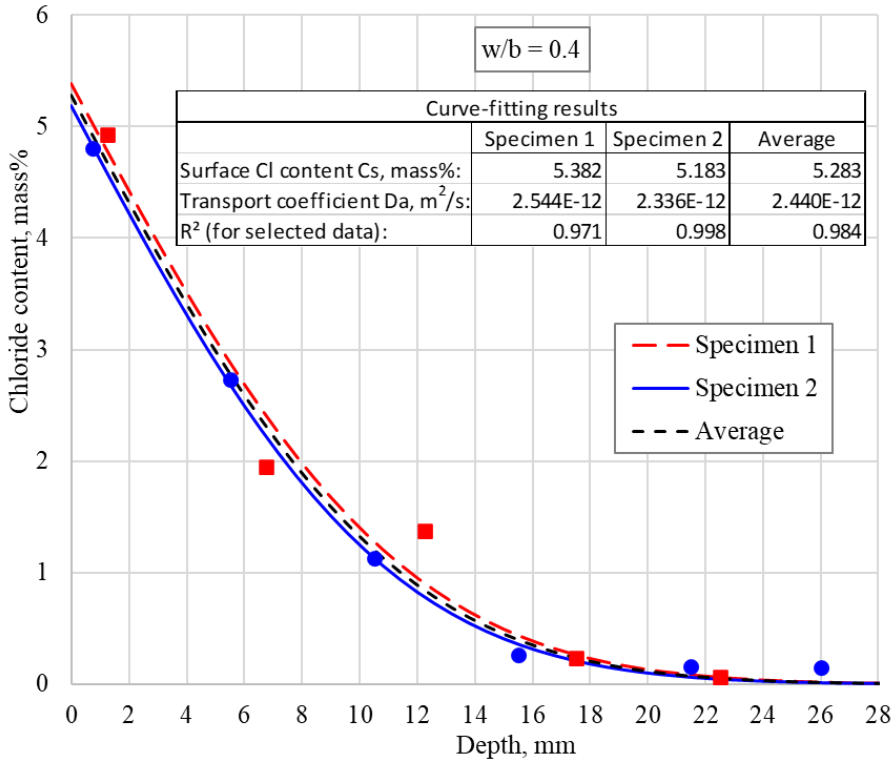

Figure VII.1: Chloride profile of the R1 (Curve fitted, Fick's 2nd law)

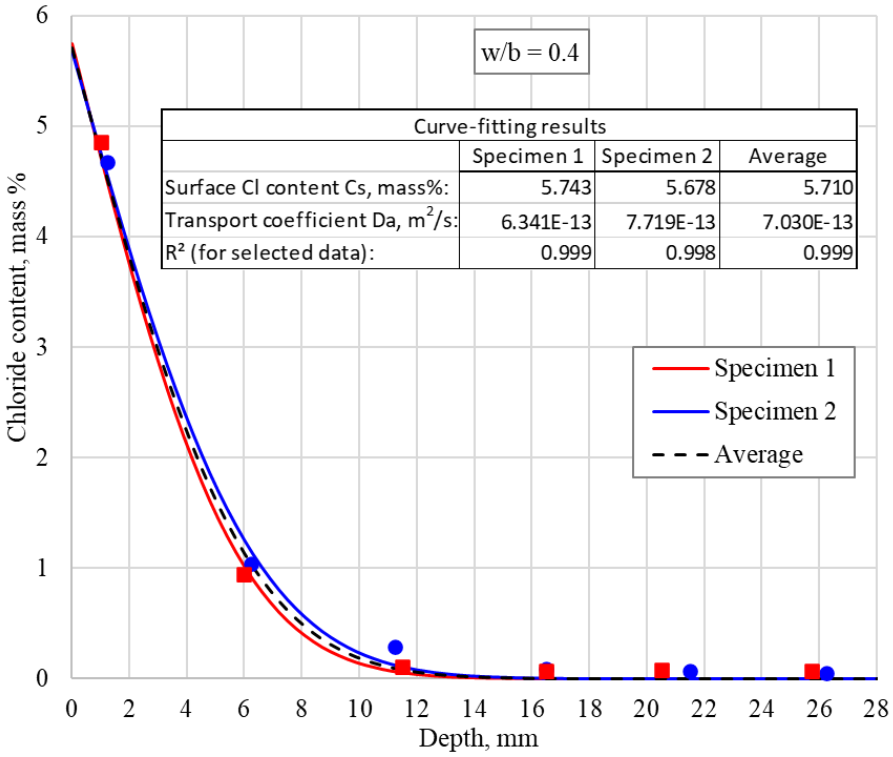

Figure VII.2: Chloride profile of the R2
(Cs estimated by extending a line joining the first two points, then Curve fitted, Fick's 2nd law)

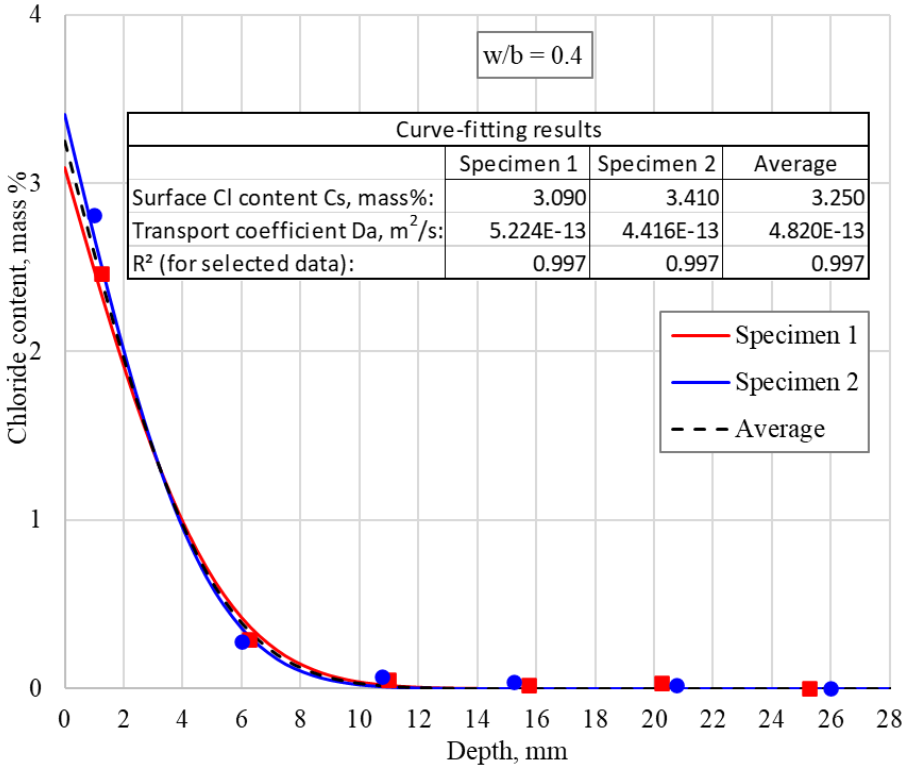

Figure VII.3: Chloride profile of the LC^3-55(B:35/10)
(Cs estimated by extending a line joining the first two points, then Curve fitted, Fick's 2nd law)

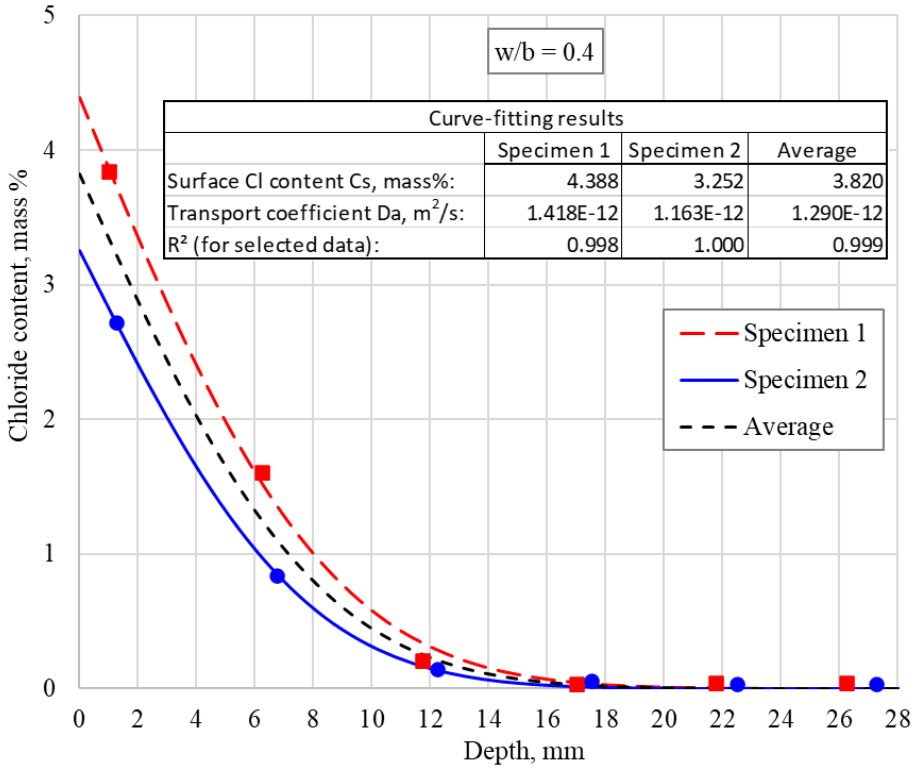

Figure VII.4: Chloride profile of the LC^3-55(H:35/10) (Curve fitted, Fick's 2nd law)

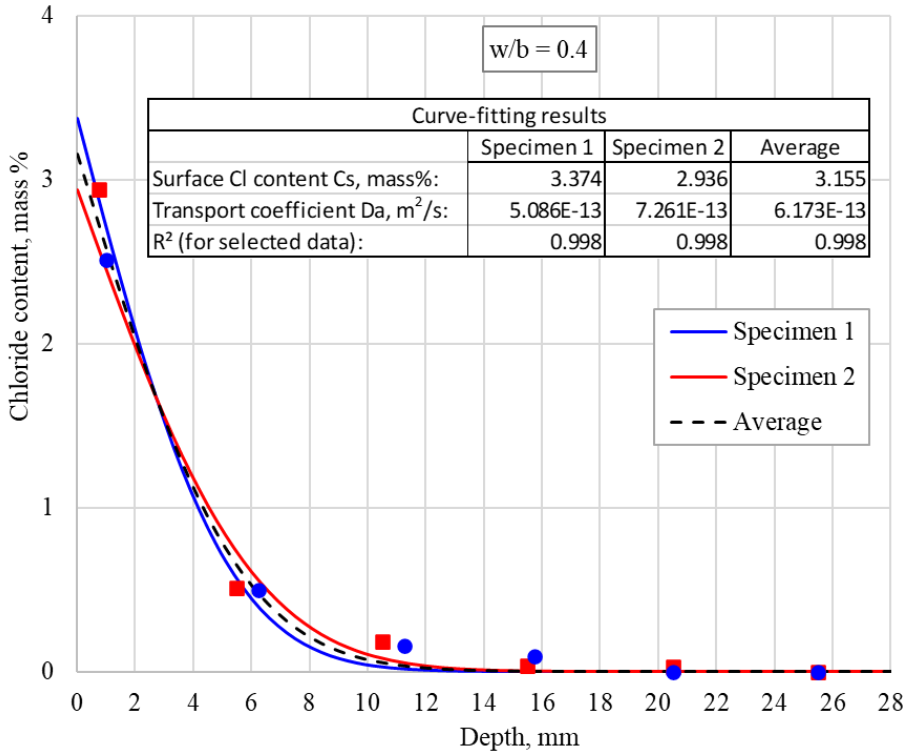

Figure VII.5: Chloride profile of the LC^3-55(PH:35/10)
(Cs estimated by extending a line joining the first two points, then Curve fitted, Fick's 2nd law)

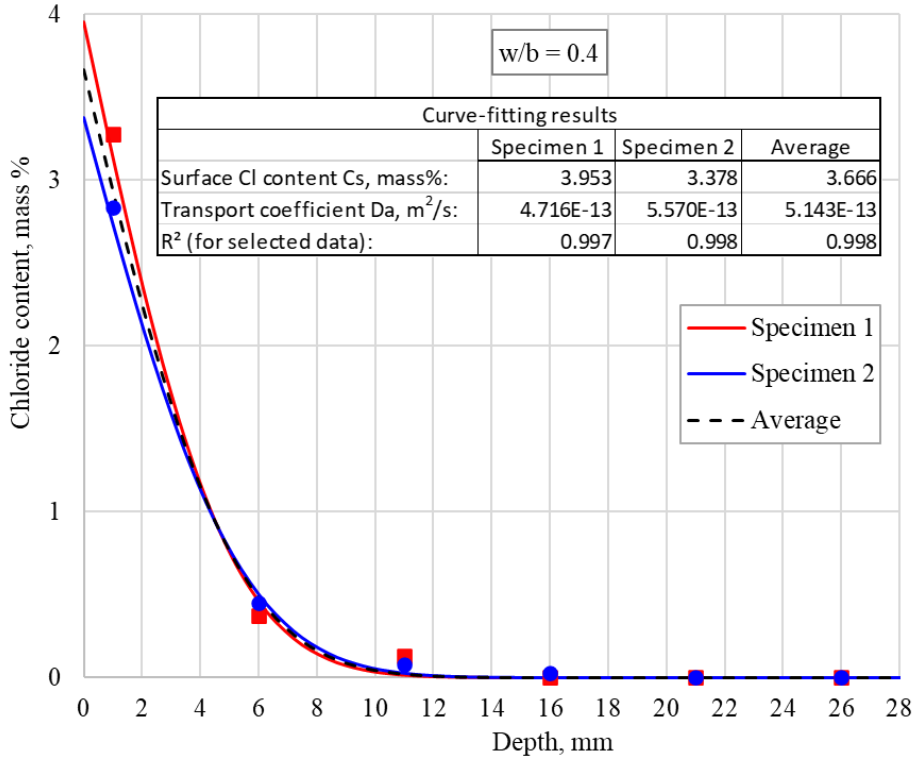

Figure VII.6: Chloride profile of the LC^3-65(B:25/10)
(Cs estimated by extending a line joining the first two points, then Curve fitted, Fick's 2nd law)

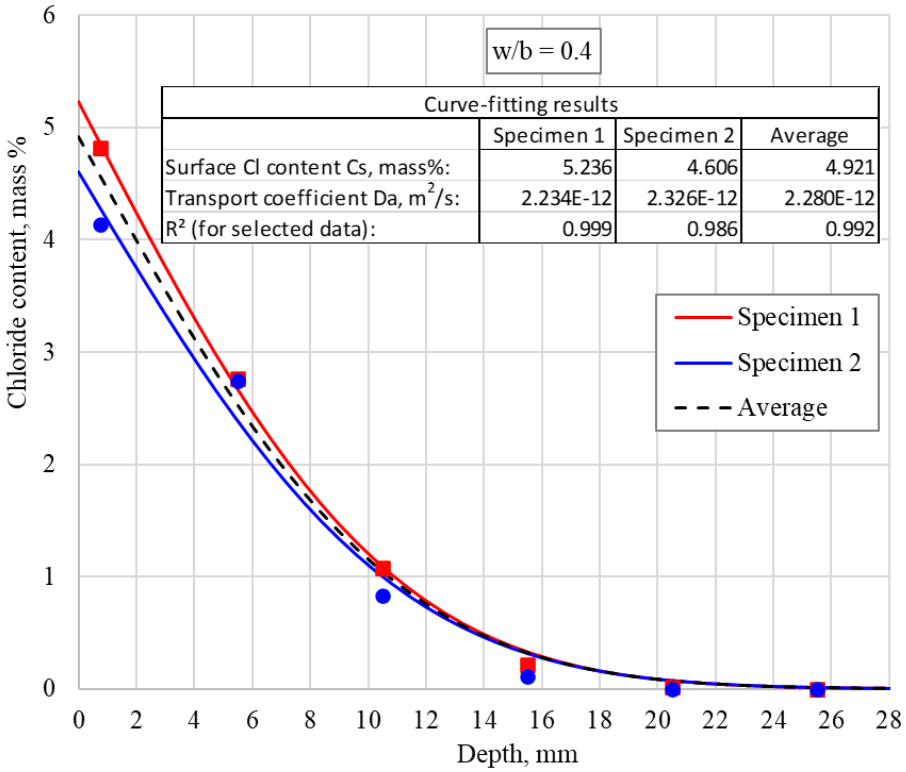

Figure VII.7: Chloride profile of the LC^3-65(H:25/10) (Curve fitted, Fick's 2nd law)

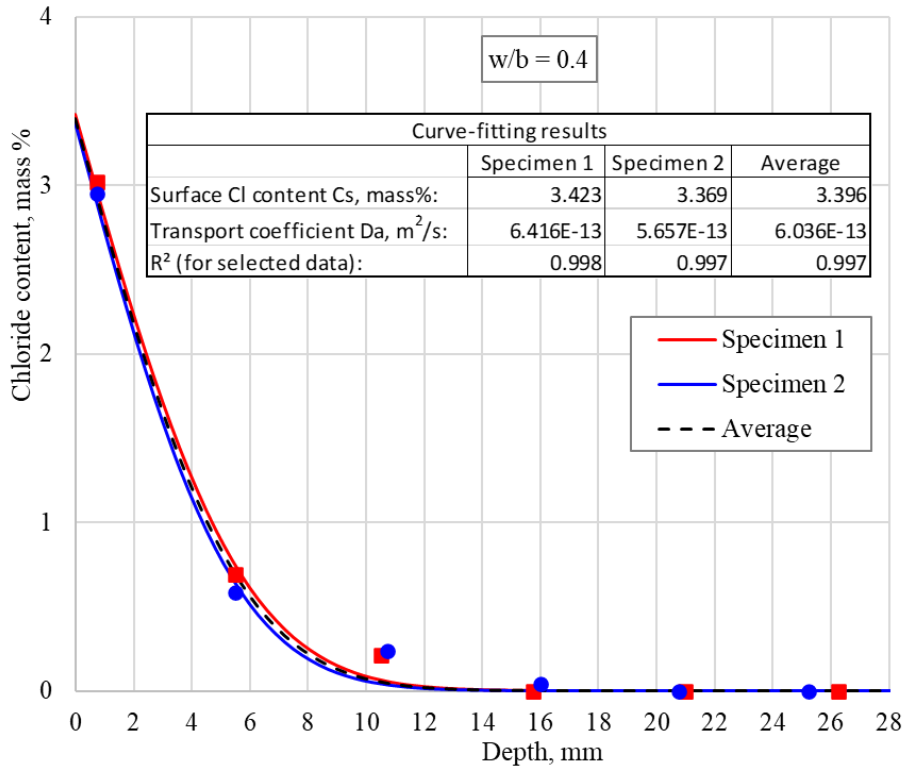

Figure VII.8: Chloride profile of the LC^3-45(B:40/10)
(Cs estimated by extending a line joining the first two points, then Curve fitted, Fick's 2nd law)

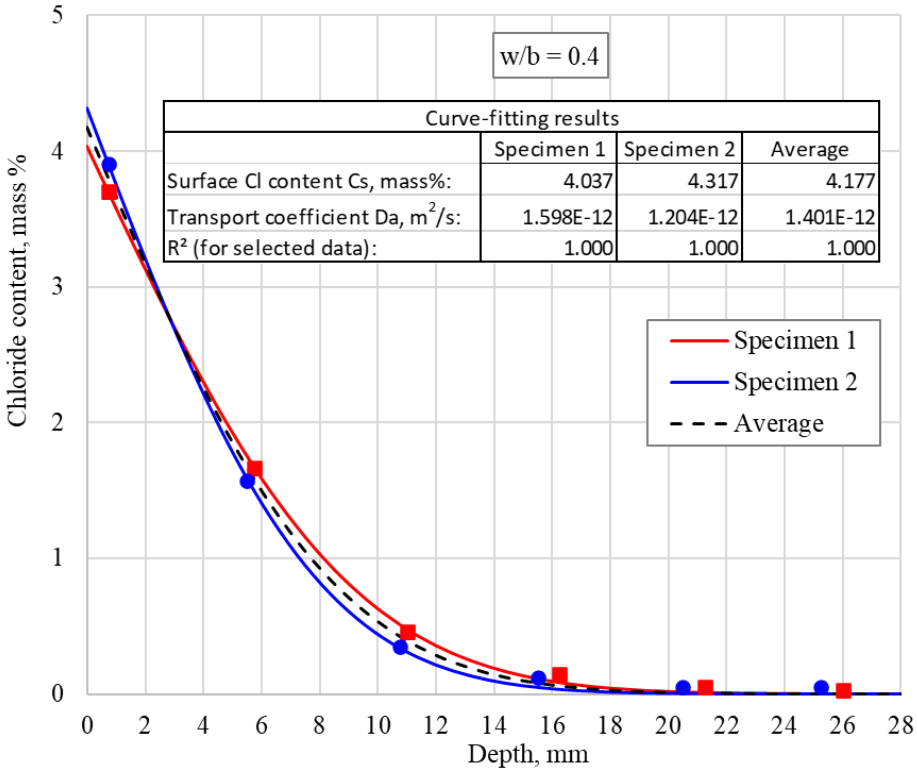

Figure VII.9: Chloride profile of the LC^3-45(H:40/10) (Curve fitted, Fick's 2nd law)

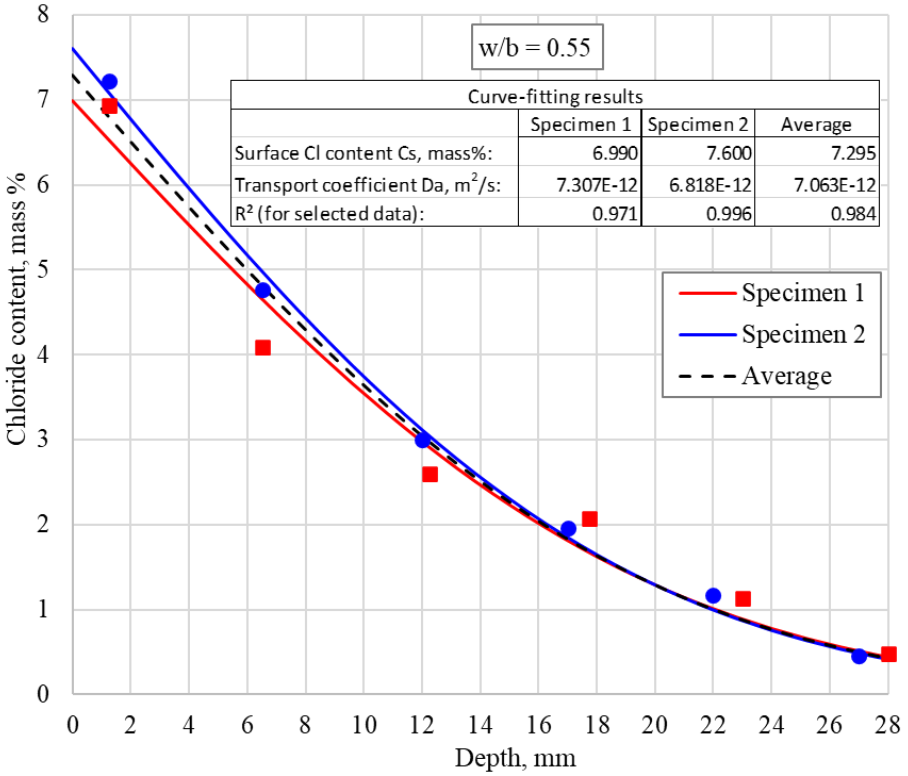

Figure VII.10: Chloride profile of the R1(w/b = 0.55, Curve fitted, Fick's 2nd law)

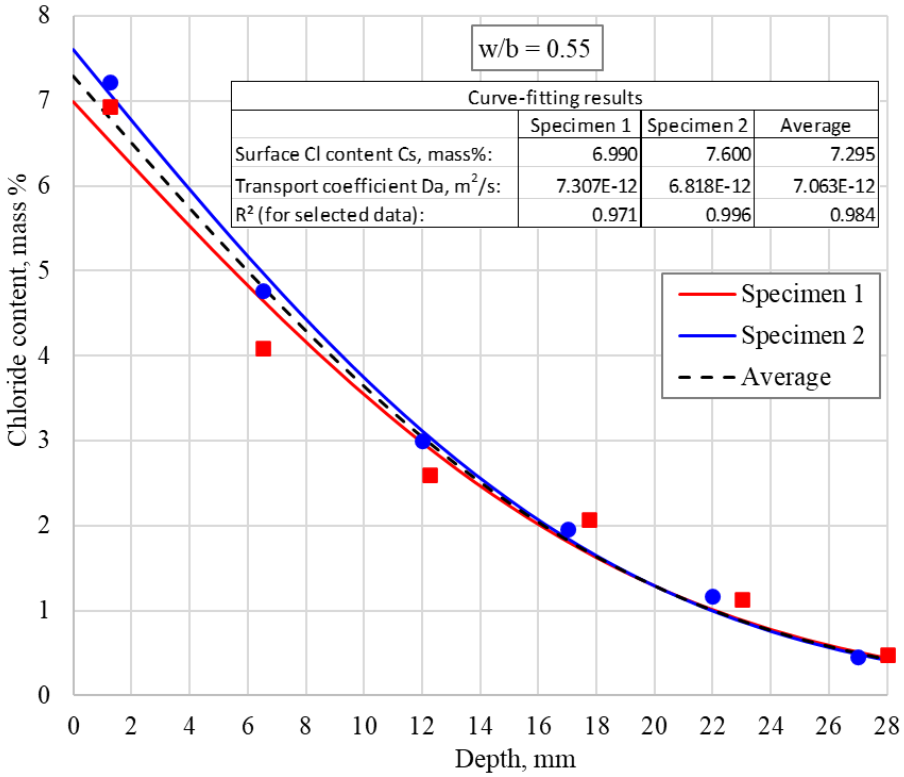

Figure VII.11: Chloride profile of the LC^3-55(B:35/10) (w/b = 0.55, Curve fitted, Fick's 2nd law)

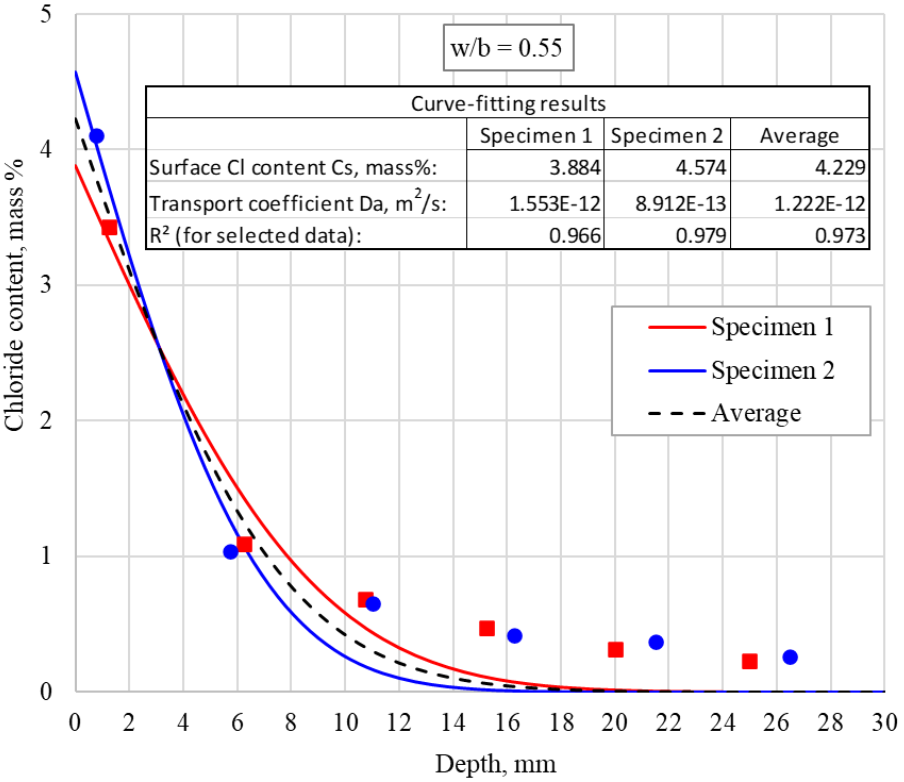

Figure VII.12: Chloride profile of the LC^3-55(H:35/10) (w/b = 0.55, Curve fitted, Fick's 2nd law)

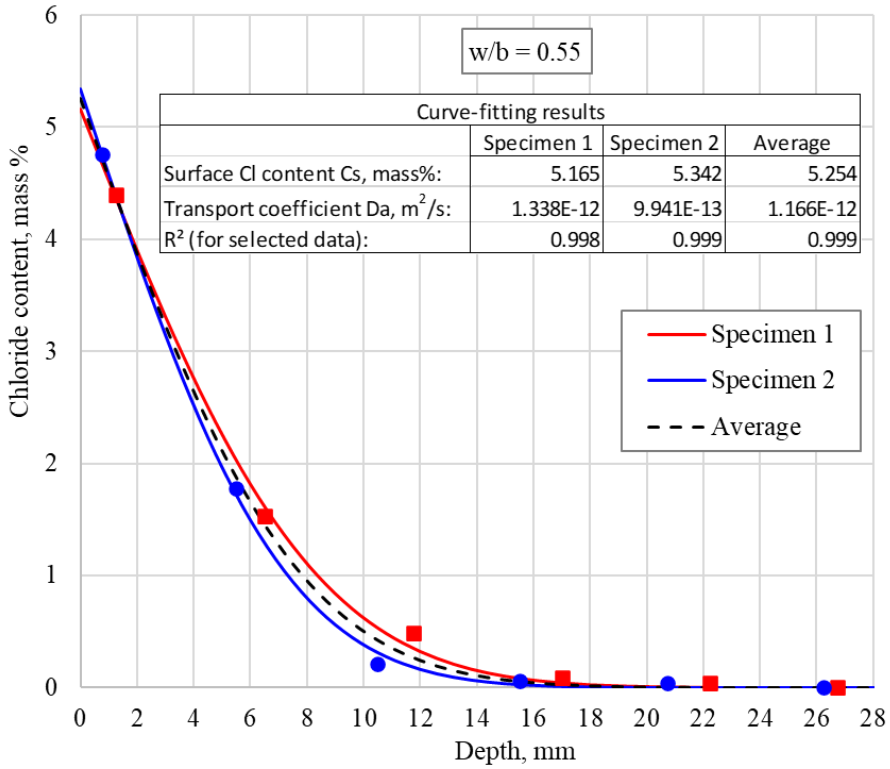

Figure VII.13: Chloride profile of the LC^3-55(HC:35/10) (w/b = 0.55, Curve fitted, Fick's 2nd law)